

# Reduction of Harmonics to Improve Power Quality in Distribution Lines using a Series Active Power Filter

T. Madhubabu  
HOD-Assistant Professor,  
Dept. of Electrical and Electronics  
Engineering  
Teegala Krishna Reddy Engineering  
College  
Hyderabad, Telangana, India.  
madhumk448@gmail.com

Akshaya Anireddy  
UG Student  
Dept. of Electrical and Electronics  
Engineering  
Teegala Krishna Reddy Engineering  
College  
Hyderabad, Telangana, India.  
anireddyakshayaareddy@gmail.com

Naam Sahithi  
UG Student  
Dept. of Electrical and Electronics  
Engineering  
Teegala Krishna Reddy Engineering  
College  
Hyderabad, Telangana, India.  
sahithinam9@gmail.com

K. Sai Krishna Suman  
UG Student  
Dept. of Electrical and Electronics  
Engineering  
Teegala Krishna Reddy Engineering  
College  
Hyderabad, Telangana, India.  
saisuman3534@gmail.com

Sokkam Vikas  
UG Student  
Dept. of Electrical and Electronics  
Engineering  
Teegala Krishna Reddy Engineering  
College  
Hyderabad, Telangana, India.  
sokkamvikas.1922@gmail.com

Kalagotla Chenchireddy  
*Assistant Professor,*  
*Dept. of Electrical and Electronics*  
*Engineering*  
*Teegala Krishna Reddy Engineering*  
*College*  
Hyderabad, Telangana, India.  
chenchireddy.kalagotla@gmail.com

**Abstract:** Electrical devices have advanced and are employed in many different applications nowadays. Personal computers, arc furnaces, and non-linear loads like fluorescent lights emit harmonics alongside utility variable frequency drives (VFD). These are the main gadgets for power quality issues. As is well known, power quality is a significant problem for consumer and distribution systems. This study explores the harmonics induced by non-linear loads. An active power filter, which can enhance power quality and compensate for reactive power has been utilized. In the electrical system at low and medium voltage, Series Active Power Filters (SAPF) are primarily employed to reduce the harmonics, over and in compensation for voltage distortions like sags, flickers, and notches. Total harmonic distortion (THD) can be minimized by SAPF, which injects voltage into the line to mitigate the distortions.

**Keywords:** Total Harmonic Distortions (THD), Series Active Power Filter (SAPF), and Variable Frequency Drives (VFD), Non-linear Loads (NLL).

## I. INTRODUCTION

A common location for the production, transmission and consumption of power at a particular amplitude and frequency is the distribution system, which reveals the quality of the electric power (EPQ). EPQ is mainly used to indicate voltage & current quality, availability of service, and supply of power, among other things [1]. Power lines have seen a variety of harmonic disturbances in recent years, mostly as a result of non-linear loads (NLL) like electric motors, power converters, arc furnaces, etc. Additionally, power electronics (PE) usage for our comfort has significantly increased in recent years. Even though these PE devices make human life more convenient, they also increase the harmonic current in the supply system and negatively impact the power factor [2]. Due to the differences in the component values and component tolerance of the filter, source impedance, and frequency of the AC source have a considerable negative impact on their performance. These might also cause the

system to experience series and load resonances [3][4]. To deal with the issues related to the quality of power, a passive power filter (PPF) is used, but it has some disadvantages such as being more-costly, due to parallel or series resonance and the source's impedance. An APF is extremely wealthy and takes up a lot of space in control theories, and harmonic extraction techniques of the APF [10]. The active filters are employed in the case of the connection for both the series and shunt systems to eliminate harmonics from the system [7]. As compared to PPFs, APFs have an increased number of advantages. They are good performance, an automated adjustment that is risk-free in resonance, and a (power factor) PF that is kept at unity [8] [9]. The APF has more desirable performances when compared to other strategies [5][6]. The traditional PPF has a high-rated capacity to eliminate all the harmonics produced by NLL [13]. On the demand side, a hybrid filter that combines an APF and a PTPF is proposed to operate for improvement in the harmonics [11] [14]. To account for voltage sag and swell, a Shunt APF fundamentally needs an energy source, like a DC battery. Typically, the required DC power for the Shunt APF is provided by a separate rectifier [12] [15]. A series APF reduces voltage distortions using suitable filters and controllers.

## II. SYSTEM CONFIGURATION

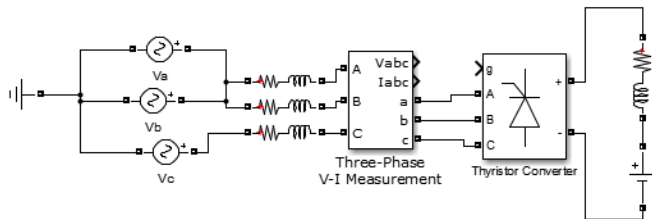


Fig 1: Circuit diagram of distribution network

The diagram of the distribution network, which includes a 3-phase supply, a 3-phase V-I measurement block, a thyristor converter, and an RL non-linear load, is shown in the picture above. The 3 phases are represented by,  $V_a$ ,  $V_b$ , &  $V_c$ . The input voltage is given to the thyristor converter, which connects to an NLL and adjusts its value as per the consumer's requirement. There are numerous distortions in the distribution lines which include voltage swag, as a result of the NLL. A series APF is employed to correct for the distortions; this is explained in detail in the sections that follow.

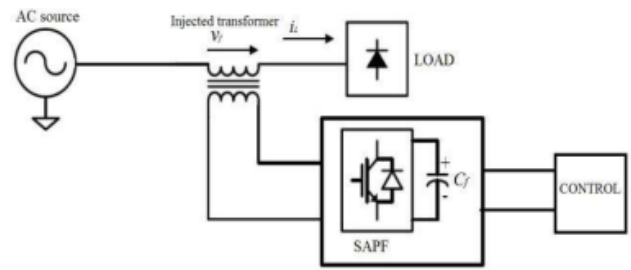


Fig 2: Basic diagram of SAPF

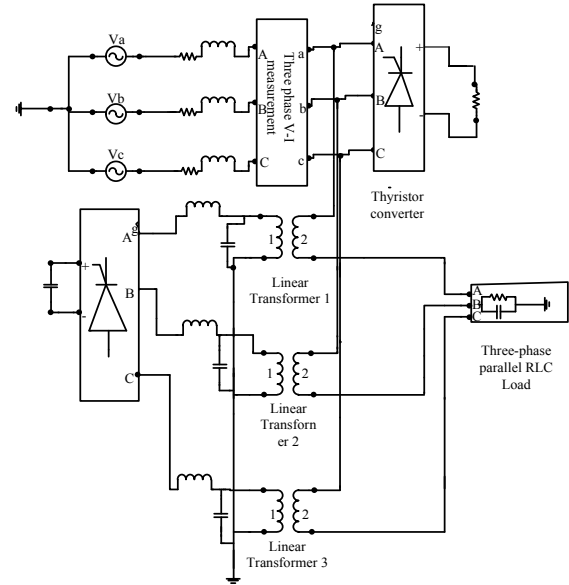


Fig 3: Circuit Diagram of distribution network with SAPF

The image up top shows the diagram of several APFs. An injection transformer, a 3- $\phi$  parallel RLC load, a 3- $\phi$  V-I measurement block, a thyristor converter, a synchronized six-pulse generator, and a three-phase supply are all shown in the diagram. The V-I measurement block, which is used to gauge the circuit's three-phase voltages and currents, is connected to a three-phase supply. When this block is linked in series with the 3-phase elements, it gives 3-phase phase-to-phase or phase-to-ground voltages and currents. Gate signals are given to all the thyristors by the pulse generator, which is powered by supply voltages. The thyristors receive the triggering pulses from this pulse generator, which also regulates how they fire. A phase-locked loop (PLL) can be used to determine the 3-phase source voltage's phase angle. The current controller receives all low-frequency currents on the DC side. The thyristor converter receives the generator's output. By doing this, high frequencies in a three-phase system are transformed into middle frequencies.

Active power filters (APF) have been successfully used to account for nonlinear loads. The shunt architecture, in which

the APF is connected in parallel with the load, has drawn the most interest. Its typical use is for the elimination of current harmonics produced by disturbance-causing harmonic current source (HCS) loads. However, parallel APF is ineffective when a load generates voltage harmonics, also known as harmonic voltage source (HVS) loads. In this case, an APF design with a series connection has been proposed known as SAPF. The SAPF is linked between the source and NLL. The voltage injected by a SAPF at the PCC ensures that the load voltages are not affected by voltage disturbances. Most three-phase unbalanced systems and voltage sags, swell, and flickers are reduced using SAPF. A converter, injection transformer, and filter are their parts. The supply lines are connected in series with these transformers. They are used to compensate for the voltage harmonics along with filtering the switching ripples in a SAPF.

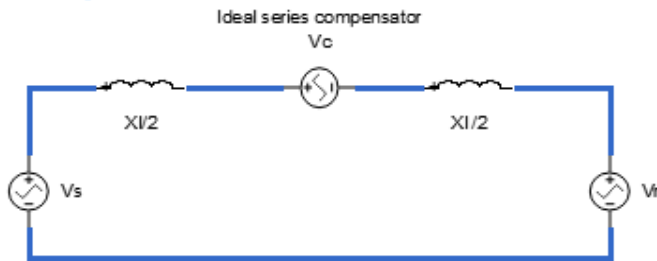


Fig 4: Ideal series compensation of a transmission line.

The equation yields the equivalent impedance value for the transmission line is,

$$X_{eq} = X - X_{comp} = X(1 - r) \quad (1)$$

Where,

$$r = \frac{X_{comp}}{X} \quad (2)$$

$r$  ---series of degrees compensate,

$X_{comp}$  ---Comparable series compensation reactance

→+, if capacitive

→-, if inductive

The transmission line's current flow is of the following magnitude:

$$I = \frac{2V}{(1-r)X} \sin \frac{\theta}{2} \quad (3)$$

The transmission line's current source of active electricity is,

$$P_c = VcI = \frac{V^2}{(1-r)X \sin \theta} \quad (4)$$

The source provides the reactive power,

$$Q_c = I^2 \times (X_{comp}) = \frac{2V^2}{X} \times \frac{r}{(1-r)^2} (1 - \cos \theta) \quad (5)$$

If the switch opens with a slanted delay relative to the line current,

$$i = I_m \cos \omega t = \sqrt{2}I \cos \omega t \quad (6)$$

The following functions can be used to express the capacitor voltage:

$$V_c(t) = \frac{1}{c} \int_{\gamma}^{int} i(t) dt = \frac{I_m}{\omega C} (\sin \omega t - \sin \gamma) \quad (7)$$

The basic voltage of a capacitor,

$$V_{cf}(\gamma) = \frac{1}{\omega C} (1 - \frac{2}{\pi} \gamma - \frac{1}{\pi} \sin 2\gamma) \quad (8)$$

Impedance about  $\gamma$ ,

$$X_c(\gamma) = \frac{V_{cf}(\gamma)}{I} = \frac{1}{\omega C} (1 - \frac{2}{\pi} \gamma - \frac{1}{\pi} \sin 2\gamma) \quad (9)$$

Where,

$$I = I_m / \sqrt{2}$$

In the sections that follow, let's talk in detail about the control technique utilized.

### III. CONTROL STRATEGY

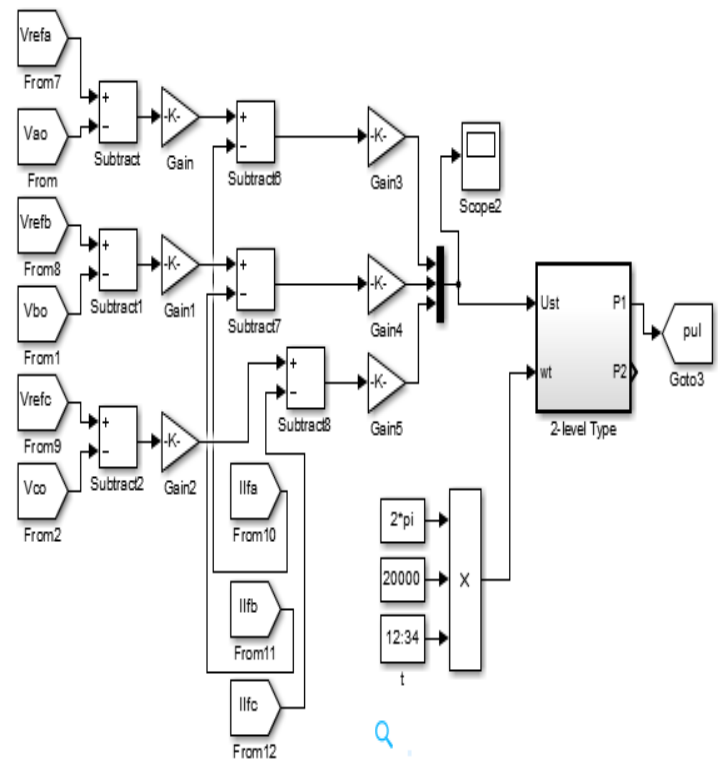


Fig 5: Control strategy for the SAPF

A SAPF is typically used to inject a voltage component to control terminal voltages and adjust for voltage sags, voltage

swells, spikes, notches, and flickers. It primarily serves to preserve delicate loads. Direct Voltage Restorer (DVR), a series APF, inserts a series voltage and corrects for the load voltages when the fault occurs on other lines. As is common knowledge, there are two different types of SPAFs: those with current-fed NLL (CFNLL) and those with voltage-fed NLL (VFNLL). In the DC link of a diode rectifier, VFNLL consists of a capacitive filter and a load. All by itself, SAPF successfully keeps the sinusoidal supply currents for the VFNLL. Coming back to CFNLL, it has a resistor and inductor connected in series in a DC link of a 3- $\phi$  diode rectifier. A sufficient voltage is injected to get rid of the harmonics and keep the voltage under control. By forcing a high impedance path to the current harmonics, SPAFs correct current system distortion brought on by non-linear loads. The series filter will act as a harmonic voltage source to produce low impedance at the fundamental frequency and prevent current harmonics from entering the ac mains. This compels the high-frequency currents to pass through the LC passive filter connected in parallel to the load. The SAPF imposes a high impedance by producing a voltage at the same frequency as the harmonic component of the current that needs to be removed. By correcting the fundamental frequency positive, negative, and zero sequence voltage components of the power distribution system, voltage control or unbalance can be fixed. The SAPF is able to account for voltage control on the load side (sags or swells) and voltage unbalance by injecting a voltage component in series with the supply voltage in this situation. To reduce the ripples caused by the voltage injection from the SAPF, a ripple filter is connected. Given that it consists of a series connection between a capacitor and a resistor, the calculation is as follows:

$$Fr = 1/(2*\pi*Rr*Cr)$$

Where,

Rr – Ripple filter Resistance

Cr – Ripple filter Capacitance

Here, a PI controller is used to enhance the performance of a SAPF with the PWM technique. The PWM controller, which in turn produces the triggering pulses for the VSC of the SAPF, receives the error signal that the PI controller calculates and the difference between the reference voltages and the detected load voltages. In real-world applications, voltage harmonics is corrected using a PWM control circuit. As seen in Fig. 5, the voltages at the load side Vao, Vbo, & Vco are linked to the input of the subtract, subtract1, and subtract2 to calculate the difference between them. The output

of the subtract is then sent to the gain, gain1, and gain2 to increase the voltage. Subtracts 6, 7, and 8 are connected to the output of the gains and the reference currents Irefa, Irefb, and Irefc. Additionally, their outputs are linked to gains 3, 4, and 5. Finally, a 2-level type that produces the output is coupled to all of these gains.

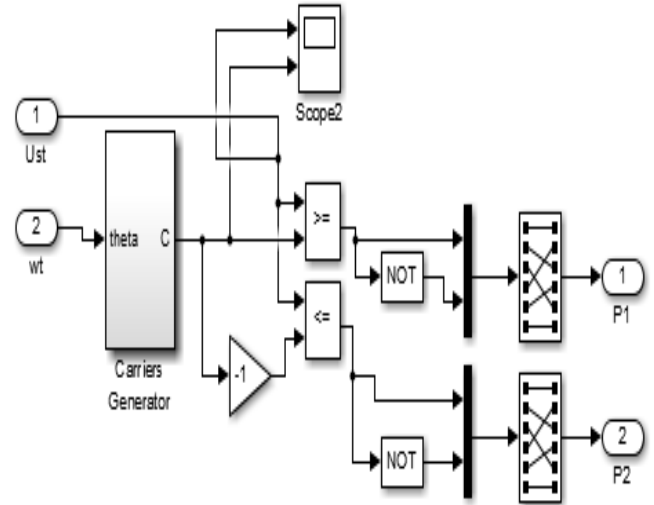


Fig 6: Subsystem

This figure shows the subsystem1 circuit diagram which consists of a carrier generator.

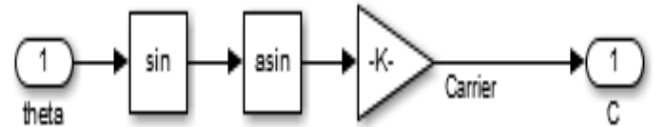


Fig 7: Subsystem 2

The circuit diagram for subsystem2, which comprises a gain block and carrier signals, is shown in the above picture.

#### IV. SIMULATION RESULTS

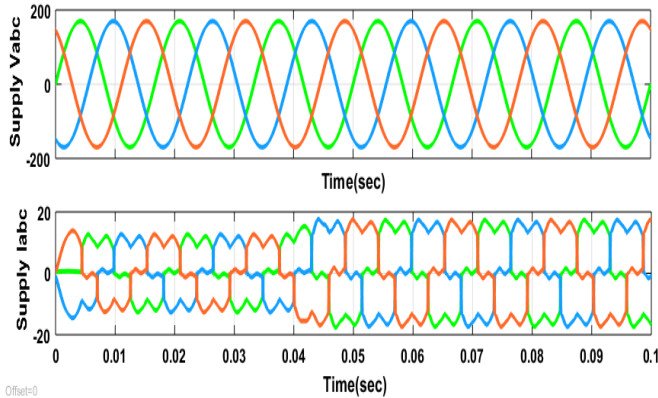


Fig 8. 3-phase Supply Voltage and Supply Current waveforms.

From fig. 8, it can be seen that there are two waveforms: supply voltage and supply current. Three phases make up each waveform. 3-phases A, B, & C marked with 3 different colours from the 3-phase supply voltage & current waveforms can be found. In this case, the colours red, blue, and green denote the A, B, and C phases, respectively. The voltage waveform's magnitude lies between -200 and 200. While the current waveforms' magnitudes range from -20 to 20. Because it is a pure sinusoidal waveform, there won't be any distortions in the voltage or current.

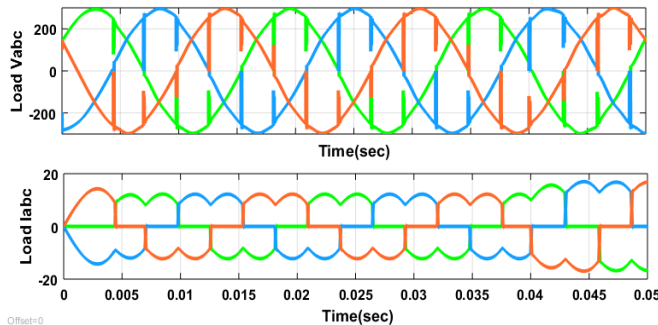


Fig 9. 3-phase Load Voltage and Current waveforms

The load current and load voltages for the three phases calculated as shown in fig 9. Two waveforms of the three-phase load voltage and load current can be seen. 3 phases A, B, and C indicated with 3 different colours from these waveforms can be found. In this case, the colours red, blue, and green denote the A, B, and C phases, respectively. The voltage waveform's magnitude lies between -200 and 200. While the current waveforms' magnitudes range from -20 to 20.

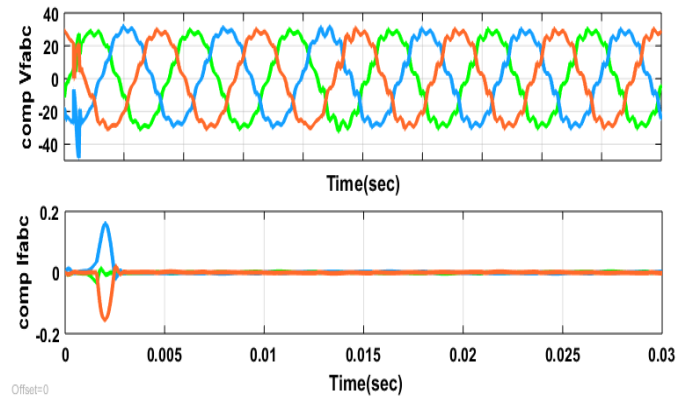


Fig 10. 3-phase Compensated Voltage and Compensating Current Waveforms.

The compensated voltages and compensated currents from the 3-phase compensating voltage & current waveforms can be found. To lessen the harmonics, these voltages are introduced into the supply lines. The magnitude of the voltage waveform spans from -200 to 200. While the current waveforms' magnitudes range from -20 to 20. The waveforms of the compensating current and voltage have been displayed above.

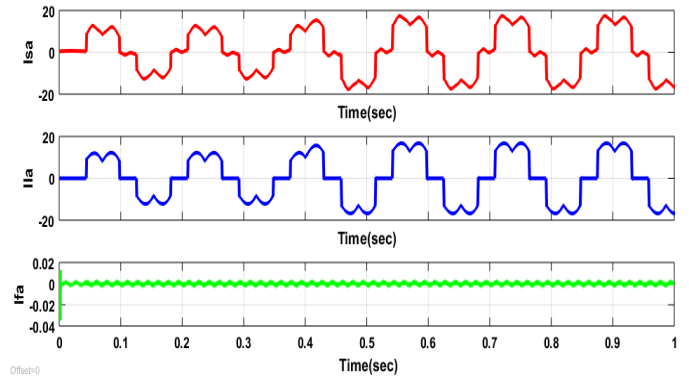


Fig 11. 1-phase Source Current, Load Current, and Compensating Current Waveforms.

The source current is shown in red, the load current is shown in blue, and the compensating current is shown in green. These are the output currents obtained at the source, load, and compensation or filter. Fig. 11 shows the waveforms of the supply, load and compensating currents in a single phase.

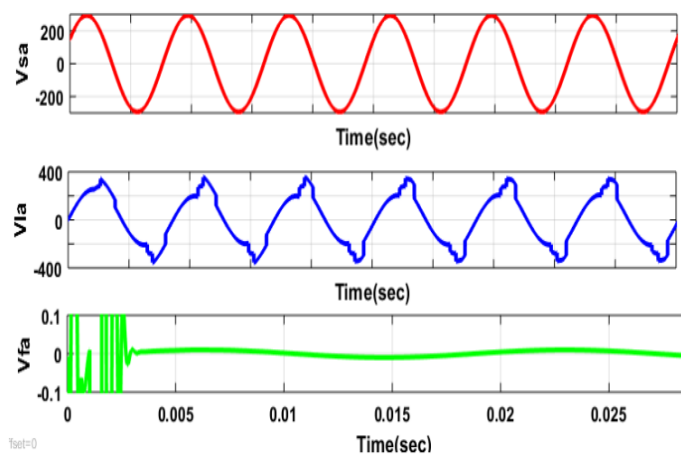


Fig 12. 1-phase Source, Load, and Compensating Voltage waveforms

The source voltage, load voltage, and compensating voltage waveforms for a single phase are shown in Fig. 12. Different colours are used to symbolize each waveform. While there is no distortion in the source voltage waveform, the load voltages do have distortions; to reduce them, the corrected voltage, which is indicated in green is used. A SAPF improves the power quality in distribution lines. By utilizing transformers to pump power into the supply lines, voltage harmonics are typically greatly decreased.

## V. CONCLUSION

This proposed research infers that employing SAPF harmonics reduces large values by looking at the supply and load voltages. The series active filter employs a hysteresis controller to minimize NLL voltage distortion compensations. The usage of SAPF has significantly enhanced the quality of the power.

## VI. REFERENCES

- [1] Chaudhari MA. Three-phase Series Active Power Filter as Power Quality Conditioner. In 2012 IEEE International Conference on Power Electronics, Drives and Energy Systems (PEDES) 2012 Dec 16 (pp. 1-6). IEEE.
- [2] K. Santhosh, K. Chenchireddy, P. Vaishnavi, A. Greeshmanth, V. M. Kumar and P. N. Reddy, "Time-Domain Control Algorithms of DSTATCOM in a 3-Phase, 3-Wire Distribution System," 2023 International Conference on Intelligent Data Communication Technologies and Internet of Things (IDCIoT), Bengaluru, India, 2023, pp. 781-785, doi: 10.1109/IDCIoT56793.2023.10053535.
- [3] J. Turunen and H. Tuusa (2007, September). Using a straightforward PI-control approach, the series active power filter's voltage compensation performance is improved. Europe Power Electronics and Applications Conference in 2007 (pp. 1-9). IEEE.
- [4] Chenchireddy, K., & Jegathesan, V. (2022, March). Multi-Carrier PWM Techniques Applied to Cascaded H-Bridge Inverter. In 2022

International Conference on Electronics and Renewable Systems (ICEARS) (pp. 244-249). IEEE.

- [5] Rao, K. Mercy Rosalina, and M. Uma Maheswara. Improvement of Microgrid Transient Stability Using Series Active Power Filters Pages 1-4 of the 2019 Fifth International Conference on Electrical Energy Systems. IEEE, 2019.
- [6] K. Chenchireddy, V. Kumar, K. R. Sreejyothi and P. Tejaswi, "A Review on D-STATCOM Control Techniques for Power Quality Improvement in Distribution," 2021 5th International Conference on Electronics, Communication and Aerospace Technology (ICECA), Coimbatore, India, 2021, pp. 201-208, doi: 10.1109/ICECA52323.2021.9676019.
- [7] Radzi, M. A. M., Usman, H., and Hizam, H. (2013, November). Improve power quality by simulating a single-phase shunt active power filter using a fuzzy logic controller. The IEEE Conference on Clean Energy and Technologies (CEAT) was held in 2013. (pp. 353-357). IEEE.
- [8] Al-Haddad K, Rahmani S, and Hamadi a unique hybrid series active filter structure that can correct reactive power, voltage and current harmonics and sag and swell in the voltage. 2009 July 5th IEEE International Conference on Industrial Electronics (pp. 286-291). IEEE.
- [9] "Comparative study on combined series active and shunt passive power filter employing two different control approaches," by Hasan, Khairul Nisak Md., and Mohd Fakhizan Romlie. 2007 International Conference on Advanced Intelligent Systems IEEE, 2007.
- [10] Xu, Hong Wang, Yonghai, Xiangning Xiao, and Hao Liu. "Hybrid active power filters operating in parallel with capacitors or passive power filters." Asia and Pacific. 2005 IEEE/PES Transmission & Distribution Conference & Exhibition, pp. 1-6 IEEE, 2005.
- [11] Chenchireddy, K., & Jegathesan, V. (2022). Three-Leg Voltage Source Converter-Based D-STATCOM for Power Quality Improvement in Electrical Vehicle Charging Station. In *AI Enabled IoT for Electrification and Connected Transportation* (pp. 235-250). Singapore: Springer Nature Singapore.
- [12] Tung NX, Horikoshi K, and Fujita G. a control method that has been modified to allow a dynamic voltage restorer to serve as a SAPF. International Power Electronics Conference 2010, ECCE ASIA, June 21, 2010 (pp. 2283-2287). IEEE.
- [13] G. W. Chang and W. C. Chen An innovative reference compensation voltage method for APF management in series. IEEE Transactions on Power Delivery, Version 21.3, Pages 1754-1756, 2006.
- [14] V. Kumar, K. Chenchireddy, M. R. Reddy, B. Prasad, B. Preethi and D. S. Raj, "Power Quality Enhancement In 3-Phase 4-Wire Distribution System Using Custom Power Devices," 2022 8th International Conference on Advanced Computing and Communication Systems (ICACCS), Coimbatore, India, 2022, pp. 1225-1228, doi: 10.1109/ICACCS54159.2022.9785339.
- [15] Anawade, Shradha Balajirao, and Atul A. Kale. "Series Active Power Filter (SAPF) For Power Quality Improvement." 2022 *Interdisciplinary Research in Technology and Management (IRTM)*. IEEE, 2022.

# Output Voltage and Power Factor Improvement for Non-Conventional Energy Generation

N.Rajashekar Varma  
*Dept. of Electrical and  
Electronics Engineering  
Teegala Krishna Reddy  
Engineering College*  
Hyderabad, Telangana, India.  
dmrsvarma@gmail.com

Dhasharatha. G  
*Dept. of Electrical and  
Electronics Engineering  
Teegala Krishna Reddy  
Engineering College*  
Hyderabad, Telangana, India  
g.dhasharatha@gmail.com

E.Harsha Vardhan reddy  
*Dept. of Electrical and  
Electronics Engineering  
Teegala Krishna Reddy  
Engineering College*  
Hyderabad, Telangana, India  
harshare321@gmail.com

A.Manisha  
*Dept. of Electrical and  
Electronics Engineering  
Teegala Krishna Reddy  
Engineering College*  
Hyderabad, Telangana, India  
manishamani.ar9@gmail.com

M.Tharun Kumar  
*Dept. of Electrical and  
Electronics Engineering  
Teegala Krishna Reddy  
Engineering College*  
Hyderabad, Telangana, India  
tarun.kumar7013@gmail.com

K.Charan  
*Dept. of Electrical and  
Electronics Engineering  
Teegala Krishna Reddy  
Engineering College*  
Hyderabad, Telangana, India  
charankamati27@gmail.com

**Abstract:** In this modern world, electricity is one of the basic and also an widely used necessity, since the universe cannot function without electrical energy. There are a variety of sources that can generate electrical energy; these include conventional energy sources and nonconventional energy sources. Due to limitation and the high cost of fossil fuels and also environmental effects, consideration of conventional source energy generation can be a trouble; therefore, the world is looking toward energy generation that has less impact on the environment as a source. Even though generation is easy, some uncertainty like high harmonic distortion and less efficient power and low power factor at consumer or load can be attested in this process due to standard conventional switches. Hence, cascaded h-bridge with increased level for nonconventional energy generation and transmission for switching operations has been suggested in this research to overcome all the loopholes and to improve the efficiency.

**Keywords:** Power Factor, non-convetional energy sources, cascaded H-bridge

## I. INTRODUCTION

The serially added H-bridge multi-layer alternator is the combination of serially linked H-bridge with a separate Direct current source which is elect acquired as of any non-conventional source [1]. Multilevel inverters have recently

gained popularity as an architecture for high voltage industrial applications. To provide elevated power demand with rising electrical energy-level, multilevel inverters have made significant advancements. Multilevel inverters provide several benefits over traditional two-level inverters, including lower switching frequencies first-class load voltage(v) and current(i) with less harmonic disturbance, and reduced voltage stress on power switching components [2-4]. These factors are the causes of the ongoing nature of several multilevel inverter investigations. Multilevel inverters come in a variety of topologies, such as diode-clamped multistep alternators, flying-capacitor multistep alternators, and serially connected H-bridge multilayer alternators. The multilevel serially added H-bridge alternator is one of these multilevel topologies that has gained popularity since it does not require clamp diodes or capacitors [5-6].

Serially added multi-step alternator is a power electrical component designed to integrate an Alternating voltage that has been converted from several levels of direct current voltages. The most enticing advancement in The multilayer inverter operates in the moderate-to-peak level voltage array, which includes applications for motor drive, energy distribution, power energy class, and power conditioning [7]. The medium voltage energy management

industry benefits from the use of multilevel voltage source inverters since they are affordable. Inverters with numerous voltage or current sources and output levels might be referred to as multilevel inverters. Different topologies can be used to create a multilayer inverter [8]. A multi-step inverter has more whip hand when compared to the normal two-level inverter which consumes an excessive rate of switching frequency. The best properties of multi-step inverters are low  $dv/dt$  generation and a very low total harmonic distortion in output voltage. Operation is done with minimum switching frequency in the case of multi-level inverters [9].

Asinusoidal voltage is required in many real-world applications because of their affordability, multi-level inverters have become a common alternative. As the step increase, wave nature class likewise improved and the need for filters decreases [10]. Multilayer alternators have often employed in medium- or peak-power system applications, such as variable-speed and stationary reactive power correction [11]. The better-switching devices are opted for better and more efficient economic operations. The layer number of the alternator must be gradually improvised and stepped up so that the whole harmonic disturbance can nearly get nullified.

## II. SERIES CONNECTED-BRIDGE MULTILAYER ALTERNATOR TOPOLOGY

The 7-level/layer alternator topology is described in fig-1 it contains three h-bridges cascaded in series and each h-bridge contains four switches igbt. Each h-bridge has one separate dc source.

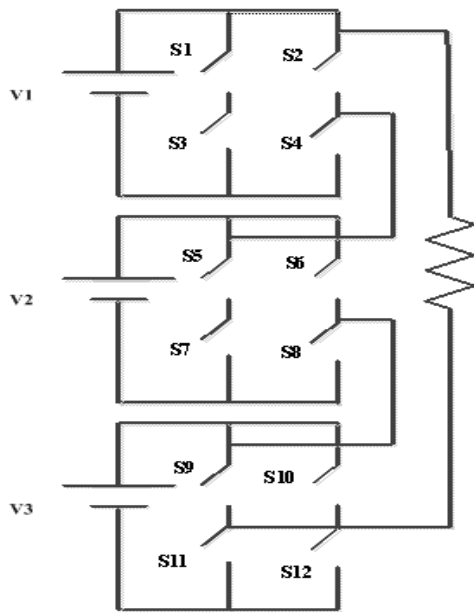


Fig. 1. Seven level inverter topology

The 7-layer series connected h-bridge alternator can be operated in many modes. To operate modes can be changed by changing the switches position (on/off), for different modes of operation, different voltage values are obtained. As 7layer series connected h-bridge multilayer alternator is considered, 7 different voltages as provided in the below table-1 are obtained.

Table-1 7- level inverter voltage levels

Voltages	VH1	VH2	VH3
-3Vdc	-Vdc	-Vdc	-Vdc
-2Vdc	0	-Vdc	-Vdc
-1Vdc	0	0	-Vdc
0	0	0	0
1Vdc	Vdc	0	0
2Vdc	Vdc	Vdc	0
3Vdc	Vdc	Vdc	Vdc

The designed multilevel inverter can be operated in many switching modes; two modes are explained below.

### A. MODE OF OPERATION -1

For 7- the series-connected h-bridge multilayer alternator, three h-bridges connected in series are used. If -3 VDC voltage as the output is considered, the switches are activated are S2, S3, S6, S7, S10, and S11. The operating condition diagram is shown below in Fig. 2. The seven-level can be used in a variety of ways. The switching sequence for the two modes of operation is explained. for the 7-level alternator. MOSFET, GTO, IGBT, and thyristor switches are just a few examples of switching devices. Based on the specifications of the switching devices and requirements, any one of the above switches can be used. These switching devices are used to achieve smoother, wiser, more efficient, and cost-effective operations.

The thyristor switching devices are suitable for the rectifiers, ac-ac voltage controllers, and cyclo converters; the MOSFET switching devices are best suited for dc-dc converters and chopper circuits; and the IGBT switches are best suited for the alternator topologies. In this manuscript, for the switching operations, the IGBT switches are used rather than any other switches because they operate at the best voltage, power, and frequency as well. Because of the



IGBT's above-mentioned characteristics, it is the most commonly used switching device in alternator internal circuits. Inverters are electronic devices that convert DC power to AC power. The operating conditions for inverters depend on several factors, including the type of inverter, the input DC voltage, the load requirements, and the switching frequency.

Here are some general recommendations for operating conditions:

**Input DC Voltage:** The recommended input DC voltage for the inverter depends on its design and load requirements. The input voltage should be within the range specified by the manufacturer to ensure safe and optimal operation.

**Switching Frequency:** The switching frequency of the inverter affects the output waveform quality and efficiency. A higher switching frequency can improve output voltage quality and efficiency but can also increase switching losses, reducing the overall efficiency. The recommended switching frequency depends on the inverter type and the application.

**Load Requirements:** The load requirements, such as voltage and current requirements, determine the output voltage and current of the inverter. The inverter must be sized to meet the load requirements, and the operating conditions must be set to ensure that the inverter can deliver the required voltage and current.

**Heat Dissipation:** Inverters generate heat during operation. The operating conditions should be set to ensure that the inverter can dissipate heat effectively and operate within its safe temperature range. It is essential to consult the manufacturer's specifications and guidelines for the specific inverter being used to ensure that it is operated within its safe and optimal operating conditions.

Overall, the best operating conditions for inverters depend on the specific application and inverter design. An IGBT (Insulated Gate Bipolar Transistor) is a type of power semiconductor device that is widely used in high-power applications.

The specifications of an IGBT may vary depending on the specific model and application, but the following are some key specifications:

**Maximum Voltage Rating:** This specification refers to the maximum voltage that an IGBT can withstand without breaking down. It is crucial to ensure that the IGBT can operate safely within the specified voltage range.

**Collector Current:** This rating specifies the maximum current that an IGBT can handle without damage. It is important to ensure that the IGBT can handle the required current for the particular application.

**Switching Frequency:** This specification defines the maximum frequency at which an IGBT can switch on and off. It is essential for applications that require fast switching, such as in inverters.

**Thermal Resistance:** This specification refers to how efficiently an IGBT can dissipate heat generated during operation. It is crucial to ensure that the IGBT can operate within its safe temperature range.

**Gate Charge:** This specification defines the amount of charge required to switch an IGBT on and off. It is essential to ensure that the IGBT can be controlled effectively and efficiently.

**On-State Voltage:** This rating is the voltage drop across the IGBT when it is conducting current. It is crucial to ensure that the IGBT can handle the required voltage for the specific application.

In summary, the specifications of an IGBT play a vital role in ensuring its safe and effective operation within the specified operating range. To ensure that an IGBT operates optimally, it is essential to consult the manufacturer's specifications and guidelines for the specific model being used.

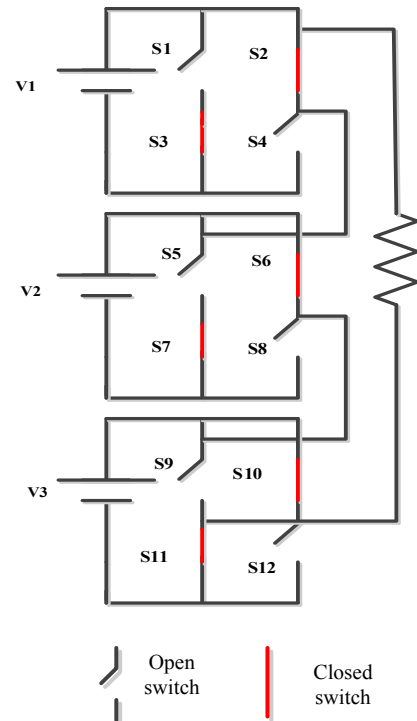


Fig.2 mode-1 operation topology

## B. MODE OF OPERATION-2

Similar to the above mode of operation, mode-2 operation of the 7-level serially connected h-bridge alternator is studied.

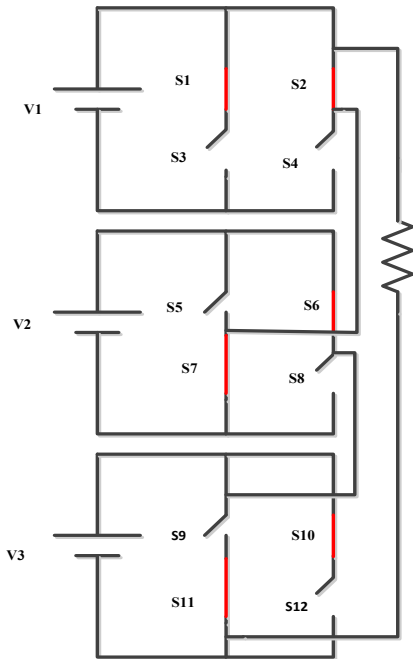


Fig.3. mode-2 operation

Apart from the above modes of operation, the 7-layer alternator has many other modes of operation. the remaining operations of the 7-layer inverter switching sequence is explained below table-2.

Table -2 switching modes for different voltages

S	S	S	S	S	S	S	S	S	S	S1	S1	S1
1	2	3	4	5	6	7	8	9	0	1	2	
0	1	1	0	0	1	1	0	0	1	1	0	
1	1	0	0	0	1	1	0	0	1	1	0	
1	1	0	0	1	1	0	0	0	1	1	0	
1	1	0	0	1	1	0	0	1	1	0	0	
1	0	1	0	1	1	0	0	1	1	0	0	
1	0	1	0	1	0	0	0	1	1	0	0	
1	0	1	0	1	0	0	0	1	0	1	0	

## IV. WORKING SCHEME

The series connected h-bridge used is operated in two modes.

### 1. OPERATION OF A SERIALY CONNECTED H-BRIDGE MULTI-LAYER ALTERNATOR IN GENERATING MODE

The operation of series connected h-bridge multilayer alternator is explored for the straightaway/linear load of 40KVA and (8/10) power-factor lagging is connected to normal 3-layer, layer and 7-layer series connected h-bridge alternators. Here one h-bridge use one DC source hence maintenance and controllability is easy. the total harmonic distortion is observed accordingly from the output voltage graphs of corresponding 3-level, 5-level and 7-level inverter. For 3-layer alternator the voltage levels are -500V, 0V, 500V for 5-layer alternator the voltage levels are -500V, -250V, 0V, 250V, 500V. For 7-layer inverter the voltage levels are -500V, -250V, 125V, 0, 125V, 250V, 500V. It is observed that the voltage profile has improved and the whole harmonic disturbance (THD) is absolutely decreased while the layer of the serially connected h-bridge is increased [13].

### 2. WORKING OF A SERIALY CONNECTED H-BRIDGE AS A COMPENSATOR

The combination of nonconventional energy sources can be used as a compensator as well as a secondary power source. By cutting the harmonics, power quality improvement can be attained. The load is not constant or linear on the load side, so the serially h-bridge alternator, as a compensator, reduces the harmonic quantity, improves the power factor, and also increases efficiency [14].

A good power factor indicates that the electrical power is being used efficiently, and this can result in several benefits, such as:

1. Lower electricity bills: A good power factor means that less electrical energy is wasted, and as a result, you will be charged less by your electricity provider.
2. Improved equipment performance: Electrical equipment operates more efficiently with a good power factor, which can result in lower maintenance costs and longer equipment lifetimes.
3. Increased capacity: A good power factor means that more electrical load can be served with the same amount of electrical power, which can result in increased capacity and fewer power outages.
4. Reduced environmental impact: A good power factor means that less electrical energy is wasted, which can result in a reduced environmental impact.

## IV. SIMULATION RESULTS:

The simulation outcomes of the 3-layer, 5-layer, and 7-layer inverters are achieved with the help of MATLAB and Simulink. The three-level inverter voltage waveforms are shown in Fig. 4, and the whole harmonic disturbance of a three-level series connected h-bridge is analyzed in Fig. 5.

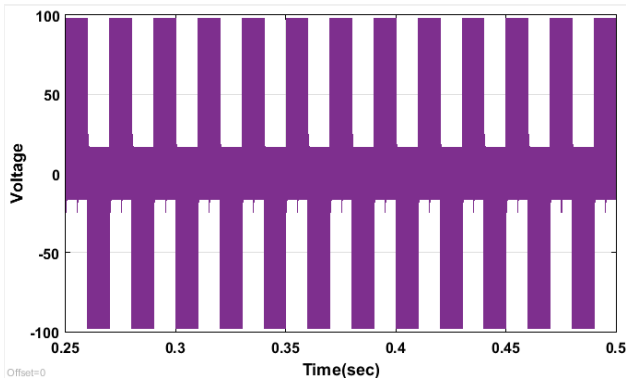


Fig.4. Voltage waveform of 3- layer serially connected h-bridge alternator

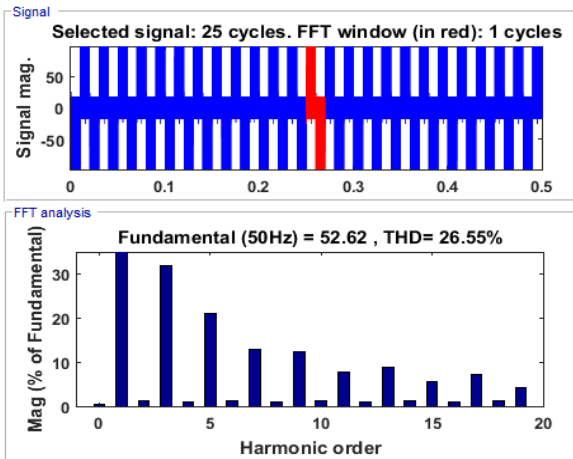


Fig.5. Whole harmonic disturbance of 3- layer serially connected h-bridge alternator

The 5- layer serially connected h-bridge alternator voltage waveforms are shown in the fig-6 and the whole harmonic disturbance of 3- layer series connected h-bridge is analyzed from fig.7.

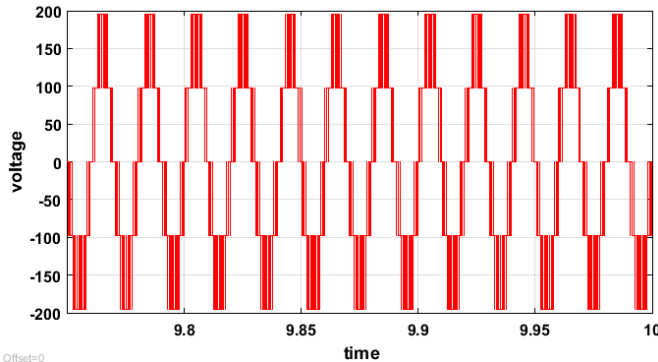


Fig.6. Voltage waveform of 5-level series connected h-bridge alternator

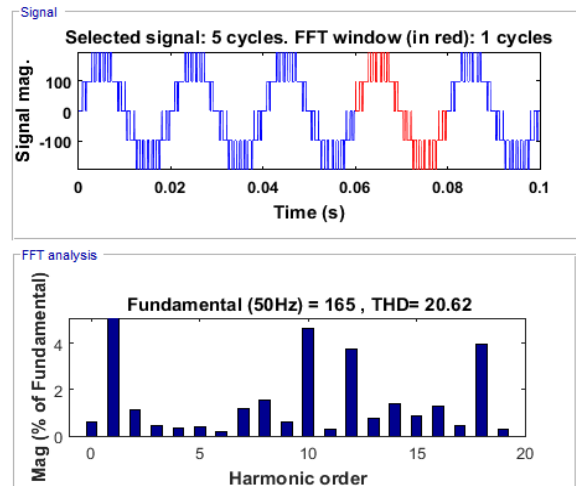


Fig.7. Whole harmonic disturbance of 5- layer series connected h-bridge alternator.

The 7- level alternator voltage waveforms are shown in the fig-8 and the whole harmonic disturbance of 7- the layer series connected h-bridge is analyzed from fig.9.

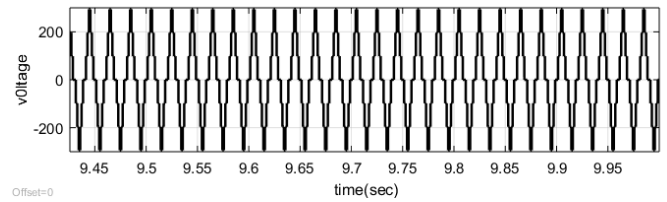


Fig.8. Voltage waveform of 7-layer series connected h-bridge alternator

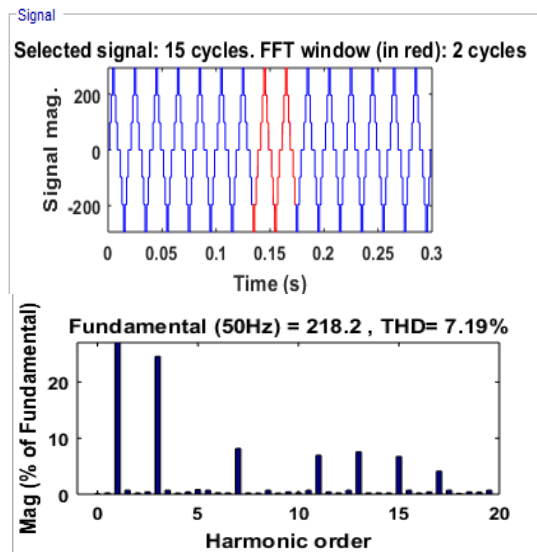


Fig.9a and 9b. Whole harmonic disturbance of 7- layer series connected h-bridge alternator.

## V.CONCLUSION

This research work has investigated the increased layers of series connected h-bridge inverter to analyze output voltage, power quality improvement, and total harmonic distortion. The simulation result clearly shows that when the level of the inverter increased then the total harmonic distortion gradually decreased. Moreover, the load power factor is improved and the overall efficiency is increased. Hence, high-level inverters are used in switching operations while the non-conventional source is needed to generate and transmitted with efficiency and quality.

## REFERENCES

- [1]. Gaikwad, Asha, and Pallavi Appaso Arbune. "Study of cascaded H-Bridge multilevel inverter." *2016 (ICACDOT)*. IEEE, 2016.
- [2]. Sim, Hyun-Woo, June-Seok Lee, and Kyo-Beum Lee. "A detection method for an open-switch fault in cascaded H-bridge multilevel inverters." *2014 (ECCE)*. IEEE, 2014.
- [3]. Chenchireddy, Kalagotla, and V. Jegathesan. "Multi-Carrier PWM Techniques Applied to Cascaded H-Bridge Inverter." *(ICEARS)*. IEEE, 2022.
- [4]. Ranjan, Abhishek Kumar, D. Viiava Bhaskar, and Nibedita Parida. "Analysis and simulation of cascaded H-bridge multilevel inverter using level-shift PWM technique." *2015 (ICCPCT-2015)*. IEEE, 2015.
- [5]. Chenchireddy, Kalagotla, and V. Jegathesan. "A Review Paper on the Elimination of Low-Order Harmonics in Multilevel Inverters Using Different Modulation Techniques." *2020 (2021)*: 961-971.
- [6]. Sreejyothi, Khammampati R., et al. "Level-Shifted PWM Techniques Applied to Flying Capacitor Multilevel Inverter." *2022 (ICEARS)*. IEEE, 2022.
- [7]. Sahoo, Rajanikanta, et al. "A seven-level cascaded H-bridge inverter topology with reduced sources." *2018 2nd (ICISC)*. IEEE, 2018.
- [8]. Dehedkar, Shilpa N., and A. G. Thosar. "Simulation of Single Phase Cascaded H-Bridge Multilevel Inverters & THD Analysis." *2018 (ICETIETR)*. IEEE, 2018.
- [9]. Abir, Ashique Anan, Tapan Kumar Chakraborty, and Khandaker Sultan Mahmood. "> An Experimental Study of Cascaded H-Bridge Multilevel Inverter for Obtaining Multiple Voltage Waveforms Containing Different Number of Levels." *2019 10th (PEDG)*. IEEE, 2019.
- [10]. Nagar, Shweta, Shazma Khan, and Balvinder Singh. "Performance of cascaded diode bridge integrated H-bridge 13 level multilevel inverter." *2017 (RDCAPE)*. IEEE, 2017.
- [11]. Jana, Kartick Chandra, Sujit Kumar Biswas, and Parasuram Thakura. "A simple and generalized space vector PWM control of cascaded H-bridge multilevel inverters." *2006 IEEE* 2006.
- [12]. Sandhu, Mamatha, and Tilak Thakur. "Modified cascaded H-bridge multilevel inverter for hybrid renewable energy applications." *IETE Journal of Research* 68.6(2022): 3971-3983.
- [13]. Anand, Vishal, and Varsha Singh. "Implementation of cascaded asymmetrical multilevel inverter for renewable energy integration (2021): 1776-1794. (IJCTA).
- [14]. Tummala, Suresh Kumar, and G. Dhasharatha. "Artificial neural networks based SPWM technique for speed control of permanent magnet synchronous motor." *E3S web of conferences*. Vol. 87. EDP Sciences, 2019.
- [15]. VENKATESH, D., G. DHASHARATHA, and K. LAHARIKA. "Reduction of Harmonics and Reactive Currents in Wind Generator Based Power system Network using D-ST ATCOM." (2015).



# Different Types of Faults Detection and Identification in Synchronous Generator Using MFO-based FL Techniques

Dr.B.Vidyasagar<sup>1</sup>, K.Sai Priya<sup>1</sup>, S.Sai Sagar<sup>1</sup>, B.Kurmi Naidu<sup>1</sup>, M.Shivakanth Reddy<sup>1</sup>

<sup>1</sup> Dept. of Electrical and Electronics Engineering, Teegala Krishna Reddy Engineering College,

Hyderabad, Telangana, India.

Email : Vidyasagar@tkrec.ac.in

---

## ABSTRACT

Synchronous generators (SGs) are expensive and essential parts of power networks that need to be safeguarded from flaws and unusual operating conditions. The performance of the power system as a whole can be negatively impacted by internal and external problems that can seriously harm SGs. Electric utilities utilize numerical, solid-state, and electromagnetic relays constructed on a differential protection scheme to protect SGs. More machine models and analyses of how synchronous machines operate with intrinsic flaws are nonetheless required. Various synchronous generators have been successfully controlled using traditional control theory and nature-inspired metaheuristic stochastic optimization techniques like evolutionary algorithms (EAs), particle swarm optimization (PSO), differential evolution (DE), genetic algorithms (GA), firefly algorithms (FA), and artificial bee colonies (ABC) algorithm. defects. Artificial neural networks (ANNs), wavelet packet decomposition, and MFO-based FLC have all been used to analyze synchronous generators with internal and external ground faults.

**Key words:** Synchronous Generator , Incipient faults , Artificial Neural Network (ANN) , MFO ,Fuzzy Logics

---

## 1. INTRODUCTION

Synchronous generators (SGs) are essential components of power systems that generate electricity and ensure an uninterrupted power supply to consumers[1]. However, SGs are susceptible to various internal and external faults that can cause significant damage to the machine and affect the performance of the entire power system[2]. Traditional protection methods have limitations in detecting and identifying faults in SGs, necessitating the development of new and effective fault detection techniques[3]. This article focuses on the detection and identification of different types of faults in SGs using MFO-based FL techniques[4]. The article highlights the importance of fault detection and identification in SGs and proposes the use of MFO-based FL techniques for this purpose[5]. The article also discusses the application of wavelet packet decomposition and artificial neural networks (ANNs) in conjunction with MFO-based FL techniques to improve fault detection and identification in SGs[6]. The proposed technique was tested on a 3 MW SG, and the results demonstrated its effectiveness in detecting and identifying different types of faults[7]. The article concludes that the proposed technique can be a valuable tool for power system operators to improve the reliability and performance of SGs[8].

## Proposed MFO-Based FLC Using Synchronous Generator and Fault Diagnosis

This section discussed the synchronous generator's fault detection and diagnostic technique using the MFO-based FLC. The block architecture of a possible method for diagnosing synchronous generator incipient faults is shown in Figure (1). The synchronous generator, offline process, online process, and diagnosis process are shown in this diagram. In this case, the output signal has produced and controlled the synchronous generator. The alternator's signal has been double-checked for errors and the data collection representing is saved for the different errors throughout the offline phase.

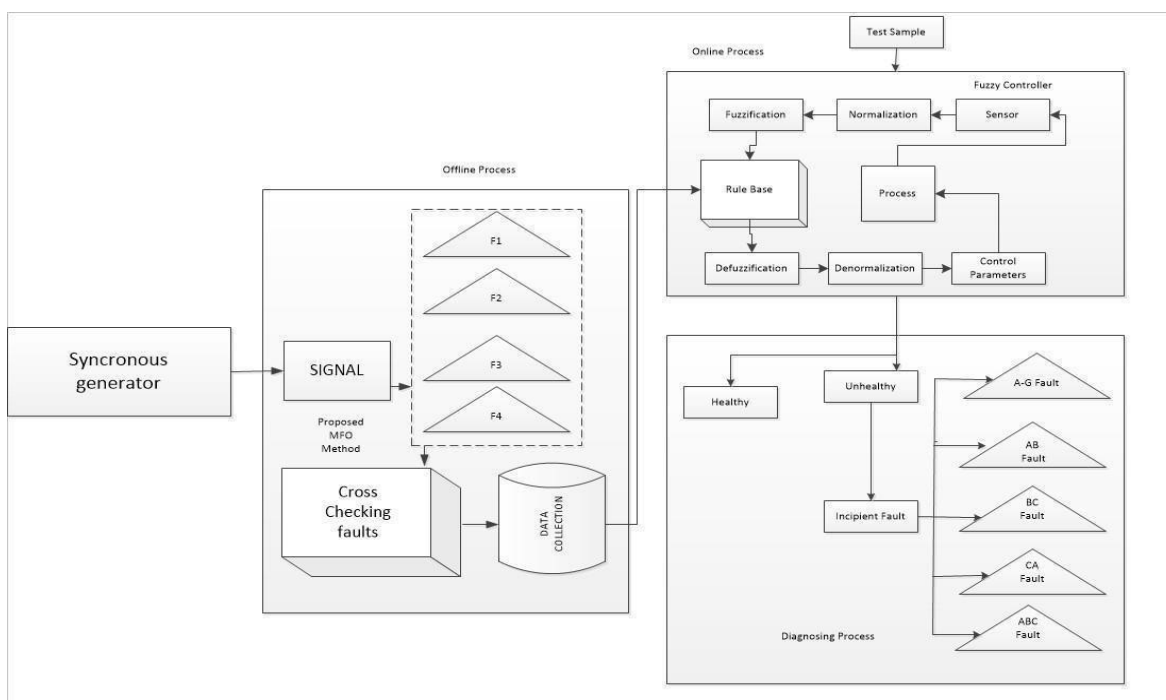


Figure.1 shows a block diagram of the suggested method for diagnosing internal faults in alternators.

The recommended technique is carried out in this case in a synchronous generator collecting data sets and identifying the new issues in two steps. The Moth flame optimization approach is used to identify the best ways to proceed from the open looking for space in light of a function of the objective kind and produce logically plausible data sets first and foremost. The Moth flame optimization technique uses the synchronous generator to provide a range of metrics that are used to determine if the generator is healthy, ill, etc. situations separately. In the second stage, the Fuzzy logic controller applies the finish of a data set and terms the es synchronous generator's nascent problems under various scenarios. The recommended diagnosis technique was developed with the specific genuine purpose of separating the fault concerns from the states of the synchronous generator. the figure1. A synchronous generator's modeling is put together, furthermore, with a combined MFO control technique, finding a synchronous generator's three-phase fault problems is made. For synchronous generator incipient defect diagnosis, the proposed method is the MFO-based FLC. The MFO technique is used in this situation to identify the best courses of action within the confines of the desired capacity and create any feasible coherent datasets. Considering the finished data set, the Fuzzy logic control performs and diagnoses Alternator nascent difficulties in various scenarios. The following are notable steps connected to the recommended calculation:

**(a) Stages in the Proposed Algorithm's Optimization:**

**Stage 1: Initialisation**

The voltage(V), speed(N), and torque(T) numbers serve as the initial constraint parameters. The number of iterations is initialized, and the power values begin as the FLC parameters are generated at random.

**Stage 2: Random generation**

V, N, and T values are used as the beginning values for the restrictions' conditions. Initialize the power values and the number of iterations. using the equation and the random generation of Fozzy logic controller parameters, respectively .

**Stage 3: Evaluation**

The V and I level that correspond to the value of the produced power are displayed during the assessment Work on. Recommended MFO and FLC method's primary goal is to minimize the deviation of the power signal from the intended location.

**Stage 4: Updation**

Using equations and the moth's position in proximity to the flame is updated based on the fitness function.

**Stage5: Final process**

Equation estimates that during the course of repetitions, the number of flaws decreases adaptively . The calculation's output is only available for the data sets that are theoretically possible to predict the optimal parameter. Access is granted to the FLC's rule base of these finished data sets so that it may simulate the fuzzification process and identify any impending problems with the synchronous gene under varied responsibility situations. The FLC is created with the particular objective of diagnosing the synchronous generator's nascent problems.

**(b) With FLC, prediction of the ideal parameter:**

Identification of impending problems with a synchronous generator is carried out using the fuzzy system. Figure 1 shows that the following succinct explanation of the technique has been provided:

**Procedure (i): Fuzzification**

This process converts the sharp input into a linguistic element in a fuzzy knowledge base using the membership function acquired. The error and the change of error, are provided as equations (1) and the fuzzy controller's input (2).

$$E(t)=V(t)-V^*(t)$$

$$\Delta E(t)=V_i(t)-V_{i-1}(t) \dots\dots(1)$$

V(t) presents the output voltage, V\*(t) refers to the standard voltage and *i* subscripts denote the value taken at the beginning of the process. **Process (ii): the system of fuzzy inference** fuzzy input, fuzzy input, and fuzzy output is changed with the help of the "If then" type fuzzy rules. Here, rules are formed with one reflecting the circumstances in which a defect occurs and the other indicating the situations in which the system is fault-free. Both levels of the fuzzy system and demulsifier can be used to recognize the membership function. After the membership function is pushed out to list phonetic words during the fuzzification and defuzzification layers; it graphs non-fuzzy information values to fuzzy semantic terms and, in contrast, fuzzy linguistic positions to non-fuzzy information values. **Procedure (iii) : Decision making** the uncertain values that the fuzzification approach is based on may be used to create fuzzy rules for every component of the methodology. The decision is based on the aforementioned criteria. The common method for the If A, then B is a vague rule. The system is faultless if A and B are both zero, but in the unlikely event that A is positive and B is negative, fault 1 is now active. The rules for the form are unclear

$$\text{If } E \text{ is } X_a \text{ and } \Delta E \text{ is } Y_b, \text{ THEN } X_a^f(t) \text{ is } F_a(t) \dots\dots(2)$$

Where X<sub>a</sub> and X<sub>y</sub> are the vague subsets and consider the singleton values of the fuzzy system. **Procedure**

**4: Defuzzification**

The decisions made when using the defuzzification process are where the fuzzy values are found. This method converts the output esteems from fuzzy to crunchy . The output variable's potential to include members serves as the foundation for the defuzzification. The framework is provided as a database.

$$F_a(t)=X_a^f(t) \dots\dots(3)$$

Where  $X_a^f(t)$  is the final result of fuzzification.

As a degree of assistance target is determined for each member of the collection, fuzzification is necessary. The fuzzy system accurately anticipates the outcomes when there is increased participation in the work. Similarly, the proposed MFO with the FLC system determines the precise SG fault while increasing the gain parameter. Figure(2) shows the MFO with FLC flowchart in action.

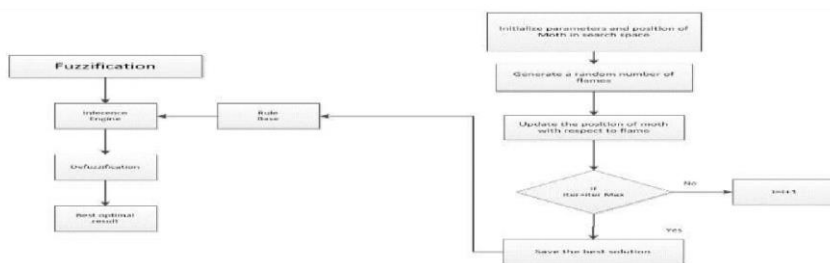


**Figure.2:** Flowchart of proposed MFO with FLC

By using a variety of approaches, including wavelet packet decomposition, artificial neural networks, and MFO-based FLC, this chapter investigates the synchronous generator's nascent flaws. To diagnose the behavior of the fault at this point, internal faulty signals are analyzed as wavelet packet decomposition to three-phase currents is decomposed into approximate and detailed signals. This method establishes the energy of the approximation signal and the maximum energy of the detail signals. By controlling both regular and irregular signals, the ANN controllers successfully get rid of internal faults. The output performance of the synchronous generator signals is assessed by the MFO-based FLC-based signal analysis to determine whether or not it is initially flawed. The subdivision gets rid of increased inquiries into the developing fault, decreased fault detection, and decreased internal fault. As a consequence, it is possible to raise the issue of the internal fault of the synchronous generator with MFO based FLC much more successfully by presenting an optimization fault issue, followed by fact-finding and the suggested techniques. The recommended MFO-based FLC-based synchronous generator's concept and plan, as well as its implementation next to the internal fault problems, are made evident. The results and discussion of the proposed approach and the existing method have been briefly presented along with comparisons to other methods.

**RESULTS:**

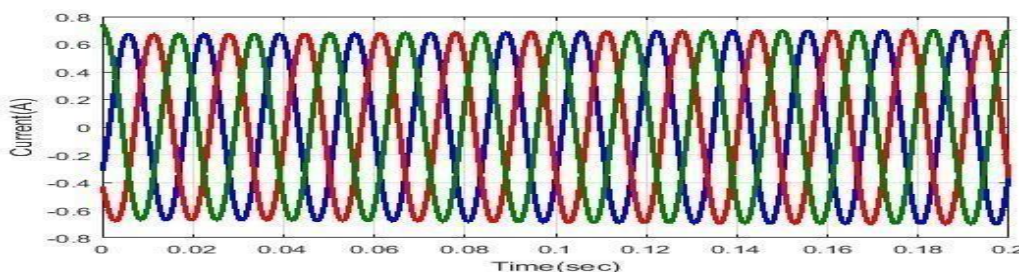


**Fig:3** Analysis of current in normal condition

**A – Earth Fault**

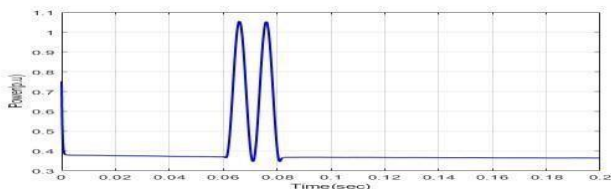


**Fig 4:** Electrical Energy

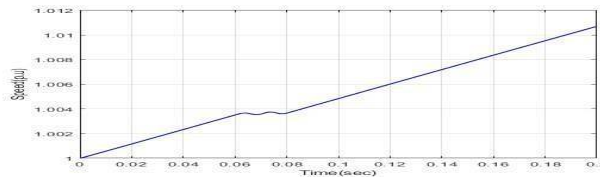


**Fig 5:** Turning Speed

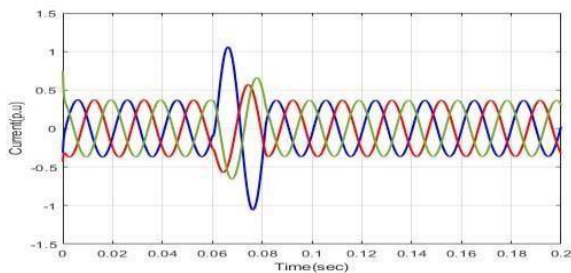


**Fig 6:** Stator-(I)

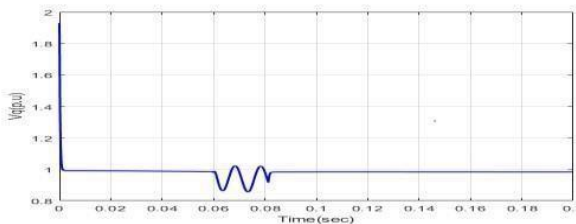


**Fig 7:** Stator (V) Vd



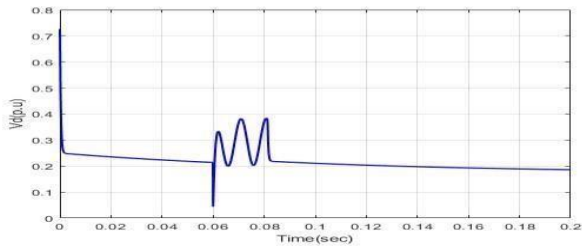


**Fig 8: Stator (V) Vq**

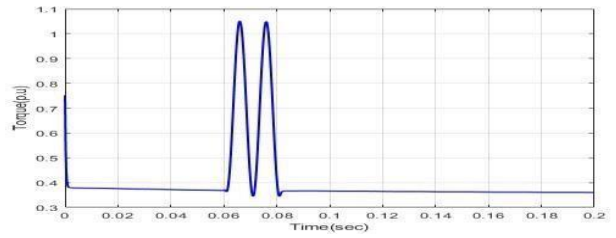


**Fig 9: TORQUE (T)**

**B – Earth Fault**

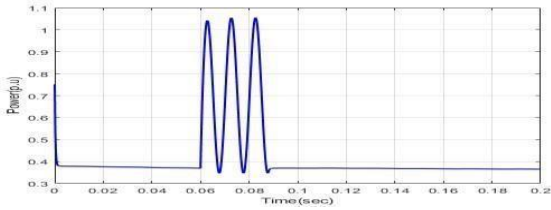


**Fig 10: Electrical Energy**

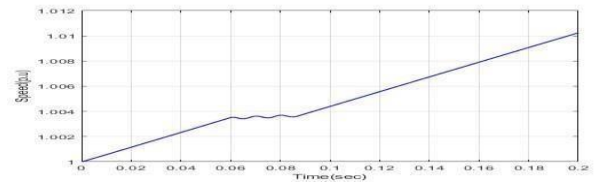


**Fig 11: Turning Speed**

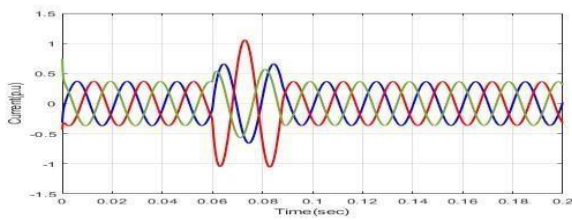


**Fig 12: Stator-(I)**

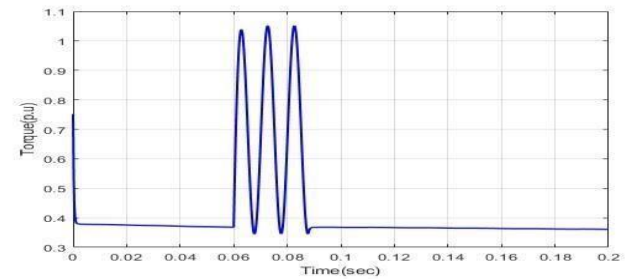


**Fig 13: Stator (V) Vd**

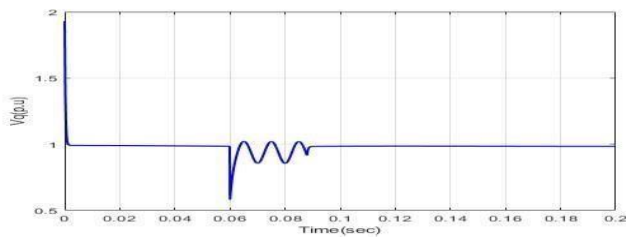


**Fig 14: Stator (V) Vq**

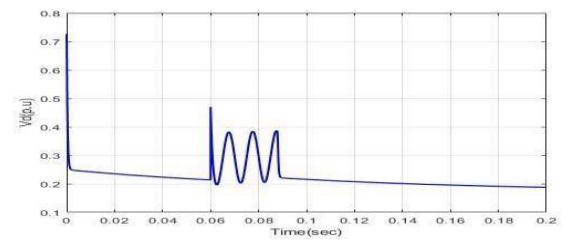


**Fig 15: TORQUE(T)**

**C – Earth Fault**

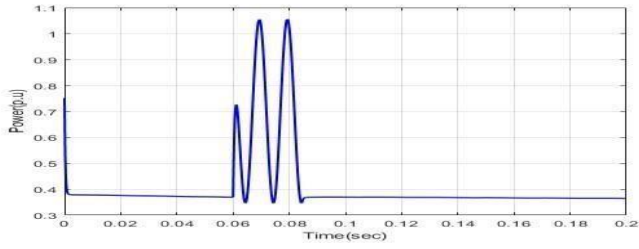


**Fig 16: Electrical Energy**

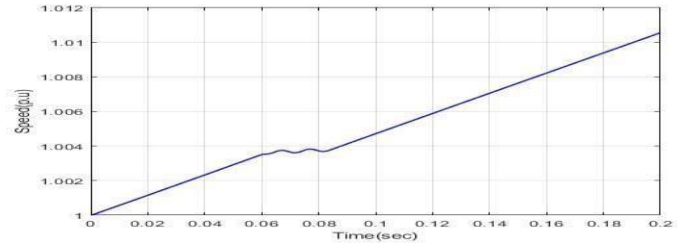


**Fig 17: Rotor Speed**

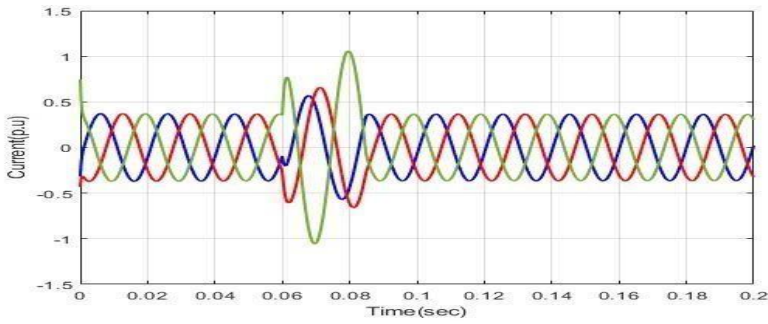


**Fig 18: stator-(I)**

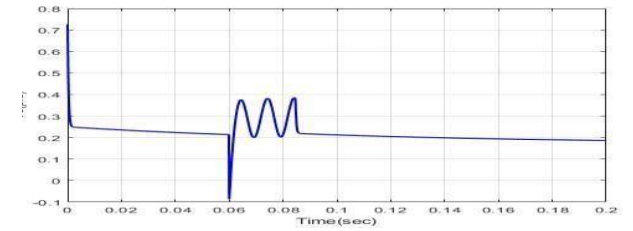


**Fig 19: stator (V) Vd**

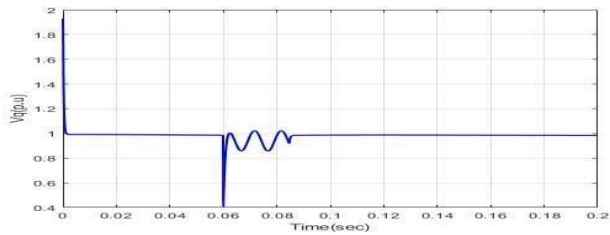


**Fig 20: Stator (V) Vq**

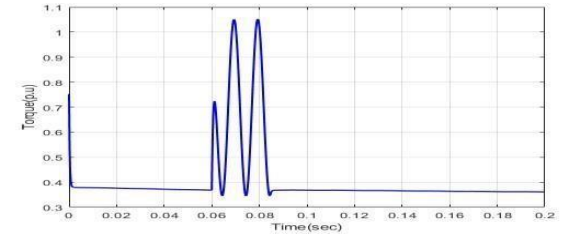


**Fig 21: TORQUE (T)**

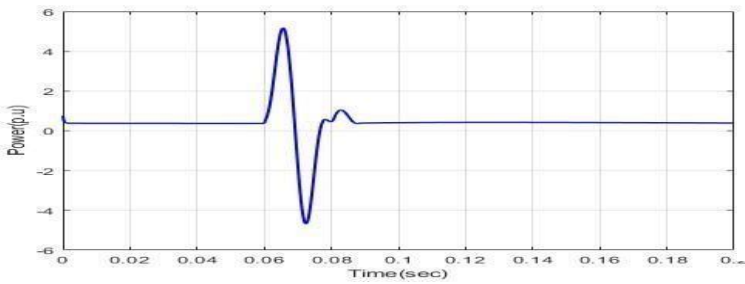


**Fig 22: Electrical Energy**

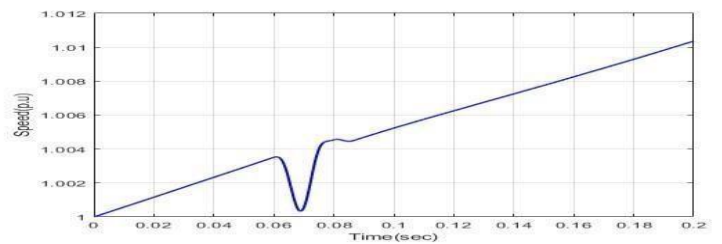


**Fig 23: Turning Speed**

**AB – Earth Fault**

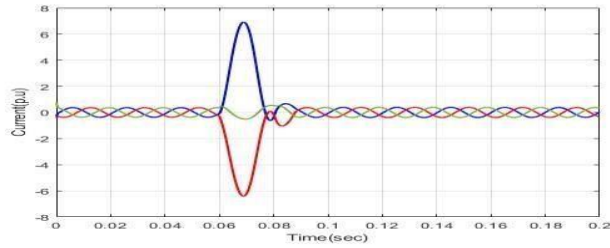


**Fig 24: Stator (I)**

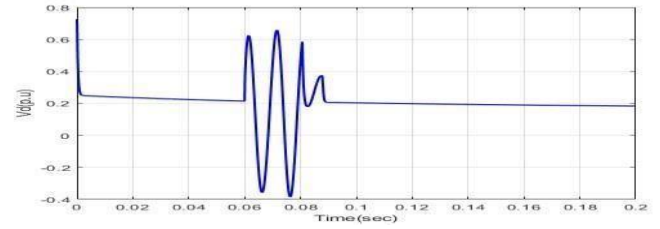


**Fig 25: Stator (V) Vd**

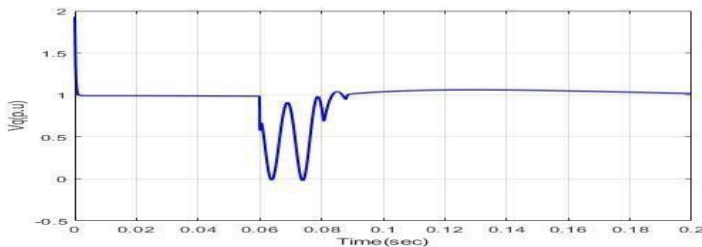


**Fig 26: stator (V) Vq**

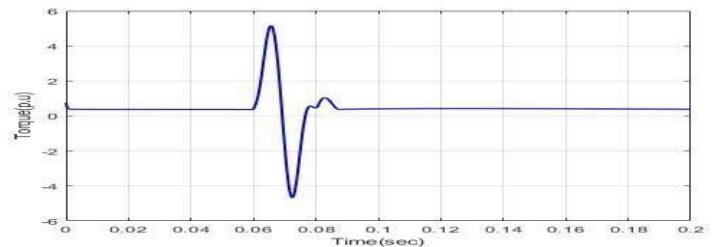


**Fig 27: TORQUE (T)**

**BC-Earth fault**

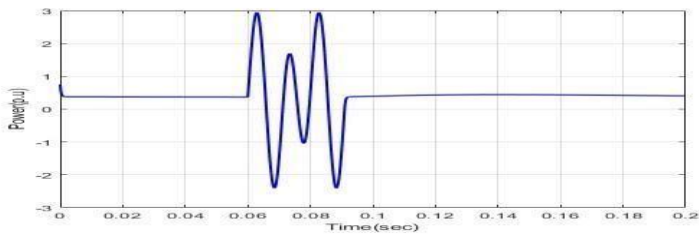


**Fig 28: Electrical Energy**

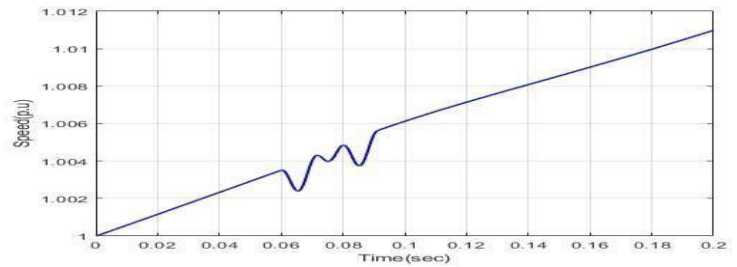


**Fig 29: Turning Speed**

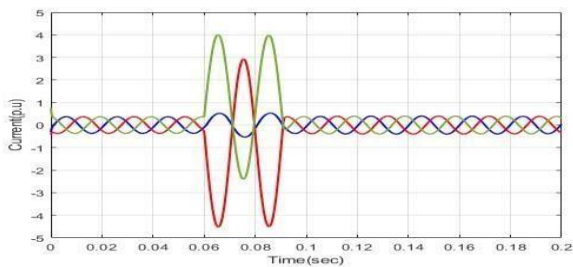


**Fig 30: Stator (I)**

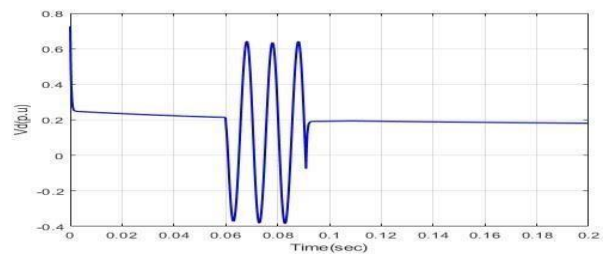


**Fig 31: Stator (V) Vd**

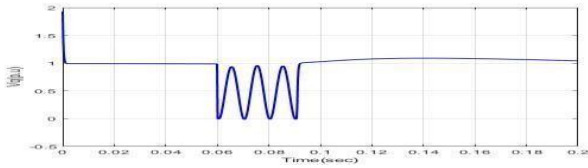


**Fig 32:** Stator (V)  $V_q$   
CA-Earth fault

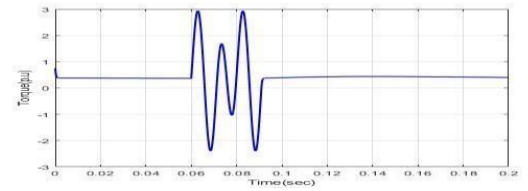


**Fig 33:** Torque

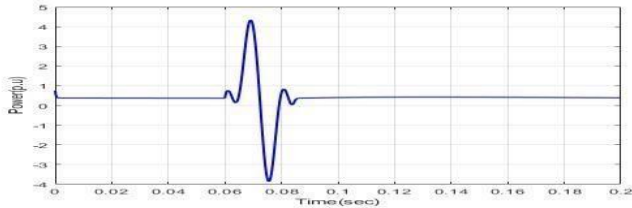


**Fig 34:** Electrical Energy

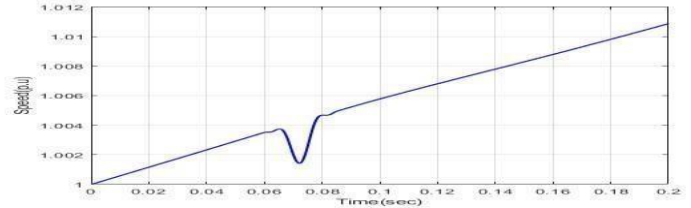


**Fig 35:** Turning speed

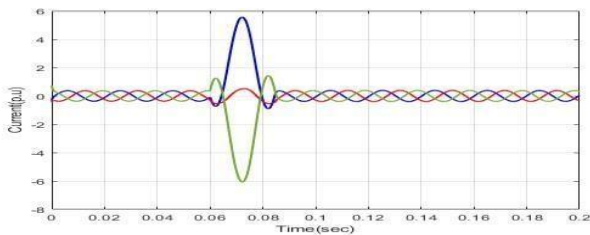


**Fig 36:** Stator (I)

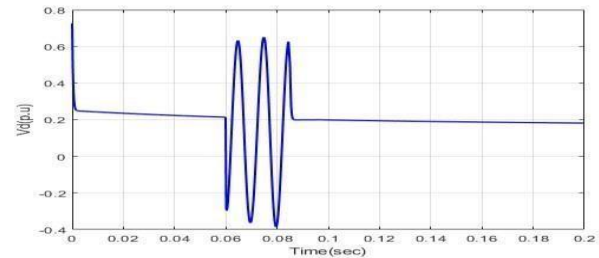


**Fig 37:** Stator (V)  $V_d$

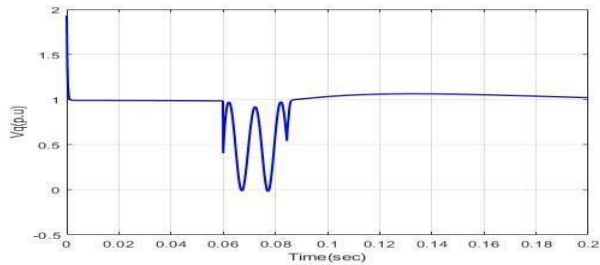


**Fig 38:** Stator (V)  $V_q$

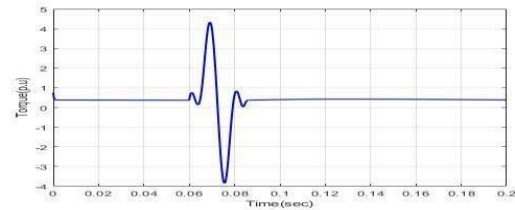


**Fig 39:** TORQUE (T)

**ABC – Earth Fault**

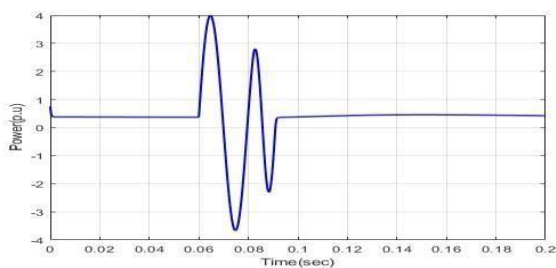


**Fig 40:** Electrical Energy

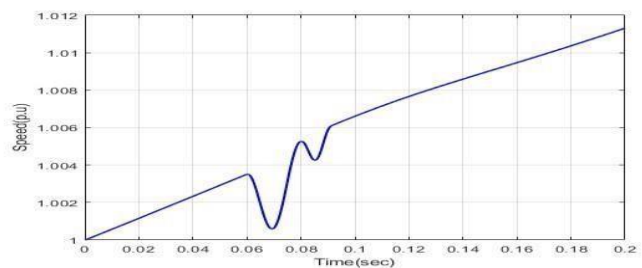


**Fig 41:** Electrical Energy

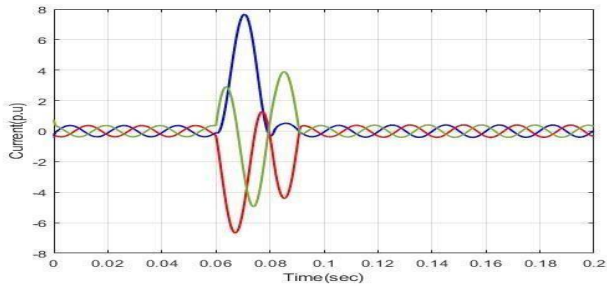


**Fig 42:** Electrical Energy

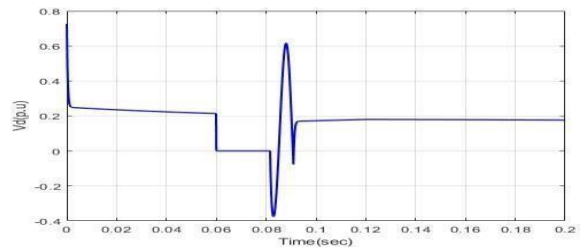


**Fig 43:** Stator (V) Vd

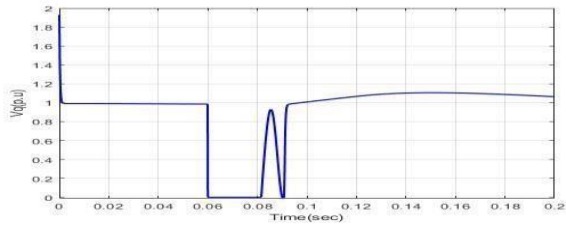


**Fig 44:** Stator (V) Vq

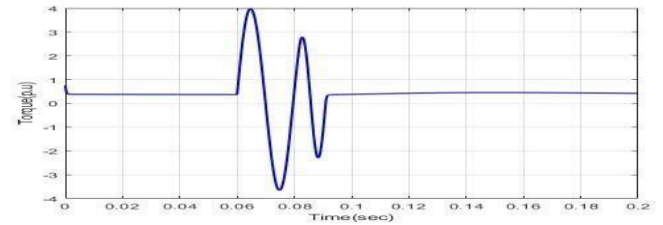


**Fig 45:** TORQUE (T)



**Fig:46 :** 3 KVA, 415 V, 4.5 A, 1440 RPM, 3- Phase Alternator

**EXPERIMENTAL DATA:**

	A Phase	B Phase	C Phase	Total
A Fault	1.1086	0.5939	0.7473	2.4499
B Fault	0.6924	1.1075	0.7473	2.5472
C Fault	0.5945	0.6927	1.1074	2.3946
AB Fault	6.9434	0.4092	0.7473	8.0999
BC Fault	0.5500	2.9050	4.0326	7.4876
AC Fault	5.5450	0.5412	1.4399	7.5261
ABC Fault	7.6566	1.2451	3.8882	12.7899

**Table 1:** Execution analysis of a suggested method through a developing fault for ten preliminary steps

Model	Proposed	ANFIS	ANN
RMSE	9.4	20.5	23.4
MAPE	1	12.0	16.2
MBE	2.3	4.6	6.1
Consumption time (s)	5	7.8	7.8

**Table 2:** A statistical analysis of a method proposed by an existing technology that detects a flaw in the first 10 preliminary results

Performance Measures	Proposed	ANFIS	ANN
Accuracy	0.96	0.87	0.58
Specificity	0.94	0.83	0.55
Recall	1	0.91	0.62
Precision	0.95	0.85	0.59

**CONCLUSION:**

The control calculation for a synchronous generator is shown in the thesis utilizing a variety of methods, including wavelet packet decomposition, artificial intelligence, BA-RNN, ANN-GSA, and MFO-FLC. In this case, the suggested approach is carried out in two stages, such as the first problems with SG-set sorting and data analysis. A synchronous generator is used to study DWT and ANN, fault detection, and character with the GSA system. The mistakes in the synchronous generator then control the RNN technique going ahead. Here, the RNA production process was used to enhance the BA. The ANN is trained using ALO, which improves ANN performance. The improved ANN is used to determine whether or not the signs are faulty. The MFO approach's best course of action is to use the space that is now available to authenticate and maybe store static data packages. The FLC employs SGs and supplementary data sets in both favorable and undesired circumstances. Using factual estimations, such as sensitivity, specificity, recall, and accuracy, has allowed researchers to examine and assess the suggested strategy's practicality. Using statistical measures including MBE, MAPE, RMSE, and use time, the proposed task's execution was verified and compared Using ANN, fuzzy, and ANFIS methods . The suggested methodology was displayed in front of several techniques relating to communication presentation methods and real techniques. The comparison of the MATLAB simulation results with the outcomes of the experimental setup demonstrated the superiority of the suggested AI approaches for fault identification in a Synchronous

Generator The suggested approach is employed to identify the stable and undesired SG states in the presence of an early deficit. Here, the suggested method is employed to diagnose emerging defects and collect informational indexes. The SG rehearsals are divided into good and bad circumstances right away. The stator-torque current views within that are normalized to their estimated peak esteem. At that point, the MFO is used to evacuate the deficiencies that directly correspond to the current symptoms. To offer the precise type of flaw, the extruded components are established using FLC. This proposed method allows for more accurate detection of new failures.

## **REFERENCES:**

- [1] B.VIDYASAGAR, Dr.SS.TULASIRAM "Incipient Fault Diagnosis in Stator winding of Synchronous Generator A CMFFLC Technique" IETE Journal of Research (Taylor and Francis online Journal) ISSN: 0377-2063, April 2018
- [2] Yushi Miura, Toshifumi Ise, Toshinobu Shintai, and Toshinobu Shintai, "Oscillation damping of a distributed generator using a virtual synchronous generator," IEEE Transactions on Power Delivery, Vol.29, No.2, pp.668-676, 2014.
- [3] B.VIDYASAGAR, DR.SS.TULASIRAM "Enhanced ANN with Ant Lion Optimization for diagnose the incipient faults of Synchronous Generator"(JARDCS) Journal of Advance Research in Dynamical Control Systems ISSN 1943-023X, 02 Sep 2019.
- [4] Deepak M. Divan and Andrew D. Paquette published a paper in IEEE Transactions on Industry Applications titled "Virtual impedance current limiting for inverters in microgrids with synchronous generators" in 2015.
- [5] Lin-Yu Lu, Chia-Chi Chu, and others, "Consensus-based Secondary Frequency and Voltage Drop Control of Virtual Synchronous Generators for Isolated AC Micro-Grids," IEEE Journal on Emerging and Selected Topics in Circuits and Systems, Vol. 5, No. 3, pp. 443-455, 2015.
- [6] "Real-time emulation of a high-speed micro turbine permanent-magnet synchronous generator using multiplatform hardware-in-the-loop realization," IEEE Transactions on Industrial Electronics, Vol. 61, No. 6, pp. 3109-3118, 2014.
- [7] "Comparison of wind power converter reliability with low-speed and medium-speed permanent-magnet synchronous generators", IEEE Transactions on Industrial Electronics, Vol. 62, No. 10, pp. 6575-6584, 2015. Zhou, Dao, FredeBlaabjerg, Toke Franke, Michael Tonnes, and Mogens Lau
- [8] Ehsan Nasr-Azadani, Claudio Caizares, Daniel E. Olivares, and Kankar Bhattacharya, "Stability analysis of unbalanced distribution systems with synchronous machine and DFIG based distributed generators," IEEE Transactions on Smart Grid, Vol. 5, No. 5, pp. 2326-2338, 2014.

# Renewable Energy Source Fed Multilevel Inverter

Ankanthi Manjula  
Dept. of Electrical and Electronics  
Engineering  
Teegala Krishna Reddy Engineering  
College  
Hyderabad, Telangana, India.  
[manju.ankathi708@gmail.com](mailto:manju.ankathi708@gmail.com)

Manish Palepu  
Dept. of Electrical and Electronics  
Engineering  
Teegala Krishna Reddy Engineering  
College  
Hyderabad, Telangana, India.  
[manishpalepu7@gmail.com](mailto:manishpalepu7@gmail.com)

Naveen Karnekanti  
Dept. of Electrical and Electronics  
Engineering  
Teegala Krishna Reddy Engineering  
College  
Hyderabad, Telangana, India.  
[k.naveen1695@gmail.com](mailto:k.naveen1695@gmail.com)

Saikiranreddy Gogireddy  
Dept. of Electrical and Electronics Engineering  
Teegala Krishna Reddy Engineering College  
Hyderabad, Telangana, India.  
[saigogireddy0905@gmail.com](mailto:saigogireddy0905@gmail.com)

Chandan Kumar Chiguru  
Dept. of Electrical and Electronics Engineering  
Teegala Krishna Reddy Engineering College  
Hyderabad, Telangana, India.  
[chandankumarchiguru1999@gmail.com](mailto:chandankumarchiguru1999@gmail.com)

**Abstract:** This article implemented a hardware structure of a single-phase inverter with Arduino with hybrid energy sources, this inverter generates an AC square wave using PWM generated by an Arduino microcontroller, and this Arduino helps in generating triggering pulses for MOSFETS switching, thereby AC voltage is developed, taking this as a reference. This paper simulated a renewable energy source fed multilevel inverter, which consists of the windmill, and PV cell as renewable sources, as there is a lot of change in power generation in the current world there is a need of using renewable energy sources for power generation, and a 9-level inverter for power conversation, the 9 level inverter is used for maximizing the output power to a higher extent when compared to other inverters, the energy generated by the renewable energy source is stored in a battery, and this circuit is parallelly connected to the inverter for the AC power generation.

**Keywords:** Single-phase inverter, hybrid energy sources, Arduino, renewable energy sources, windmill, PV cell, multilevel inverter.

## INTRODUCTION

Multilevel energy inverters were studied highly in the latest years. The advantages of using multilevel inverters are that it has low harmonic distortion acquired due to the multilevel voltage range at the output and reduced stresses on the switching devices used [1]. In comparison with traditional two-level voltage deliver inverters, multilevel inverters can output higher voltage rankings without the usage of the collection connection of low sustain voltage devices and function a decreased dv/dt of the output voltage and spectrum better harmonic. The use of multilevel inverters become one of the inexperienced techniques for immoderate energy medium voltage applications [2]. The popular kinds of multi-stage inverters are categorized into three primary groups Neutral point Clamped multilevel inverters, flying capacitor multilevel inverters, and protruded H- ground multilevel inverters. The Neutral Point Clamped multilevel inverters have a few step backs that weaken the reliability of these structures because it desires one-of-a-kind clamping diodes which are rated. The incorrectly balanced capacitor hassle and an additional range of

switches, capacitors etc, are required for growing the machine energy rating [3]. A nonpartisan point-braced inverter with a dynamic countdown of nine levels 9Level R D C, A N P C Inverter). The shortcomings of the 5L ANPC are eliminated by this inverter, which also reduces control unfortunate and improves yield waveform quality [13]. Inverters with three stages are used in high-power applications. Two-changed SVPWM computations were reported by Yong-Chao, and these techniques reduced regular mode voltages in a three-level inverter [4]. Comparable negative aspects of the Flying capacitor multilevel inverters additionally have been recorded including a massive quantity of cumbersome and more capacitors highly priced, the improperly balanced capacitor problem, and bad efficiency [14]. The concept of the output voltage which is stepped up became commenced with the handiest 3 ranges withinside the output voltage of the waveform withinside the Neutral factor clamped multilevel inverters inverter additionally referred to as a diode-clamped multi-level inverter in the year 1981. The subsequent change of this inverter comes in the way of means of including outside ranges [5]. The fundamental output voltage is improved, and harmonics are reduced with the aid of multilevel inverters. They are more electromagnetically compatible, have higher voltage capabilities, and have fewer harmonics [15]. They also have fewer switching losses. Five-level and nine-level multilevel inverters are both available. They make accurate comparisons with the aid of inverters, IGBTs, and switching devices [6]. The characteristics checking based on space-vector modification was proposed by Quang Wei and others. The 3-stage current source inverter's 5, 7, 11, and 13 sound requests were silenced as a result of this technique. 10 kilo-volts ampere consecutive current from source-converter modules were tested by equipment [7]. This technology can assist in achieving efficiency of the system and the usage of energy from renewable sources incorporated into hybrid systems [12]. Different energy from renewable sources, such as PV and wind, have been combined to satisfy the necessary load because of the fluctuating natural conditions [8]. Now, these systems aid in reaching the desired optimum output when used in conjunction with multilayer inverters. Pulse width modulation aids in



lowering harmonic distortion output and significantly raises the voltage from the 5-level inverter output. For power electronic applications consisting of bendy AC transmission systems, renewable electricity sources, uninterruptible electricity supplies, and lively electricity filters, multilevel inverters have become crucial. Here, an approach for implementing pulse width modulation is suggested. The output is minimised with the aid of PWM. The PWM's overall distortions of harmonic aids in raising the output voltages [9]. The PV wind-battery-based hybrid system manages power flow by connecting to the grid via a multiple-input of transformer. The output waveform distortion is the biggest negative. Efficiency increases when harmonics are reduced. Utilising the suggested multi-level inverter is achievable [10]. A switched capacitor was used in the Flying capacitor clamped 5-degree inverter. The quality of the output waveforms could be raised [11]

## II. HYBRID ENERGY SOURCES

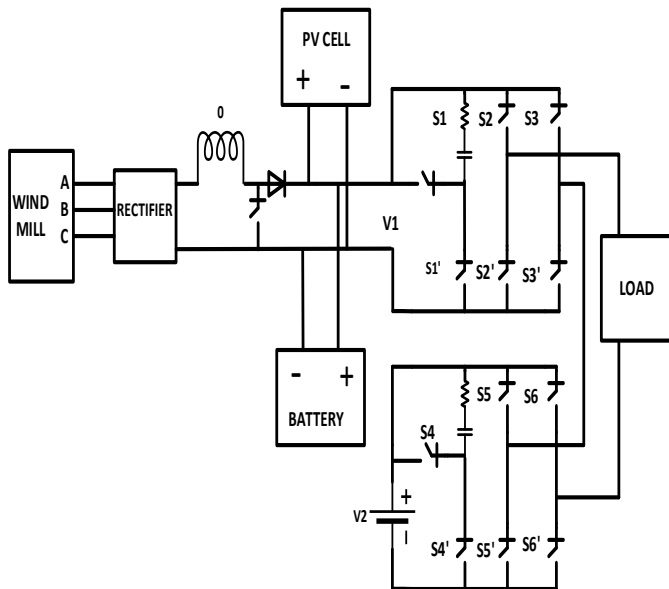


Fig.1. The hybrid-energy source system diagram.

The above fig.1. is a hybrid electric energy sources system. The circuit consists of two hybrid electric energy sources, a windmill & PV cell, a windmill is an electric energy generating device which converts wind energy into electrical energy, and the windmill consists of a turbine which rotates in the wind direction making kinetic energy and the shaft of the turbine is connected to the motor shaft and this motor shaft is connected to the generator where it converts kinetic to mechanical energy and thereby it converts and develops into electrical energy, PV cell is a device which converts light energy into electrical energy by the means of sun rays which is nothing but photovoltaic effect. A storage unit which is a battery is used for storing the energy received from the windmill and PV cell, the boost-converter is used to step up the voltage from the windmill to a desired higher level, and the 9-level inverter circuit consists of 3 pairs of MOSFETS in each set making it 12 which are connected parallelly. Input for the 1 set of MOSFETS pair will be given from the hybrid circuit which is V1, whereas the second set of MOSFETS pair will be given input from a battery

which is V2. The battery is connected as V2 because of the circuit complexity. The rectifier circuit input will be fed from the windmill, the rectifier is used for reducing the distortions from the windmill output, after the rectification process, the output of the rectifier is given to the boost converter for increasing the voltage to a higher extent. Mutually to the output of the converter, the PV cell and battery are connected parallelly, and the total output of this circuit is given to the input of the 9-level inverter input 1 which is V1. And after connecting the input sources of the inverter V1 & V2 the MOSFETs will get into their switching action and thereby it is converted to AC from DC. And the output from the inverter is given to desired the load.

### A. Full wave rectifier

A full-wave rectifier is useful in converting the output-Ac of the windmill to Dc, the rectifier input is given to the output of the windmill and the output received from the rectifier is hereby given for the boost converter for increasing the voltage to a higher level.

Full wave rectifier output voltage,

$$V_0 = \frac{1}{\pi} \int_{\alpha}^{\pi+\alpha} V_m \sin \omega t. d(\omega t) = \frac{2V_m}{\pi} \cos \alpha \quad (1)$$

### B. Boost converter

The boost converter is useful for stepping up the received voltage to a higher level. The circuit of the boost converter is shown below from fig.2. The input of the boost converter is given from the output of the rectifier, in which the dc output of the windmill is converted to Ac using a rectifier. In the boost converter, there are two modes of operation which can be seen in fig.3, & fig.4.

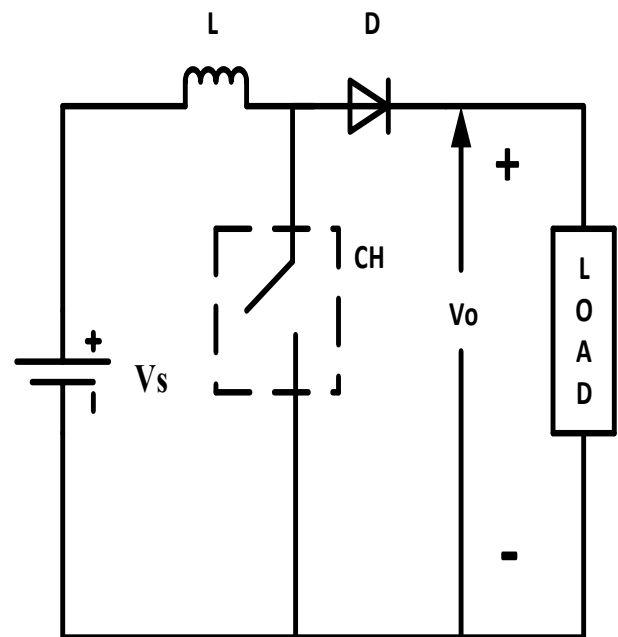


Fig.2. circuit diagram of the boost converter.

There are two modes of operation which undergoes a boost converter, which is shown below.

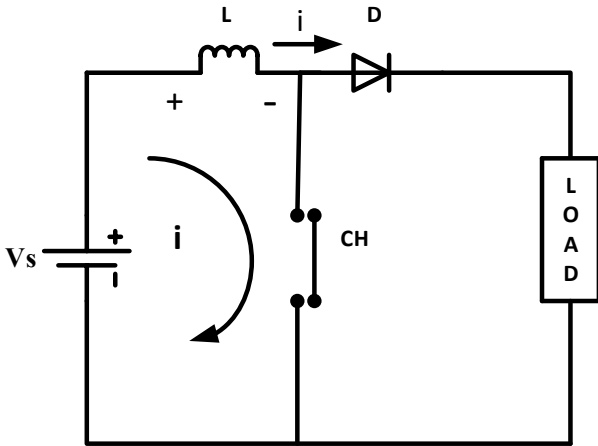


Fig.3. The boost converter for the first mode of operation.

From fig.3, This is one of the modes of operation in the Boost converter in which the switch CH is in the ON condition which is nothing but the circuit being short at the node, in which current is being divided at the node, flows through the first loop, and then flows through the load. This is the first mode of operation.

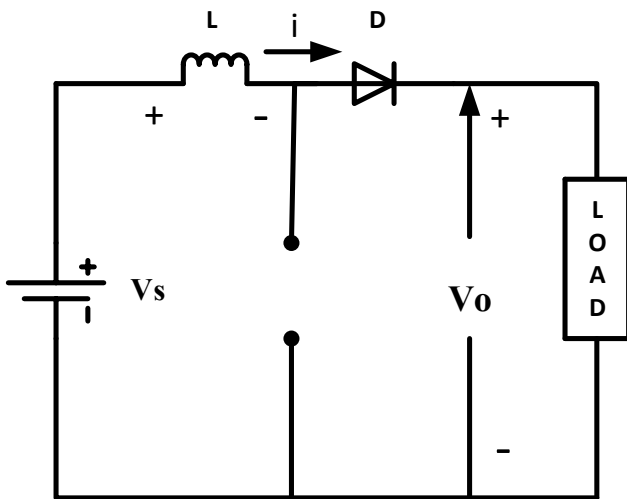


Fig.4. The boost-converter for the second mode of operation.

From fig.4, This is another mode of operation in the Boost converter in which the switch CH is in the OFF condition which is nothing but the circuit being open at the node, in which current flows in One direction is nothing but through the load side. This is the second mode of operation.

Boost converter output voltage

$$V_0 = \frac{V_{in}}{1-D} \quad (2)$$

Where D= duty ratio

$$D = \frac{T_{on}}{T}$$

$$V_0 = V_s \frac{T}{T-T_{on}} = V_s \frac{1}{1-\alpha} \quad (3)$$

### C. Inverter

The inverter in this circuit is useful for converting the Dc power to Ac using switching devices which are MOSFETS, the input of the inverter is given from the battery which stores the energy received from the hybrid sources, after receiving the input, the inverter converts the received input DC supply to Ac-voltage with the help of switching devices then the output of the inverter is given to the load which is nothing but stand-alone applications.

The output voltage of Half bridged Inverter

$$V_0 = \frac{V_s}{2} \dots\dots 0 < t < \frac{T}{2} \quad (4)$$

$$V_0 = -\frac{V_s}{2} \dots\dots \frac{T}{2} < t < T \quad (5)$$

The output voltage of Full bridged Inverter

$$V_0 = V_s \dots\dots 0 < t < \frac{T}{2} \quad (6)$$

$$V_0 = -V_s \dots\dots \frac{T}{2} < t < T \quad (7)$$

## III SIMULATION RESULTS

### A. Control scheme

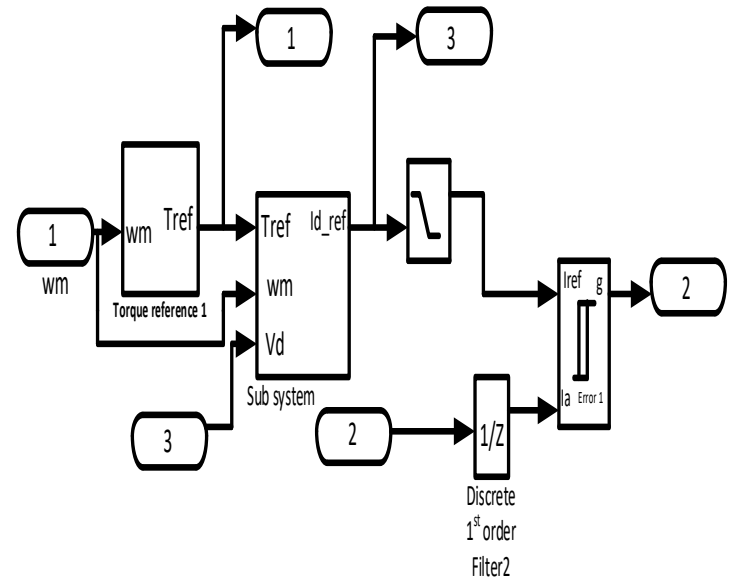


Fig.5. The control scheme of the windmill.

The above fig.5 displays the control scheme of the windmill the output of the windmill is given to the torque reference 1 subsystem and the output of the torque reference 1 is given to the sub system 2 which is connected to the saturation for the desired output and is compared with references.

B. Subsystem 1 (torque reference1)

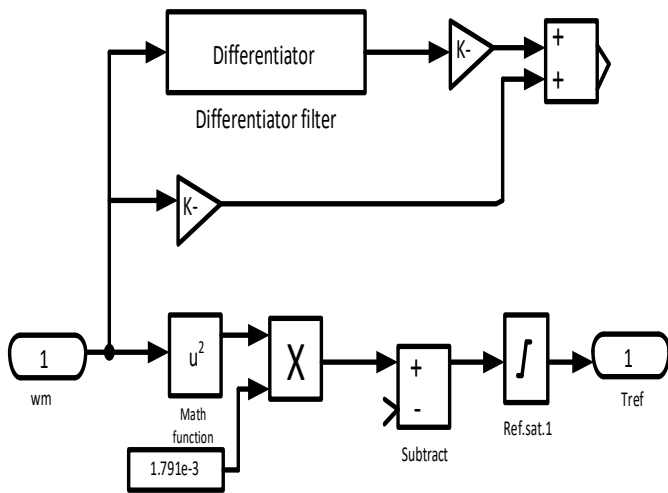


Fig.6 Diagram of subsystem1(torque reference1) from the control scheme.

The above fig.6 shows subsystem 1 of the windmill control scheme which is the torque reference 1. which contains differentiator and other mathematical components.

C. Subsystem 2

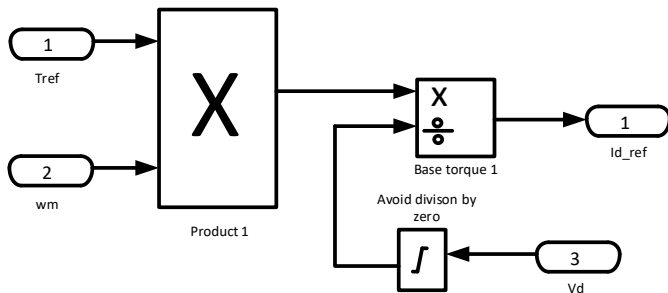


Fig.7. Diagram of subsystem 2 from the control scheme.

The above fig.7 shows subsystem 2 of the windmill control scheme which contains mathematical logic blocks.

D. Battery control scheme

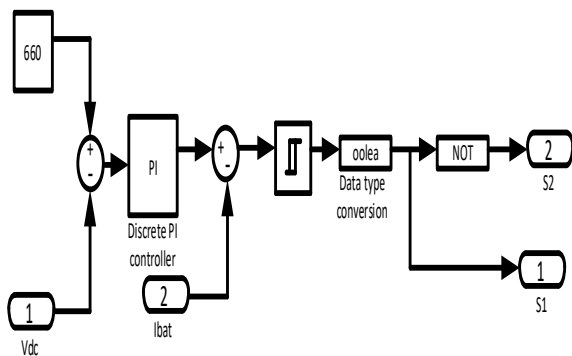


Fig.8.Diagram of the battery control scheme.

From fig.8, we can observe the control scheme of the battery which involves a discrete Pi controller, logical gates and references for comparison, and saturation for the constantly desired output.

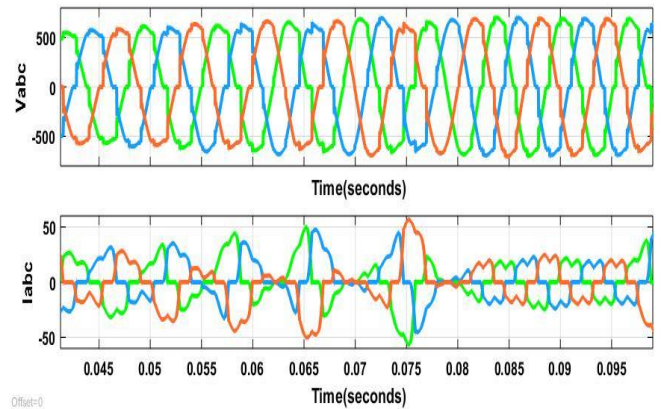


Fig.9. wind turbine output voltage & current

From the fig.9, we can observe the output voltage obtained & current waveforms of a permanent motor synchronous generator, the wind turbine, which is three-phase, from the voltage waveform we can observe three phases R, Y, & B three red colour lines indicating the R phase while the green colour indicating the Y phase and blue colour indicating the B phase. similarly, from the current waveform, we can observe three phases R, Y, & B three red colour lines indicate the R phase while the green colour indicating the Y phase and the blue colour indicating the B phase. The magnitude of voltage waveforms is ranging from -500 to +500. whereas the magnitude of current waveforms are ranging from -50 to 50.

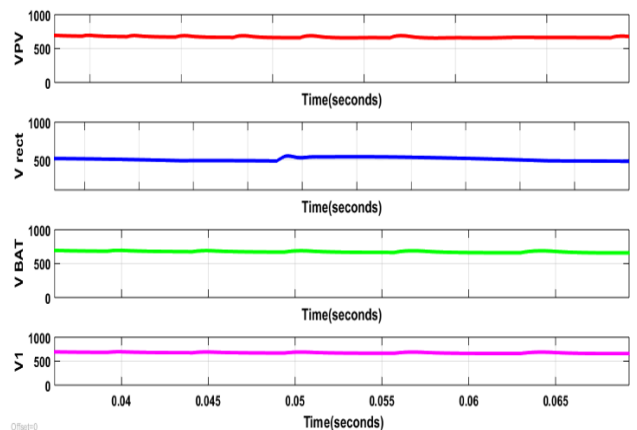


Fig.10. Boost converter output voltages.

The above fig.10 shows the output voltages of the photovoltaic cell, rectifier voltage, battery voltage & inverter input 1 voltages. As all voltages are of DC the waveforms are constant. The RED line indicating the output voltage obtained from the photovoltaic cell and its magnitude is ranging from 0 to 1000. The blue line indicates the output voltage obtained from the rectifier and it is ranging from 0 to 1000. The green line indicating the output voltage obtained from the battery and its magnitude is ranging from 0 to 1000. The pink line indicates the output voltage of inverter input 1, and its magnitude is ranging from 0 to 1000.

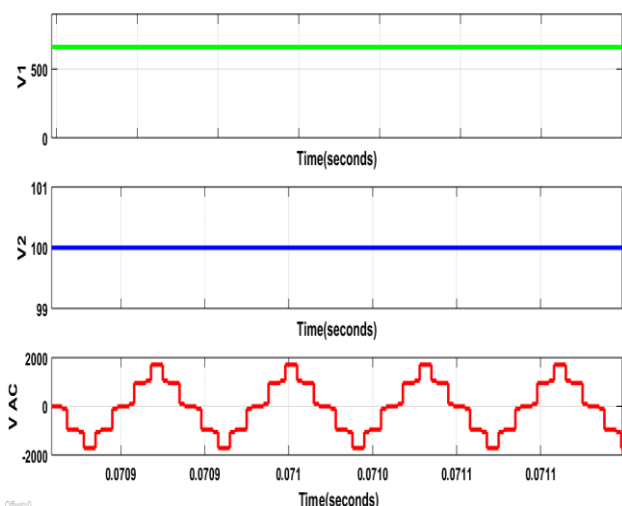


Fig.11. Input & output voltages obtained from the inverter

from fig.11, we can observe the input and output voltage waveforms obtained from the inverter. Usually, this inverter consists of two inputs 1 & 2. input 1 voltage is given as V1 and indicated with green colour. its magnitude is ranging from 0 to 500. The inverter input 2 is given as V2 and indicated with blue colour. and its magnitude is ranging from 99 to 101. As the voltages V1 & V2 are of DC the waveforms are constant. Finally, the last waveform displays the waveform of the output voltage obtained from the inverter V AC, the 9-level inverter output waveform is indicated with red colour and its magnitude is ranging from -2000 to 2000.

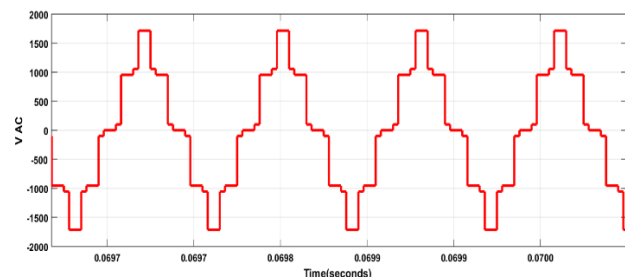


Fig.12. the voltage obtained from the inverter output

From above fig.12, we can observe the output waveform obtained from the inverter V AC which is 9 level inverter output indicated with red colour and the magnitude is ranging from -2000 to 2000.

#### IV HARDWARE IMPLEMENTATION

This article implemented a hardware structure of a single (1)-phase inverter with Arduino by hybrid electric sources, which mainly consists of, one Arduino Uno which is a microcontroller, two MOSFETs for the inverter, one 12v rechargeable battery for an energy storage unit, a step-up transformer a Dynamo for windmill 40×40 solar panel for photo voltaic power generation, and lamp load for the output, the above-mentioned components were used can be seen in the below fig.13. The Arduino uno is the heart of this inverter in which it helps in generating the PWM pulses. It helps in switching of MOSFETS.

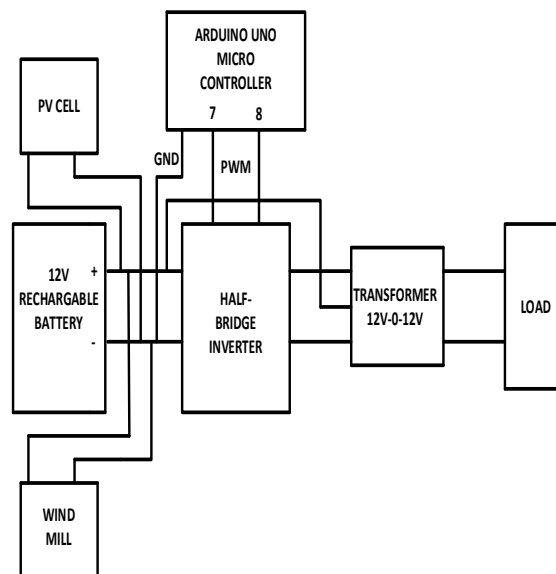


Fig.13. single-phase inverter using Arduino with hybrid energy sources

The above block diagram from fig.13, of a single-phase inverter using Arduino with hybrid electric sources, exposes the total construction of the project. In this circuit, two hybrid electric sources were built which are a windmill and a PV cell, and are connected parallelly to a 12V rechargeable battery which is the storage unit, there by a single phase half bridge inverter is built using two MOSFETs which is the main component, used for power conversion DC-AC, the triggering pulses for the MOSFETs will be given by the Arduino Uno which is the microcontroller used for controlling the output voltage at the desired level, and now the 12v battery is fed to the inverter input, through this inverter the DC supply given to the inverter is converted to AC by the MOSFETs and the output obtained of the inverter is fed to the input of the step-up transformer for increasing the voltage level and thereby the output of the transformer is connected to a lamp load.



Fig.14. Hardware kit of the single-phase inverter with hybrid sources

The above fig.14 indicates the hardware implementation of the single-section inverter that's linked to a lamp load.

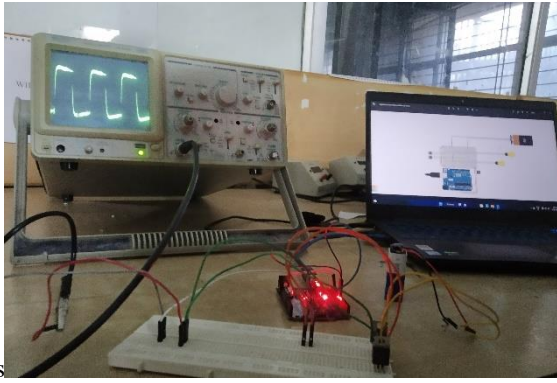


Fig.15. Single phase inverter output displayed on CRO.

The above circuit was successfully implemented and out was generated with 220V 50HZ supply at the output side, which is our desired output level, the inverter generated a square wave which is nothing but AC voltage and this generated output and waveform is displayed on CRO which can be seen on the above fig.15.

## V CONCLUSION

This paper implemented the simulation of the renewable energy sources fed multilevel inverter and the output of the proposed system was shown. Hardware structure was implemented with a single-phase inverter using Arduino, which generated a square pulse by PWM with the help of an Arduino microcontroller and the output of the hardware displayed on CRO is shown.

## REFERENCES

- [1] Akira Nabae, et al, "A New Neutral Point-Clamped PWM Inverter," IEEE-Trans. Ind. Applicant.1981, 17(3): 518-523.
- [2] M. D. Manjrekar and T.A.Lipo, "A hybrid multilevel inverter topology for drive applications," in, Con/ Rec. 1998 IEEEAPECCon/ vol. 2, pp. 523-529.
- [3] C. Feng, J.Liang, and V.G.Agelidis, "Modified phase-shifted PWM control for flying capacitor multilevel converters," IEEE-Transactions on Power Electronics, vol.22, pp. 178-185, 2007.
- [4] Chenchireddy, K. et, al 2020. Different topologies of inverter: a literature survey Innovations in Electrical and Electronics Engineering pp 35-43
- [5] L.G.Franquelo, et, al, "The age of multilevel converters arrives," IEEE, industrial electronics magazine, vol. 2, pp. 28-39, 2008.
- [6] C. Liu, K. T. Chau and X. Zhang, "An efficient wind-photovoltaic hybrid generation system using the doubly excited permanent-magnet brushless machine," IEEE, Trans. Ind. Electron., vol. 57, no. 3, pp. 831- 839, Mar. 2010.
- [7] Chenchireddy, K., Jegathesan, V. and Kumar, L.A., 2019. Design and Simulation of a Single Phase Four Level Neutral Point Clamped Inverter. International Journal of Recent Technology and Engineering (IJRTE) ISSN, pp.2277-3878..
- [8] C.W. Chen, C.Y.Liao, K.H. Chen and Y. M. Chen, "Modeling and controller design of a semi-isolated multi-input converter for a hybrid PV/wind power charger system," IEEE, Trans. Power Electron., vol. 30, no. 9, pp. 4843-4853, Sept.2015.
- [9] R. Wandhare & V. Agarwal, "Novel integration of a PV-wind energy system with enhanced efficiency," IEEE, Trans. Power Electron., vol. 30, no. 7, pp. 3638-3649, Jul. 2015
- [10] B. Mangu, et.al., "Grid-Connected PVWind-Battery based Multi-Input Transformer Coupled Bidirectional DC-DC Converter for household Applications", IEEE Journal of Emerging and Selected Topics in Power Electronics, 2016.

- [11] Chenchireddy, K. and Jegathesan, V., 2022. Three-Leg Voltage Source Converter-Based D-STATCOM for Power Quality Improvement in Electrical Vehicle Charging Station. In AI Enabled IoT for Electrification and Connected Transportation (pp. 235-250). Springer, Singapore.
- [12] Mahalakshmi, R. and Thampatty, K.S., 2015. Grid connected multilevel inverter for renewable energy applications. *Procedia Technology*, 21, pp.636-642.
- [13] Sengamalai U, Ramasamy P, Thentral T, Balasubramani K, Alagarsamy M, Muthusamy S, Panchal H, Sachithanandam MP, Sadasivuni KK. A simplified methodology for mitigating the harmonics and common-mode voltage using multi-level inverters for renewable energy applications. *Energy Sources, Part A: Recovery, Utilization, and Environmental Effects*. 2021 Sep 25:1-23.
- [14] Sinha, A., Jana, K.C. and Das, M.K., 2018. An inclusive review on different multi-level inverter topologies, their modulation and control strategies for a grid connected photo-voltaic system. *Solar Energy*, 170, pp.633-657.
- [15] Kumar NB. Design And Analysis Of Different Multi-Level Inverter Topologies For Single Phase Im Drive. *Turkish Journal of Computer and Mathematics Education (TURCOMAT)*. 2021 Apr 28;12(10):4104-17.

# Time-Domain Control Algorithms of DSTATCOM in a 3-Phase, 3-Wire Distribution System

K.Santhosh  
Dept. of EEE  
Teegala Krishna Reddy  
Engineering College  
Hyderabad, Telangana, India  
santhosh.btech245@gmail.com

Kalagotla Chenchireddy  
Dept. of EEE  
Teegala Krishna Reddy  
Engineering College  
Hyderabad, Telangana, India  
chenchireddy.kalagotla@gmail.com

Pulluri Vaishnavi  
Dept. of EEE  
Teegala Krishna Reddy  
Engineering College  
Hyderabad, Telangana, India  
vysnavipulluri2@gmail.com

A.Greeshmanth  
Dept. of EEE  
Teegala Krishna Reddy  
Engineering College  
Hyderabad, Telangana, India  
Greeshmanth1166@gmail.com

V.Mahesh kumar  
Dept. of EEE  
Teegala Krishna Reddy  
Engineering College  
Hyderabad, Telangana, India  
maheshkumar9400@gmail.com

Police Nandakishore reddy  
Dept. of EEE  
Teegala Krishna Reddy  
Engineering College  
Hyderabad, Telangana, India  
pnandakishorerreddy24@gmail.com

**Abstract:** In this paper, A crystal clear explanation is seen regarding improvement in a power quality distribution system. When the electrical power system appears to be out of phase that is either unbalanced of power on the source side or load side irrespective of any case FACTS (Flexible AC Transmission system) devices are used FACTS is nothing more than a program that uses electronic controllers to boost the effectiveness of current power systems. Over the past few years, research on new developing technologies has also been ongoing. STATCOM is one of the important FACTS controller devices. Overall from a cost point of view, VSI (Voltage source inverter) is preferred. DSTATCOM (Supply static compensator) is placed at PCC (point of the mutual link) to solve the above problem which is to get into the phase of currents and voltages. A DSTATCOM has different theories to explain but here SRFT (Synchronous reference frame theory) and IRPT (Instantaneous reactive power theory) are explored. After processing, the results are simulated by using MATLAB/SIMULINK

**Keywords:** FACTS, DSTATCOM, SRFT, IRPT

## I. INTRODUCTION

Quality of power is important for distribution and utilization. This quality of power depends on voltage, current, and frequency to some extent. If any disturbances/ variations occur then this quantity tends to change from the actual value, Author [1] said that in this type of case power quality problem arises. According to [2]'s comprehensive explanation of the distribution system's power quality issues, the issues are due to transients, voltage variations (V<sub>sag</sub> and V<sub>swell</sub>), voltage imbalance, voltage fluctuations, frequency variations, and waveform distortions (noise, harmonics...). To get out of this problem they implemented DSTATCOM. In reference [3] author suggested that for power quality compensation and also for power quality enhancement a PI controller DSTATCOM is used. A FACTS can be placed in different ways in a system that is it may be in series, shunt, or shunt-

series. A shunt-connected device is STATCOM it is connected at PCC if the link is disturbed due to more power DSTATCOM consumes power or else it also supplies power when the power is needed when there are non-linear load circumstances on the scheme. The active power filters used for harmonics and power compensation are described in [4]. In different phases, with and without neutral wires in the AC distribution system. And also they presented the different AF configurations for harmonics and reactive power compensation. It was all about the survey regarding the selection of AF which is very helpful for manufacturers. About [5] active filters are connected in parallel to nothing Nevertheless, shunt active cleans are used to reduce harmonics, recompense for reactive power, and maintain the quality of the power supply. At PCC they send equal and opposite harmonics to eliminate the harmonics present in the AC link. And also analyzed the performance of SAF by considering two different loads and observed various results of THD (Total harmonic distortion). In [6] complete observation on the capacitor planning and sizing to enhance the distribution system's quality of power, they divided their work in two ways the very first concerns with identification and combination of voltage factors, and the second is all about using PSO techniques the capacitor sizing is implemented because they help in reducing power loss and in voltage profile improvement. Author [7] considered only applications of FACTS in the distribution system that is shunt connected to one DSTATCOM application are regulation of voltage and compensation of reactive power. He said that at first power electronics used are Thyristor-based controllers but now technology is improving day by day in our lives as the PWM technique replaces the outdated methods. Clear details about the DSTATCOM SRFT (synchronous reference frame theory) control technique are provided in [8]. is observed and simulated the results in MATLAB and those outcomes are compared with the real-time outcomes, they

choose this SRFT because it is effectively improving power quality in the distribution network. The paper [9] can give knowledge on ASFC (adaptively switched filter compensator) and DSTATCOM using PID controller, they compared those two studies and resulted in Simulink/MATLAB which shows the power quality improvement in different aspects such as PF improvement, reactive power compensation, voltage stability and harmonics reducing effects. Paper [10] gave advanced information that to reduce the problems related to power quality they introduced a device named PTDS (power transfer integrating supercapacitor) name itself says that a supercapacitor is placed for the transfer of power in the network and also they verified the control strategy of PTDS, here PTDS makes the connection between both AC and DC networks in addition to power quality improvement it also reduces the load demand issues. In [11] concerns about a non-linear load with variations in power are removed with the help of FACTS shunt-connected device DSTATCOM for three-phase, they used voltage controllers of AC for the extraction of harmonics and balancing the load and also implemented the work on salp swarm optimization. Here they observed and performed for both modes of operation those are UPF (unity power factor) and ZVR (zero voltage regulation) of imbalance in both current and phase. As we know there are different control algorithms for DSTATCOM [12] explained by PPFNN (polynomial Petri fuzzy neural network) controller for the improvement in PF, unbalanced currents, and THD. In droop-controlled microgrids, the power quality problems are very seriously considered and these can be improved by using DSTATCOM controllers like online trained PPFNN and also IPRT, which are successfully implemented. I've now discussed each author's goals and efforts to increase the system's power quality. Our primary goal is to provide consumers with quality power since, as we are all aware, quality is important in all aspects of our everyday lives.

This is possible when we employ various tools, such as FACTS, to handle every issue, such as enhancing steady-state and dynamic stability as well as reducing voltage instabilities. The FACTS devices can be connected in three different ways.

- Shunt connection • Series connection
- Shunt-Series connection

STATCOM is the name of a FACTS device that is coupled to a shunt.

A static compensator, also known as a voltage source converter or current source converter, is an electronic device that controls power using IGBTs, MOSFETs, and other devices.

## II. TOPOLOGY

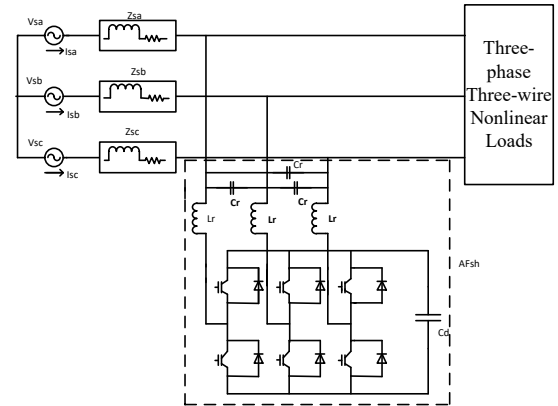


Fig. 1. Three-phase, Three-Wire Distribution for STATCOM

Fig 1 demonstrates a 3-wire shunt active filter's basic schematic representation in a 3-phase 3-wire supply network.

The designs of the inductor, capacitor and voltage across the capacitor must be taken into account for the STATCOM, and once that device has been designed, its location must be considered. Before starting, the following explanation of what we're going to perform in this section[13].

As we all know the supply is from generating station where electrical power is generated and transmitted over long distances to reach the distribution station, from this station loads are connected to satisfy the consumer needs. Here in daily life, we observe non-linear loads are more compared to linear loads. There will be a disturbance in the transmission sector. To overcome this unbalance/disturbance we are going to introduce some devices which are useful for balancing these problems. DSTATCOM is a FACTS device used for the solution of all power quality issues which is shunt-connected to the point of mutual connection through the supplied link (PCC)[14].

It has two different operating modes.

- i) voltage mode
- ii) current mode

In the voltage mode of operation, we consider all voltage values for respective calculations and whereas for the current mode of operation we consider current values for the mathematical calculations.

The very first main function of DSTATCOM is to generate or absorbs the reactive power present at PCC, so that power quality issue can be eliminated successfully[15]. So, before solving the power quality problem it is better to know what precisely are these power quality issues.

The following are a few power quality issues that I am aware of:

- Disruptions in power frequency
- Transients in the power system
- Harmonics in the power system
- power factor

As electrical and electronics engineers, we must minimize these problems and issues as well as the numerous others that are connected to power quality. When we consider a voltage source converter, Fig. 1 depicts an active shunt filter linked to a link in parallel with inductors, capacitors, and six diodes. We can also see six IGBTs in parallel with the diodes.

There are primarily two forms of systemic imbalance.

Unbalanced on the source side

Unbalanced on the load side

Our device can generate or absorb active and reactive power to balance out an unbalance on either the source side or the load side. For instance, if the load side needs  $z$  amount of power and the source side only takes  $y$  amount, our STATCOM will supply  $x$  amount, which is  $z$  power is alike to the sum of  $x$  power and  $y$  power. However, to obtain this STATCOM power, some control techniques for the needed power are needed to achieve a balanced system and eliminate unbalances in load, The next section goes into a detailed discussion of control algorithms.

### III. CONTROL SCHEME

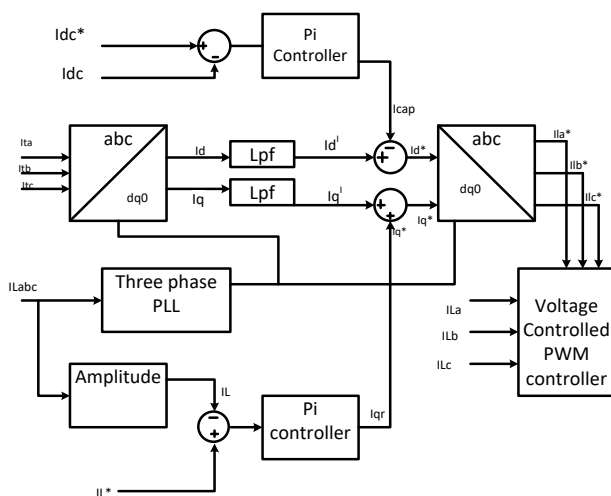


Fig. 2. Control algorithm for DSTATCOM

The above figure shows the control technique used for our DSTATCOM. There are different kinds of control algorithms/theories used for the implementation of DSTATCOM. which are classified into two categories and those are as follow:

i) Time domain control algorithm

ii) Frequency domain control algorithm

We examine the two basic kinds of time domain control methods, namely: The two categories mentioned above are further divided into numerous types.

SRF and IRP

The 3-phase 3-wire supply system is explored by both of these ideas. As a DSTATCOM, VSC is used. In both algorithms, the main aim is to create the gate pulses for the IGBTs with the help of the PWM current regulator, It is used to match the supply fluxes with the transformed mentioned

currents. The calculations of these transformed reference currents are different in both theories.

1) IP

This model is founded on Clark's renovation, which reduces 3-phase quantities to 2-phase equivalents in the alpha-beta structure.

Rapid active and reactive power calculation stands to be done. (1) gives the alpha and beta values of voltages by using

Three-phase supply voltages after the alpha-beta transformation, similarly (2) for currents

(3) Shows active and reactive powers in the dc component. After converting those dc component values into ac components instantaneous active and reactive powers are (4)

In (5) we calculated reference three-phase supply currents by using previous calculations. (6) power factor correction is done.

This transform is applied to the voltages & currents which generate reference currents for controlling at gate signals of VSC( voltage source converter )

Applications: Mainly used for reactive power compensation

$$\begin{bmatrix} V_\alpha \\ V_\beta \end{bmatrix} = \sqrt{\frac{2}{3}} \begin{bmatrix} 1 & -\frac{1}{2} & -\frac{1}{2} \\ 0 & \frac{\sqrt{3}}{2} & -\frac{\sqrt{3}}{2} \end{bmatrix} \begin{bmatrix} V_{sa} \\ V_{sb} \\ V_{sc} \end{bmatrix} \quad (1)$$

$$\begin{bmatrix} I_\alpha \\ I_\beta \end{bmatrix} = \sqrt{\frac{2}{3}} \begin{bmatrix} 1 & -\frac{1}{2} & -\frac{1}{2} \\ 0 & \frac{\sqrt{3}}{2} & -\frac{\sqrt{3}}{2} \end{bmatrix} \begin{bmatrix} I_{sa} \\ I_{sb} \\ I_{sc} \end{bmatrix} \quad (2)$$

$$\begin{bmatrix} p_L \\ q_L \end{bmatrix} = \begin{bmatrix} V_\alpha & V_\beta \\ V_\beta & -V_\alpha \end{bmatrix} \begin{bmatrix} I_\alpha \\ I_\beta \end{bmatrix} \quad (3)$$

$$P_L = \overline{p_L} + p_L \quad (4)$$

$$Q_L = \overline{q_L} + q_L$$

$$\begin{bmatrix} I_{sa}^* \\ I_{sb}^* \\ I_{sc}^* \end{bmatrix} = \sqrt{\frac{2}{3}} \begin{bmatrix} 1 & 0 \\ -\frac{1}{2} & \frac{\sqrt{3}}{2} \\ -\frac{1}{2} & -\frac{\sqrt{3}}{2} \end{bmatrix} \begin{bmatrix} V_\alpha & V_\beta \\ -V_\beta & V_\alpha \end{bmatrix}^{-1} \begin{bmatrix} p^* \\ q^* \end{bmatrix}$$

(5)

$$p^* = \overline{p_L} + p_{loss} \quad (6)$$

$$q^* = q_L - q_{vr}$$



2) *SRF*

This theory, often referred to as the DQ mention frame scheme is based on the change of currents in a synchronously rotating d-q structure. This means that the controller uses source side voltages  $V_a, V_b,$  and  $V_c$  as well as load side currents  $I_{La}, I_{Lb},$  and  $I_{Lc}$  to generate appropriate reference currents.

A phase-locked loop (PLL) converts voltage signals into current sine cosine signals.

Park's transformation transforms current signals into the DQ frame, which is then filtered and turned back into the ABC structure ( $I_{sa}, I_{sb},$  and  $I_{sc}$ ), which is then supplied to an indication maker to create the changing signals for VSC.

Reference direct axis supply current is equal to the total of the direct axis load current's dc component and DSTATCOM losses current. The difference between the quadrature axis load current's dc component and the quadrature axis current is the reference quadrature axis supply current (8).

9) Achieved through the reverse park's transition are three-phase reference supply currents, At PCC (10) calculated.

Applications: Mainly used for the THD and load imbalance

$$I_d^* = I_{dDC} + I_{loss} \quad (7)$$

$$I_q^* = I_{qDC} - I_{qr} \quad (8)$$

$$(9) \quad \begin{bmatrix} I_{sa}^* \\ I_{sb}^* \\ I_{sc}^* \end{bmatrix} = \begin{bmatrix} \cos \theta & \sin \theta & 1 \\ \cos \left( \theta - \frac{2\pi}{3} \right) & \sin \left( \theta - \frac{2\pi}{3} \right) & 1 \\ \cos \left( \theta + \frac{2\pi}{3} \right) & \sin \left( \theta + \frac{2\pi}{3} \right) & 1 \end{bmatrix} \begin{bmatrix} I_d^* \\ I_q^* \\ I_0^* \end{bmatrix}$$

$$V_{sp} = \sqrt{\frac{2}{3} (V_{sa}^2 + V_{sb}^2 + V_{sc}^2)} \quad (10)$$

IV. SIMULATION RESULTS

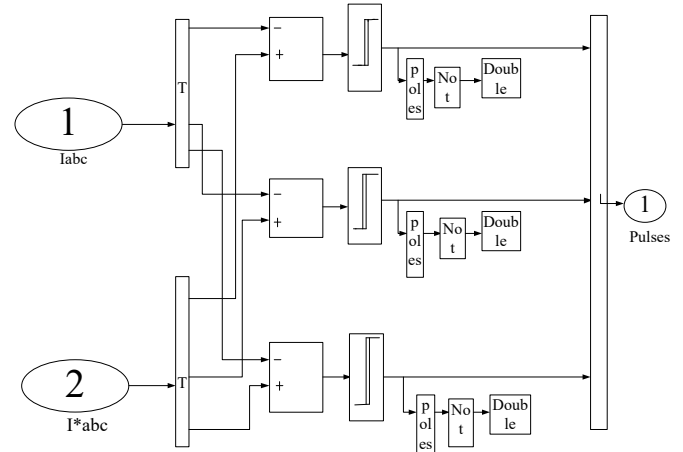


Fig. 3. Hysteresis Control Scheme

In this control scheme, we are getting pulses to operate VSC

The procedure for The supply currents and reference currents are added to produce these pulses, as indicated in Fig 3. After the control system was finished, we simulated the outcomes in the form of graphs, as shown in the corresponding figures below. Single-phase voltages and currents as well as three-phase voltages and currents of both sides that is source side and load side are simulated in MATLAB. Compensating voltage and current are also simulated in fig 8 and fig 9 respectively.

All of the simulated results display the voltage or current value at that specific instant of time on the x-axis (time in seconds) and the y-axis (respective voltage or current value, either load side or source side).

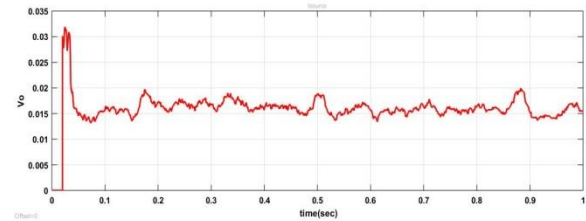


Fig. 4. Shows the output voltage

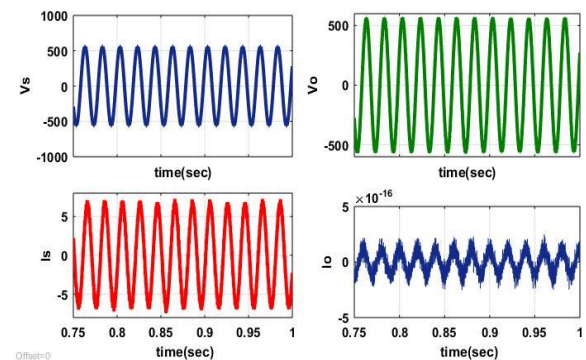


Fig. 5. shows the  $V_s, V_o, I_s,$  and  $I_o$

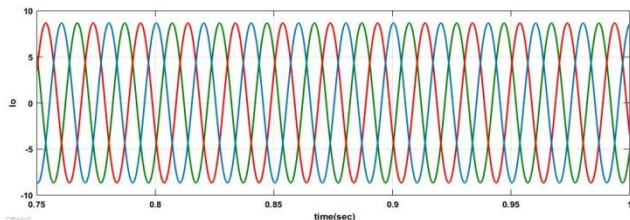


Fig. 6. Three-phase output current

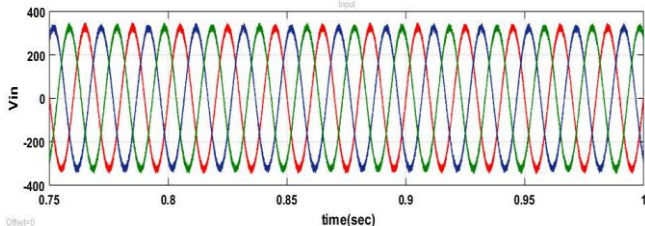


Fig. 7. Three-phase input voltage

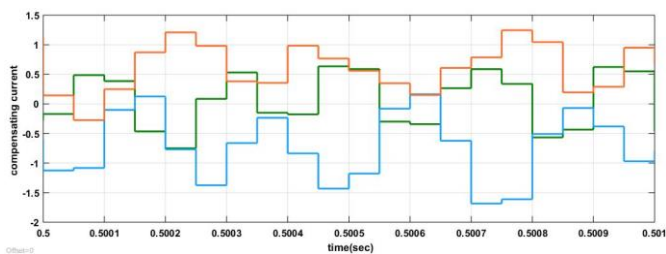


Fig. 8. shows compensating current

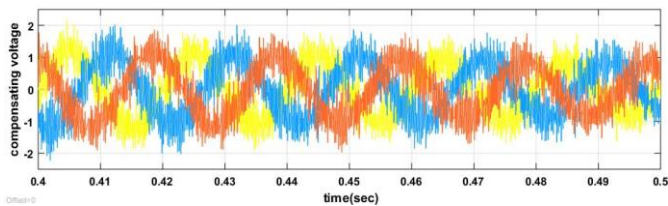


Fig. 9. shows compensating voltage

## V. CONCLUSION

This article has discussed about the FACTS shunt connected DSTATCOM for the power quality improvement and explained different control theories of DSTATCOM like SRFT and IRPT additionally to the explanation they also compared and their performance is investigated accordingly, simultaneously the results are simulated in MATLAB/SIMULINK.

## REFERENCES

[1] Chenchireddy, Kalagotla khammampati.R. sreejyoti, and V. Kumar. "Comparative investigation on single-phase distribution Grid-connected with and without DSTATCOM." In E3S web of meetings, vol. 309. EDP sciences, 2021.  
 [2] Kumar, V., et al. "Power Quality Enhancement In 3 phase 4-wire Distribution system using Convention Power Devices." 2002  
 [3] Chenchireddy, K. et al. ( 2021 December), A review on regulator techniques for power quality improvement in the Supply system.

2021 5<sup>th</sup> international meeting in electronics, communication and aerospace technology (ICECA) (pp. 201-208). IEEE.  
 [4] Singh, B., Al-Haddad, K. and Chandra, A ., 1999. A review of active filters for power quality improvement. IEEE transactions on industrial electronics,46(5), pp.960-971.  
 [5] Shah, A., Vaghela. N, shunt active power filter for power quality improvement in the distribution system. International journal of engineering development and research. 2005.  
 [6] Wang Z, Liu H, Li J. Reactive Power Planning in Distribution Network Considering the Consumption Capacity of Distribution Generation. In 2020 5<sup>th</sup> Asia Conference on Power and Electrical Engineering (ACPEE) 2020 Jun 4 (pp. 1122-1128). IEEE.  
 [7] Padiyar KR. FACTS controllers in power transmission and distribution. New Age International; 2007.  
 [8] Mahela, O.P. and Shaik, A.G., 2016. Power quality improvement in the distribution network using DSTATCOM with battery energy storage system. International Journal of Electrical Power & Energy System, 83, pp.229-240.  
 [9] Elmetwaly, A.H., Eldesouky, A.A. and Sallam, A.A., 2020. An adaptive D-FACTS for power quality enhancement in an isolated microgrid. IEEE Access, 8, pp.57923-57942.  
 [10] Lai J, Chen M, Dai X, Zhan N. Energy Management Strategy Adopting Power Transfer Device Considering Power Quality Improvement and Regenerative Braking Energy Utilization for Double-Modes Traction System CPSS Transaction on Power Electronics and Applications. 2022 Apr 20:7(1):103-11.  
 [11] Sikakolapu, J., Arya, S.R. and Maurya, R., 2021. Distribution static compensator using an adaptive observer-based control algorithm with salp swarm optimization algorithm. CPSS Transactions on Power Electronics and Applications, 6(1), pp.52-62  
 [12] Tan KH, Li MY, Weng XY. Droop Controlled Microgrid with DSTATCOM for Reactive power Compensation and Power Quality Improvement. IEEE Access. 2022 Nov 18.  
 [13] Grunbaum R. FACTS for voltage control and power quality improvement in distribution grids.  
 [14] Kewat S, Singh B. Modified amplitude adaptive control algorithm for power quality improvement in multiple distributed generation system. IET Power Electronics. 2019 Aug;12(9):2321-9.  
 [15] Singh B, Arya SR. Design and control of a DSTATCOM for power quality improvement using cross correlation function approach. International Journal of Engineering, Science and Technology. 2012;4(1):74-86.

# Power Generation of Wind-PV-Battery based Hybrid Energy System for Standalone AC Microgrid Applications

Nagasridhar Arise  
Dept of EEE, Assistant professor  
Teegala Krishna Reddy Engineering  
College  
Hyderabad  
[sridhar0106@gmail.com](mailto:sridhar0106@gmail.com)

Veluma Bhoomika  
Dept of EEE, UG Student  
Teegala Krishna Reddy Engineering  
College  
Hyderabad  
[bhoomika83411@gmail.com](mailto:bhoomika83411@gmail.com)

Nalla Ajay Reddy  
Dept of EEE, UG student  
Teegala Krishna Reddy Engineering  
College  
Hyderabad  
[ajayreddynalla2612@gmail.com](mailto:ajayreddynalla2612@gmail.com)

Sama Harika  
Dept of EEE, UG student  
Teegala Krishna Reddy Engineering College  
Hyderabad  
[harikasama1603@gmail.com](mailto:harikasama1603@gmail.com)

Adimulam Koushik  
Dept of EEE, UG Student  
Teegala Krishna Reddy Engineering College  
Hyderabad  
[koushikadhi143@gmail.com](mailto:koushikadhi143@gmail.com)

**Abstract:** This article describes the power generation of wind, PV, and, battery-based hybrid energy systems for standalone AC microgrid applications. There are many results for resolving issues with the supply of electrical power, particularly in rural places where electrical networks are difficult to access. The usage of networks that are not linked to electrical systems allows for the provision of electricity to remote places, which is one way for determining this issue. They are denoted to as standalone microgrid systems. The standalone microgrid has its sources of electricity, extension (or) addition with an energy storage system. They are utilized where power transmission and distribution from a major centralized energy source is too far and costly to operate. In this article, a standalone AC microgrid scheme with a hybrid power system comprised of wind, photovoltaic, and batteries are designed and managed.

**Keywords:** Hybrid energy system, PV (Solar Cell), Wind, Battery, Microgrid.

## I. INTRODUCTION

Nowadays, electricity plays an energetic role for lightening, heating, refrigerating, operating computer appliances, etc., For less emission of gases, while producing energy when it allocating energy to different energy generation systems renewable such as Pv, wind, and storage device maintain a crucial role. Because of the inclusion of variable non-conventional energy resources when running in standalone mode, it requires various control techniques for continuous and systematic power transfer. In [1], they proposed an article about the system which has the ability to perform experimental research and studies in the field of non-

conventional energy resources. They used control procedures which are cast off for real-time control environments. In this paper, an experimental scale microgrid of distributing non-conventional energy resources with battery storage, EMS, and a controller scheme is developed. In [2], they introduced the methodology in which dissimilar methods were used for the optimization of hybrid-based non-conventional energy resources. They used different algorithms which include optimization including hybrid algorithms. This generation used Artificial intelligence algorithms as they have better precision and good convergence. So, finally, they decided that unlike procedures have different accuracy and precision level and also there is a difference in convergence speed. So, the choice of an algorithm or methodology may vary with user requirements. In [3] they proposed an article about the ideal planning of Hybrid renewable power resources. They used the (HOMER)Hybrid optimization model for electrical renewables software system, which was developed by the National renewable energy laboratory (NREL), US. They determined that more than grid-connected mode HRES modeled in standalone mode. In [4] this article they used multiple algorithms for optimization of non-conventional energy resources based microgrid systems. The algorithms are multi-objective multi-verse optimization (MOMVO) algorithm, DE, and PSO are used. The outcome show a high accuracy rate compared to other techniques. In [5] they introduced the mathematical modeling of hybrid non-conventional power systems which recapitulate the HRES,

mainly solar cells, wind, hydro, and storage devices such as batteries. They presented the MPPT technique and to extract maximum power PV, wind requires special techniques because of non-linear power characteristics. In [6] they proposed an article about the hybrid renewable energy resource's-based DC microgrid which they concluded that DCMG is pollution-free and also low cost. In [11] they used multi-objective optimization algorithm for decreasing the load losses, maintenance cost. [12] the study proposed the cost analysis and the worth of standalone microgrid related area of Bangladesh.

## II. HYBRID ENERGY POWER GENERATION

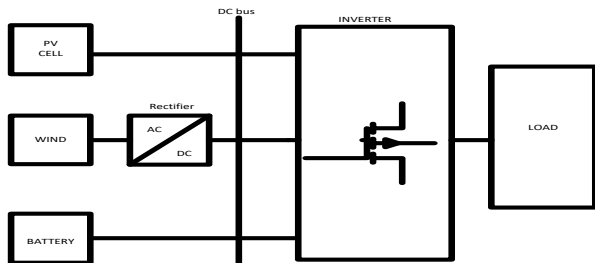


Fig-1: Hybrid Energy generating station

The block diagram for the hybrid energy generation station is shown in Fig-1 and includes PV cells or solar cells, wind energy, Battery, and inverter. It tells that the solar cell, wind, and battery are the inputs that generate some energy and pass it to the inverter. The inverter stores the energy and sends that energy to the load. As we are seeing a DC bus over there, it is also identified as the DC link which serves as an interface between the AC-DC converter and inverter. The proposed system is going to generate the power using Non-conventional energy resources that are shown below;

### A. Pv Model

Solar or photovoltaic (PV) generation of power is the procedure of converting radiant energy from the sun into electricity using solar panels. Solar panels also called PV panels, PV systems can too be installed in grid-connected or off-grid (stand-alone) configurations. Pv cell has many advantages than wind model such as less maintenance and its installation is very easy [7].

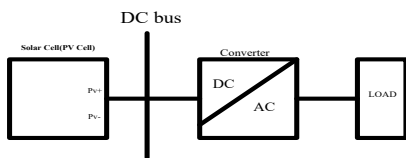


Fig-2: PV model

The PV model is made known in Fig. 2, which demonstrates how the PV cell is linked to the DC bus, then to the DC-AC converter, also known as an inverter, and ultimately to the load. So here first PV model generates the power in the

form of DC and then it passes through the converter, that converter converts the DC power to the AC and sends it to the load.

### B. Wind Generation Model

By transforming the kinetic energy of moving air into electricity, wind energy is castoff to generate power. The wind moves the rotor blades of modern wind turbines, changing moving energy into rotational energy. This rotational energy is then converted into electrical energy with the support of a generator. When the speed exceeds more than the cutout speed pitch angle controller is used to limit the speediness of the wind turbine [8].

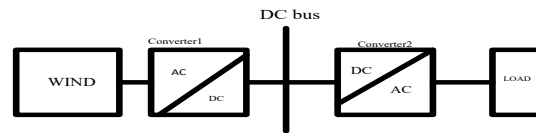


Fig-3: Wind Generation

The full-wave rectifier output voltage is given by;

$$V_o = V_{in} \frac{T}{T - T_{on}} = V_{in} \frac{1}{1 - \alpha} \quad (1)$$

Where  $V_o$ -Output voltage

$V_{in}$ -Input voltage

Figure 3 depicts the production of electricity utilizing wind energy. In this diagram, the generated power is routed through Converter1, an AC-DC converter, and through Converter2, a DC-AC converter also identified as an inverter, with the aid of the DC bus. The line between the rectifier and inverter is known as a DC bus or DC link, and the output of the inverter is linked to the load in AC.

### C. Battery System Model

The Battery is completed up of a DC-DC boost converter and a nickel-metal-hydrde battery. Through the PI controller, this converter is in charge of maintaining the dc bus voltage.

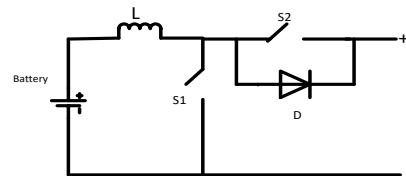


Fig-4: Battery and DC-DC converter

The production voltage of the boost converter is given by;

$$V_o = \frac{V_{in}}{1 - D} \quad (2)$$

$$D = \frac{T_{on}}{T} \quad (3)$$

Where  $V_o$ -Output voltage

$V_{in}$ -Input voltage

$D$ -Duty ratio



are well aware that the rotor blades in the wind convert moving energy into rotational energy, and that generator terminals are used to transform rotational energy into electrical energy. From the figure the  $W_m$  block is associated to the square math function then the result of the math function and some constant value are the input to the product block, the output of the product block is coupled to the subtract and then after saturation it is associated to the output port  $T_{ref}$ . The output port  $T_{ref}$  is now input to the subsystem which involves the product, base torque block as made known in fig 7. And this subsystem is coupled to a discrete first-order filter then to a current controller and finally to a generator terminal.

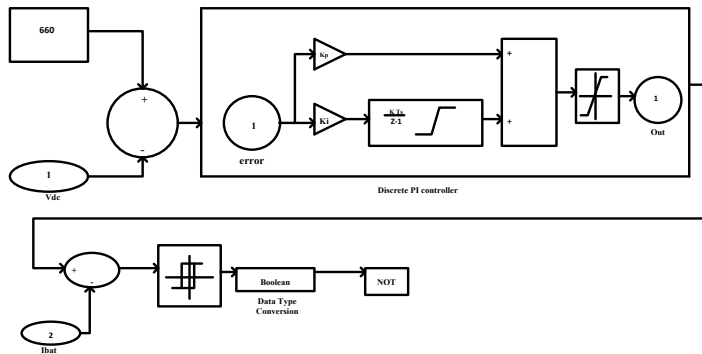


Fig-8: Battery/Electrolyzer controller

A battery/electrolyzer controller is represented in Fig. 8 where a constant value and dc voltage input are distributed to the summation point before being coupled to a discrete PI controller. Conferring to the form of feedback, the discrete PI controller block calculates the control signal using the backward Euler discretization method, which is a commonly used method in control systems for the correction of error between the commanded setpoint and the actual value. The relay is now connected to the discrete PI

controller block via the summation point, and the data type conversion, which is Boolean, is attached after that. The logic gate, NOT the block, is linked to it at the end. When shortage of wind and Pv power generation takes place battery acts an active power source as a backup [10]

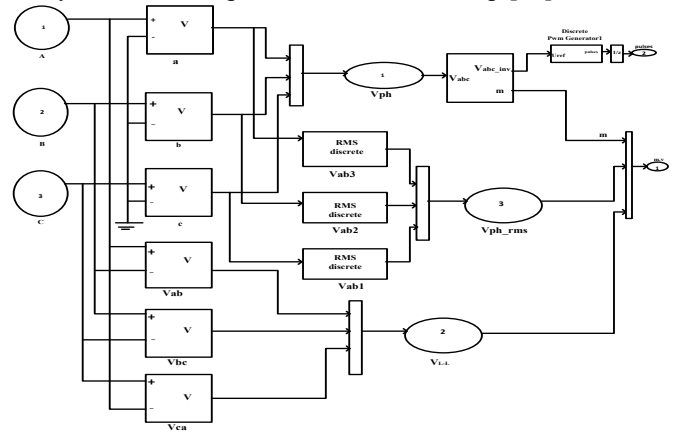


Fig-9: Control of inverter

Fig 9 shows the controller of the inverter is in three phases, the variables A, B, and C is associated to phase blocks and then connected to multiplexers and also connected to RMS discrete blocks, now connected to phase RMS voltage blocks and  $V_{LL}$  blocks and then connected to discrete PWM generator, thus to generate some pulses.

#### IV. SIMULATION RESULTS

After designing the MATLAB/simulation diagram. The PV model, wind model, battery, inverter, and load side input and output current and voltage wave form are made known below and were extracted using MATLAB/Simulink. The designed MATLAB/simulation diagram is shown below figure10.

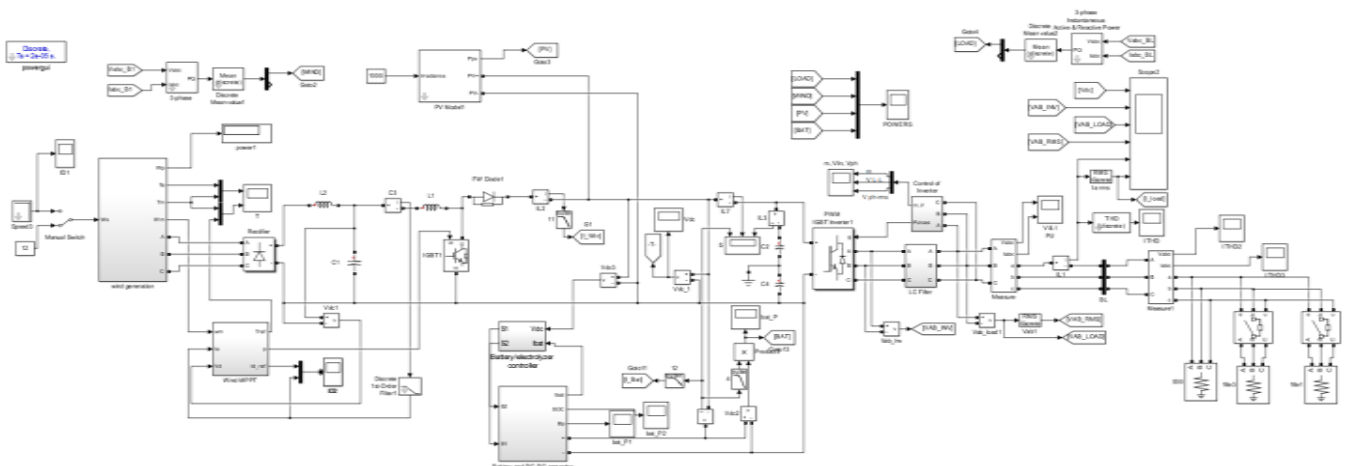


Fig-10: MATLAB/Simulation diagram

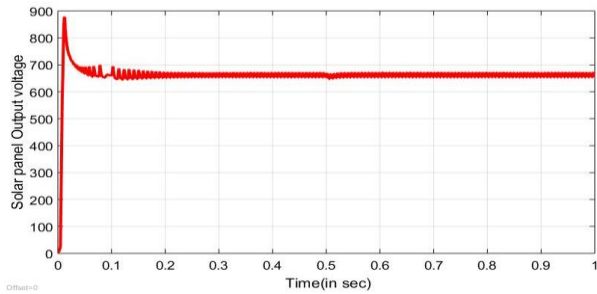


Fig-11: Solar panel output voltage

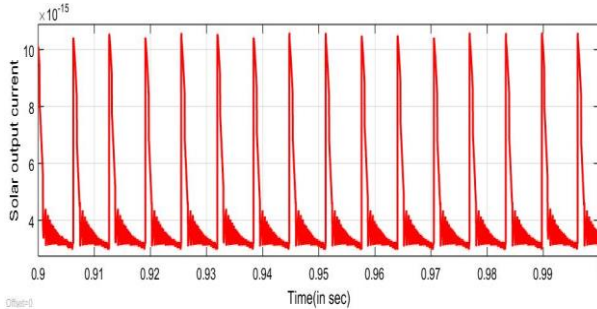


Fig-12: Solar panel output current

Fig-11 and Fig-12 which are depicted above defines solar panel output voltage and solar panel output current respectively. From the Fig-11 we can see that there is an output voltage which rises maximum up to 880 v then it is decreased to 655.8 v nearly.

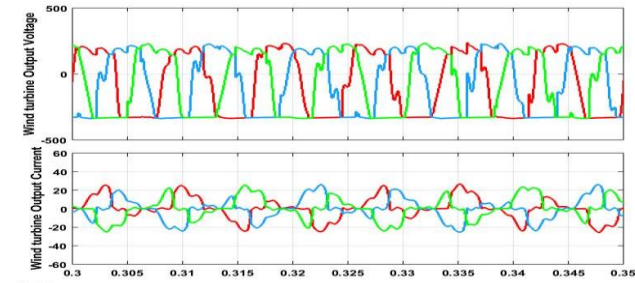


Fig-13: Wind turbine output voltage and current

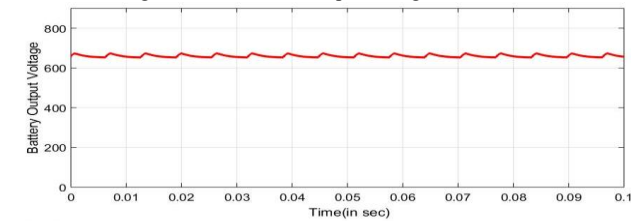


Fig-14: Battery output voltage

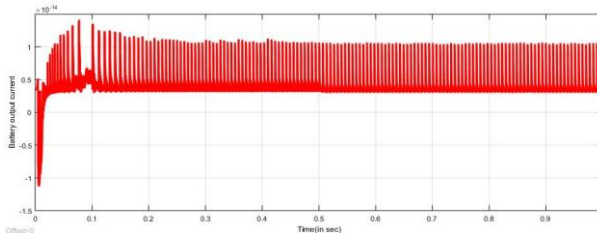


Fig-15: Battery Output current

Fig-13, Fig-14, and Fig-15 which are represented above are the wind output current and voltage, Battery output voltage, and Battery output current respectively. So, from the Fig-13 the voltage is nearly to 260 volts and current is from -20 to +20 amperes. From Fig-14 the voltage is constant around 660 nearly.

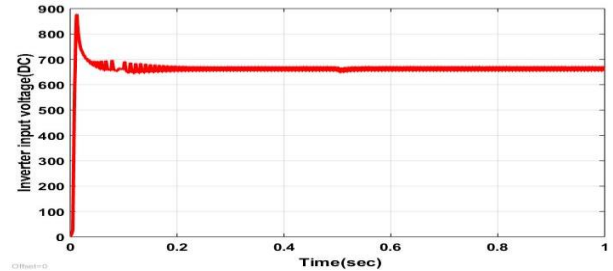


Fig-16: Inverter input voltage (DC)

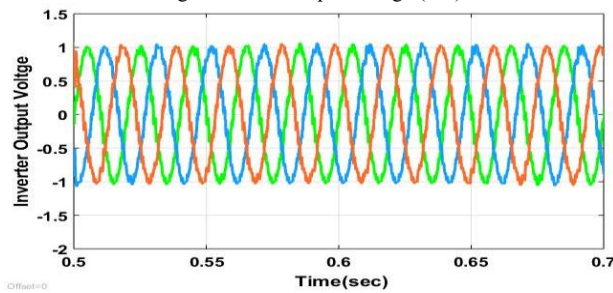


Fig-17: Inverter output voltage

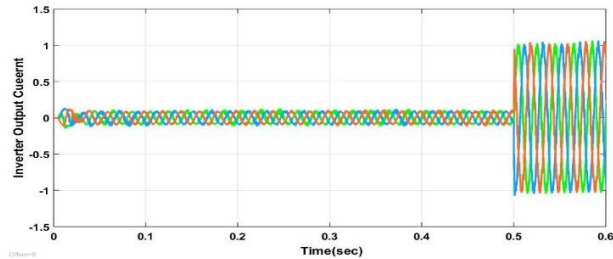


Fig-18: Inverter output current

Fig-16, Fig-17, and Fig-18 shows the inverter input voltage, inverter output voltage and current respectively. From the Fig-16 we can see that x-axis represents input voltage of an inverter and y-axis shows the time in seconds. So, it maintains constant voltage DC from 0 to 1 seconds. From Fig-17 there is a constant output voltage varies from -1 to +1 volts with respect to time in seconds.

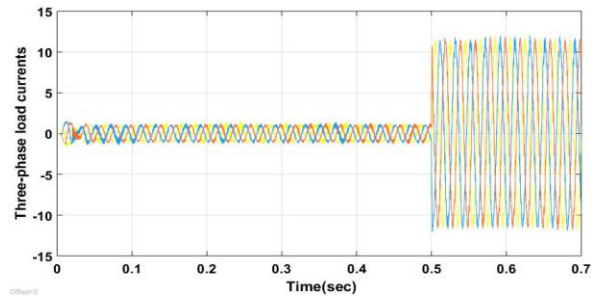


Fig-19: Three phase load currents

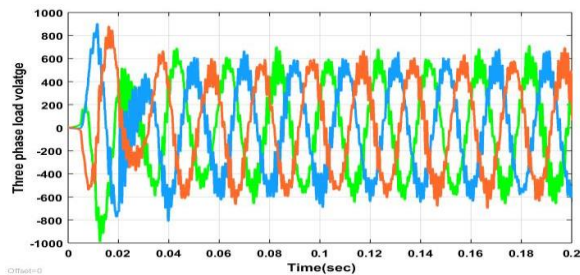


Fig-20: Three-phase load voltage

Fig-19 and Fig-20 depicted above are the three phase load currents and voltages respectively. From the Fig-19 we can see that it maintains constant value up to 0.5 seconds which is nearly to 2 amperes and then suddenly rises after 0.5 seconds to 10 amperes and that is continuous to 0.7 seconds.

#### V. CONCLUSION

This paper proposes control techniques for power generation of wind-Pv-Battery based hybrid energy system for standalone AC microgrid applications. The proposed techniques introduced power management under variable conditions like solar irradiance and wind speed variations, where the generation of power is used for standalone AC microgrid applications.

#### REFERENCES

- [1] Merabet, A., Ahmed, K.T., Ibrahim, H., Beguenane, R. and Ghias, A.M., 2016. Energy management and control system for laboratory scale microgrid-based wind-PV battery. *IEEE transactions on sustainable energy*, 8(1), pp.145-154.
- [2] Sinha, S. and Chandel, S.S., 2015. Review of recent trends in optimization techniques for solar photovoltaic-wind based hybrid energy systems. *Renewable and Sustainable Energy Reviews*, 50, pp.755-769.
- [3] Bahramara, S., Moghaddam, M.P. and Haghifam, M.R., 2016. Optimal planning of hybrid renewable energy systems using HOMER: A review. *Renewable and Sustainable Energy Reviews*, 62, pp.609-620.
- [4] Hemeida, A.M., Omer, A.S., Bahaa-Eldin, A.M., Alkhalaf, S., Ahmed, M., Senjyu, T. and El-Saady, G., 2022. Multi-objective multi-verse optimization of renewable energy sources-based microgrid system: Real case. *Ain Shams Engineering Journal*, 13(1), p.101543.
- [5] Bhandari, B., Poudel, S.R., Lee, K.T. and Ahn, S.H., 2014. Mathematical modeling of hybrid renewable energy system: A review on small hydro-solar-wind power generation. *international journal of precision engineering and manufacturing-green technology*, 1(2), pp.157-173.
- [6] Shaikh, P.H., Leghari, Z.H., Mirjat, N.H., Shaikh, F., Solangi, A.R., Jan, T. and Uqaili, M.A., 2018. Wind-PV-Based Hybrid DC Microgrid (DCMG) Development: An Experimental Investigation and Comparative Economic Analysis. *Energies*, 11(5), p.1295.
- [7] Hemeida, A.M., El-Ahmar, M.H., El-Sayed, A.M., Hasanien, H.M., Alkhalaf, S., Esmail, M.F.C. and Senjyu, T., 2020. Optimum design of hybrid wind/PV energy system for remote area. *Ain Shams Engineering Journal*, 11(1), pp.11-23.

- [8] Krishan, O. and Suhag, S., 2019. Techno-economic analysis of a hybrid renewable energy system for an energy poor rural community. *Journal of Energy Storage*, 23, pp.305-319.
- [9] Badwawi, R.A., Abusara, M. and Mallick, T., 2015. A review of hybrid solar PV and wind energy system. *Smart Science*, 3(3), pp.127-138.
- [10] Kumar P, Palwalia DK. Feasibility study of standalone hybrid wind-PV-battery microgrid operation. *Technology and Economics of Smart Grids and Sustainable Energy*. 2018 Dec;3(1):1-6.
- [11] Baghaee, H.R., Mirsalim, M., Gharehpetian, G.B. and Talebi, H.A., 2016. Reliability/cost-based multi-objective Pareto optimal design of stand-alone wind/PV/FC generation microgrid system. *Energy*, 115, pp.1022-1041.
- [12] Chenchireddy, K., Jegathesan, V. (2022). Three-Leg Voltage Source Converter-Based D-STATCOM for Power Quality Improvement in Electrical Vehicle Charging Station. In: Marati, N., Bhoi, A.K., De Albuquerque, V.H.C., Kalam, A. (eds) *AI Enabled IoT for Electrification and Connected Transportation*. Transactions on Computer Systems and Networks. Springer, Singapore.
- [13] Das, H.S., Dey, A., Tan, C.W. and Yatim, A.H.M., 2016. Feasibility analysis of standalone PV/wind/battery hybrid energy system for rural Bangladesh. *International Journal of Renewable Energy Research (IJRER)*, 6(2), pp.402-412.
- [14] Hu, J., Shan, Y., Xu, Y. and Guerrero, J.M., 2019. A coordinated control of hybrid ac/dc microgrids with PV-wind-battery under variable generation and load conditions. *International Journal of Electrical Power & Energy Systems*, 104, pp.583-592.
- [15] Chenchireddy, K., & Jegathesan, V. (2021). A Review Paper on the Elimination of Low-Order Harmonics in Multilevel Inverters Using Different Modulation Techniques. *Inventive Communication and Computational Technologies*, 961-971.



# Case study on Ni-MH Battery

N. Ramesh babu  
Department of EEE  
Teegala Krishna Reddy  
Engineering college  
Hyderabad, Telangana, India  
[rameshbabu3889@tkrec.ac.in](mailto:rameshbabu3889@tkrec.ac.in)

Kalagotla Chenchireddy  
Department of EEE  
Teegala Krishna Reddy  
Engineering college  
Hyderabad, Telangana, India  
[chenchireddy.kalagotla@gmail.com](mailto:chenchireddy.kalagotla@gmail.com)

V.Harsha Vardhan Reddy  
Department of EEE  
Teegala Krishna Reddy  
Engineering college  
Hyderabad, Telangana, India  
[Vanukuriharsha123@gmail.com](mailto:Vanukuriharsha123@gmail.com)

D.samhitha  
Department of EEE  
Teegala Krishna Reddy  
Engineering college  
Hyderabad, Telangana, India  
[Samsamhitha481@gmail.com](mailto:Samsamhitha481@gmail.com)

P.Apparao  
Department of EEE  
Teegala Krishna Reddy  
Engineering college  
Hyderabad, Telangana, India  
[Pinniapparao098@gmail.com](mailto:Pinniapparao098@gmail.com)

Ch.pavan Kalyan  
Department of EEE  
Teegala Krishna Reddy  
Engineering college  
Hyderabad, Telangana, India  
[Cherukuripavankalyan2001@gmail.com](mailto:Cherukuripavankalyan2001@gmail.com)

**Abstract:** In the current world, where we depend on a variety of systems and technologies, batteries play a critical role. They are necessary for supplying portable power for cellphones, laptops, and other mobiles as well as for regenerative energy sources including solar and wind, electric cars, And home energy storage systems. Rechargeable nickel-metal hydride (NiMH) batteries have grown in significance as a result of their many advantages due to great performance, Extended life, and eco-friendly alternative to throwing away batteries, these batteries have grown in popularity for years. As a result, we examine in this research how well a Ni-MH battery performance when coupled to a boost converter for boosting and battery state of charge

**Keywords:** Boost converter, Nickel-metal hydride battery, state of charge

## I.INTRODUCTION

System for managing energy A technology that makes it possible to store energy for later uses is an energy storage system (ESS).[2] It is a crucial element in the development of renewable energy sources, one way to address the intermittent production of sources such as solar and wind is to store excess energy during periods of low demand, and then utilize that stored energy to meet demand during times of high demand.[1] ESS can assist regulate the supply of electricity and balance the grid.[6]

Batteries, flywheels, compressed air systems and pumped hydro storage are s few of the many distinct types of ESS. Batteries, which store electric energy in a chemical form for later use, are the most widely used ESS technology.[3] Some types of ESS, including flywheels and compressed air systems, store energy and mechanical forms as compressed air systems and flywheels, o in forms of potential energy, such as pumped hydro storage.[7] As the world moves rapidly towards a future

controlled completely by environmentally friendly power sources interest in energy capacity gadgets rising rapidly as well as supporting the Commeal joining of environmentally friendly power essays.[4] May likewise bring down top interest offer crisis reinforcement power and upgrade the effectiveness of ESS will increment as the expense of innovation keeps on dropping contributing to the improvement of a more reasonable energy framework.[8]

At the point when required a battery hence compounds over 2 electrical energy it is one of the most utilized kinds of energy stockpiling fueling anything from a little electronic device to enormous scope electric vehicles and power frameworks batteries or compromised of at least one cell that each has a positive and a negative cathode isolated by an electrode light.[5] As you charge a battery synthetic response happens that permits particles to move to start with one terminal and then onto the next putting away electrical energy in the process as a battery is discharged the particles return to their Cortana areas in the put-away energy is delivered as electric flow. [9]There are a few kinds of batteries each with its arrangement and applications lead corrosive, lithium-particle, cadmium, and nickel metal hydride batteries are the two most generally utilized sorts of batteries.[12]

Lead storage cells are among the oldest & most extensively usable types of batteries.[11]They are commonly utilizing automotive applications and backup power systems. They are generally expensive and deliver strong currents, making them ideal for starting engines.[10] Lithium-ion batteries are becoming increasingly popular because of their high-quality energy density, extended cycle life, and low self-discharge rates. They're common in portable electronics, electric cars, and energy storage systems. Nickel-cadmium and nickel-metal

hydride batteries are commonly utilized in portable electronic devices and power tools.[15]

They have a better energy density than lead-acid batteries and supply larger currents.[11] Battery technology is always growing and improving, with continual research to boost energy density, lower costs, and enhance safety.[14] As renewable energy sources such as solar and wind become more prevalent, the requirement for energy storage devices to balance the grid and provide backup power is likely to expand.[13]

## II. NI-MH BATTERY AND BOOST CONVERTER TOPOLOGY

Rechargeable nickel-metal hydride (Ni-MH) batteries are commonly used in various electronic devices., including cameras, toys, and portable music players. These batteries outperform the nickel-cadmium (NiCd) batteries that came before them in terms of energy density and longevity. NiMH batteries are composed of an alkaline electrolyte solution, a hydrogen compound negative terminal, and a positive cathode made of nickel oxyhydroxide.

During the charging process of NiMH batteries, the hydrogen-absorbing alloy negative electrode takes in hydrogen while the nickel oxyhydroxide positive electrode releases oxygen. This sparks a chemical process that causes the battery to store electric energy. NiMH batteries have the benefit of being able to maintain their charge for extended periods which makes them perfect for usage in inactive gadgets. As they don't contain any harmful metals, they are also more ecologically friendly than NiCD batteries. NiMH battery so has certain drawbacks; thorough however they gradually lose their charge even while not in use since they are more likely to self-discharge. They are also less powerful and have lesser capacity than other battery kinds, as such lithium-ion batteries. NiMH batteries are a suitable option for many users, especially in low-drain devices where longer battery life is needed. these might not be the ideal option for high-power, high-drain devices, though, since they might not be able to supply enough energy to keep the item operating for extended periods

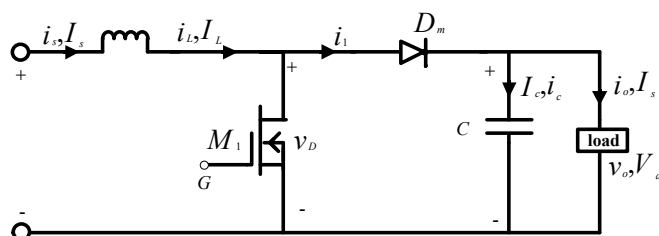


Figure 1: Dc boost converter

**Boost converter:** Boost converters are DC-to-DC converters that increase the input voltage to higher output voltages, and

they operate primarily in two modes: continuous conduction mode (PCM) and Broken conduction mode (BCM).

Persistent conduction method: boost converter can work in persistent condition mode PCM in which the inductor current never arrives at zero during an exchanging cycle in CCM, the inductor receives the input voltage and stores energy as a magnetic field. The inductor delivers this accumulated energy to load when the adjustment is switched on, increasing the o/p voltage. The inductor continues to give energy to the load even after the switch is turned off, causing a constant flow of current through the inductor.

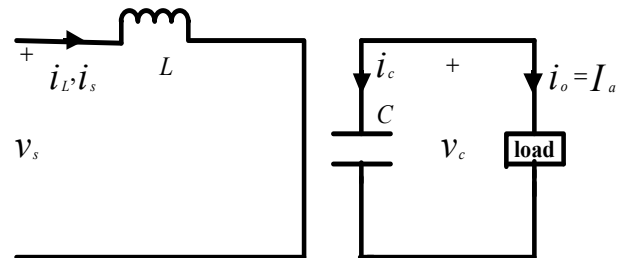


Figure 2: persistent conduction mode

PCM is superior to conventional modes of operation in several ways, including smoother output voltages and greater efficiency. There is no voltage spike after each switch since the inductor current never goes to zero. This can lower efficiency and create electromagnetic interference (EMI). In addition, misfortunes brought about by obstruction and center misfortunes are diminished by the state's current coursing through the inductor. The inductor must be designed correctly to ensure that the inductor current is constantly larger than zero throughout each switching cycle to sustain PCM. This necessity careful consideration of the inductor value and switching frequency to prevent saturation and decreased efficiency from the inductor current exceeding the maximum permitted current. In higher power applications where input and output voltage levels are quite steady, PCM is frequently employed. It is frequently used in power factor correction circuits as well, where it helps to lower harmonic distortion and enhance power factor. As a whole, PCM is a dependable and effective way for boost converters to operate.

In Broken conductance mode, the moving charge in the inductor reaches zero during a certain period\_ each switching cycle when a DC-to-DC mechanism operates in Broken conductance mode (BCM) in lower power applications where the i/o and o/p voltage heights differ significantly, this mode of the process is frequently employed. In BCM, the inductance current is let to reach 0 just before each switching cycle is completed. This may lead to an output voltage waveform that is discontinuous, which may produce an output voltage ripple and lower efficiency

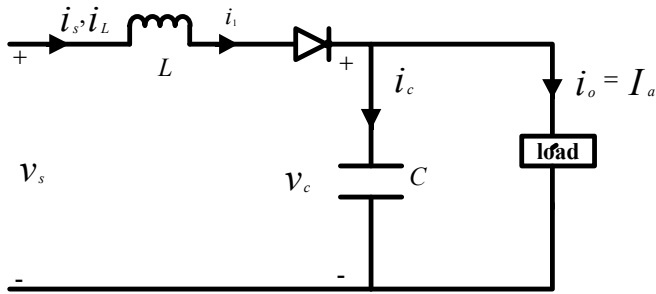


Figure 3: Broken conduction mode

Yet, compared to other modes of operation, BCM has the advantage of having the option to offer a less difficult and more reasonable arrangement at the point when the switches turn on the info voltage is given to the inductor which makes the inductor current increment directly than when the switch is the resulting voltage begins rising. The inductor current ultimately reaches zero and the diode starts to conduct as a result. This enables the inductor to release its stored energy into the output capacitor and the load, producing an output voltage waveform with discontinuities. converters that employ boost, buck, or buck-boost can use BCM. Nonetheless, it is frequently utilized in low-power applications, such as battery-power gadgets, in situations where the voltage levels of both the input and output are unregulated. A DC-to-DC method of stilling the air by the recipes of specific applications including the power level in formation and result in voltage levels wanted effectiveness and result voltage Well, the choice between PCM and BCM depends on the specific prerequisites of utilization both modes have benefits and drawbacks

Undertaking inductor current increases from  $I_1$  to  $I_2$  over time.

$$V_s = L \frac{I_2 - I_1}{t_1} = L \frac{\Delta I}{t_1} \quad (1)$$

Equation (1) shows the voltage supply

Or

$$t_1 = \frac{\Delta IL}{V_s} \quad (2)$$

Furthermore, the inductor current falls straightly from

$$V_s - V_a = -L \frac{\Delta I}{t_2} \quad (3)$$

Or

$$t_2 = \frac{\Delta IL}{V_a - V_s} \quad (4)$$

$\Delta I$  is the top-top wave current of L.

$$\Delta I = \frac{\Delta V_s t_1}{L} = \frac{(V_a - V_s) t_2}{L} \quad (5)$$

Replacing  $t_1 = kT$  and  $t_2 = (1-k)T$  produces the typical result voltage

$$V_a = V_s \frac{T}{t_2} = \frac{V_s}{1-k} \quad (6)$$

Which gives

$$(1-K) = \frac{V_s}{V_a} \quad (7)$$

Substituting  $k = t_1/T = t_1/f$  into yields

$$t_1 = \frac{V_a - V_s}{V_a f} \quad (8)$$

Expecting a lossless circuit,

$$I_s = \frac{I_a}{1-K} \quad (9)$$

The exchanging time frame T can be found from

$$T = \frac{1}{f} = t_1 + t_2 = \frac{\Delta IL}{V_s} + \frac{\Delta IL}{V_a - V_s} = \frac{\Delta IL V_a}{V_s (V_a - V_s)} \quad (10)$$

What's more, this gives the top to top wave current:

$$\Delta I = \frac{V_s (V_a - V_s)}{f L V_a} \quad (11)$$

or

$$\Delta I = \frac{V_s k}{f L} \quad (12)$$

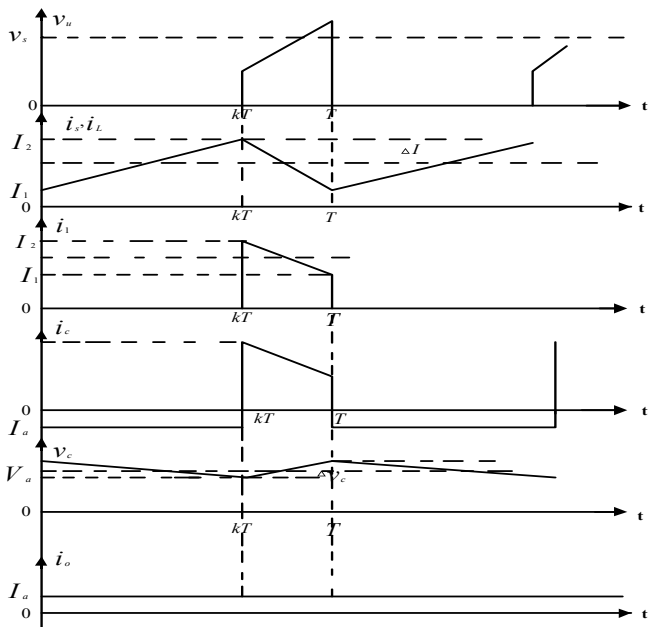


Figure 4: wave forms

At the point when the semiconductor is turned on. The capacitor conveys the heap current for a length of  $t=t_1$  and during this time, the typical capacitor current is  $i_c=i_a$  while the top voltage of the capacitor still up in the air

$$\Delta v_c = v_c - v_c(t=0) = \frac{1}{C} \int_0^{t_1} I_c dt = \frac{1}{C} \int_0^{t_1} I_a = \frac{I_a t_1}{C} \quad (13)$$

Eq(13) shows the small change in capacitance-voltage

Substituting  $t_1 = (v_a - v_s) / v_a f$

$$\Delta v_c = \frac{I_a (v_a - v_s)}{v_a f C} \quad (14)$$

or

$$\Delta v_c = \frac{I_a K}{f C} \quad (15)$$

Condition for ceaseless inductor and capacitor voltage

$$\frac{K v_s}{f L} = 2 I_L = 2 I_a = \frac{2 v_s}{(1-K) R} \quad (16)$$

Which gives the basic worth of the inductor

$$L_c = L = \frac{K(1-K)R}{2f} \quad (17)$$

Eq(17) shows the inductance current

Assuming  $v_c$  is the typical the ripple voltage of the capacitor is equal to 2 times the value of the capacitor voltage.  $\Delta v_c = 2v_a$

$$\frac{I_a k}{C f} = v_a (2) = 2 R I_a \quad (18)$$

Which gives the critical value of the capacitor

$$C_c = C = \frac{K}{2fR} \quad (19)$$

### III. WORKING SCHEME

The Ni-MH battery was used in 2 operations

Working

1. Procedure of Ni-MH battery

The battery is associated with constant load and parallel with the dc machine where a rate limiter for the signals rises and down. Having a relay with some limitations is linked to the battery. At the point when the territory of charge (soc) the of battery goes below 0.1 [10%], a negative burden force of 200Nm is functional to the machine Thus it goes about as a creator to re-energize the battery. At the point when the SOC was more than 0.9 [90%], the heap force is eliminated So just the battery supplies the constant load.

2. performance checking of Ni-MH battery associated with step-up converter:

In this mode, the Ni-MH cell will be associated with a boost converter in which there are PID controller, MOSFET, and DIODE mask are there. Which relational operators are there in the step-up converter these all are connected to a dc voltage source and the performance of the battery such as soc, current, and voltage are measured using a scope.

### IV. SIMULATION RESULTS:

With the help of MATLAB/SIMULINK software. The Simulation outcomes of Ni-MH batteries at different stages are achieved.

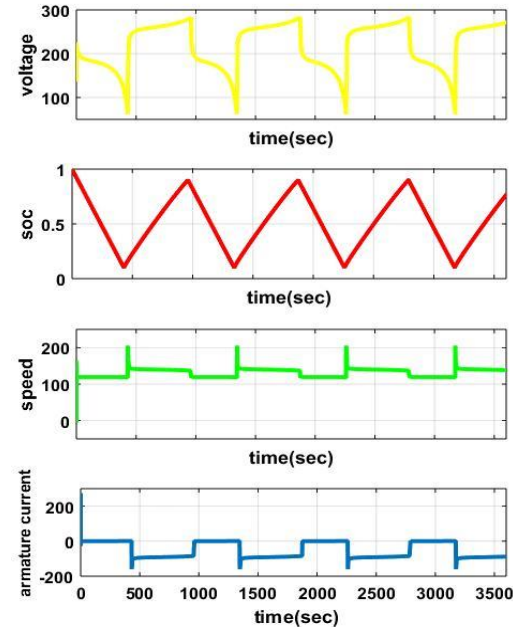


Figure 5: voltage, soc, speed, and armature current waveforms which are connected to the scope where both battery and machine are associated parallel.

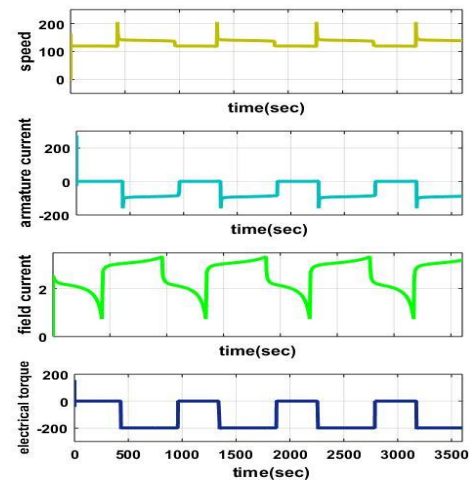


Fig (6): waveforms of dc machine in different with different parameters like electrical torque, field current, armature current, speed

State of charge, current, and voltage of a battery which stands connected with constant load and a dc machine then the characteristic waveform will occur on the scope

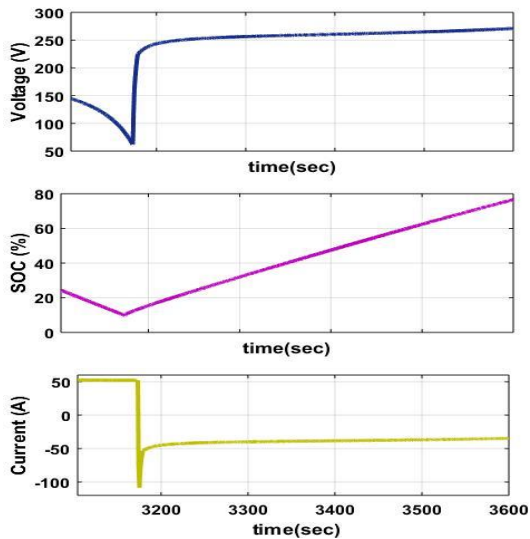


Fig7: voltage, current, and soc waveforms of the battery  
 When the battery is allied to the boost converter the waveform of the Ni-MH cell will occur

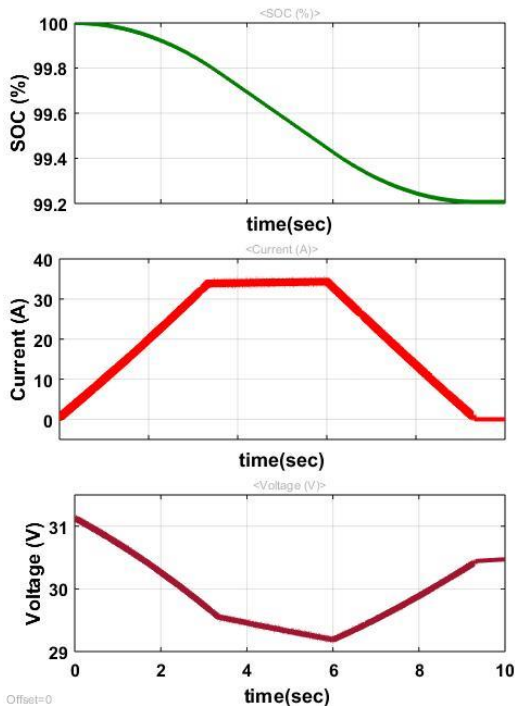


Fig8: current, voltage, soc, the voltage of Ni-MH battery connected to the step-up converter

## V.CONCLUSION

In this paper, we went through the Ni-MH battery which we placed in different conditions like associating it parallelly with the dc machine and boost converter. The speed, soc, current, and voltage are rising and falling depending upon the time where we saw that from the simulation result. We use a rate limiter and relay for the Ni-MH battery model which is connected to the dc machine and the PID controller in the boost converter which is connected to the Ni-Mh battery.

## REFERENCES:

- [1]. . Park, Sang-Jun, et al. "Depth of discharge characteristics and control strategy to optimize electric vehicle battery life." *Journal of Energy Storage* 59 (2023): 106477.
- [2]. VENKATESH, D., G. DHASHARATHA, and K. LAHARIKA. "Reduction of Harmonics and Reactive Currents in Wind Generator Based Power system Network using D-STATCOM." (2015)..
- [3]. Krishnamoorthy, Umapathi, et al. "Efficient Battery Models for Performance Studies-Lithium Ion and Nickel Metal Hydride Battery." *Batteries* 9.1 (2023): 52.
- [4]. Chenchireddy, Kalagotla, and V. Jegathesan. "Three-Leg Voltage Source Converter-Based D-STATCOM for Power Quality Improvement in Electrical Vehicle Charging Station." *AI-Enabled IoT for Electrification and Connected Transportation*. Singapore: Springer Nature Singapore, 2022. 235-250.
- [5]. Martínez-Sánchez, Rafael, et al. "A Low-Cost Hardware Architecture for EV Battery Cell Characterization Using an IoT-Based Platform." *Sensors* 23.2 (2023): 816.
- [6]. Qiao, Jialu, et al. "A chaotic firefly-Particle filtering method of dynamic migration modeling for the state-of-charge and state-of-health co-estimation of a lithium-ion battery performance." *Energy* 263 (2023): 126164.
- [7]. Sreejyothi, Khammampati R., et al. "Zero Voltage Switching (ZVS)-Based DC-DC Converter for Battery Input Application." *AI-Enabled IoT for Electrification and Connected Transportation*. Singapore: Springer Nature Singapore, 2022. 219-234.
- [8]. Russo, Antonio, and Alberto Cavallo. "Stability and Control for Buck-Boost Converter for Aeronautic Power Management." *Energies* 16.2 (2023): 988.
- [9]. Guo, Qihao, et al. "Model predictive control and linear control of DC-DC boost converter in low voltage DC microgrid: An experimental comparative study." *Control Engineering Practice* 131 (2023): 105387.
- [10]. Mansour, Arafa S., and Mohamed S. Zaky. "A new extended single-switch high gain DC-DC boost converter for renewable energy applications." *Scientific Reports* 13.1 (2023): 264.
- [11]. Chenchireddy, Kalagotla, et al. "Performance Verification of Full-Bridge DC To DC Converter Used for Electric Vehicle Charging Stations" 2022 8th International Conference on Advanced Computing and Communication Systems (ICACCS). Vol. 1. IEEE, 2022
- [12]. Choi, Changki, Seongyun Park, and Jonghoon Kim. "Uniqueness of multilayer perceptron-based capacity prediction for contributing state-of-charge estimation in a lithium primary battery." *Ain Shams Engineering Journal* 14.4 (2023): 101936.
- [13]. Tummala, Suresh Kumar, and G. Dhasharatha. "Artificial neural networks based SPWM technique for speed control of permanent magnet synchronous motor." *E3Sweb of conferences*. Vol. 87. EDP Sciences, 2019.

- [14]. Lie, Jenni, and Jhy-Chem Liu. "Selective separation of lanthanide group in spent NiMH battery acidic leaching solutions." *Separation and Purification Technology* 307 (2023): 122671.
- [15]. Rahimpour Golroudbary, S., Kraslawski, A., Wilson, B.P. and Lundström, M., 2023. Assessment of environmental sustainability of nickel required for mobility transition.

See discussions, stats, and author profiles for this publication at: <https://www.researchgate.net/publication/372608076>

# Closed-loop control of BLDC motor using Hall effect sensors

Article in *International Journal of Applied Power Engineering (IJAPE)* · September 2023

DOI: 10.11591/ijape.v12.i3.pp247-254

---

CITATIONS

0

READS

90

1 author:



**Kalagotla Chenchireddy**  
Karunya University

53 PUBLICATIONS 160 CITATIONS

SEE PROFILE

## Closed-loop control of BLDC motor using Hall effect sensors

**B. Ramesh, Kalagotla Chenchireddy, Baddam Nikitha Reddy, Bellamkonda Siddharth,  
Chelmala Vinay Kumar, Putta Manojkumar**

Department of Electrical and Electronic Engineering, Teegala Krishna Reddy Engineering College, Hyderabad, India

---

### Article Info

#### Article history:

Received Mar 31, 2023

Revised Apr 27, 2023

Accepted May 7, 2023

---

#### Keywords:

BLDC motor  
Hall effect sensors  
PID controller  
Speed  
Torque

---

### ABSTRACT

Due to its key advantages of top performance, strong torque, and simple volume, brushless direct current (BLDC) motors are now extensively employed in a variety of industrial sectors, including the automotive industry, robotics, and electrical vehicles. Yet, in some circumstances, it can be challenging to use speed control techniques for specific devices. The major goal of this work is to use a proportional integral derivative (PID) converter to regulate the speed characteristics of BLDC. PID converter is preferred over all other converters because of its straightforward design and straightforward implementation. Using MATLAB simulation results are verified at different reference speed changing conditions, the motor input current and back electromotive force (EMF) values are verified. The speed and torque characteristics are verified during steady and transient state conduction.

*This is an open access article under the [CC BY-SA](https://creativecommons.org/licenses/by-sa/4.0/) license.*



---

### Corresponding Author:

Kalagotla Chenchireddy

Department of Electrical and Electronic Engineering, Teegala Krishna Reddy Engineering College

Hyderabad, Telangana 500097, India

Email: [chenchireddy.kalagotla@gmail.com](mailto:chenchireddy.kalagotla@gmail.com)

---

## 1. INTRODUCTION

The significance of brushless direct current (BLDC) motor drives has gained more in the last decades due to their power quality improvement and their extraordinary performance compared with other drives [1], [2]. Field windings and armature windings are located on the stator and rotor, respectively, in DC motors. Because there are brushes and dust has built up in them, upkeep is more expensive. Due to their tendency to arc, DC motors can only be used in certain hazardous industries [3], [4]. The BLDC motor could be changed to resolve this. Because it is more efficient, requires less money, has a large ratio of torque to weight and is simple to operate at all speeds [5], [6]. The importance of taking into account a large ratio of torque to weight is that it has a long operational life, is silent, and is more effective than others [7]. The BLDC motor can solve the issue of electrical erosion and mechanical friction. Hall sensors are used to determine the motor's position [8]. To achieve a smooth speed operation and torque with a low ripple content, the motor must be controlled]. Electronic commutation of the BLDC motors results in trapezoidal back electromotive force (EMF) signals. The proportional integral derivative (PID) controller adjusts the motor's input voltage continually based on the discrepancy between the intended speed and the true speed. The PID controller's proportional, integral, and derivative gains are adjusted to produce the desired responsiveness and stability [9]. In an open loop, BLDC motor the control technique involves voltage control, pulse width modulation (PWM), and frequency control [10]. The open-loop speed control is more accurate than the closed-loop speed control as external factors like temperature and load variations are included [11]–[15]. The open loop BLDC motor model is used in MATLAB, and the responses are used to study under various circumstances.



## 2. BRUSHLESS DC MOTOR

Figure 1 shows the permanent magnet rotor (moving component) and stator windings make up a BLDC motor (fixed part). The brushless DC motor is an AC synchronous motor without brushes or commutators [16]–[19]. It has a compact form, noiseless operation, long operation life, and high efficiency, unlike DC motors. Hall effect sensors (H) monitor the coil's position concerning the motor's magnetic field.

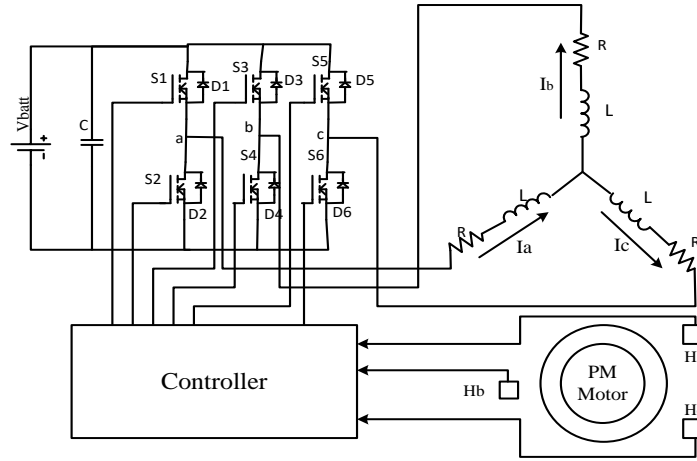


Figure 1. Equivalent circuit of brushless DC motor [4]

A stator is connected in Y in a BLDC motor type, and each phase's resistance and inductance are equal. Losses like those caused by iron cores, eddy currents, and hysteresis are disregarded. The BLDC motor's phase voltage formula is displayed as (1).

$$\begin{bmatrix} u_A \\ u_B \\ u_C \end{bmatrix} = \begin{bmatrix} R & 0 & 0 \\ 0 & R & 0 \\ 0 & 0 & R \end{bmatrix} \begin{bmatrix} i_A \\ i_B \\ i_C \end{bmatrix} + \begin{bmatrix} L - M & 0 & 0 \\ 0 & L - M & 0 \\ 0 & 0 & L - M \end{bmatrix} \frac{d}{dt} \begin{bmatrix} i_A \\ i_B \\ i_C \end{bmatrix} + \begin{bmatrix} e_A \\ e_B \\ e_C \end{bmatrix} \quad (1)$$

Figure 2 shows the back EMF waveforms, Hall effect sensor waveforms and current waveforms of the BLDC motor. The wave forms are varied each 60°, the back EMFs are at each instant one positive, one negative and third EMF zero. A brushless DC motor's electromagnetic torque is computed as (2).

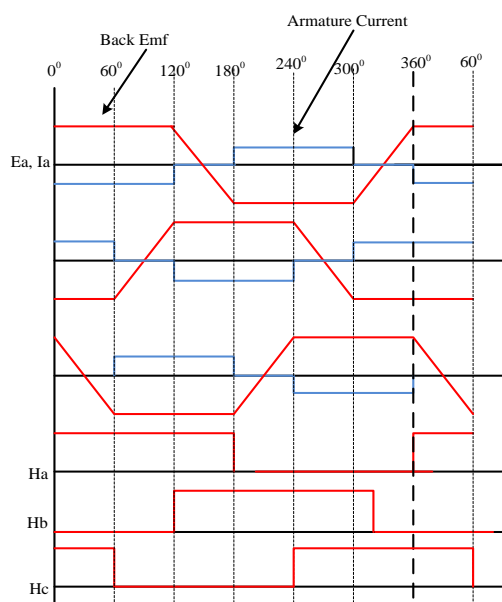


Figure 2. Characteristic waveforms of a BLDC motor [5]

$$T_e = \frac{e_A i_A + e_B i_B + e_C i_C}{\omega_m} \quad (2)$$

Where  $\omega_m$  is the rotational angular velocity in radians per second and  $T_e$  is the electromagnetic torque. To calculate the motion of the BLDC motor:

$$T_e - T_L = J \frac{d\omega_m}{dt} + B_v \omega_m \quad (3)$$

where,  $T_L$  is load torque,  $J$  is the moment of inertia of the motor a  $B_v$  is the friction coefficient. The equation for the relationship between the rotor's location and speed is (4).

$$\frac{d\theta}{dt} = \frac{P}{2} \omega_m \quad (4)$$

Where  $P$  is the number of poles and is the rotor's pole position.

### 3. CONTROL SCHEME

#### 3.1. Brushless DC motor speed adjustment

Figure 3 shows the most popular method of controlling BLDC motors is by the use of Hall sensors, which serve the dual purposes of position and speed sensors. Nevertheless, its primary flaw is that it collects current speed data, which is displayed as inaccurate [20]–[22]. In this paper, we use pulse width modulation (PWM) for controlling the power to the device. The main advantage of this technique is low power losses while switching the devices. Two loops are shown in the block diagram above, one of which is used to measure the speed of the BLDC motor, and the other of which is used to power a three-phase, six-step inverter. The generated torque must match the driver's desired torque and be in control of the brake and accelerate pedals. Torque control is a need. In the range up to the rated speed, torque remains constant. The BLDC motor can operate at its top speed, but the torque may decrease. Torque control can be mainly used in traction units and electric cars.

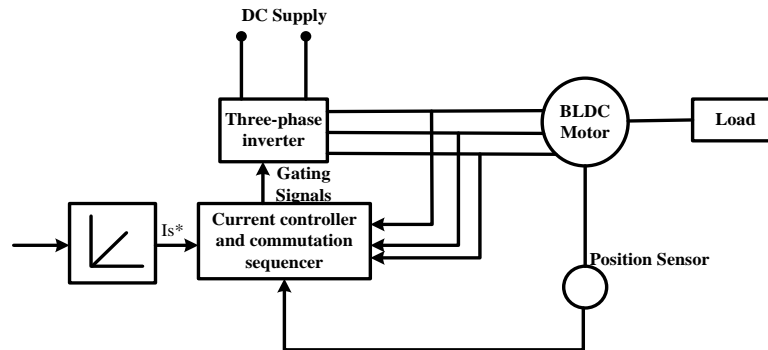


Figure 3. Block chart of the torque control scheme

#### 3.2. PID controller mathematical equations

The motor's speed, torque, and voltage are measured and relayed back as feedback using a PID controller [23]–[25]. The terms proportional (P), integral (I), and derivative (D) make up a PID controller. The controller can shorten the rise time and dampen oscillations.

- The transfer function of the PID controller

$$u(s) = \left[ K_p + \frac{K_i}{s} + K_d s \right] E(s) \quad (5)$$

- Controller equation in the time frame

$$u(t) = K_p e(t) + K_i \int_0^t e(t) dt + K_d \frac{de}{dt} \quad (6)$$

$$u(t) = K_p \left( e(t) + \frac{K_i}{K_p} \int_0^t e(t) dt + \frac{K_d}{K_p} \frac{de}{dt} \right) \quad (7)$$

$$T_i = \frac{K_p}{K_i} \text{ and } T_d = \frac{K_d}{K_p} \tag{8}$$

$$u(t) = K_p \left( e(t) + \frac{1}{T_i} \int^t e(t) dt + T_d \frac{de}{dt} \right) \tag{9}$$

**3.3. Commutation logic**

A brushless DC engine is an electric motor that requires an electronic commutation system to control its speed and direction. Unlike DC motors BLDC motors do not use brushes to transfer the power instead they use a controller to send electric signals to motor windings to generate a rotating magnetic field. Figure 4 shows the logic gate circuit for switching on the inverter circuit. Figure 4(a) shows the Hall effect signal to EMF signal. Figure 4(b) shows the EMF signal to GATES. The Hall effect sensors are used in the control scheme. The Hall effect sensors are a key role in the BLDC motor circuit.

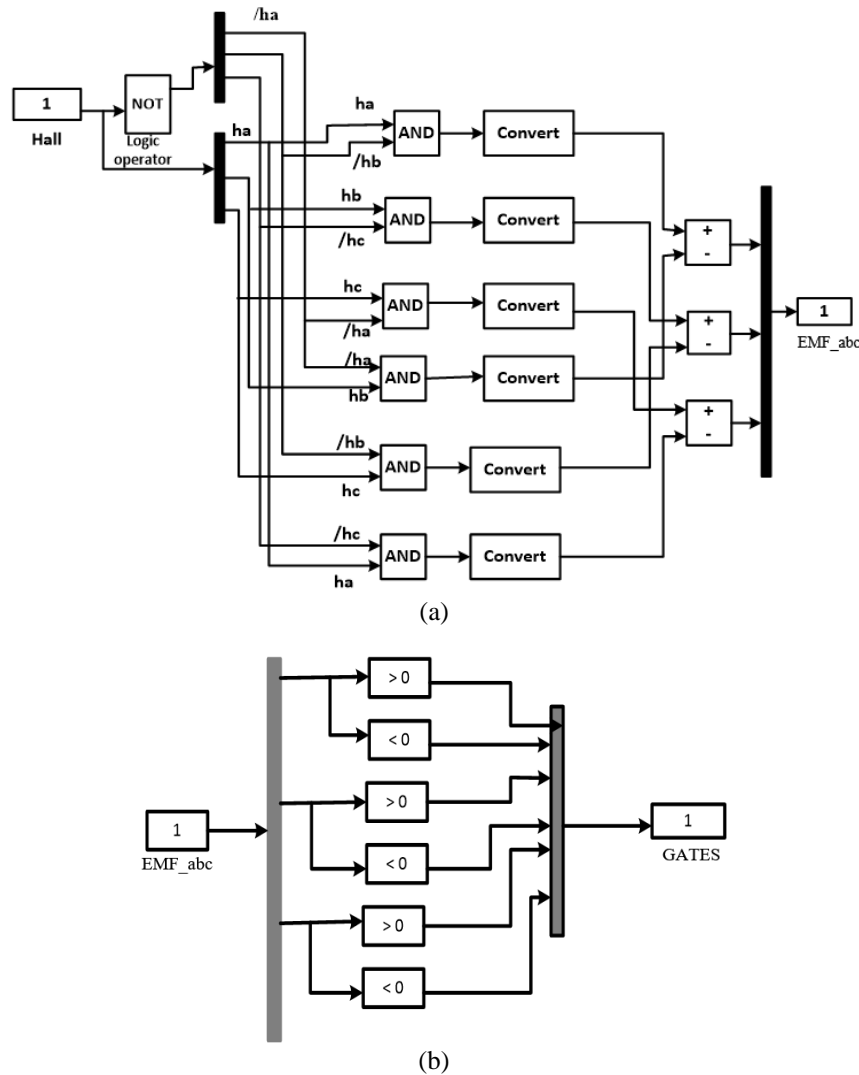


Figure 4. Logic circuit connecting from (a) Hall to EMF and (b) EMF to GATES

**4. SIMULATION RESULTS**

Figure 5 depicts the output response of stator currents of A, B, and C to time. The maximum amplitude of the waveform is 3 A. Phase B and C are the same as phase A but 120 electrical degrees phase shift to each other. Figure 6 depicts the output response of the back EMFs of the engine. The signal is called a TRAPEZOIDAL SIGNAL. The three-phase stator back EMF magnitudes are shown in the figure. The magnitude is 200 V. The magnitude of voltage is 0 to 0.1 s is a very less and transient state.

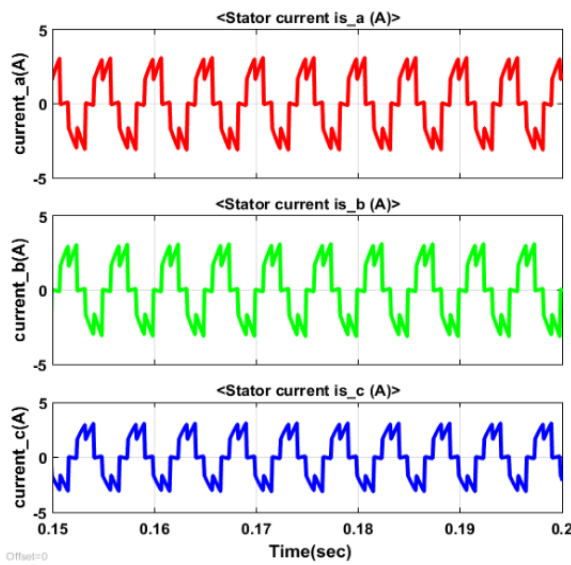


Figure 5. Three-phase stator current characteristics

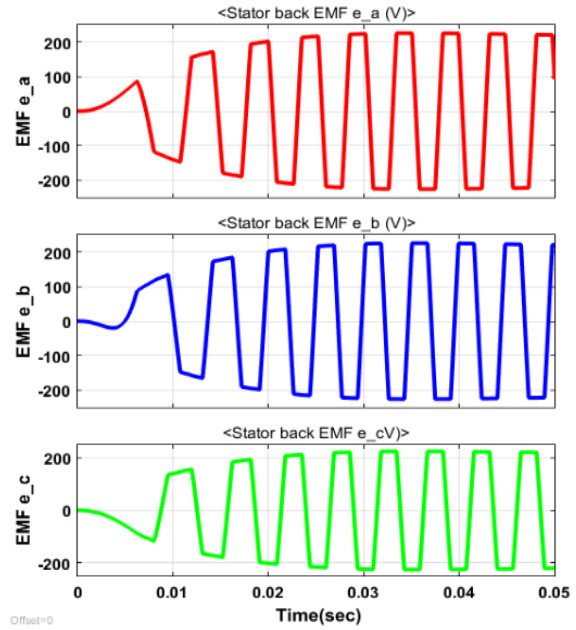


Figure 6. Back EMF characteristics

Figure 7 depicts the output response of the speed-torque characteristics. Here the supply voltage is constant. Speed took 3000 rpm. Here torque is inversely proportional to the speed. Speed is measured in rpm and torque is taken as newton per meter. The motor's rate of spinning depends on the relation between the applied voltage and the loaded torque. Figure 8 depicts the output responses of the Hall effect signals for phases A, B, and C. The signals represent the density of a magnetic field around the device.

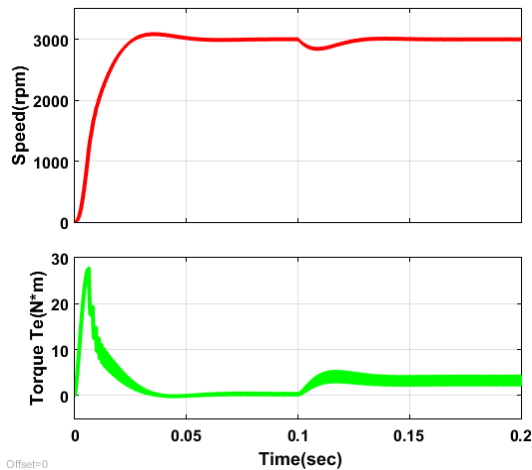


Figure 7. Speed-torque characteristics

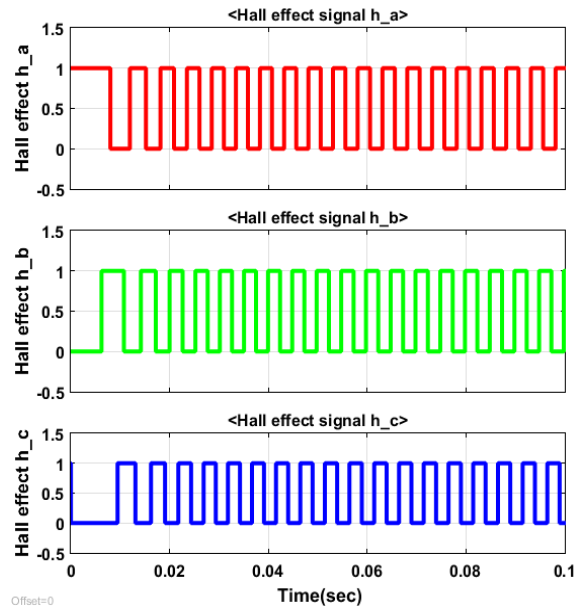


Figure 8. Hall effect signal characteristics

Figure 9 shows the output responses of the motor in two different speed conditions. The Figure 9(a) is taken when the motor speed is 3500 rpm. The Figure 9(b) is taken when the speed is 2500 rpm. From the above speed-torque characteristics we can conclude that the output result doesn't change even if the speed varies.

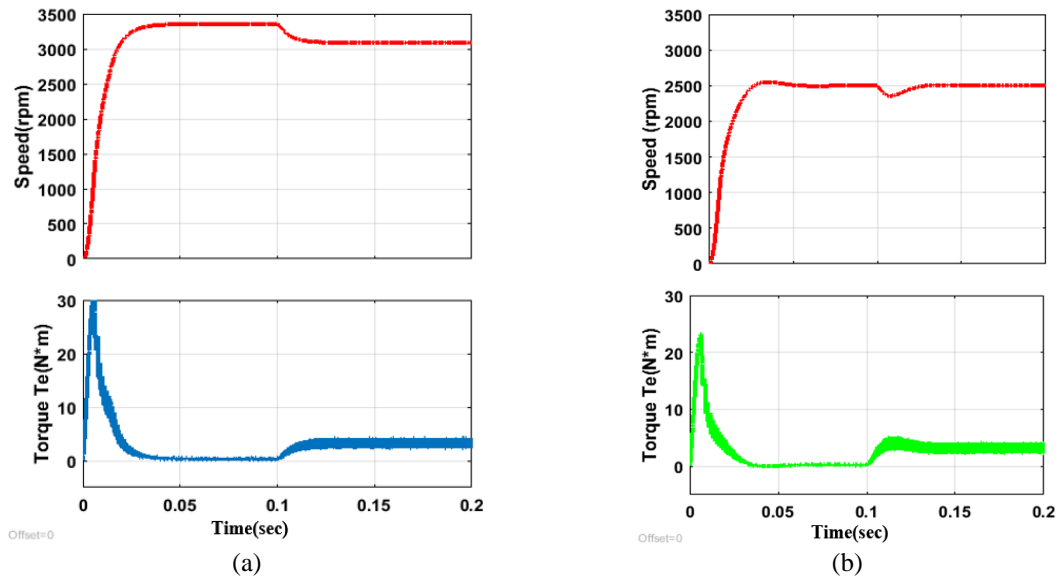


Figure 9. Speed-torque characteristics in different speed conditions (a) reference speed 3000 rpm and (b) reference speed 2500 rpm

## 5. CONCLUSION

This study described how to effectively control the speed of an open loop brushless DC motor. A BLDC engine's pace can be controlled using a PID controller in a variety of applications. Moreover, it offers improved precision and lessens motor wear and tear. The paper's primary goal is to demonstrate how long a motor can operate reliably. MATLAB/SIMULINK software is used to verify the characteristics, including stator current, back EMF, and speed-torque characteristics, which are considered under various speed situations.





## REFERENCES

- [1] R. Prakash and M. Sangeetha, "A Power Factor improvement and Speed Control of BLDC Motor Drive using ANFIS Controller," vol. 3, no. 5, pp. 462–467, 2016.
- [2] K. Chenchireddy, V. Kumar, G. Eswaraiiah, K. R. Sreejyothi, S. A. Sydu, and L. B. Ganesh, "Torque Ripple Minimization in Switched Reluctance Motor by Using Artificial Neural Network," *2022 IEEE 2nd International Conference on Sustainable Energy and Future Electric Transportation, SeFeT 2022*, 2022, doi: 10.1109/SeFeT55524.2022.9909305.
- [3] M. A. A. Aziz *et al.*, "A Review on BLDC Motor Application in Electric Vehicle (EV) using Battery, Supercapacitor and Hybrid Energy Storage System: Efficiency and Future Prospects," *Journal of Advanced Research in Applied Sciences and Engineering Technology*, vol. 30, no. 2, pp. 41–59, 2023, doi: 10.37934/araset.30.2.4159.
- [4] B. N. Kommula and V. R. Kota, "Direct instantaneous torque control of Brushless DC motor using firefly Algorithm based fractional order PID controller," *Journal of King Saud University - Engineering Sciences*, vol. 32, no. 2, pp. 133–140, 2020, doi: 10.1016/j.jksues.2018.04.007.
- [5] P. Suganthi, S. Nagapavithra, and S. Umamaheswari, "Modeling and simulation of closed loop speed control for BLDC motor," in *2017 Conference on Emerging Devices and Smart Systems, ICEDSS 2017*, 2017, pp. 229–233, doi: 10.1109/ICEDSS.2017.8073686.
- [6] V. R. Walekar and S. V. Murkute, "Speed Control of BLDC Motor using PI Fuzzy Approach: A Comparative Study," *2018 International Conference on Information, Communication, Engineering and Technology, ICICET 2018*, 2018, doi: 10.1109/ICICET.2018.8533723.
- [7] K. S. Devi, R. Dhanasekaran, and S. Muthulakshmi, "Improvement of speed control performance in BLDC motor using fuzzy PID controller," in *Proceedings of 2016 International Conference on Advanced Communication Control and Computing Technologies, ICACCCT 2016*, 2017, pp. 380–384, doi: 10.1109/ICACCCT.2016.7831666.
- [8] A. Jaya, E. Purwanto, M. B. Fauziah, F. D. Murdianto, G. Prabowo, and M. R. Rusli, "Design of PID-fuzzy for speed control of brushless DC motor in dynamic electric vehicle to improve steady-state performance," in *Proceedings IES-ETA 2017 - International Electronics Symposium on Engineering Technology and Applications*, 2017, pp. 179–184, doi: 10.1109/ELECSYM.2017.8240399.
- [9] P. H. Krishnan and M. Arjun, "Control of BLDC motor based on adaptive fuzzy logic PID controller," *Proceeding of the IEEE International Conference on Green Computing, Communication and Electrical Engineering, ICGCCEE 2014*, 2014, doi: 10.1109/ICGCCEE.2014.6922372.
- [10] M. Mahmud, S. M. A. Motakabber, A. H. M. Zahirul Alam, and A. N. Nordin, "Adaptive PID Controller Using for Speed Control of the BLDC Motor," in *IEEE International Conference on Semiconductor Electronics, Proceedings, ICSE*, 2020, pp. 168–171, doi: 10.1109/ICSE49846.2020.9166883.





- [11] M. A. Akhtar and S. Saha, "Positive Current Reference Generation based Current Control Technique for BLDC Motor Drives Applications," in *2019 5th International Conference on Advanced Computing and Communication Systems, ICACCS 2019*, 2019, pp. 496–500, doi: 10.1109/ICACCS.2019.8728349.
- [12] K. Chenchireddy, V. Kumar, and K. R. Sreejyothi, "Investigation of Performance Vector Control Single-Phase Induction Motor," in *2021 7th International Conference on Advanced Computing and Communication Systems, ICACCS 2021*, 2021, pp. 887–891, doi: 10.1109/ICACCS51430.2021.9441773.
- [13] P. Pillay and R. Krishnan, "Modeling, simulation, and analysis of permanent-magnet motor drives. I. The permanent-magnet synchronous motor drive," *IEEE Transactions on Industry Applications*, vol. 25, no. 2, pp. 265–273, 1989, doi: 10.1109/28.25541.
- [14] V. Kumar, K. Chenchireddy, K. R. Sreejyothi, and G. Sujatha, "Design and Development of Brushless DC Motor Drive for Electrical Vehicle Application," pp. 201–217, 2022, doi: 10.1007/978-981-19-2184-1\_10.
- [15] T. Y. Lee, M. K. Seo, Y. J. Kim, and S. Y. Jung, "Motor Design and Characteristics Comparison of Outer-Rotor-Type BLDC Motor and BLAC Motor Based on Numerical Analysis," *IEEE Transactions on Applied Superconductivity*, vol. 26, no. 4, 2016, doi: 10.1109/TASC.2016.2548079.
- [16] S. O. Kwon, J. J. Lee, B. H. Lee, J. H. Kim, K. H. Ha, and J. P. Hong, "Loss distribution of three-phase induction motor and BLDC motor according to core materials and operating," *IEEE Transactions on Magnetics*, vol. 45, no. 10, pp. 4740–4743, 2009, doi: 10.1109/TMAG.2009.2022749.
- [17] H. W. Kim, K. T. Kim, Y. S. Jo, and J. Hur, "Optimization methods of torque density for developing the neodymium free SPOKE-type BLDC motor," *IEEE Transactions on Magnetics*, vol. 49, no. 5, pp. 2173–2176, 2013, doi: 10.1109/TMAG.2013.2237890.
- [18] A. Usman and B. S. Rajpurohit, "Comprehensive Analysis of Demagnetization Faults in BLDC Motors Using Novel Hybrid Electrical Equivalent Circuit and Numerical Based Approach," *IEEE Access*, vol. 7, pp. 147542–147552, 2019, doi: 10.1109/ACCESS.2019.2946694.
- [19] J. Shao, "An improved microcontroller-based sensorless brushless DC (BLDC) motor drive for automotive applications," *IEEE Transactions on Industry Applications*, vol. 42, no. 5, pp. 1216–1221, 2006, doi: 10.1109/TIA.2006.880888.
- [20] J. Gao and Y. Hu, "Direct self-control for BLDC motor drives based on three-dimensional coordinate system," *IEEE Transactions on Industrial Electronics*, vol. 57, no. 8, pp. 2836–2844, 2010, doi: 10.1109/TIE.2009.2036027.
- [21] G. H. Jang and C. I. Lee, "Dual winding method of a BLDC motor for large starting torque and high speed," *IEEE Transactions on Magnetics*, vol. 41, no. 10, pp. 3922–3924, 2005, doi: 10.1109/TMAG.2005.854967.
- [22] H. Wang, J. Wang, X. Wang, S. Lu, C. Hu, and W. Cao, "Detection and Evaluation of the Interturn Short Circuit Fault in a BLDC-Based Hub Motor," *IEEE Transactions on Industrial Electronics*, vol. 70, no. 3, pp. 3055–3068, 2023, doi: 10.1109/TIE.2022.3167167.
- [23] B. Bairwa, M. Murari, M. Sahapur, M. R. Kavya, and M. F. Khan, "Drive Cycle Based Speed Control of BLDC Motor Using Pulse Width Modulation," *ICRTEC 2023 - Proceedings: IEEE International Conference on Recent Trends in Electronics and Communication: Upcoming Technologies for Smart Systems*, 2023, doi: 10.1109/ICRTEC56977.2023.10111848.
- [24] T. Yazdan, W. Zhao, T. A. Lipo, and B. Il Kwon, "A novel technique for two-phase BLDC motor to avoid demagnetization," *IEEE Transactions on Magnetics*, vol. 52, no. 7, 2016, doi: 10.1109/TMAG.2016.2521874.
- [25] P. Li, W. Sun, and J. Shen, "Flux observer model for sensorless control of PM BLDC motor with a damper cage," *2017 12th International Conference on Ecological Vehicles and Renewable Energies, EVER 2017*, 2017, doi: 10.1109/EVER.2017.7935909.

## BIOGRAPHIES OF AUTHORS






**B. Ramesh**     is received the B.Tech. and M.Tech. from JNTU Hyderabad, Hyderabad, India, in 2010 and 2012 respectively and pursuing Ph.D. in KLU university, Vijayawada, India. He is working presently as Assistant Professor in Teegala Krishna Reddy Engineering College, Hyderabad, India. He has presented technical papers in various national and international journals and conferences. He can be contacted at email: r.bonigala@gmail.com.






**Kalagotla Chenchireddy**     is received the B.Tech. and M.Tech. from JNTU Hyderabad, Hyderabad, India, in 2011 and 2013 respectively and pursuing Ph.D. in Karunya Institute of Technology and Sciences, Karunyanagar, Coimbatore, TN, India. He is working presently as Assistant Professor in Teegala Krishna Reddy Engineering College, Hyderabad, India. He has presented technical papers in various national and international journals and conferences. His area of interest includes power electronics, power quality, and multilevel inverters. He is regular reviewer ISA Transactions, Cybernetics and Systems SCIE journals. He can be contacted at email: chenchireddy.kalagotla@gmail.com.






**Baddam Nikitha Reddy**    is presently UG Student in Electrical and Electronics Engineering, Teegala Krishna Reddy Engineering College, Hyderabad, India. She has presented technical papers in various national and international journals and conferences. Her area of interest includes power electronics, power quality, and multilevel inverters. She developed electromagnetic train in Teegala Krishna Reddy Engineering College, Hyderabad. She can be contacted at email: [nikithareddy508@gmail.com](mailto:nikithareddy508@gmail.com).






**Bellamkonda Siddharth**    is presently UG Student in Electrical and Electronics Engineering Department, Teegala Krishna Reddy Engineering College, Hyderabad, India. He has presented technical papers in various national and international journals and conferences. His area of interest includes power electronics, power quality, and multilevel inverters. He developed hybrid vehicle in Teegala Krishna Reddy Engineering college Hyderabad. He can be contacted at email: [sidharthbellamkonda@gmail.com](mailto:sidharthbellamkonda@gmail.com).



**Chelmala Vinay Kumar**    is presently UG Student in Electrical and Electronics Engineering Department, Teegala Krishna Reddy Engineering College, Hyderabad, India. He has presented technical papers in various national and international journals and conferences. His area of interest includes power electronics, power quality, and multilevel inverters. He got first prize national level project expo 2023 in NNRG College Hyderabad. He can be contacted at email: [vinaychelimala2422@gmail.com](mailto:vinaychelimala2422@gmail.com).



**Putta Manojkumar**    is presently UG Student in Electrical and Electronics Engineering Department, Teegala Krishna Reddy Engineering College, Hyderabad, India. He has presented technical papers in various national and international journals and conferences. His area of interest includes power electronics, power quality, and multilevel inverters. He developed solar inverter in Teegala Krishan Reddy Engineering College, Hyderabad. He can be contacted at email: [manojyadav7306@gmail.com](mailto:manojyadav7306@gmail.com).

See discussions, stats, and author profiles for this publication at: <https://www.researchgate.net/publication/370558948>

# Grid-Connected 3L-NPC Inverter with PI Controller Based on Space Vector Modulation

Conference Paper · May 2023

DOI: 10.1109/ICACCS57279.2023.10113092

---

CITATIONS

0

---

READS

27

1 author:



[Kalagotla Chenchireddy](#)

Karunya University

53 PUBLICATIONS 160 CITATIONS

SEE PROFILE



# Grid-Connected 3L-NPC Inverter with PI Controller Based on Space Vector Modulation

**Kalagotla Chenchireddy**

Department of EEE  
Teegala Krishan Reddy Engineering  
College  
chenchireddy.kalagotla@gmail.com

**Mulla Gouse Basha**

Department of EEE  
Geethanjali College of Engineering  
and Technology  
m.gousebasha@gmail.com

**Sandhya Dongari**

Department of EEE  
Teegala Krishan Reddy Engineering  
College  
sandhyadongari19@gmail.com

**Praveen Kumar**

Department of EEE  
Teegala Krishan Reddy Engineering  
College  
praveenkumarmadagoni@gmail.com

**G Karthik**

Department of EEE  
Teegala Krishan Reddy Engineering  
College  
karthikgaddam252@gmail.com

**G Maruthi**

Department of EEE  
Teegala Krishan Reddy Engineering  
College  
maruthi13031999@gmail.com

**Abstract**—For a three-level grid-connected neutral point clamped (3L-NPC) inverter, a closed-loop space vector modulation-based PI controller is presented in this paper. The clamp diodes and cascaded dc capacitors used in the diode-clamped multilevel inverter produce multiple-level ac voltage waveforms. Low THD and creating pure sine waves are the key benefits of MLIs. Generally speaking, the inverter can be set up with a three-level, five-level, seven-level, etc. architecture. However, a NPC inverter is only ever referred to as a 3-level inverter. The SVM is one of the well-liked period modulation techniques and is widely used for the digital management of VSIs. The SVM is principally used for generating change pulses. The project SVM results are compare with carrier-based curved PWM (SPWM). The enforced 3L-NPC simulation results are verified in MATLAB/SIMULINK software.

**Keywords**—SVM, PI Controller, Grid-Connected 3-Level 3-Phase NPC Inverter.

## I. INTRODUCTION

The inverts are plays vital role in modern electrical engineering like Electrical Vehicles, robotics and Solar plants. Authors in [1] implemented A novel high-power ANPC Inverter. The implemented inverter is controlled by an improved fault-tolerant control strategy. The control strategy is well operated under short-circuit fault conditions. Reference [2] grid connected three-level inverter had implemented. The inverter is controlled by general mode resonance damp and DC voltage complementary techniques. The implemented controller reduced output current distortion reduced power loss and switching loss. The proposed controller had verified under different load change conditions. The 3-Ph 3-level inverter is controlled by a model predictive controller. The control strategy had well operated in a closed loop. The planned controller is well-operated under steady-state and active conduction [3]. Authors in [4] introduced 3-phase and 4-wire T-Type inverters with the neutral inductor. The zero-sequence voltage controller is implemented for the inverter. The

implemented controller eliminated lower-order harmonics. The reduced device count 4-level 3-phase inverter is presented in [5]. The DC-Link capacitor voltage complementary system had been implement and the low-frequency modulation scheme, as well as level, shifted PWM technique implemented this reference.

Grid-connected three-phase three-wire NPC inverter had implemented in [6]. The implemented controller had controlled by a de-coupled control scheme. The experimental results were verified at different PLL conditions. This paper had different mathematical equations analyzed.

Reference [7] presented an MPC controller for a 3-L NPC inverter. The inverter-controlled PMSM is in this paper. The MPC controller was robust, well operated steady state, and had dynamic conduction. Different topologies of inverters and different SVM techniques are reviewed in [8]-[9]. The infinite-level induction motor is discussed in [10]. The motor was controlled by three-phase VSI, the experimental results verified different load conditions. A modified Z-Source inverter had implemented in [11]. A novel technique is implemented in this reference for balancing DC-Link capacitors. Three-level inverter reduced torque ripples in the induction motor [12]. Level-shifted PWM techniques implemented in [13] for MLI. This SVM-based three-level grid-connected inverter was implemented, in section II inverter topology explained, the section III control technique implemented and the section IV results explained.

## II. GRID-CONNECTED INVERTER

A single pole triple throw switch is also called a three-level inverter. in its place of a two-level inverter, We are using a three-level inverter because we need a multi-level converter. In a three-level inverter, there is a pole R where a load terminal is connected to it. So that we can apply either +V<sub>dc</sub> or -V<sub>dc</sub> to it, which is measured concerning 0 at R. So the quality of waveform will be improved if we connect this R to the midpoint 0 either by positive bus or by negative

bus. This connection is not available in a two-level inverter so we are using a three-level inverter. Three-Level NPC Grid Connected Inverter is shown in Fig. 1.

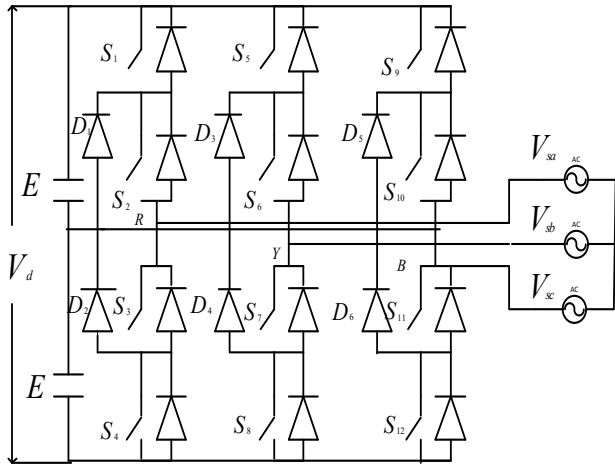


Fig. 1. Three-Level NPC Grid Connected Inverter

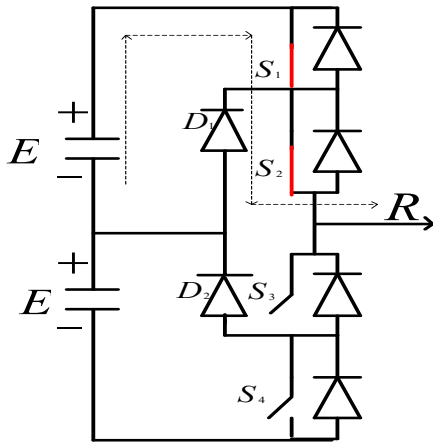


Fig. 2. Mode-I operation

Fig. 2 shows the Mode 1 operation: when the switches S1 and S2 are in the ON position and S3 and S4 are in the OFF position. Then +vdc will goes to the pole R.

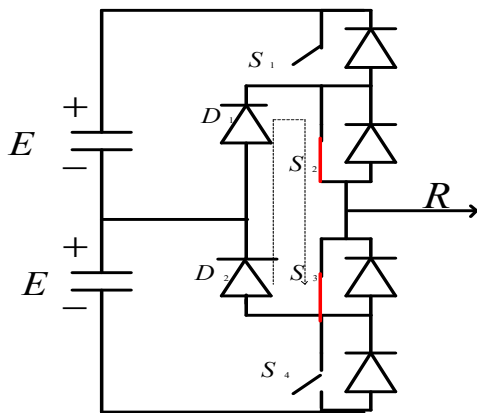


Fig. 3. Mode-II operation

Fig. 3 shows the Mode II operation: whenever the switches S3 and S4 are in the ON position and S1 and S2 are in the OFF position. Then -Vdc will go to the pole R.

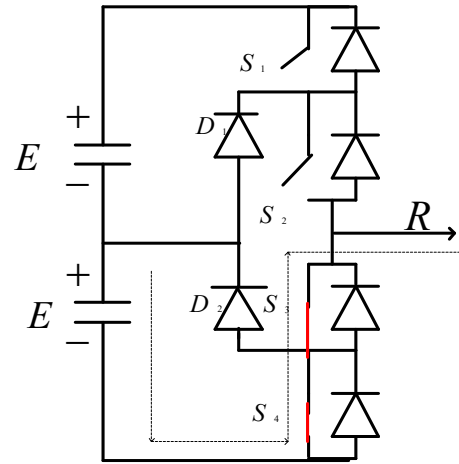


Fig. 4. Mode-III operation

Fig. 4 shows the Mode III process: it is also possible to connect R to O. When the switch S2, and S3 are in the ON position and S1, and S4 are in the OFF position. So that R could establish a connection with O.

Here readily available are two different paths depending on the consignment current i.e., O to R (or) R to O directions. This O is sometimes called DC neutral i.e., neutral point clamped inverter. here we used two diodes which are called clamping diodes, which connect the two midpoints R and O. sometimes these are called Diode clamped inverters or Active clamped inverters. This converter can apply either +Vdc or 0 or -Vdc at the pole regardless of the current direction. We also have another possibility of the case that is case 4.

CASE 4: When the switch S1 and S4 are ON and S2 and S3 are in the OFF position.

Here we neglect this condition because S2, and S3 are open-circuited and there is no load possibility and the NPC inverter is open circuit. Table 1 is showing the positions of switches and their voltage conditions.

TABLE 1

S <sub>1</sub>	S <sub>2</sub>	S <sub>3</sub>	S <sub>4</sub>	V <sub>RO</sub>
ON	ON	OFF	OFF	+V <sub>dc</sub>
OFF	ON	ON	OFF	0
OFF	OFF	ON	ON	-V <sub>dc</sub>

Let switching states for three cases are: P(+), 0, N(-)

By observing the above table 1 we find that

1. S1 and S3 are complimentary. when S1 is low then S3 is high and vice versa.

2.S2 and S4 are complimentary. When S2 is low then S4 is high and vice versa.

In a three-level inverter there are two pairs of complementary switches. For two pairs of complementary switches, we need to generate two getting signals. Which will significantly change. For the two-level, we generate one sine wave with one triangle. but for the three-level, we need to generate one sine wave with two carriers and sometimes it can also be two sine waves with one carrier.

Instantaneous pole voltages, line-line voltages and line-neutral load voltages

$$V_{RO}=0, \pm V_{dc}/2; \quad V_{YO}=0, \pm V_{dc}/2; \quad V_{BO}=0, \pm V_{dc}/2$$

When the middle two switch in the R phase then  $V_{RO}=0$  and  $\pm V_{dc}/2$ . Similarly  $V_{YO}$  and  $V_{BO}$ .

$$\begin{aligned} V_{RY} &= V_{RO} - V_{YO}; & V_{RN} &= (V_{RY} - V_{BR})/3. \\ V_{RY} &= \pm V_{dc}, \pm V_{dc}/2, 0 & V_{RN} &= \pm 2V_{dc}/3, \pm V_{dc}/2, \pm V_{dc}/3, \\ & & & \pm V_{dc}/6, 0 \end{aligned}$$

### III. SPACE VECTOR MODULATION

For the three-level NPC inverter, several SVM schemes have been suggested. The NPC inverter is presented using conventional SVM, and then the even command vocal elimination is achieved using a customized SVM system. SVPWM diagram is shown in Fig. 5.

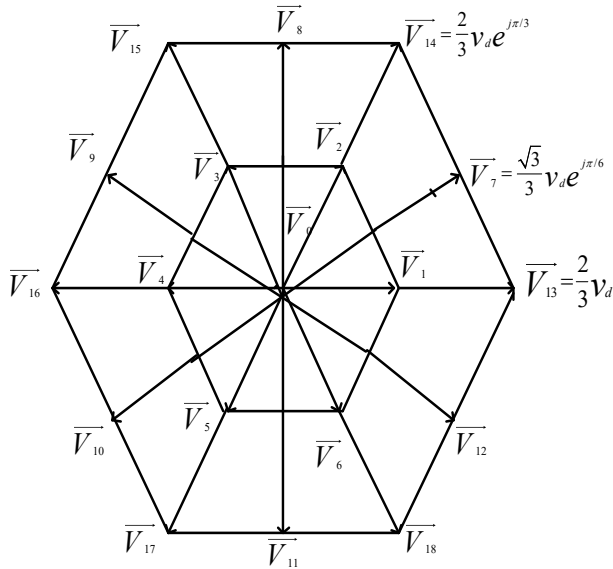


Fig. 5. SVPWM diagram

Synchronous reference frame (SRF) theory-based PI controlled implemented in this project. The SRF theory converts three-phase to two-phase and two-phase three-phase. This total conversion is used for controlling direct-axis and quadrature-axis currents. In AC currents we need to control magnitude and phase angle; in DC systems we need

to control only magnitude. This is the main advantage of the conversion system. The SVM-based PWM generator will implement in this project, these PWM techniques total 21 vectors, six tiny vectors, six intermediate vectors, six fat vectors and two zero vectors.

Base on their scale (length), the voltage vectors be able to be classified into four groups, as shown in the vector diagram above.

VECTOR ZERO: The magnitude of  $v_0$  in the three switching states [+++] [000] and [---] is zero.

SMALL VECTOR: The magnitudes of (V1 to V6) are all equal to  $V_d/3$ . There are two switching states for each tiny vector. One was classed as a P-type minute vector and the other as an N-type minute vector since one contained [+ ] and the other contained [-].

Large vectors (V13–V18) have a scale of  $2V_d/3$ , while medium vectors (V7–V12) have a scale of  $3V_d/3$ .

Here in the R-phase top two devices are ON and in the Y-phase top two devices are ON and in the B-phase bottom two devices are ON and the pole voltages are  $+V_{dc}/2, +V_{dc}/2, -V_{dc}/2$ . This case is also possible in a two-level inverter and vectors 2, 3,4,5,6 are like to that of the two-level inverter. Here R phase has three possibilities and Y phase has 3 possibilities and the B phase has three possibilities. This means that there are 27 possible switching state combinations. Only 6 states out of 27 have been accounted for. We can determine the connection between the switching states and the related voltage vector by looking at the diagram above. Out of 27 inverter states, these 6 vectors lead to 6 active vectors, all having a magnitude of  $V_{dc}/2$ . So that two of them produce the same vector. The three-level inverter gives us much more opportunities to explore and design new PWM methods than a two-level inverter.

### DWELL TIME CALCULATION

$$\begin{cases} \overline{V}_{ref} T_s = \overline{V}_1 T_a + \overline{V}_2 T_b + \overline{V}_o T_o \\ T_s = T_a + T_b + T_o \end{cases} \quad (1)$$

The SV drawing can be alienated into six triangular sector, which are then additional alienated into four triangular region based on the SVM algorithm to calculate the dwell time. As is well known, the SVM is founded on the 'volt-second balancing' principle. The reference voltage and sampling time are combined to form the term "voltage second balancing," which is equal to the sum of voltage times the duration of space vectors.

Let us take a triangular region whose tip falls in it as shown in Fig. 6.

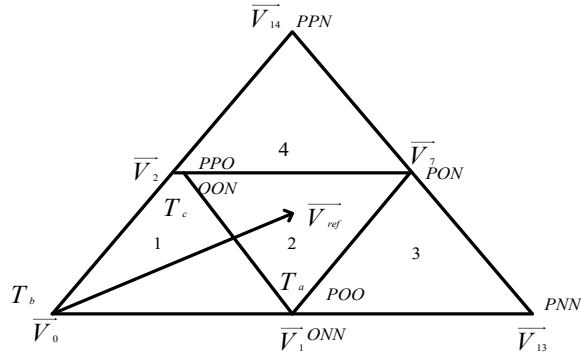


Fig. 6. Triangle VECTOR diagram

Whenever we are applying the two active vectors, the error is very high due to the longest duration. To reduce this error, we need to apply the three closest vectors. so that the error is so small. This error voltage vector is nothing but the harmonics and the ripple voltages in all three phases. if we transform the ripple voltages in all three phases into the space vector domain that becomes the error vector

If the instantaneous error vector is low then the integral instantaneous stator flux ripple and instantaneous current ripple are going to be low. That is the reason why a three-level inverter gives us better waveform quality.

#### IV. SIMULATION RESULTS

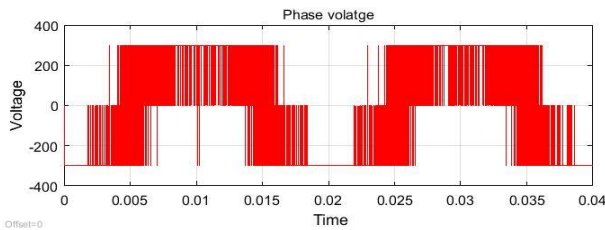


Fig. 7. Three levels NPC inverter phase voltage

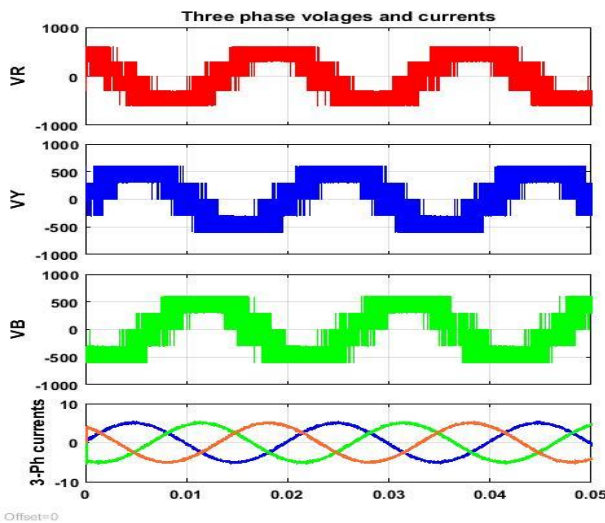


Fig. 8. Three-phase line voltages and currents

The inverter output phase voltage is exposed in Fig. 7. Peak to peak, the phase voltage is 300V in magnitude. The wave shows like square wave. The three-phase voltages and currents be displayed in Fig. 8. The three-phase voltages are 1200 phase shift each other. The magnitude of the line voltage is 500V. The magnitude of three phase currents is 5A.

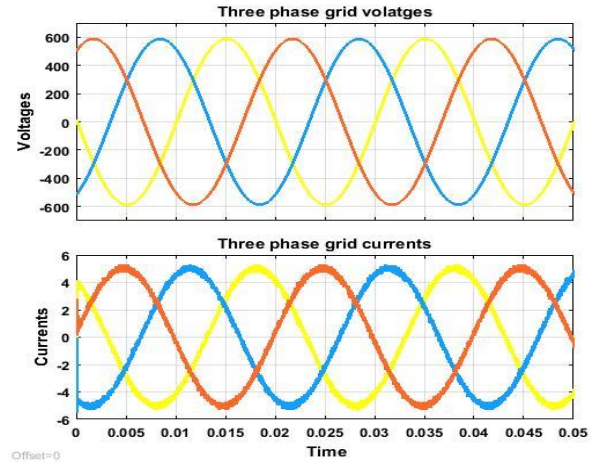


Fig. 9. Three phase grid side line voltage and currents

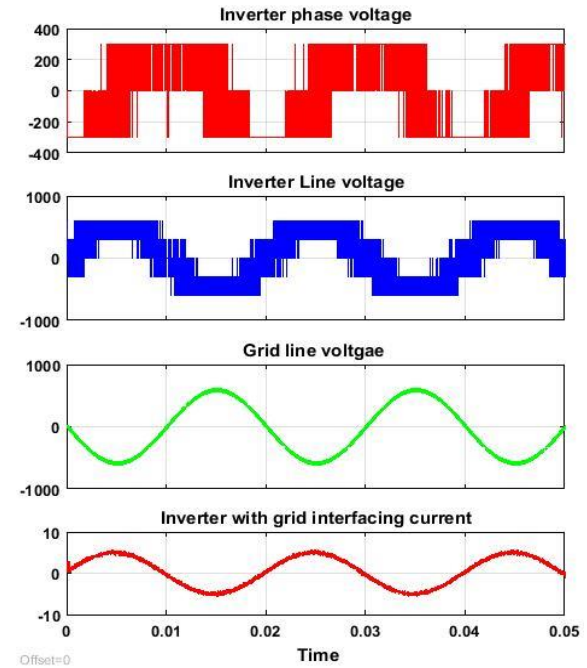


Fig. 10. Inverter phase voltage, line voltage, grid line voltage and current

Fig. 9 shows the three-phase grid side currents as well as current waveforms. Fig. 10 shows the single-phase inverter output voltage and current. The magnitude of the current is 5A. Fig. 11 show the THD value of the grid side current.

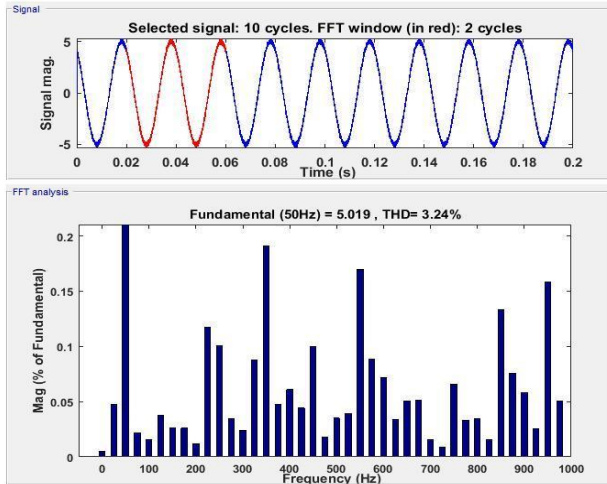


Fig. 11. Phase current THD value

When we compare the average pole voltage in 2L and 3L inverters the error is very high in 2-level inverters. Whereas the error is low in 3-level inverters. This indicates the low harmonic content of the current. So that we can vary it sinusoidal [VRO, VYO, VBO]. In the case of 3-level inverters, we have two pairs of complementary switches, which is different from 2-level inverters. So that we have 2-level shifted carriers.

Here, there is a torque that runs between 0 and 1 and the other torque runs between 0 and -1. so R, Y, and B are un compared here but with help of switching logic, their voltage is known. We can also do a phase shifting of level-shifted carriers for 3-level inverters which will not affect the fundamental voltage. The final experimental findings demonstrate the system's robustness without any outside disturbances and high dynamic performance with reduced THD.

## V. CONCLUSION

For a grid-connected, three-level NPC inverter, a potential integral control method based on SVM has been carried out in this paper. Due to their high importance, MLIs acquires more vogue for both low and high-power applications in research, medical and other industrial applications. Known as a feedback control loop, a potential integral controller determines the error signal by comparing the output of each system in the grid. This is due to NPC inverters requiring DC. In this project switching of SVM and PI control is integrated with the voltage balancing technique.

The main reason to design this system is to generate a pure sine wave without any external perturbations and unwanted harmonics. This PI control-SVM grid technique allows low THD current, high power factor, and has low ripples, this also operates at a steady switching frequency. Also, the competence of the planned topology is elevated.

## REFERENCES

- [1] Xu, S. Z., Wang, C. J., & Wang, Y. (2019). An improved fault-tolerant control strategy for high-power ANPC three-level inverter under short-circuit fault of power devices. *IEEE Access*, 7, 55443-55457.
- [2] Zhao, R., Wang, C., Yan, Q., Xu, H., & Blaabjerg, F. (2020). Common-mode resonance damping and DC voltage balancing strategy for LCCL-filtered three-level photovoltaic grid-tied inverters. *IEEE Access*, 8, 13228-13239.
- [3] Andino, J., Ayala, P., Llanos-Proano, J., Naunay, D., Martinez, W., & Arcos-Aviles, D. (2022). Constrained modulated model predictive control for a three-phase three-level voltage source inverter. *Ieee Access*, 10, 10673-10687.
- [4] Zhang, L., Yang, H., Wang, K., Yuan, Y., Tang, Y., & Loh, W. K. (2021). Design methodology for a three-phase four-wire T-type inverter with the neutral inductor. *CPSS Transactions on Power Electronics and Applications*, 6(1), 93-105.
- [5] Salem, A., Van Khang, H., & Robbersmyr, K. G. (2021). Four-Level Three-Phase Inverter With Reduced Component Count for Low and Medium Voltage Applications. *IEEE Access*, 9, 35151-35163.
- [6] Zhang, B., Du, X., Zhao, J., Zhou, J., & Zou, X. (2020). Impedance modeling and stability analysis of a three-phase three-level NPC inverter connected to the grid. *CSEE Journal of Power and Energy Systems*, 6(2), 270-278.
- [7] Gu, M., Wang, Z., Yu, K., Wang, X., & Cheng, M. (2021). Interleaved model predictive control for three-level neutral-point-clamped dual three-phase PMSM drives with low switching frequencies. *IEEE Transactions on Power Electronics*, 36(10), 11618-11630.
- [8] Chenchireddy, K., Jegathesan, V., & Ashok Kumar, L. (2020). Different topologies of inverter: a literature survey. *Innovations in Electrical and Electronics Engineering*, 35-43.
- [9] Chenchireddy, K., & Jegathesan, V. (2021). A Review Paper on the Elimination of Low-Order Harmonics in Multilevel Inverters Using Different Modulation Techniques. *Inventive Communication and Computational Technologies*, 961-971.
- [10] Hareesh, A., & Jayanand, B. (2021). Scalar and vector controlled infinite level inverter (ILI) topology fed open-ended three-phase induction motor. *IEEE Access*, 9, 98433-98459.
- [11] Huynh, A. T., Ho, A. V., & Chun, T. W. (2020). Three-phase embedded modified-z-source three-level T-type inverters. *IEEE Access*, 8, 130740-130750.
- [12] Hakami, S. S., Alsofyani, I. M., & Lee, K. B. (2019). Torque ripple reduction and flux-droop minimization of DTC with improved interleaving CSFTC of IM fed by three-level NPC inverter. *IEEE Access*, 7, 184266-184275.
- [13] Sreejyothi, Khammampati R., et al. "Level-Shifted PWM Techniques Applied to Flying Capacitor Multilevel Inverter." 2022 International Conference on Electronics and Renewable Systems (ICEARS). IEEE, 2022.

# Fuel Cell based Grid Connected Two-Level Inverter

Khammampati R Sreejyothi  
Assistant Professor

Dept. of Electrical and Electronics  
Engineering  
Teegala Krishna Reddy Engineering  
College  
Hyderabad, Telangana, India.  
krs.jyothi@gmail.com

Kalagotla Chenchireddy  
Assistant Professor

Dept. of Electrical and Electronics  
Engineering  
Teegala Krishna Reddy Engineering  
College  
Hyderabad, Telangana, India  
[chenchireddy.kalagotla@gmail.com](mailto:chenchireddy.kalagotla@gmail.com)

Musku Jahnavi  
UG Student

Dept. of Electrical and Electronics  
Engineering  
Teegala Krishna Reddy Engineering  
College  
Hyderabad, Telangana, India  
janureddy2912@gmail.com

Siddu Boini  
UG student

Dept. of Electrical and Electronics  
Engineering  
Teegala Krishna Reddy Engineering  
College  
Hyderabad, Telangana, India.  
boinisiddu1526@gmail.com

Rakesh Ganna  
UG student

Dept. of Electrical and Electronics  
Engineering  
Teegala Krishna Reddy Engineering  
College  
Hyderabad, Telangana, India  
rakeshganna18@gmail.com

Vatti Prashanth  
UG Student

Dept. of Electrical and Electronics  
Engineering  
Teegala Krishna Reddy Engineering  
College  
Hyderabad, Telangana, India  
prashanthvatti123@gmail.com

**Abstract:** This study introduces a grid-connected inverter powered by fuel cells (FC). Though comparable to a battery, the fuel cell does not store energy. DC voltage is continuously supplied to the fuel cell. Oxygen (O<sub>2</sub>) and hydrogen (H<sub>2</sub>) are used as fuel inputs. In this research study, fuel cell is connected to a two-level inverter, and the inverter output is linked to a segregation transformer, whose output is connected to the grid. The primary goal of this study is to use renewable energy sources to lessen air pollution. There has been a lot of recent study on EVs powered by fuel cells. MATLAB/ Simulation software is used to validate the fuel cell results.

**Keywords:** fuel cell, micro-grid, voltage, current

## I INTRODUCTION

The smart micro grid design in reference [1], has different input sustainable efficiency sources like wind, solar and photovoltaic. The inverter is used for converting DC-AC. Fuel cells and hydrogen technology can provide clean, efficiency and sustainable electrical power wherever and whenever it is needed. The designed micro grid was used for Electric Vehicle battery charging and domestic loads. Modified teaching learning algorithm is implemented in this study. The algorithm controlled the micro-grid system. The hybrid electric vehicle is presented in [2]. The hybrid vehicles have two different input sources one is battery and other one is fuel cell. The fuel cell has clean and green energy generating power. The fuel cell used a secondary source in HEV. Fuel cell based distribution system is implemented in [3]. Frequency control technique was introduced in this study. In this study mathematical formulas are analyzed. The implementation of micro grid technology can emphasize the dependability of the power systems by beneficence of self-heal performance at low voltage levels and reducing air pollution. Generally speaking, fuel cells are employed mostly for transportation technology, household applications, portable use and stationary power generation [5]. The characteristics of fuel cells are partly

distributed and nonlinear, which are mainly required for the analyzing of the system design [6]. In general, the fuel cell's contribution to the frequency control approach can be divided into two categories: frequency regulation and island grids [8]. With a set-point reference frequency, it was possible to regulate the fuel cell inverters for output power requirements [9]. Through local control systems, frequency modulation of the fuel cells is discovered to be outsourced [10]. This research presents FC based grid connected system. Fuel cells are ecofriendly distributed generation systems. They are environmentally responsible because the demand for electric power and environmental restrictions may rise as a result of the greenhouse gas emissions [9]. The electrochemical cells convert the chemical energy into electrical energy [10]. One of the most attractive distributed generation techniques for power transmission is fuel cells [3]. The economic operation of microgrids can vary the topology of the feeder only through the reconfiguration process, which is another feature of them [4]. The two-level inverter provides a clean and stable power supply for grid-tied applications. It offers a sustainable energy solution that can help in mitigating the energy crisis and environmental problems [5]. With continuous technological advancements in fuel cell technology and inverter scheme, the fuel cell is based grid connected two-level inverter is predictable to play an important part in the upcoming energy generation and distribution [9]. Due to their energy conversion efficiency is more and emissions are low, FC have developed a popular clean and effective choice for converting energy. The two-level inverter is the key component of the system and is responsible for converting the DC signal into an AC signal suitable for grid connection [7]. The benefit of AC Micro grids is that they utilize some converters to supply AC power straight to AC then DC loads. The effective control plan is used to plan the hybrid energy sources in AC micro grid to generate an ideal energy management system [4]. Fuel cells generate power by a unit cell that contains a strong current but a low voltage. Grid voltage wave can result in lowest frequency

ripples in the FC output current in a FC built power production scheme which is linked to the network. The low-frequency ripple should not exceed 15% of the fuel cell's output (100–120 Hz), as this will boost the FC proficiency and prolong its lifecycle [6]. As same as the battery, the primary frequency control can also be used by FC power plants. Dependent on the FC technology, a fuel processor is employed to deliver hydrogen-rich fuel to the fuel cell. FC frequency management is more locally controlled thanks to local systems [7]. Because the fuel cells won't be able to react quickly to such rapid load changes, the batteries must be allied to the fuel cells either in parallel or in series to serve as an impermanent energy storing part that supports setup or unexpected load adjustments. An organic model or a primary/additional order typical is utilized for the analysis of FC systems in order to understand the sluggish dynamic of the FC [1]. Each element in fuel cell architecture is evaluated based on its power, energy capacity, and voltage boundary conditions [2]. FC are broadly used in many countries for their specific purposes. FC work by merging a fuel, as hydrogen, with an oxidizing agent, such as oxygen, in the presence of an electrolyte. This reaction produces electricity, heat and water. The electricity can be used to power a wide range of applications, from cars to buildings [6]. One of the main advantages of FC is they have high efficiency. With this they can convert up to 60 % of energy in fuel into usable electricity, compared to around 20% for internal combustion engines. FC have the potential to be a very efficient and clean source of power [3]. They produce electricity with very little pollution, emitting only water vapor and heat. FC are a promising technology that has the potential to revolutionize the way we generate power [1]. These are becoming increasingly popular as a clean, efficient, and versatile power source for a variety of applications. In the electric vehicles the FC are used as alternative to batteries [6]. FC electric vehicles are already being deployed in some countries and major automakers are investing heavily in their development. These are being developed for use in portable electronic devices such as laptops, smartphones, and drones. These FC offer longer run times than batteries and can be refueled quickly and easily, they are developed by a number of companies and are expected to become more widely available in the coming years [8]. FC offer a promising alternative to traditional power sources in a variety of applications offering low noise levels. As research and development continues, FC are likely to become even more widely adopted in the years to come [10]. These FC are likely to play an increasingly important role in global energy landscape, driven by their potential to reduce the greenhouse gas emissions, increase energy efficiency, and provide power in a wide variety of settings [9]. Two-level inverter can be easily integrated into overall system design, and they require minimal maintenance and upkeep [2]. As FC technology continues to improve and costs continue to decline. One key advantage of a two-level inverter is its ability to provide high-quality power that is synchronized. It does not cause disruptions or other problems on the electric grid [8].

## II FUEL CELL

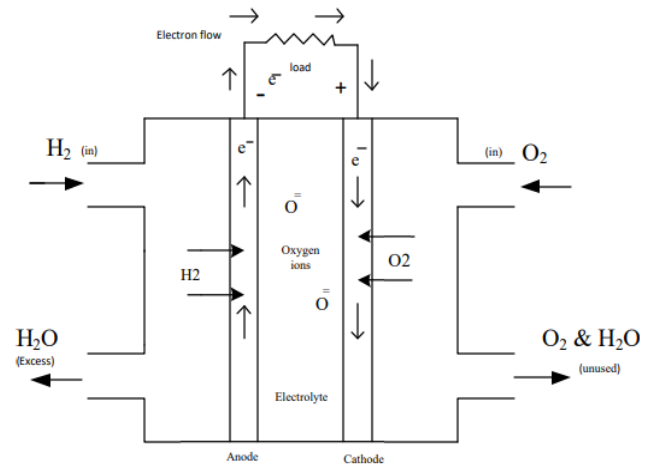


Fig.1 fuel cell illustration

Figure.1 shows the diagram of the fuel cell. The FC is like a battery but they do not need recharge. They produce voltage continuously. The Fuel cell is operating at high efficiency in combustion engine. In this cell, chemical energy will be transformed into electrical energy. Both the anode and cathode which are in fuel cell are two electrolytic plates that are divided by an electrolyte membrane. Oxygen (O<sub>2</sub>) passes via the cathode and hydrogen (H<sub>2</sub>) passes over the anode.

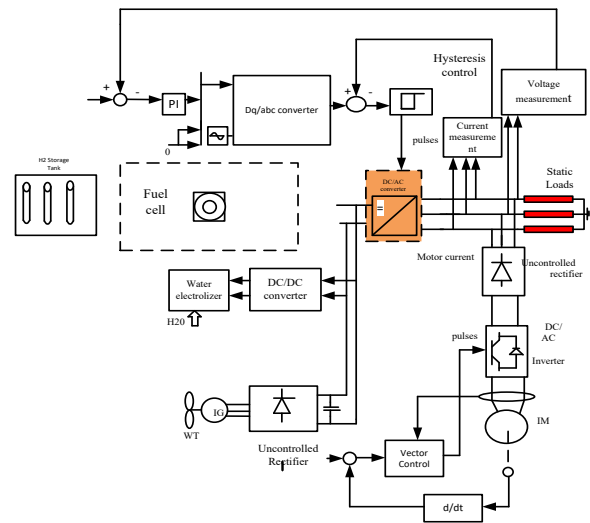


Fig.2 micro grid system with wind/fuel cell [11]

Fig.2 shows the micro-grid connected hybrid energy source. Wind and fuel cells are examples of hybrid sources. The DC-AC converter input is coupled to the fuel cell and wind outputs. In this paper inverter pulses are generated HCC. The active power controller has controlled this paper.

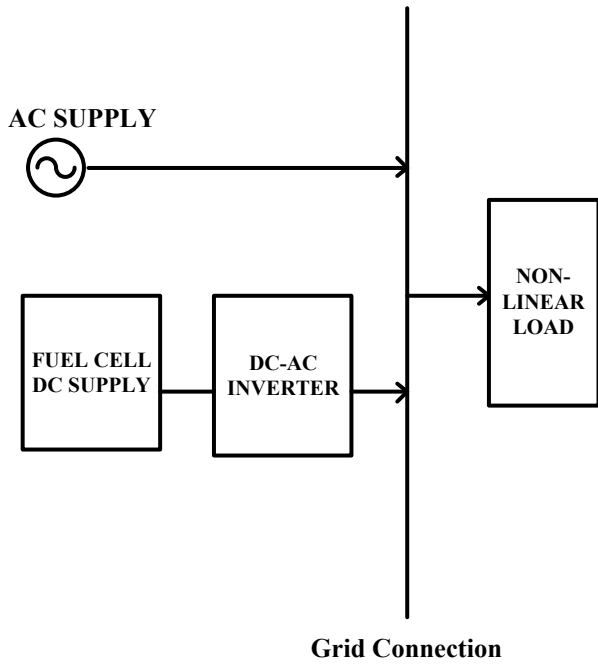


Fig.3 proposed block diagram

Figure.3 displays the single line diagram of the FC and grid connection. Single line diagrams have mainly four blocks one is supply, Non-linear load, fuel cell DC supply and inverter.

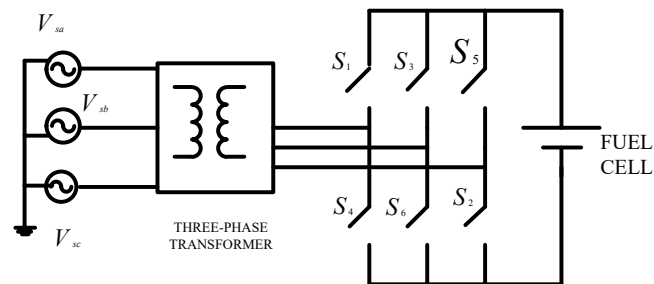


Fig .4 proposed schematic picture

Figure.4 represents the grid-connected FC. A fuel cell, a three-phase two-level inverter, an isolation transformer, and a three-phase supply are all involved in this circuit. The three-phase grid supply is connected to transformer's other end, the inverter output is connected to the transformer's one end, and the FC output voltage is connected to the inverter's input.

$$V_{ab} = \sum_{n=1,3,5}^{\infty} \frac{4V_s}{n\pi} \cos \frac{n\pi}{6} \sin n(\omega t + \frac{\pi}{6}) \quad (1)$$

$$V_{ab} = \sum_{n=1,3,5}^{\infty} \frac{4V_s}{n\pi} \cos \frac{n\pi}{6} \sin n(\omega t - \frac{\pi}{2}) \quad (2)$$

$$V_{ab} = \sum_{n=1,3,5}^{\infty} \frac{4V_s}{n\pi} \cos \frac{n\pi}{6} \sin n(\omega t + \frac{5\pi}{6}) \quad (3)$$

Equation (1), (2) and (3) are the three-phase inverter output voltages.

### III CONTROL SCHEME

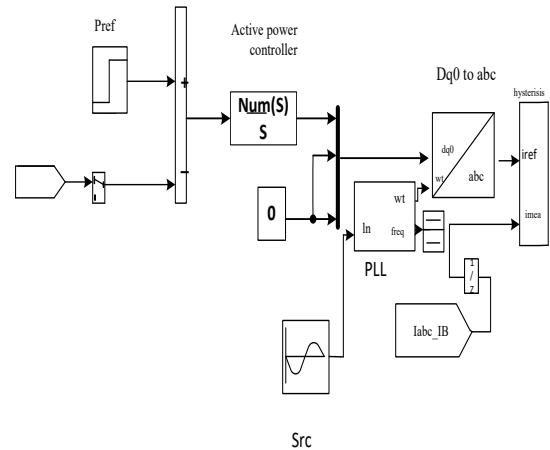


Fig.5 shows the control strategy

The figure.5 displays the control strategy of inverter, this control scheme has major components power reference represented Pref, grid power PQ\_IB, active power controller, mux block, inverse park transformation, reference current Iref and Imean.

The powers are taken from grid and reference power. The active power controller block it controllers active power, the reactive power zero in above controller and zero sequence power also zero. The mux block has three input powers active and reactive power, third one is zero sequence power. The inverse park transformation outputs are three-phase reference currents. [11-14]

This control scheme has PLL. The PLL is generated phase angle and it locks the input and output voltage.

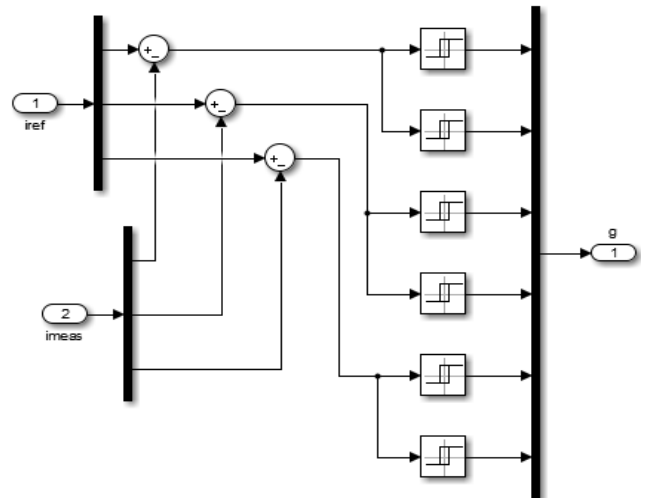


Fig.6 shows hysteresis controller

The fig.6 shows the hysteresis current controller (HCC). The current controllers have two reference currents one is Iref and other is Imean. The HCC is used for controlling current saturation, upper limit or lower limit of current values.



### IV SIMULATION RESULTS

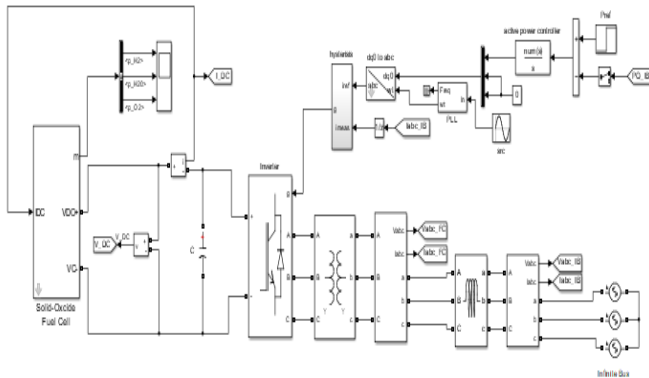


Fig.7 Fuel cell simulation Diagram

Fig.7 shows the fuel cell simulation has mainly four blocks. These are fuel cell, inverter, transmission and supply. The fuel cell block has an input terminal called  $I_{dc}$  and two output voltage terminals labelled  $+V_{dc}$  and  $-V_{dc}$ . The output current is represented as  $I_{DC}$  and the output voltage is represented as  $V_{DC}$ . The inverter input is linked to the complete cell output terminals. The three-phase transformer is linked to the single-phase two-level inverter's output terminals. Three-phase measurement port is associated to the three-phase output terminals. Three-phase measurement port has two output ports, one of which represents the three-phase output voltage as  $V_{abc\ FC}$  and the output current as  $I_{abc\ FC}$ . The simulation diagram has connected three-phase grid supply.

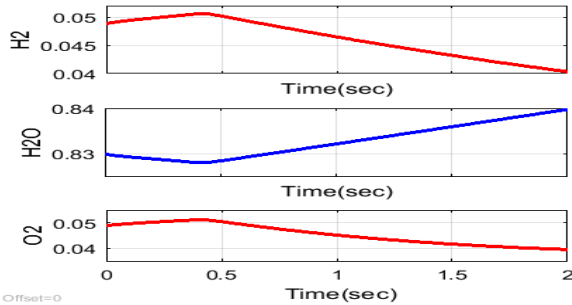


Fig.8 Oxygen (O<sub>2</sub>), Hydrogen (H<sub>2</sub>) and H<sub>2</sub>o

The fig.8 shows the hydrogen and oxygen the output is redox. The fuel cell inputs are H<sub>2</sub>, O<sub>2</sub> and outputs is H<sub>2</sub>o. When the inputs are H<sub>2</sub> and O<sub>2</sub> decreasing the output is increasing.

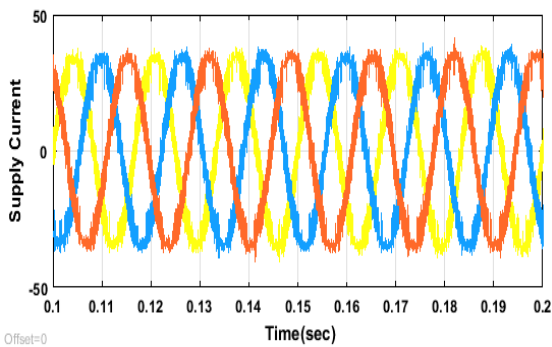


Fig.9 demonstrates the supply current

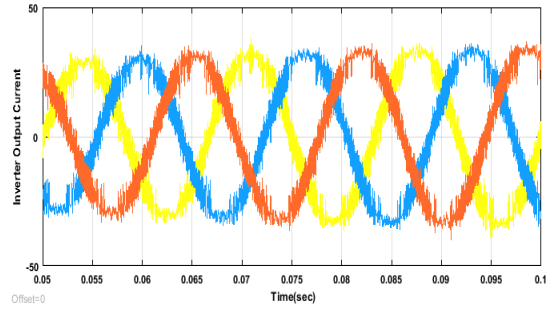


Fig.10 demonstrates the inverter output current.

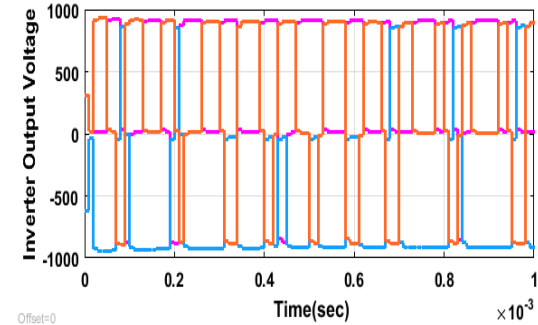


Fig.11 demonstrates the inverter's output voltage.

Fig.9 demonstrates the three-phase supply current. There are certain distortions in the wave shape. Fig.10 demonstrates the distorted inverter output current. Fig.11 Square wave is the wave form used to represent the inverter output voltage.

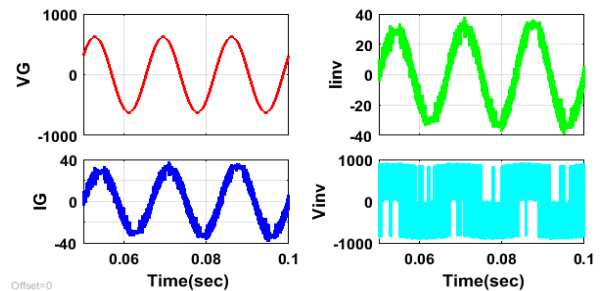


Figure.12 displays the system single phase waveforms.

Figure 12 displays the single-phase waveforms. In which X-axis and Y-axis are taken as time(sec) and output current, output voltage (ground current, ground voltage) respectively.

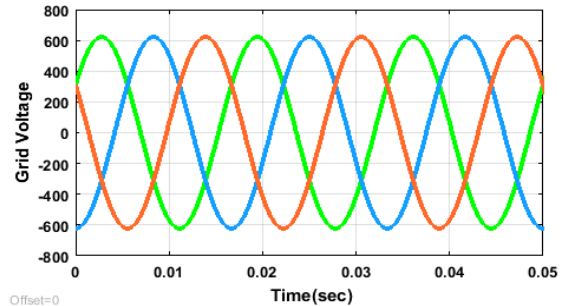


Fig.13 displays the three-phase grid voltage.

figure.13 demonstrates the three-phase grid voltage, which has an amplitude of 600V. This section total represents the simulation results; Grid current, inverter output current, grid voltage, and various single phase output waveforms are the outcomes for the fuel cell.

## V CONCLUSION

This article discussed grid-connected fuel cells. The fuel cell is comparable to a battery but does not store energy. The fuel cell operates on a constant DC voltage supply. Oxygen (O<sub>2</sub>) and hydrogen (H<sub>2</sub>) serve as the fuel inputs (O<sub>2</sub>). The output of the two-level inverter linked to the isolation transformer, and the output of the isolation transformer associated to the grid. This fuel cell in this study uses renewable energy sources to achieve its principal goal of lowering air pollution. Recent day's lots of researches are going on fuel cell based EV. Using the MATLAB/ Simulation programmed the fuel cell results are confirmed. The output results are fuel cell inputs oxygen and hydrogen.

## REFERENCES

- [1]. Dejie Zhao, et all (2021). "Dispatching Fuel-Cell Hybrid Electric Vehicles toward Transportation and Energy Systems Integration." CSEE Journal of power and Energy Systems.
- [2]. Jesus A Oliver et all. "High Level decision methodology for the selection of a fuel cell-based power distribution architecture for an aircraft application.
- [3]. Santhosh, K., Chenchireddy, K., Vaishnavi, P., Greeshmanth, A., Kumar, V. M., & Reddy, P. N. (2023, January). Time-Domain Control Algorithms of DSTATCOM in a 3-Phase, 3-Wire Distribution System. In 2023 International Conference on Intelligent Data Communication Technologies and Internet of Things (IDCIoT) (pp. 781-785). IEEE.
- [4]. Gong, Xuan, Feifei Dong, Mohamed A. Mohamed, Omer M. Abdalla, and Ziad M. Ali. Secured energy management architecture for smart hybrid microgrids considering PEM-fuel cell and electric vehicles." Ieee Access 8 (2020): 47807-47823.
- [5]. Chenchireddy, K., Goud, B. S., Mudhiraj, C. M. S., Rajitha, N., Kumar, B. S., & Jagan, V. (2022, March). Performance Verification of Full-Bridge DC To DC Converter Used for Electric Vehicle Charging Stations. In 2022 8th International Conference on Advanced Computing and Communication Systems (ICACCS) (Vol. 1, pp. 434-439). IEEE.
- [6]. Gyoung-Jong, et all. "Grid Connection Using A Structure That Combines a Buck Converter And a Push-Pull Converter To Reduce The Low Frequency Current Ripple Of The Fuel-Cell." IEEE Access 10 (2022): 95823.
- [7]. Kumar, V., Chenchireddy, K., Reddy, M. R., Prasad, B., Preethi, B., & Raj, D. S. (2022, March). Power Quality Enhancement In 3-Phase 4-Wire Distribution System Using Custom Power Devices. In 2022 8th International Conference on Advanced Computing and Communication Systems (ICACCS) (Vol. 1, pp. 1225-1228). IEEE.
- [8]. Sylvain Gelfi, et all. "Dynamics of Low-Pressure and High-Pressure Fuel Cell Air Supply System".
- [9]. Kouros Sedghisigarchi, et all. "Dynamic and Transient Analysis of Power Distribution Systems with Fuel-Cells". IEEE Transactions on energy conversion, Vol.19, No.2, June 2004.
- [10]. Estebansari, Abouzar, et all. "Frequency Control of Low Inertia Power Grids with Fuel Cell Systems in Distribution Networks." IEEE Access 10 (2022): 71530-71544.
- [11]. A. Vazquez, et all. "Integrated Power Conditioner Topology for Fuel cell-based Power Supply Systems".
- [12]. Chenchireddy, K., & Jegathesan, V. (2022). Three-Leg Voltage Source Converter-Based D-STATCOM for Power Quality Improvement in Electrical Vehicle Charging Station. In AI Enabled IoT for Electrification and Connected Transportation (pp. 235-250). Singapore: Springer Nature Singapore.
- [13]. M. Tanrioven, et all. "Modeling, Control and Power Quality Evaluation of a PEM Fuel cell-based Power Supply System for Residential Use".
- [14]. Yuedong Zhana, Jianguo Zhu, Youguang Guob, and Hua Wang. "An Intelligent Uninterruptible Power Supply System with Backup Fuel cell/battery Hybrid Power Sources".

# Design and Implementation of Three-phase Three Level NPC Inverter

Dhasharatha G,  
Assistant Professor  
Dept. of Electrical and Electronics  
Engineering  
Teegala Krishna Reddy Engineering  
College  
Hyderabad, Telangana, India.  
g.dhasharatha@gmail.com

N.Rajasekhar Varma,  
Professor  
Dept. of Electrical and Electronics  
Engineering  
Teegala Krishna Reddy Engineering  
College  
Hyderabad, Telangana, India  
dnrsvarma@gmail.com

Ageeru Spandana  
UG student  
Dept. of Electrical and Electronics  
Engineering  
Teegala Krishna Reddy Engineering  
College  
Hyderabad, Telangana, India  
ageeruspandana@gmail.com

Padmanabuni Arun Kumar  
UG student  
Dept. of Electrical and Electronics  
Engineering  
Teegala Krishna Reddy Engineering  
College  
Hyderabad, Telangana, India  
Padmanabuniarunkumar456@gmail.com

Bommakanti Venumadhav  
UG student  
Dept. of Electrical and Electronics  
Engineering  
Teegala Krishna Reddy Engineering  
College  
Hyderabad, Telangana, India  
bommakantivenumadhav@gmail.com

Boyanapally Prem kumar  
UG student  
Dept. of Electrical and Electronics  
Engineering,  
Teegala Krishna Reddy Engineering  
College  
Hyderabad, Telangana, India  
Premkumarboyanapally1234@gmail.com

**ABSTRACT:** The three-level NPC PWM inverter is a type of multilevel inverter that provides a higher quality of output wave form compared to traditional two-level inverter. It is a type of power electronic converter that is used in renewable energy such as wind turbine and PV system. It convert DC power source into AC power source. It is also capable of handling high power levels and provides better efficiency compared to other inverter topologies. Since, inverter uses PWM technique to control the switching power of semiconductor devices.

**Keywords:** Multilevel inverter, Neutral point clamped inverter, Three level inverter, SPWM technique.

## I. INTRODUCTION

In comparison to other inverters that have been researched and used in the past, NPC inverters are one of the most significant multilevel inverter structures. Low volts is needed to power the devices using this kind of inverter, and the output voltage needs to have minimal harmonic content. The topological structure cannot be expanded because of the inherent neutral voltage balance issue. [1] [12]

The primary approach for a three-level NPC inverter uses SVPWM and PWM to manage the average value of NP currents at zero in a switching instance (PWM) [2]. Nabae, Takahashi, and Akagi created the neutral point converter in 1981; it was essentially a 3-level diode-clamped inverter. The multi-level inverter is more capable and effective power applications nowadays [3]. This inverter is utilised in high voltage, high power efficiency applications with a wide

variety of machine speeds [4]. Three-level NPC inverter benefits include: maximising efficiency at switching times.

At the appropriate voltage level, the capacitors can recharge once more. Due to the sharing of all phases to a single set of DC links, the inverter's capacitance can be kept to a minimum. [5]

Since new approaches for controlling the switches in inverters were introduced. For Example, Pulse Width Modulation (PWM). [6]

The most common used for the PWM technique is sinusoidal PWM technique (SPWM). The NPC multi level inverter can be operated as 3 modes operations. i.e. Dipolar, Unipolar and Partial dipolar. [7]

As a result, the dc link voltage in an NPC 3-level inverter can be divided into two equal capacitors. The fluctuation in NP voltage is the 3-level inverter's serious issue [8].

In this study, an SPWM project was constructed that offers an NPC multi-level inverter with voltage balance control and waveform for switching between levels of three and five. [9][10] Only the measurement of load current and DC link voltage is required for this project. The load performance is not high flow because the balancing voltage strategy is based on adding the appropriate diagonals/angles to the provided order of the voltage. [11]

## II. TOPOLOGY OF 3-LEVEL NPC INVERTER

### A. Three level inverter

There are three possible levels for the pole voltage:  $+V_{dc}$  by two zeros,  $-V_{dc}$  by two, and zero. There are some another who would count the number of levels. Let us say in R and Y, you will have five different levels because it has  $+V_{dc}$  and  $+V_{dc}$  by two or it can be zero or it can be  $-V_{dc}$  and or  $-V_{dc}$  by two. So these are the five different levels.

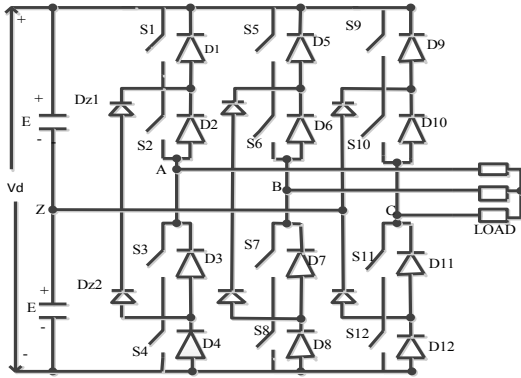


Fig 1: Three-level NPC inverter

You may something getting referred as five level inverter but convention is quite less. The relationship between the levels and voltage poles. Just two levels of pole voltages,  $+V_{dc}/2$  and  $-V_{dc}/2$ , are possible in a two-level inverter in terms of both the pole voltage and the number of levels. Hence the three level inverter has three levels:  $+V_{dc}/2$ ,  $-V_{dc}/2$ , and zero.

### B. One leg of a three level inverter

The top two devices are  $S_1$  and  $S_2$  on the bottom two will be off  $S_3$  and  $S_4$ . In this case R will be connected  $0.5 V_{DC}$ . So this is the pole getting connected to the top throw, the pole getting connected to the bottom throw is again straight forward to c.

The  $S_1$  and  $S_2$  are OFF  $S_3$  and  $S_4$  are ON. Therefore you will might get pole connected to the bottom throw. So  $V_{RO}$  will be equal to  $-0.5V_{DC}$  earlier it was  $0.5V_{DC}$  and it is also possible to connect K to O turn off  $S_4$  turn on  $S_2$  and  $S_3$ . So R could establish connection with O and through which part there are two different parts that would depend on the load current.

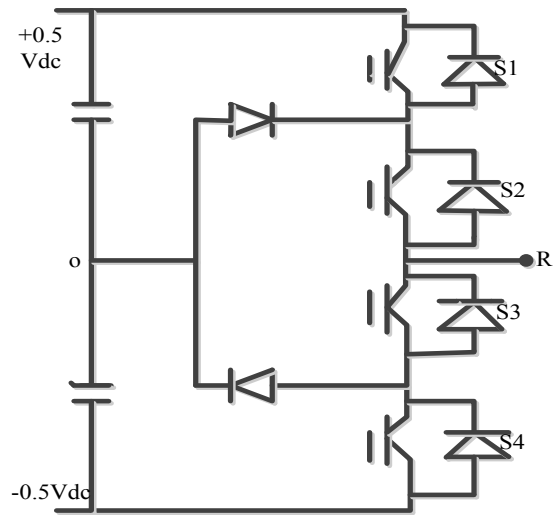


Fig 2: One leg of a 3-level inverter

$S_1$	$S_2$	$S_3$	$S_4$	$V_{RO}$
1	1	0	0	$+0.5V_{dc}$
0	1	1	0	0
0	0	1	1	$-0.5V_{dc}$

Table 1: Relationship between switching devices and output levels

$S_1$  and  $S_3$  are complementary. If  $S_1$  is high then  $S_3$  is low, if  $S_1$  is low then  $S_3$  is high. In the same way  $S_2$  and  $S_4$  are complementary with one another. In this, there are two pairs of complementary switches. So there it is sufficient for the generate one gating signal and other gating signal would come by taking its compliment. Here, two gating signals may be  $S_1$  and  $S_2$  and  $S_3$  would come by complementary  $S_1$  and  $S_4$  would come by complementary  $S_2$ . So two gating signals should be produced, and that is going to significantly change. It have one sine wave with two carriers.

## III. CONTROL SCHEME

The most commonly used modulation scheme for an NPC inverter is the SPWM technique. The basic concept of SPWM involves comparing a reference sinusoidal wave form with high frequency carrier wave form. The magnitude and frequency of the carrier wave form are typically much higher than the reference wave form.

In an NPC inverter, the DC voltage is split into multiple levels using capacitors and diodes, resulting in several voltage levels that can be used to generate a quasi-sinusoidal output wave form. The SPWM technique is then applied to

each level of the NPC inverter to generate the appropriate switching signals for the power electronics. The basic concept of SPWM involves differential a reference sinusoidal waveform with a high- frequency carrier waveform. The amplitude and frequency of the carrier waveform are typically much higher than the reference waveform. The resulting modulated waveform has the same frequency as the reference waveform and a variable amplitude determined by the width of the pulses in the carrier waveform.

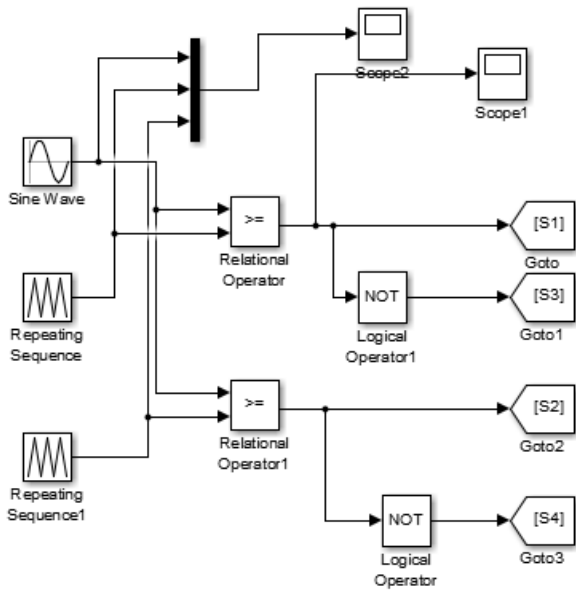


Fig 3: Overall system of SPWM technique

To implement SPWM in an NPC inverter, the reference sinusoidal waveform is typically generated using a microcontroller or DSP. The carrier waveform is generated using a high- frequency oscillator or a PWM generator. The reference waveform is then compared with the carrier waveform to generate the modulated waveform. The resulting modulated waveform is then used to generate the switching signals for the power electronics. The rate of the carrier waveform controls the exchanging rate of the power electronics, while the width of the pulses in the carrier waveform dictates the amplitude of the output voltage.

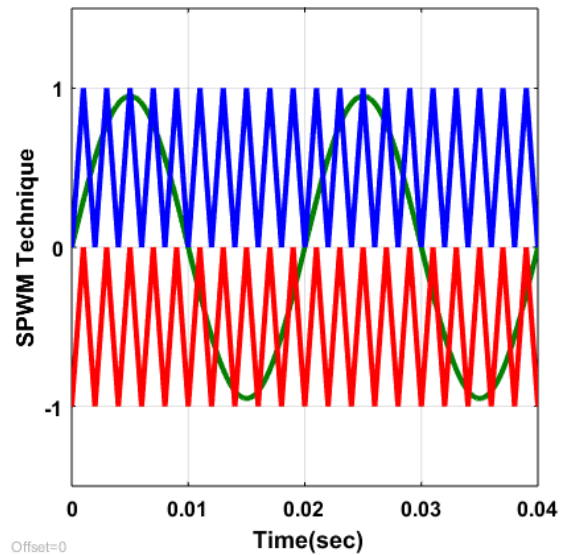


Fig 4: Output of SPWM technique

Figure shows the simulation wave form of SPWM technique. X-axis indicates time(sec) and Y-axis indicates SPWM technique.

Overall, the SPWM technique is a widely used method for generating quasi-sinusoidal waveforms in power electronics. When applied to NPC inverters, it allows for precise control of the output voltage while minimizing harmonic distortion and improving efficiency.

#### IV.RESULTS

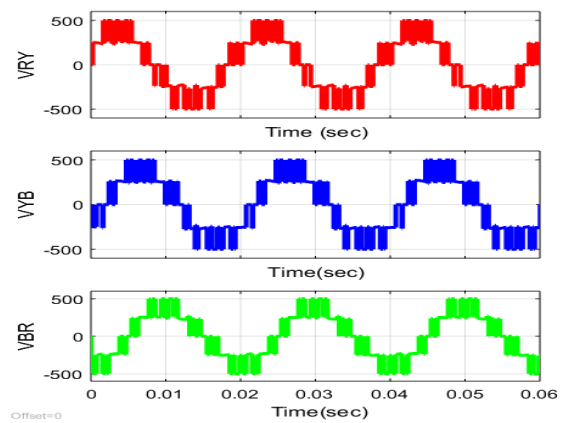


Fig 5 output waveform of individual R,Y,B line voltage

Figure(5) shows the simulation wave form of 3-phase line voltage of individual R,Y,B. X-axis indicates the time(sec) and Y-axis indicates the VRY, VYB, VBR.

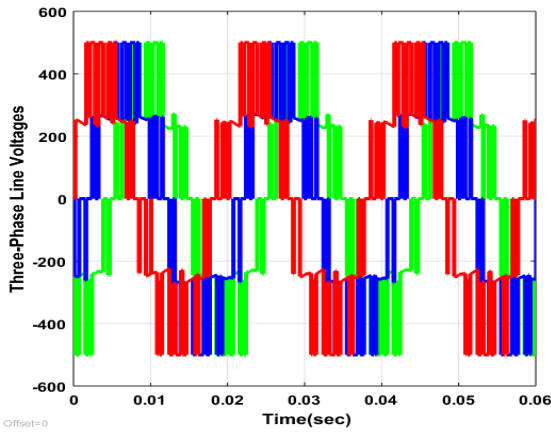


Fig:6 output waveform of combined RYB line voltage

Figure(6) shows the simulation wave form of 3-phase line voltage of combined RYB. X-axis indicate the time(sec) and Y-axis indicate the 3-phase line voltage.

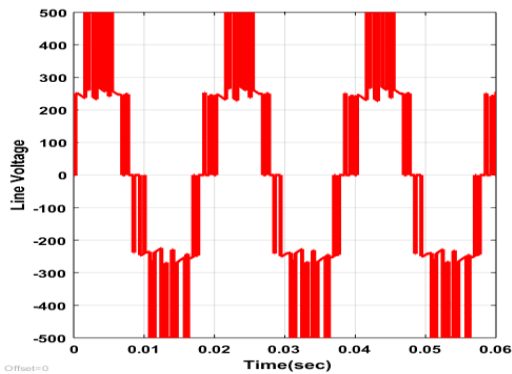


Fig:7 output waveform of 1-phase line voltage

Figure(7) shows the imitation wave form of 1-phase line voltage of R or Y or B. X-axis indicate the time(sec) and Y-axis indicate the line voltage.

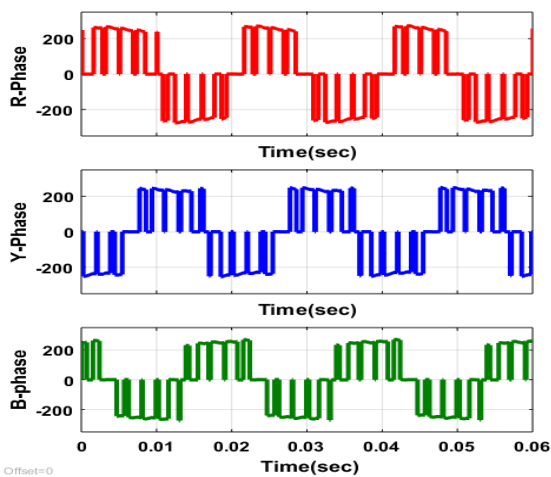


Fig:8 output waveform of individual R,Y,B phase voltage

Figure(8) shows the simulation wave form of 3-phase phase voltage of individual R,Y,B. X-axis indicate the time(sec) and Y-axis indicate the R-phase, Y-phase, B-phase.

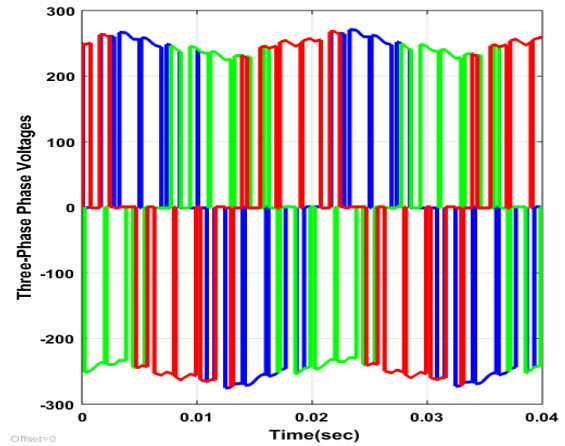


Fig:9 output waveform of combined RYB phase voltage

Figure(9) shows the simulation wave form of 3-phase phase voltage of combined RYB. X-axis indicate time(sec) and Y-axis indicate 3-phase phase voltage.

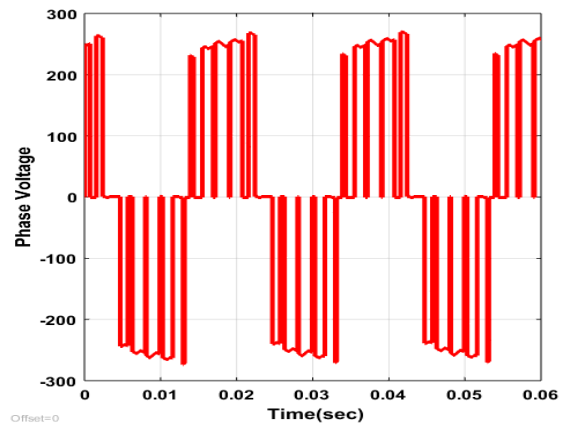


Fig:10 output waveform of 1-phase voltage

Figure(10) shows the simulation wave form of 1-phase phase voltage of R or Y or B. X-axis indicate time(sec) and Y-axis indicate phase voltage.

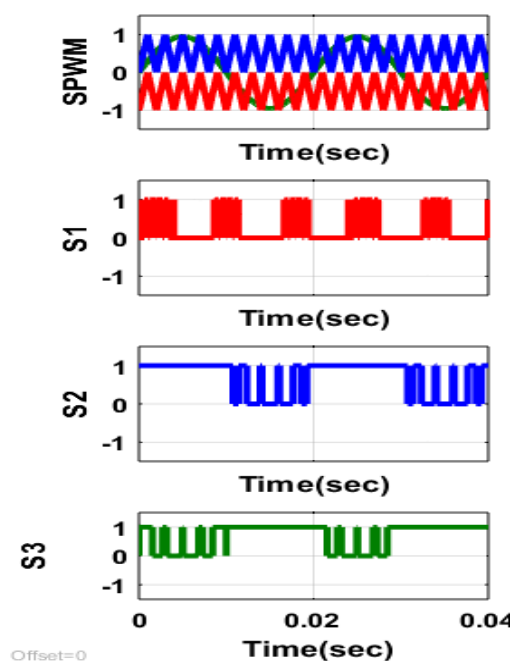


Fig:11 output waveform of switching sequency of SPWM

Figure(11) shows the switching sequence of SPWM technique of S1,S2,S3. X-axis indicate time(sec) and Y-axis indicate S1,S2,S3.

## V. CONCLUSION

In conclusion, the 3- level NPC inverter with PWM technique is highly efficient and effective method for providing high quality AC power. It offers numerous benefits over traditional two level inverters and has become increasingly popular in a range of applications. Its ability to provide precise control over the output waveform makes it an excellent choice for many different type of power systems.

## REFERENCES

- [1] Chenchireddy,et.all (2020). Different topologies of inverter: a literature survey. *Innovations in Electrical and Electronics Engineering: Proceedings of the 4th ICIEEE 2019*, 35-43.
- [2] Ahmadzadeh, Taher, Mehran Sabahi, and Ebrahim Babaei. "Modified PWM control method for neutral point clamped multilevel inverters." *2017 14th International Conference on ECTI-CON*. IEEE, 2017.
- [3] Muthukuri, Narendra Kumar, and Ravindranath Tagore Yadlapalli. "Comparison of carrier based PWM technique for Active Neutral Point Clamping Multilevel Inverter." *2020 4th International Conference on ICICCS*. IEEE, 2020.
- [4] Hashir, Shaziya, Jebin Francis, and R. Sreepriya. "A novel hybrid PWM method for DC-link voltage balancing in a three level neutral point clamped inverter." *2018 International Conference on EPSCICON*. IEEE, 2018.
- [5] Ko, Yoon-Hyuk, et al. "A simple space vector PWM scheme with neutral point balancing for three-level neutral point clamped inverter." *2011 IEEE Industry Applications Society Annual Meeting*. IEEE, 2011.

- [6] Chenchireddy, K. et al. (2021). A Review Paper on the Elimination of Low-Order Harmonics in Multilevel Inverters Using Different Modulation Techniques. *Inventive Communication and Computational Technologies: Proceedings of ICICCT 2020*, 961-971.
- [7] Jiang, Weidong, et al. "A novel discontinuous PWM strategy to control neutral point voltage for neutral point clamped three-level inverter with improved PWM sequence." *IEEE Transactions on Power Electronics* 34.9 (2018): 9329-9341.
- [8] Pairedamonchai, Pennapa. "Impact of PWM Modulation Schemes on Common-Mode Voltage Generated by 3-Level Neutral-Point-Clamped Inverters." *2018 Third International Conference on EST*. IEEE, 2018.
- [9] Srirattana-wichaikul, W., et al. "A carrier-based PWM strategy for three-level neutral-point-clamped voltage source inverters." *2011 IEEE Ninth International Conference on PE and DS*. IEEE, 2011.
- [10] Raju, K. Narasimha, M. Venu Gopala Rao, and M. Ramamoorthy. "Hybrid modulation technique for neutral point clamped inverter to eliminate neutral point shift with minimum switching loss." *TENCON 2015-2015 IEEE Region 10 Conference*. IEEE, 2015.
- [11] Azer, Peter, Saeed Ouni, and Mehdi Narimani. "A new fault-tolerant method for 5-level active neutral point clamped inverter using sinusoidal PWM." *2019 IEEE ECCE*. IEEE, 2019.
- [12] Lee, June-Seok, Seungjong Yoo, and Kyo-Beum Lee. "Novel discontinuous PWM method of a three-level inverter for neutral-point voltage ripple reduction." *IEEE Transactions on Industrial Electronics* 63.6 (2016): 3344-3354.
- [13] Chenchireddy et. all (2019). Design and Simulation of a Single Phase Four Level Neutral Point Clamped Inverter. *International Journal of Recent Technology and Engineering (IJRTE)* ISSN, 2277-3878.
- [14] Jiang, Weidong, et al. "A carrier-based PWM strategy providing neutral-point voltage oscillation elimination for multi-phase neutral point clamped 3-level inverter." *IEEE Access* 7 (2019): 124066-124076.
- [15] Swamy, Manthri, K. Anuradha, and B. Ganesh Babu. "DC level stabilization in Neutral Point Clamped multilevel inverters." *2015 Conference on PCCCTSG*. IEEE, 2015.

See discussions, stats, and author profiles for this publication at: <https://www.researchgate.net/publication/369475775>

# Induction Motor Speed Control Through Vector Control Approach

Conference Paper · March 2023

---

CITATIONS

0

READS

54

1 author:



[Kalagotla Chenchireddy](#)

Karunya University

53 PUBLICATIONS 160 CITATIONS

SEE PROFILE



# Induction Motor Speed Control Through Vector Control Approach

Rosaiah Mudigondla  
Assistant professor  
Dept. of Electrical and Electronics  
Engineering  
Teegala Krishna Reddy Engineering  
College  
Hyderabad, Telangana, India.  
rosaiah0228@gmail.com

kalagotla Chenchireddy  
Assistant professor  
Dept. of Electrical and Electronics  
Engineering  
Teegala Krishna Reddy Engineering  
College  
Hyderabad, Telangana, India.  
chenchireddy.kalagotla@gmail.com

Rekapalli Madhu Sudhan  
UG student  
Dept. of Electrical and Electronics  
Engineering  
Teegala Krishna Reddy Engineering  
College  
Hyderabad, Telangana, India.  
madhusudhan1606r@gmail.com

Pendem Akshay Kumar  
UG student  
Dept. of Electrical and Electronics  
Engineering  
Teegala Krishna Reddy Engineering  
College  
Hyderabad, Telangana, India.  
pendemakshay921@gmail.com

Yada Swamy  
UG student  
Dept. of Electrical and Electronics  
Engineering  
Teegala Krishna Reddy Engineering  
College  
Hyderabad, Telangana, India.  
swamyada193@gmail.com

Potharaveni Shiva Priya  
UG student  
Dept. of Electrical and Electronics  
Engineering  
Teegala Krishna Reddy Engineering  
College  
Hyderabad, Telangana, India.  
shivapriyapotharaveni@gmail.com

**Abstract:** The technique of vector control, often stated to as field-oriented control (FOC), is frequently utilize in Factory made applications to regulate speed and torque of IM drives. Vector control enables precise control of motor speed and torque by segmenting the stator current into components that produce torque and flux. The 3-phase Alternating current(AC) voltage & current signals are altered into a rotating reference frame, where the stator currents are divided into their torque and flux components, to achieve this. A PI controller uses the converted signals to produce the reference values for the torque ( $T_c$ ) & flux components of the stator's current. The inverse Park transform is then used to turn these values back into three-phase signals, which creates the control signals for the motor drive.

**Keywords:** Field oriented control (FOC), PI Converter, inverse park transform , Vector control, Alternating Current

## I.INTRODUCTION

Induction motors continue to be the most widely used motors in the industry, as is well known, due to their excellent performance and affordable price.[2]

Advantageous operational characteristics of AC induction motors include power, durability, and ease of control. They are extensively used in a variety of applications, ranging from mechanical control mechanisms for residential appliances.[1] Despite this, using induction motors at their highest productivity levels is a challenging task because of their complicated numerical representation and non-straight trademark during immersion.[14]These elements lead to acceptance engine control issues and necessitate the use of advanced control computations, such as vector control.[4]Due to their high performance and low price, induction motors continue to be the most popular motors in the industry. It comprises great dependability, low cost, and widespread use in industrial applications, induction motors are practically completely maintenance-free.[10]When compared to a DC motor, it is robust, lighter, cheaper, more reliable, and nearly maintenance-free. The induction motor(IM) can be controlled in a variety of ways. V/f control is the oldest technique used among these.[9]This approach has poor dynamic performance because induction motors require coordinated control of the stator current's amplitude, frequency, and phase, which is not attainable with V/f induction motor drives. [5]An option is

vector control, commonly mentioned as field oriented control ,(FOC). Dissociated control of flux and torque is a component of vector control. For managing the speed and torque of induction motor drives in industrial applications, vector control is a potent technique.[8] Vector control enables fine control of the motor's speed and torque by individually managing these two stator current components.[3] On basis of the idea of converting the three-phase AC voltage and current(I) signals into a rotating reference frame, in which stator currents are categorized into their torque and flux components, vector control is used to drive motors.[13] A PI controller uses the converted signals to produce the reference values for torque( $T_c$ ) & flux components of the stator current.[11] VC also acknowledged as field oriented control, is a control approach used for achieving high-performance control of induction motors.[15] This technique involves transforming the three-phase AC power supply into a two-phase system, with the first phase being the magnetizing component and the second phase being the torque component.[6]

The advantages of vector control include:

1. High performance: Vector control provides accurate and fast control of the motor's speed, torque, and position.[12]
2. Energy efficiency: Vector control minimizes losses in the motor, resulting in improved energy efficiency.
3. Reduced maintenance: Vector control reduces the stress on the motor, resulting in lower maintenance requirements.
4. Increased lifespan: Vector control extends the lifespan of the motor by reducing the stress and wears on its components.

In summary, vector control is a powerful control strategy used to achieve high-performance control of induction motors, resulting in improved energy efficiency, reduced maintenance requirements, and increased lifespan.[7]

## II. CONTROL METHODS

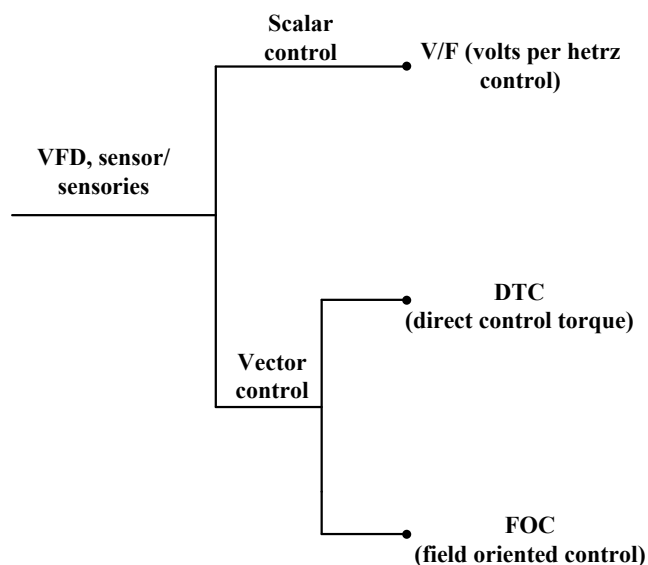


Fig.1. Control for induction motor(IM) using scalar and vector methods.

From figure (1), Vector control and scalar control are two common methods used for controlling the speed & torque ( $T_c$ ) of IM using variable frequency drive (VFD) sensors. Both methods use VFD sensors to vary the frequency of AC supply for the motor, which in turn affects the motor speed and torque.

FOC is a more sophisticated control procedure that allows for precise and independent control of the motor speed & torque. In VC method, the AC voltage (V) and current are transformed into a two-dimensional space vector representation using Clarke and Park transformations. This transformation allows the relationship between the d-axis & q-axis components of the voltage (V) & current (I) to stand independently controlled, which can be used for controlling torque ( $T_c$ ) and flux of the motor.

The controlling of  $T_c$  and flux is accomplished utilizing a PI controller which regulates voltage (V) and frequency (f) of the AC supply founded on the variance between desired torque & magnetic flux and the actual quantities. The PI controller adjusts the voltage and frequency by governing the duty cycle of the PWM inverter signal generated by VFD sensors.

Scalar control, also known as V/f control, is a simpler control method that uses a scalar relationship between the voltage and frequency of the AC supply to control motor speed & torque ( $T_c$ ). In scalar control, the VFD sensor adjusts the frequency of the AC supply which is given to the motor based on the desired speed. The voltage is then adjusted proportionally to maintain a constant V/f ratio.

The V/f ratio is described as the ratio between the voltage and frequency of AC supply to the motor. This ratio is maintained constant in scalar control to ensure that the motor operates at a constant flux level. The constant flux level ensures that the motor operates efficiently and does not overheat.

Both vector control and scalar control using VFD sensors have their advantages and disadvantages. Vector control provides more precise and independent control of the motor speed and torque, but it requires more complex control algorithms and is more expensive. Scalar control is simpler and more cost-

effective, but it is less precise and may result in lower energy efficiency.

In general, vector control is preferred for applications that require high precision and fast response times, such as robotics and automation. Scalar control is suitable for applications where cost is a significant factor and where the control requirements are less demanding, such as in HVAC systems and pumps.

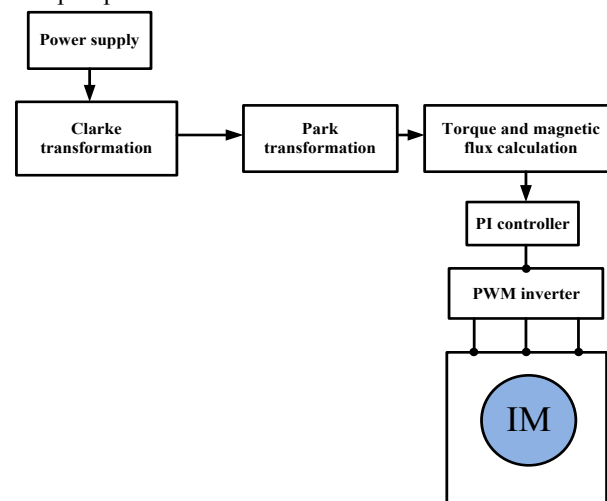


Fig.2. Topology illustration of vector control of IM.

From figure (2), VC is a procedure used for controlling the speed & torque ( $T_c$ ) of IM. The main idea behind this control scheme is to treat the induction motor as a separately excited Direct current motor with a field flux & an armature current. This way, the induction motor (IM) can be controlled as a DC motor, even though it is an AC motor.

The vector control scheme involves transforming the 3-phase Alternating Current-voltage and current (I) of the induction motor into 2-phase DC quantities, which can be used for controlling the motor's speed &  $T_c$ . The transformation is done using Clarke and Park transformations.

Clarke transformation can be used to alter the 3 phase quantities into two-phase DC quantities. The 2 phase DC quantities are then transformed into two-phase AC quantities via Park transformation. Then two-phase AC quantities are utilized to control the torque ( $T_c$ ) and flux of the motor.

The torque & flux of the motor can be controlled autonomously by supervisory of two-phase AC quantities. The torque can be maintained by monitoring the q-axis current, while flux can be also maintained by governing the d-axis current. By controlling the torque and flux, the speed and direction of the motor can be controlled as well.

The PI controller adjusts the voltage and frequency of the AC supply founded on the change that occurs between desired torque, magnetic flux, and the actual quantities. The PI controller regulates the voltage and frequency by controlling the duty cycle of the pulse width modulation (PWM) inverter signal produced by PWM inverter.

The PWM inverter converts the DC voltage from a DC link capacitor into a 3-phase AC voltage through adjustable amplitude, and frequency to control motor speed, and torque.

The control scheme is created on a mathematical model of the IM, which is used to predict the behaviour of the motor under diverse working conditions. Mathematical model includes equations for the torque & flux, as well as the voltage, and current of the motor.

The VC scheme for an IM provides several benefits over other control schemes. It provides precise and accurate control of motor speed & torque, which results in improved energy efficiency, reduced maintenance requirements, and increased lifespan. It also provides a better dynamic response, which means the motor can respond quickly to changes in load or speed.

### A. Induction motor

An induction motor (IM) is described as an AC motor that translates electrical energy into mechanical energy through the interaction of magnetic fields. The operation of an IM can be defined mathematically using some equations known as induction motor equations.

The induction motor equations are a set of differential equations that describe the electrical, & mechanical behaviour of a motor. Equations are typically written in terms of stator & rotor voltages, currents, and magnetic fields. They are based on the principles of electromagnetism and are derived from the laws of physics.

The basic equations for an induction motor are:

Rotor Voltage equation:

$$sE_r = R_r I_s + (2\pi f)L_{lr} I_r$$

$$E_r = \left(\frac{R_s}{s}\right) I_r + j(2\pi f)L_{lr} I_r$$

While the motor is in running condition,

$$T_{run} = \frac{K_s E_2^2 R_2}{R_2^2 + (sX_2)^2}$$

$$(K) = \frac{3}{2\pi N_2}$$

### III. CONTROL SCHEME

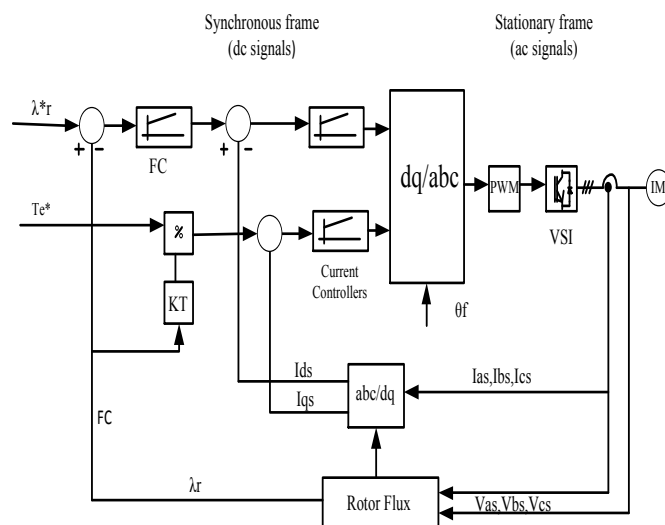


Fig.3.DFOC through Rotor Flux Orientation

DFOC is nothing but a control scheme used for induction motors that offer a fast dynamic response and high accuracy.

The control scheme of DFOC involves the following steps:

1. Measuring stator voltages & currents: The stator voltage & current can be measured using appropriate sensors.
2. Estimating rotor flux: Rotor flux is assessed using the measured stator currents & voltages. The rotor flux assessed using a mathematical model or lookup table based on the motor parameters.
3. Calculating the torque: The electro\_magnetic torque developed by the motor can be calculated using the assumed rotor flux & the measured stator current.
4. Generating the switching signals: Based on the calculated torque, the control scheme generates the appropriate switching signals to the inverter that drives the motor.
5. Controlling the fluxes of stator & rotor: control scheme adjusts amplitude & phase of the current from stator & flux of rotor for achieving the desired\_torque and speed.

DFOC control scheme uses a mathematical model or lookup table to calculate the switching signals required to control the current from stator & the flux from rotor. The table is depending up on the parameter's of the motor, such as stator resistance & inductance, rotor resistance & inductance.

DFOC provides precise control of the motor with a fast dynamic response, which makes it suitable for robotics, and electric vehicles. However, it requires complex control algorithms and is more expensive than traditional control schemes.

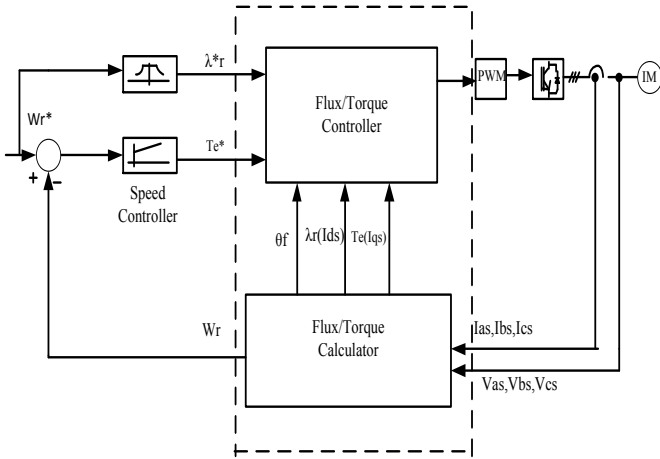


Fig.4. General Diagram Of Rotor Flux FOC

Field-Oriented Control method named for (FOC) is the control scheme for induction motors that offer a fast dynamic response and high accuracy.

The working of FOC involves the following steps:

1. Measuring stator voltages & currents: The stator voltages & currents were measured using appropriate sensors.
2. Estimating rotor flux: Rotor flux is estimated using the measured stator currents & voltages. The rotor flux developed will be estimated using a mathematical model or lookup table based on the motor parameters.
3. Transforming the stator current: The stator current is transformed with in the stationary reference to the rotor reference structure using a Park transform. This transformation simplifies the control of the motor by separating the torque-producing component from the magnetizing component.
4. Controlling the magnetizing component: A magnetizing component from the stator current is controlled to regulate the rotor flux.
5. Controlling the torque-producing component: The torque producing component's from the stator current is controlled to regulate the electromagnetic torque.
6. Generating the switching signals: Based on the controlled stator current, the control scheme generates the appropriate switching signals to the inverter that drives the motor.
7. Inverter output: DC power supply to AC power and supplies it to the motor windings is fed by the inverter and converter.

FOC provides precise control of the motor with a fast dynamic response, which makes it perfectly good for robotics, electric vehicles. FOC has become a popular control scheme for induction motors because of its effectiveness in achieving high torque and speed control. However, FOC requires complex control algorithms and is more expensive than traditional control schemes.

In Field oriented reference axis frame,

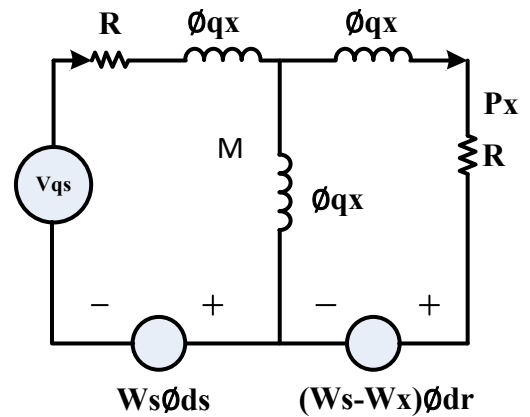


Fig.5. Field oriented reference axis frame

From the given circuit diagram,

Imaginary component,

$$\phi_{qr} = 0$$

From rotor circuit,

$$\frac{d}{dq} \phi_{qr} = 0$$

So voltage across R,

$$(w_s - w_r) \phi_{dr} + R_x i_{qr} = 0$$

From flux equation in terms of \$i\_{qs}\$,

$$M i_{qs} + L_{xr} i_{qr} = 0 \Rightarrow i_{qr} = -\frac{M}{L_{xr}} i_{qs}$$

$$(w_s - w_x) \phi_{dr} = \frac{M}{L_{xr}} i_{qs} R_x$$

$$w_{slip} \phi_r = \frac{M}{L_{xr}} i_{qs} R_x$$

By above, We Can Say that \$W\_{slip}\$ is proportional to \$i\_{qs}\$.

IV SIMULATION RESULTS

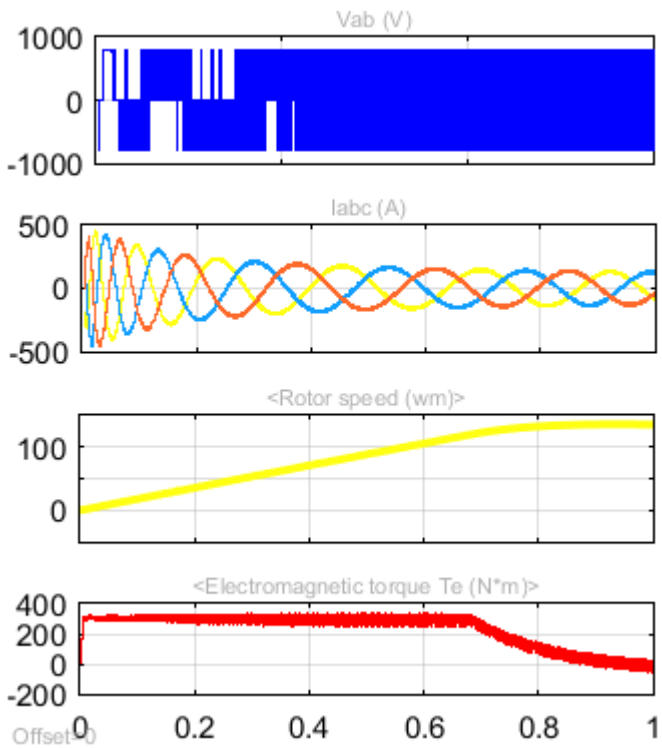


Fig.6.Output Waveforms

Fig.6.depicts the waveforms of Voltage (Vab), Current (Iabc), Rotor speed, Electromagnetic Torque (Te) in induction motor under vector control reference frame.

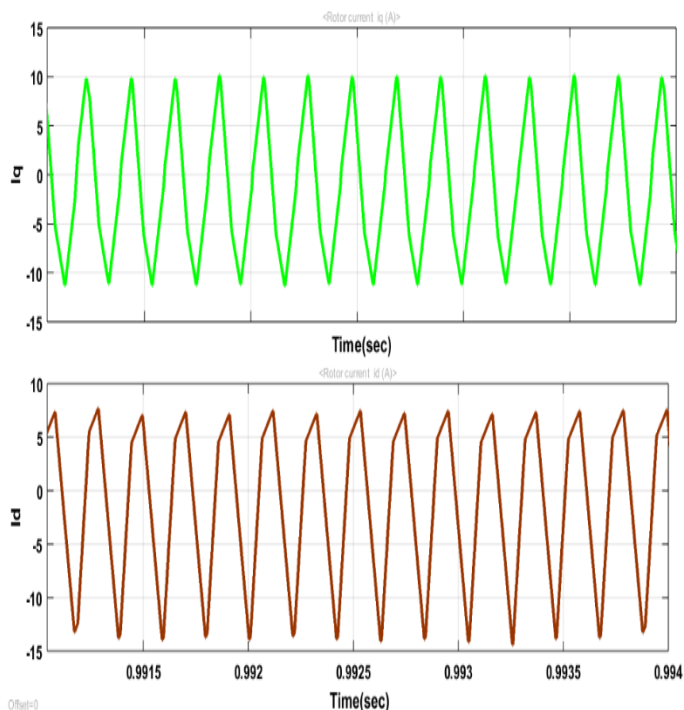


Fig.7.Rotor's Iq Id currents waveforms

Fig.7. shows the waveforms of Rotor's Quadrant current (Iq), Direct current (Id) which have a magnitude ranging from +10A to -10A

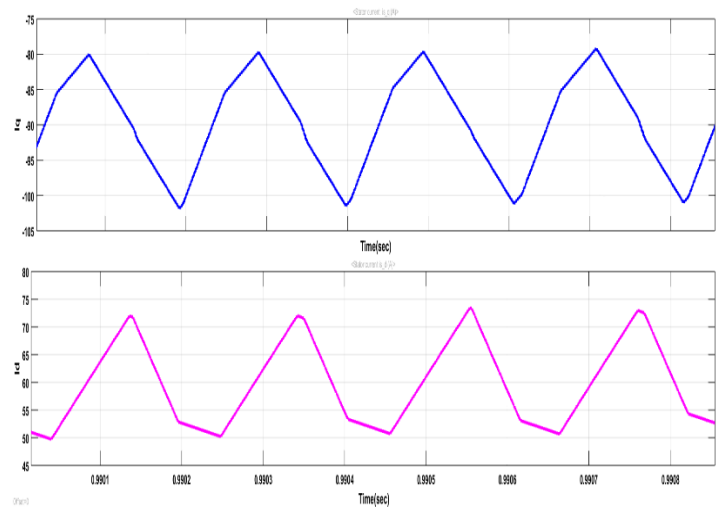


Fig.8. Stator's Iq,Id currents waveforms

Fig.8. describes the waveforms of Stator's Quadrant current(Iq),Direct current(Id) which consists of X-axis as Time(sec) and Y-axis as Current(A).The Iq waveform exists in between the -100A to -80A range. And Id waveform lies in between +50A to +75A values.

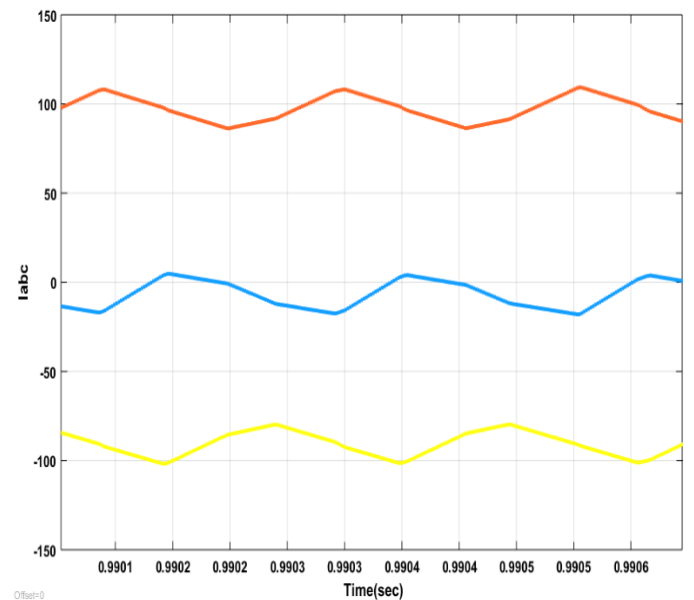


Fig.9. Three phase Iabc waveform

Fig.9. demonstrates the wave forms of Iabc in which X-axis is taken as Time(sec) and Y-axis is taken as Current(A).It is three phase current waveform in which red coloured waveform is considered as Ia,the blue coloured waveform is considered as Ib,and the yellow coloured waveform is considered as Ic.

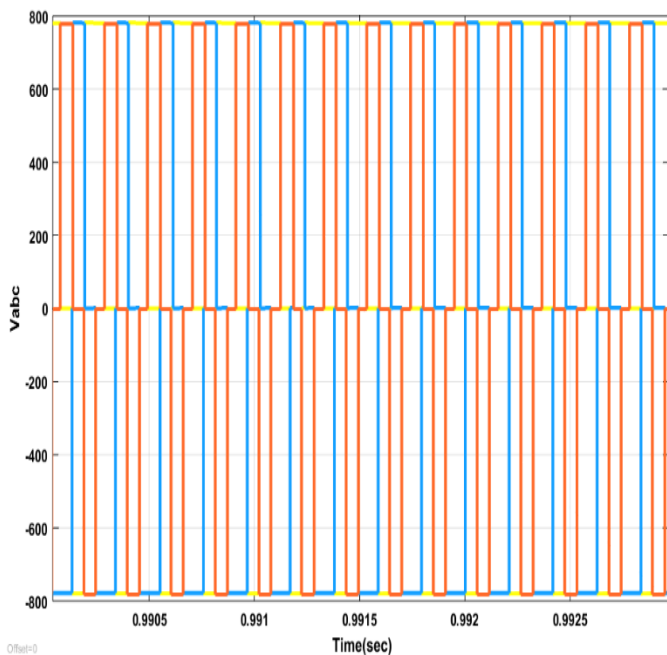


Fig.10. Three phase voltage waveform(Vabc)

Fig.10. displays the waveform of three phase voltage (Vabc). From the figure, we can see that the waveform varies the magnitude ranging from -800V to +800V.

## V.CONCLUSION

In conclusion, VC can be said as Field-Oriented Control is a sophisticated control scheme for induction motors that offers precise control of the motor's speed and torque with high dynamic response and accuracy. The control scheme involves controlling the stator current, rotor flux separately by a mathematical model to estimate motor's parameters Vector Control has been widely adopted in various industrial applications, including electric vehicles, robotics, and machine tools, due to its effectiveness in achieving high performance and efficiency. However, Vector Control requires complex algorithms and additional hardware, which makes it more expensive compared to other control schemes. Nonetheless, the benefits of Vector Control have made it a popular choice for applications that require high-performance motor control.

## REFERENCES

[1] Al Azze, Qasim, and Imad Abdul-Rida Hameed. "Reducing torque ripple of induction motor control via direct torque control." *International Journal of Electrical and Computer Engineering* 13.2 (2023): 1379.  
 [2] Kumar, V., Chenchireddy, K., Reddy, M. R., Prasad, B., Preethi, B., & Raj, D. S. (2022, March). Power Quality Enhancement In 3-Phase 4-Wire Distribution System Using Custom Power Devices. In *2022 8th International Conference on Advanced Computing and Communication Systems (ICACCS)* (Vol. 1, pp. 1225-1228). IEEE.

[3] Elnaghi, Basem E., M. N. Abelwhab, Ahmed M. Ismaiel, and Reham H. Mohammed. "Solar Hydrogen Variable Speed Control of Induction Motor Based on Chaotic Billiards Optimization Technique." *Energies* 16, no. 3 (2023): 1110.  
 [4] Ruan, Z., Song, W., Zhao, L., Zhang, Y., & Guo, Y. (2023). A Variable Switching Frequency Space Vector Pulse Width Modulation Control Strategy of Induction Motor Drive System with Torque Ripple Prediction. *IEEE Transactions on Energy Conversion*.  
 [5] Srivastav, Ashwani, M. Rizwan, and Vinod Kumar Yadav. "Comparative Analysis of Conventional and Intelligent Methods for Speed Control of Induction Motor." *Control Applications in Modern Power Systems*. Springer, Singapore, 2023. 63-75.  
 [6] Chenchireddy, K., Kumar, V., Eswaraiiah, G., Sreeivothi, K. R., Svdu, S. A., & Ganesh, L. B. (2022, August). Torque Ripple Minimization in Switched Reluctance Motor by Using Artificial Neural Network. In *2022 IEEE 2nd International Conference on Sustainable Energy and Future Electric Transportation (SeFeT)* (pp. 1-6). IEEE.  
 [7] Tousizadeh, Mahdi, et al. "A Generalized Fault Tolerant Control Based on Back EMF Feedforward Compensation: Derivation and Application on Induction Motors Drives." *Energies* 16.1 (2023): 51..  
 [8] Kali, Yassine, et al. "Enhanced Reaching-Law-Based Discrete-Time Terminal Sliding Mode Current Control of a Six-Phase Induction Motor." *Machines* 11.1 (2023): 107.  
 [9] Anagreh, Yaser, and Asma Al-Ibbini. "Low cost high performance self-starting sensorless single phase induction motor drive." *International Journal of Power Electronics and Drive Systems* 14.1 (2023): 123.  
 [10] Chenchireddy, K., Kumar, V., & Sreeivothi, K. R. (2021, March). Investigation of performance vector control single-phase induction motor. In *2021 7th International Conference on Advanced Computing and Communication Systems (ICACCS)* (Vol. 1, pp. 887-891). IEEE.  
 [11] Law, Kah Haw. "Closed loop bidirectional rotation and speed controls for three-phase induction motor." *AIP Conference Proceedings*. Vol. 2643, No. 1. AIP Publishing LLC, 2023.  
 [12] Al Azze, Qasim, and Imad Abdul-Rida Hameed. "Reducing torque ripple of induction motor control via direct torque control." *International Journal of Electrical and Computer Engineering* 13, no. 2 (2023): 1379.  
 [13] Che, Haijun, et al. "A New SMO for Speed Estimation of Sensorless Induction Motor Drives at Zero and Low Speed." *IEEJ Transactions on Electrical and Electronic Engineering* (2023).  
 [14] Karupusamy, Sathishkumar, et al. "Torque control-based induction motor speed control using Anticipating Power Impulse Technique." *The International Journal of Advanced Manufacturing Technology* (2023): 1-9.  
 [15] Kumar, V., Chenchireddy, K., Sreeivothi, K. R., & Sujatha, G. (2022). Design and Development of Brushless DC Motor Drive for Electrical Vehicle Application. In *AI Enabled IoT for Electrification and Connected Transportation* (pp. 201-217). Singapore: Springer Nature Singapore.

# Grid-Connected Inverter Fed from PV Array

V Kumar  
Dept. of EEE  
Teegala Krishna Reddy Engineering  
College  
Hyderabad, Telangana, India.  
kumarpoma@gmail.com

M Prashanth,  
UG Student,  
Dept. of EEE  
Teegala Krishna Reddy Engineering  
College  
Hyderabad, Telangana, India.  
Prashanthmanga4@gmail.com

Y Maniteja Reddy,  
UG Student,  
Dept. of EEE  
Teegala Krishna Reddy Engineering  
College  
Hyderabad, Telangana, India.  
yasamaniteja@gmail.com

J Srilakshmi,  
UG Student,  
Dept. of EEE  
Teegala Krishna Reddy Engineering  
College  
Hyderabad, Telangana, India.  
Julakantisrilakshmi2109@gmail.com

P Meghana  
UG Student,  
Dept. of EEE  
Teegala Krishna Reddy Engineering  
College  
Hyderabad, Telangana, India.  
Perumandlameghana88@gmail.com

Kalagotla Chenchireddy  
Assistant Professor,  
Dept. of EEE  
Teegala Krishna Reddy Engineering  
College  
Hyderabad, Telangana, India.  
chenchireddy.kalagotla@gmail.com

**Abstract:** This manuscript presents a grid-connected two-level inverter. The presented inverter is controlled by SRF theory with a PI controller. The two-level inverter switching pulses are generated from the space vector modulation technique. The main advantages of two-level inverters are less number of switches, low switching loss, low cost and, suitable for low power rating applications. Software called MATLAB/Simulink is used to reproduce the depicted circuit. The inverter output voltage, grid voltage, grid current, and PV module voltage are all confirmed by the simulation findings.

**Keywords:** Inverter, PV panel, Grid.

## I INTRODUCTION

This paper presents a Two-level voltage source inverter. This type of inverter is used for low-voltage and low-power range applications. Regarding [1], Model predictive control is used to regulate a better T-Type grid-linked inverter. The implemented control scheme decoupled active and reactive powers by using the DQ reference frame. This paper improved T-Type results compared with conventional T-type results. Authors in [2] Trinary hybrid CHB MLI had implemented. The implemented inverter generated more number of output voltage levels. The controller eliminated DC-offset voltages. The second-order controller controlled active, and reactive powers and irradiation. This paper three-phase three-level inverter implemented for grid connection. The

implemented inverter is controlled by a one-cycle controller. The presented controller has low switching loss and robust performance [3]. In [4] implemented a multi-string five-level inverter with a work of fictitious PWM technique. The implemented topology has an input solar panel, auxiliary circuit, DC-DC converter circuit, and inverter. This paper is a DSP controller implemented.

The yield current THD is 1.76%. Reference [5] different sliding mode control strategies applied single stage PWM inverter. Different SMC procedures are regular SMC, fundamental PWM inverter controlled by SMC, terminal attractor, and crucial terminal attractor. For an LCL-GCI shut circle architecture, To stop the mutilation of the matrix current, reference [6] has presented a better current SMC technique with capacitor current feed-forward control. Reference [7] reported on a modified sliding mode control for a single-stage VSI. In this control system is decreased burden of current aggravations and gapping issues. Jose Antonio et al [8] presented another SMC for a single-stage inverter in a photovoltaic MPPT application. The SMC had contrasted tentatively and a traditional PI regulator; SMC got a superior dynamic and unsettling influence dismissal. En-jaw change [9] introduced clever SMC for VSI. 1KW VSI trial tests had. Thought about consistent state and dynamic reaction test results, the general framework had tried under fluctuating working conditions, to be specific

state-load changing, the channel boundary varieties, and rectifier load.

Another SMC system was proposed by satishkumargudey et. al [10] which control voltage source inverter-based higher-request circuit. The VSI yield results accomplished great following capacity and hearty execution. AshnaMohan et.al [11] a versatile all-out sliding mode control (ATSMC) conspires intended for framework-associated photovoltaic frameworks. The framework associated inverter with an ATSMC had assessed by PC recreation MATLAB/Simulink power framework tool compartment. Authors explained different inverter topologies in [12]-[15].

### II GRID-CONNECTED INVERTER

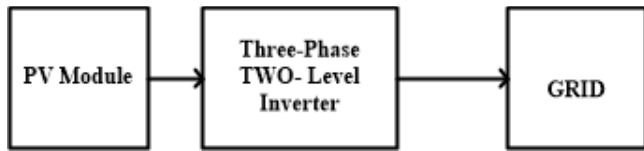


Fig.1 grid-connected PV module

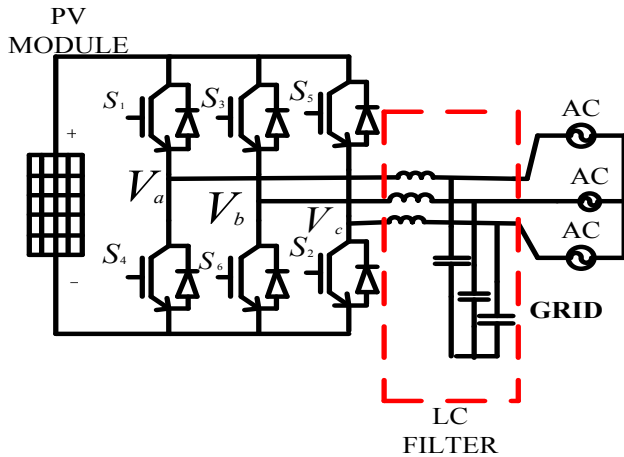


Fig.2 grid interfaced three-phase two-level inverter

Fig.1 shows the grid interfacing inverter. The block diagram has three blocks of PV Module, a two-level inverter, and a grid. Fig.2 shows a grid-interfaced three-Phase two-level inverter. The circuit has PV Module, six IGBT switches, an LC filter, and a three-phase grid supply. The LC filter circuit is used for reducing ripples in the Inverter output voltage. In this circuit  $V_a$ ,  $V_b$  and  $V_c$  are common coupling voltages grid and inverter. The Main Reasons for choosing IGBT switches are operating high voltage, high current, and high power. The other power electronics switches like MOSFET and SCRare not suitable

for inverters; MOSFET is suitable for choppers because it will operate at a high frequency. The two-level inverter advantages are fewer power electronic switches, low switching loss, easily control. The operation two-level inverters  $S_1$  and  $S_4$ ,  $S_3$ , and  $S_6$ , as well as  $S_5$  and  $S_2$ , are working in a complementary manner. The inverter switches are selected based on voltage-blocking capacity.

### III SYNCHRONOUS REFERENCE FRAME THEORY

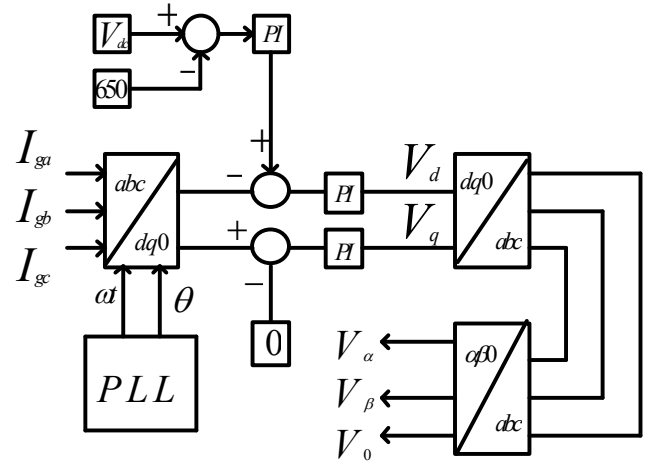


Fig.3 synchronous reference frame theory

The SRF theory is presented in fig.3. The SRF theory mainly is used for controlling three-phase quintets. The circuit  $I_{ga}$ ,  $I_{gbo}$ , and  $I_{gco}$  are the three-phase grid currents. The controller unit vector-based PLL is presented in fig.3. The main aim of this paper is the inverter output voltage synchronizing grid. The PLL synchronizes the grid voltage with the inverter output while also locking voltages with a small continuous phase error. Three-phase voltages are required for PLL input, PLL gives amplitude, frequency and phase angle. The outputs of PLL are  $\omega$  and  $\theta$ .

$$\begin{bmatrix} I_d \\ I_q \\ I_0 \end{bmatrix} = \frac{2}{3} \begin{bmatrix} \sin \omega t & \sin \left( \omega t - \frac{2\pi}{3} \right) & \sin \left( \omega t + \frac{2\pi}{3} \right) \\ \cos \omega t & \cos \left( \omega t - \frac{2\pi}{3} \right) & \cos \left( \omega t + \frac{2\pi}{3} \right) \\ \frac{1}{2} & \frac{1}{2} & \frac{1}{2} \end{bmatrix} \begin{bmatrix} I_{ga} \\ I_{gb} \\ I_{gc} \end{bmatrix} \quad (1)$$



$$\begin{bmatrix} V_a \\ V_b \\ V_c \end{bmatrix} = \begin{bmatrix} \sin \omega t & \cos \omega t & 1 \\ \sin\left(\omega t - \frac{2\pi}{3}\right) & \cos\left(\omega t - \frac{2\pi}{3}\right) & 1 \\ \sin\left(\omega t + \frac{2\pi}{3}\right) & \cos\left(\omega t + \frac{2\pi}{3}\right) & 1 \end{bmatrix} \begin{bmatrix} V_d \\ V_q \\ V_0 \end{bmatrix} \quad (2)$$

$$\begin{bmatrix} V_\alpha \\ V_\beta \\ V_0 \end{bmatrix} = \sqrt{\frac{2}{3}} \begin{bmatrix} 1 & -\frac{1}{2} & -\frac{1}{2} \\ 0 & \frac{\sqrt{3}}{2} & -\frac{\sqrt{3}}{2} \\ \frac{1}{2} & \frac{1}{\sqrt{2}} & \frac{1}{\sqrt{2}} \end{bmatrix} \begin{bmatrix} V_a \\ V_b \\ V_c \end{bmatrix} \quad (3)$$

#### IV SPACE VECTOR DIAGRAM FOR TWO-LEVEL INVERTER

Each phase-leg of the carrier-based modulation scheme techniques must be controlled separately.

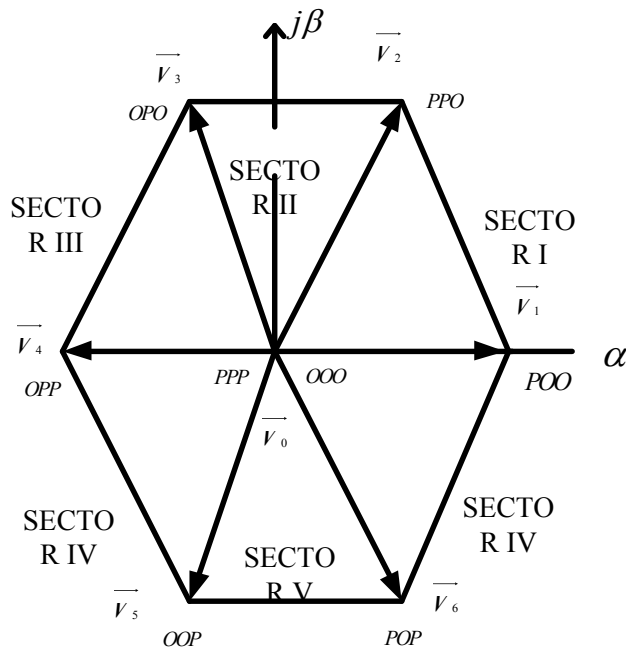


Fig.4 space vector modulation  
 TABLE: 1 ZERO VECTORS

SPACE VECTOR		SWITCHING STATES	ON-STATE SWITCH
ZERO VECTOR	$\vec{V}_0$	PPP	$S_{1^*} S_{3^*} S_5$
		OOO	$S_{4^*} S_{6^*} S_2$

Table: 2 Active Vectors

	SPACE VECTOR	SWITCHING STATES	ON-STATE SWITCH
ACTIVE VECTOR	$\vec{V}_1$	POO	$S_{1^*} S_{6^*} S_2$
	$\vec{V}_2$	PPO	$S_{1^*} S_{3^*} S_2$
	$\vec{V}_3$	OPO	$S_{4^*} S_{3^*} S_2$
	$\vec{V}_4$	OPP	$S_{1^*} S_{3^*} S_5$
	$\vec{V}_5$	OOP	$S_{4^*} S_{6^*} S_5$
	$\vec{V}_6$	POP	$S_{1^*} S_{6^*} S_5$

The space vector can be generically represented by the two-phase voltage in the alpha-beta plane. (4) Adding (2) to (3) results in (5)

Where and x = 0 or 2/3 or 4/3.

The load section voltages produced for the active switching state [POO] are

$$\begin{aligned} V_{AO}(t) &= \frac{2}{3} V_d \\ V_{BO}(t) &= -\frac{1}{3} V_d \end{aligned} \quad (6)$$

and

$$V_{CO}(t) = -\frac{1}{3} V_d$$

The analogous space vector indicated can be determined by plugging (6) into (5). (7)

The same process can be used to derive all six vivacious

$$\text{vectors. } \vec{V}_k = \frac{2}{3} V_d e^{j(k-1)\frac{\pi}{3}} \quad k = 1, 2, \dots, 6 \quad (8)$$

#### A. Dwell time calculation

The volt-second balancing equation is

$$\begin{cases} \vec{V}_{ref} T_s = V_1 T_a + V_2 T_b + V_0 T_0 \\ T_s = T_a + T_b + T_0 \end{cases} \quad (9)$$

TABLE: 3 COMPARISON TABLE

Topology	Control Technique	Outcome
Improved T-type grid-connected inverter [1]	Model predictive control	Controlled active and reactive power. Improved T-type topology has better results compared to T-type topology.
Trinary Hybrid CHB-MLI implemented [2]	Modified second-order generalized integral control scheme implemented.	The implemented inverter produced the maximum number of output voltage levels. The presented system operated at critical load conditions.
Three-phase three-level inverter [3]	One cycle control method implemented	Robust performance Low switching loss Interfaced with grid
Multi-string five-level inverter [4]	Carrier and reference signal PWM technique implemented	The implemented inverter fed PV Unity power factor Both voltage and current in the phase

IV SIMULATION DIAGRAM

TABLE: 3 Circuit Parameters

S.No	Parameter	Rating
1	PV module short-circuits current	8.01A
2	PV module open circuit voltage	36.90V
3	PV module cutting-edge at most power	7.10A
4	PV module cutting-edge at most power	30.3V
5	Phase-phase RMS voltage	400V
6	Filter inductance value	4.5mH
7	The capacitor across PV Module	2200e-6

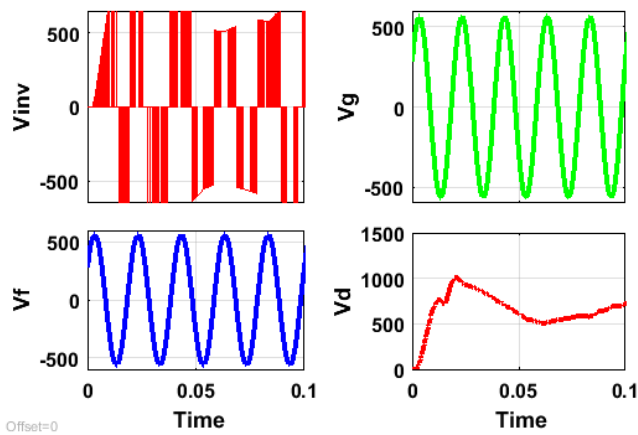


Fig.5 shows  $V_{inv}$ ,  $V_f$ ,  $V_g$  and  $V_d$  voltage waveforms

Different voltage waveforms are shown in fig.5. The inverter output voltage represents before filtering ( $V_{inv}$ ) and after filter voltage represents ( $V_f$ ). The  $V_{inv}$  shows like a square waveform and  $V_f$  shows like a pure sinusoidal waveform. The grid voltage represents  $V_g$  and PV module output voltage  $V_d$ .

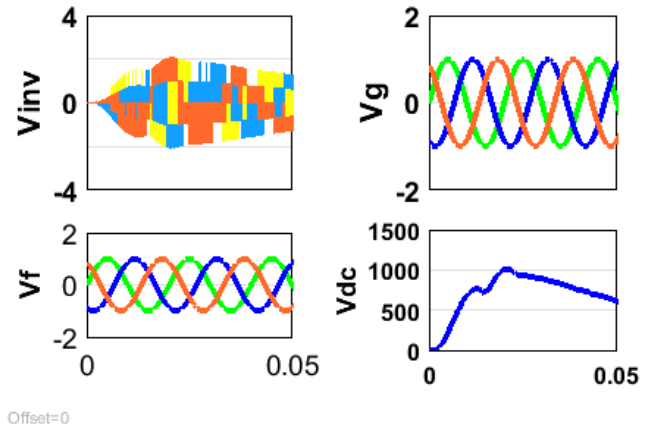


Fig.6 shows three-phase  $V_{inv}$ ,  $V_f$ ,  $V_g$  and  $V_{dc}$

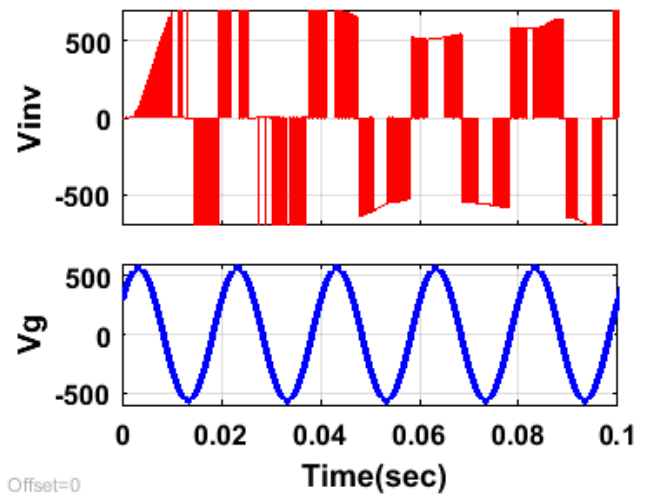


Fig.7 shows the inverter output and grid voltage

Fig.6 indicates the three-section inverter output voltage, inverter output voltage after LC clear-out circuit, three-section grid voltage and PV module voltage. The inverter output voltage looks like a square wave with a harmonic spectrum. The voltages  $V_f$  and  $V_g$  are both the same waveforms.

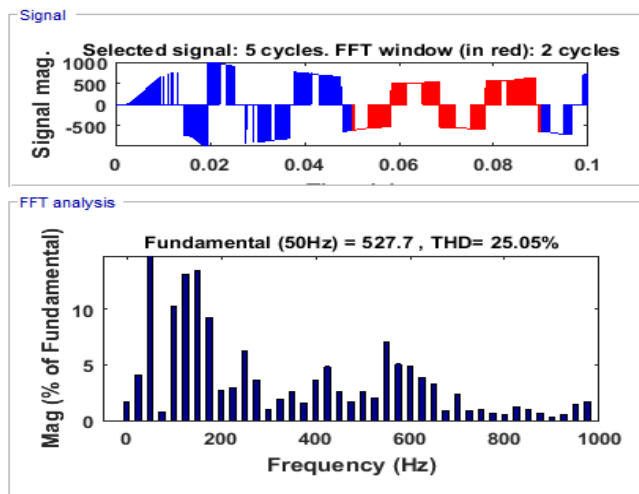


Fig.8 shows inverter output voltage with THD value

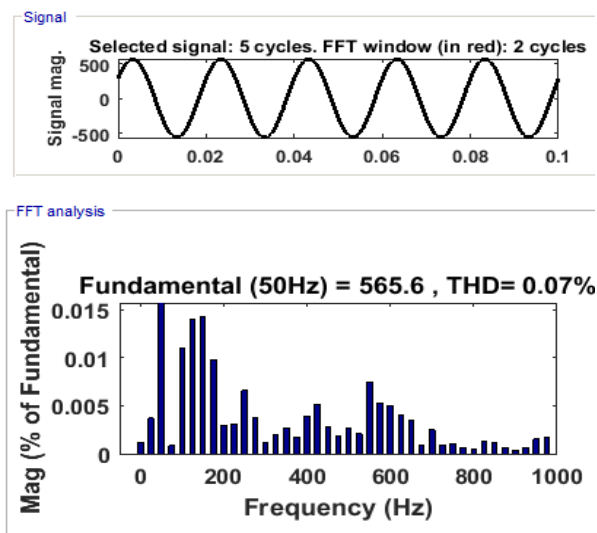


Fig.9 shows grid side voltage with THD value

Fig. 8 shows the THD value of the inverter production voltage is 25.06%. Fig. 9 shows the THD value of grid voltage is 0.07%.

## V CONCLUSION

This paper presented a grid-connected PV fed Inverter. The implemented inverter is a three-phase three-level topology. The inverter topology is controlled by the SVPWM technique and SPWM-generated PWM pulses for the inverter. The different simulation results verified grid supply voltage, current and inverter output voltage, and current. The DC-Link capacitor balancing voltage is shown in the results. The THD of the output current is 0.07%. The

THD of the inverter output voltage is 25.05%. The overall system performance is very good.

## References

- [1] Yang, G., Hao, S., Fu, C., & Chen, Z. (2018). Model predictive direct power control based on improved T-type grid-connected inverter. *IEEE Journal of Emerging and Selected Topics in Power Electronics*, 7(1), 252-260.
- [2] Mukundan, N. M. C., Pychadathil, J., Subramaniam, U., & Almkhles, D. J. (2020). Tertiary hybrid cascaded H-bridge multilevel inverter-based grid-connected solar power transfer system supporting critical load. *IEEE Systems Journal*, 15(3), 4116-4125.
- [3] Chen, Yang, and Keyue Ma Smedley. "One-cycle-controlled three-phase grid-connected inverters and their parallel operation." *IEEE Transactions on Industry Applications* 44.2 (2008): 663-671.
- [4] Rahim, Nasrudin A., and Jeyraj Selvaraj. "Multistring five-level inverter with novel PWM control scheme for PV application." *IEEE transactions on industrial electronics* 57.6 (2009): 2111-2123.
- [5] Chang, En-Chih, Yow-Chyi Liu, and Chien-Hsuan Chang. "Experimental performance comparison of various sliding modes controlled PWM inverters." *Energy Procedia* 156 (2019): 110-114.
- [6] Dang, Chaoliang, Xiangqian Tong, and Weizhang Song. "Sliding-mode control in dq-frame for a three-phase grid-connected inverter with LCL-filter." *Journal of the Franklin Institute* 357.15 (2020): 10159-10174.
- [7] Hou, B., Liu, J., Dong, F., Wang, M., & Mu, A. (2016, May). Sliding mode control strategy of voltage source inverter based on load current sliding mode observer. In 2016 IEEE 8th International Power Electronics and Motion Control Conference (IPEMC-ECCE Asia) (pp. 1269-1273). IEEE.
- [8] Cortajarena, J. A., Barambones, O., Alkorta, P., & De Marcos, J. (2017). Sliding mode control of grid-tied single-phase inverter in a photovoltaic MPPT application. *Solar Energy*, 155, 793-804.
- [9] Chang, E. C. (2018). Study and application of intelligent sliding mode control for voltage source inverters. *Energies*, 11(10), 2544.
- [10] Gudey, S. K., & Gupta, R. (2015). Sliding-mode control in voltage source inverter-based higher-order circuits. *International Journal of Electronics*, 102(4), 668-689.
- [11] Mohan, A., Mathew, D., & Nair, V. M. (2013, December). Grid-connected PV inverter using adaptive total sliding mode controller. In 2013 International Conference on Control Communication and Computing (ICCC) (pp. 457-462). IEEE.
- [12] Chenchireddy, K., Jegathesan, V., & Ashok Kumar, L. (2020). Different topologies of inverter: a literature survey. *Innovations in Electrical and Electronics Engineering*, 35-43.
- [13] Chenchireddy, K., & Jegathesan, V. (2021). A Review Paper on the Elimination of Low-Order Harmonics in Multilevel Inverters Using Different Modulation Techniques. *Inventive Communication and Computational Technologies*, 961-971.
- [14] Sreejyothi, Khammampati R., et al. "Level-Shifted PWM Techniques Applied to Flying Capacitor Multilevel Inverter." 2022 International Conference on Electronics and Renewable Systems (ICEARS). IEEE, 2022.

- [15] Chenchireddy, K., Jegathesan, V., & Kumar, L. A. (2019). Design and Simulation of a Single Phase Four Level Neutral Point Clamped Inverter. International Journal of Recent Technology and Engineering (IJRTE) ISSN, 2277-3878.

See discussions, stats, and author profiles for this publication at: <https://www.researchgate.net/publication/369475826>

# Wind –Battery Controller Based Standalone Alternating Current Microgrid Applications

Conference Paper · March 2023

---

CITATIONS

0

READS

80

1 author:



[Kalagotla Chenchireddy](#)

Karunya University

53 PUBLICATIONS 160 CITATIONS

SEE PROFILE

# Wind - Battery Controller Based Standalone Alternating Current Microgrid Applications

Rosaiah Mudigondla  
Assistant professor  
Dept of Electrical and electronics  
engineering,  
Teegala Krishna Reddy Engineering  
College  
Hyderabad  
[rosaiah0228@gmail.com](mailto:rosaiah0228@gmail.com)

Bellampally Shree Gagan Reddy  
UG student  
Dept of Electrical and electronics  
engineering,  
Teegala Krishna Reddy Engineering  
College  
Hyderabad  
[connect2shreegagan@gmail.com](mailto:connect2shreegagan@gmail.com)

Bandela Vinitha  
UG student  
Dept of Electrical and electronics  
engineering,  
Teegala Krishna Reddy Engineering  
College  
Hyderabad  
[vinithabandela@gmail.com](mailto:vinithabandela@gmail.com)

Pasham Vishwateja  
UG student  
Dept of Electrical and electronics  
engineering,  
Teegala Krishna Reddy Engineering  
College  
Hyderabad  
[pashamvishwateja@gmail.com](mailto:pashamvishwateja@gmail.com)

Akhilesh Kamble  
UG student  
Dept of Electrical and electronics  
engineering,  
Teegala Krishna Reddy Engineering  
College  
Hyderabad  
[kambleakhilesh055@gmail.com](mailto:kambleakhilesh055@gmail.com)

Kalagotla Chenchireddy  
Assistant professor  
Dept of Electrical and electronics  
engineering,  
Teegala Krishna Reddy Engineering  
College  
Hyderabad  
[chenchireddy\\_kalagotla@gmail.com](mailto:chenchireddy_kalagotla@gmail.com)

**Abstract:** *This research paper describes a wind-battery-based standalone AC micro grid system that can provide reliable and uninterrupted power to off-grid applications. The proposed system consists of a wind turbine, a battery bank, and an inverter that work together to generate and store electricity, which can be utilized to power critical loads in a standalone micro grid.*

*The microcontroller controls the energy flow between the wind turbine, battery bank, and load to ensure a stable and continuous power supply. The system's performance is evaluated using simulation, which demonstrates that the proposed system is capable of effectively providing reliable and uninterrupted power to standalone micro grids, making it a promising solution for remote and off-grid areas.*

**Keywords:** *Battery, Wind turbine, Micro Grid, Controller.*

## I INTRODUCTION

A wind-battery-based standalone AC micro grid is a new technology that has been proven to be a dependable and sustainable way to supply energy to off-the-grid and remote locations.[1] This kind of micro grid creates and distributes electricity using wind turbines, battery storage, and an AC power system.[2] Several studies have investigated the feasibility and performance of wind-battery-based standalone AC micro grids in various locations. For example, a study conducted by researchers at the University of Manchester and.[3] the University of Edinburgh

evaluated the performance of a wind-battery-based standalone AC micro grid in a remote area of Scotland and found it to be a cost-effective and sustainable solution.[4]. Another study conducted by researchers at the University of Waterloo and the University of Ontario Institute of [14]. Technology evaluated the most efficient wind-battery standalone AC micro grid design and operation for distant communities in Canada and discovered it to be a dependable and affordable source of electricity.

[5] Also, a University of Michigan study investigated the potential of freestanding.[6] AC micro grids powered by wind and batteries lower carbon emissions and enhance access to energy in poor nations.[7] According to the study, these micro grids might supply dependable and sustainable electricity to rural areas, hence lowering the demand for conventional electricity generation from fossil fuels. [8] Standalone AC micro grids powered by wind batteries have demonstrated significant promise as a trustworthy and sustainable way to supply power to rural and off-grid locations. [9] This technology has the potential to be adopted widely as a means of producing and distributing sustainable energy with continued study and development.[10]. Electricity generated by wind turbines can be stored in batteries to ensure a consistent supply of power during periods of low wind or high demand. This enables the stored energy to be utilized for electricity production at

a later time, contributing to a reliable and stable energy grid. [11] The batteries can also be utilized to balance the micro grid's power supply and demand. As a stand-alone system.[12]By doing this, the micro grid is guaranteed to be able to continue supplying electricity even during power outages or other disturbances in the primary grid.[13]The type of electrical power generated and supplied by the micro grid is known as AC (alternating current).[15]

## II WIND ENERGY POWER GENERATION

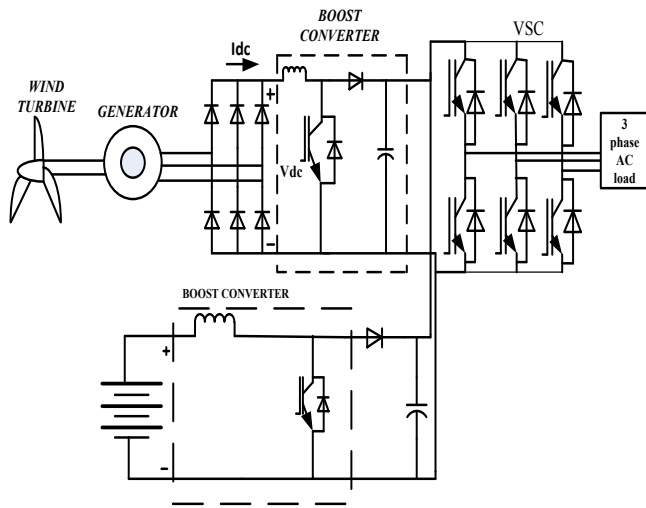


Figure-1: WIND Energy generating station

### a. Wind energy power generation

A self-sufficient electrical power system, a battery wind-based standalone AC micro grid combines renewable energy sources like wind turbines and batteries to deliver electricity to a nearby neighborhood or facility. Using the kinetic energy of the wind and transforming it into electrical power, wind turbines produce electricity.

The batteries can also be utilized to balance the micro grid's power supply and demand. As a stand-alone system, By doing this, the micro grid is guaranteed to be able to continue supplying electricity even during power outages or other disturbances in the primary grid. The type of electrical power generated and supplied by the micro grid is known as AC (alternating current). Alternating current (AC) is the primary form of electricity that is utilized in residences and commercial establishments, and it is usually supplied via the main grid. Overall, a standalone AC micro grid powered by wind and batteries is a dependable and sustainable way to supply electricity to a company or local community.

The micro grid can lessen its reliance on fossil fuels and contribute to a cleaner, more sustainable energy future by using renewable energy sources like wind turbines and batteries.

### b. Battery Wind-Based Standalone AC Micro grid Components:

**Wind Turbines:** In a battery-powered freestanding AC micro grid, wind turbines serve as an important energy source. These wind turbines transform wind kinetic energy into electrical energy that can be utilized to power electrical loads in a micro grid or stored in batteries.

**Batteries:** A freestanding AC micro grid powered by batteries and wind has two main uses for its batteries. In the beginning, they store the electrical energy produced by the wind turbines so that it may be used when there is no wind. Second, by delivering electricity during sudden spikes in demand or drops in supply, they assist in maintaining a balance between the micro grid's power supply and demand.

Power electronics play a crucial role in converting the electrical energy produced by batteries and wind turbines into the necessary AC power required to operate the electrical loads in the micro grid. Furthermore, they assist in managing the power flow and maintaining a balance between the power supply and demand within the micro grid.

A battery-wind-based standalone AC micro grid's control system is in charge of overseeing the system's overall performance. It keeps an eye on the micro grid's power supply and demand, regulates the power flow between the wind turbines and batteries, and makes sure the micro grid is running effectively and safely.

### c. Battery model

The battery model for an AC micro grid typically includes several parameters that describe the behavior of the battery. These parameters include:

1. **Capacity:** This refers to the total energy that can be stored in the battery. It is typically measured in kilowatt-hours (kWh) and depends on the size and type of the battery.
2. **Efficiency:** This parameter describes how efficiently the battery can convert stored energy into usable AC power. Various factors, such as battery chemistry, temperature, and charge/discharge rate, can impact the efficiency of batteries. **Charging and Discharging Characteristics:** This parameter describes how the battery charges and discharges over time. The charging and discharging rate of a battery can affect its lifetime and performance.
3. **Charge Status:** The parameter describes the amount of energy stored in the battery at any given time, expressed as a percentage of the battery's capacity.
4. The charge status is an important parameter to monitor as it can affect the battery's performance

and lifetime. Voltage and Current: These parameters describe the electrical attributes of the battery. The battery's effectiveness and efficiency can be influenced by variables such as voltage and current.

**d. Mathematical Model**

Charge status Model:

The charge status of the battery can be represented as a function of charging and discharging currents, battery capacity, and efficiency.

$$dSOC / dt = (I_{ch} - I_{dis}) / C - (1 / E) * I_{ch}$$

Where: dSOC/ dt: rate of change of the state of charge with time (in Ah/s)

I<sub>ch</sub>: charging current (in A)

I<sub>dis</sub>: discharging current (in A) C: battery capacity (in Ah)

E: battery efficiency (dimensionless)

Battery Voltage Model:

The battery's voltage can be expressed as a function of its state of charge, internal resistance, and open-circuit voltage, among other factors.

$$V_{bat} = V_{oc} - R_i * I - K_{soc}$$

Where: V<sub>bat</sub>: battery voltage (in V) V<sub>oc</sub>: The voltage of the battery when it is not connected to a load, (in V) R<sub>i</sub>: The battery's inner resistance. (in ohms) I: current flowing through the battery (in A) K<sub>SOC</sub>: voltage correction factor due to state of charge

Wind Turbine Model:

The wind turbines power output can be mathematically expressed by the wind speed and power coefficient.

$$P_{wt} = 0.5 C_p rho A V^3$$

where: P<sub>wt</sub>: wind turbine power output (in W) C<sub>p</sub>: The power coefficient of the wind turbine (unitless), which is influenced by variables such as air density (in kg/m<sup>3</sup>), the area of the wind turbine blades (in m<sup>2</sup>), and the wind speed (in m/s).

AC Power Distribution Model:

The AC power distribution model can be represented by a set of linear or nonlinear equations that describe the flow of power between different sources and loads in the micro grid. These equations may include factors such as the impedance of the transmission lines, the reactive power flow, and the phase angle of the AC voltage.

Overall, these equations can be used to simulate the behavior of the battery-wind-based standalone AC micro grid and optimize its performance under different operating conditions. However, it's important to note that the specific mathematical model used will depend on the specific design of the micro grid and the desired level of accuracy.

**e. Benefits of a Wind-Based Battery-Based Standalone AC Micro grid:**

Reducing Dependency on Fossil Fuels: By using renewable energy sources to power a battery-wind-based standalone AC micro grid, we may lessen our reliance on fossil fuels and move towards a cleaner, more sustainable energy future.

Enhanced Resilience: A standalone AC micro grid powered by batteries and wind is independent of the main power system. This makes it more dependable and resilient because it can keep supplying electricity despite blackouts or other major grid disturbances.

Cost Savings: By providing electricity at a lower cost than the main grid, a battery-based wind-based standalone AC micro grid can contribute to the reduction of energy expenses. This is especially true in rural locations where it could be prohibitively expensive to connect to the main grid.

Lower Environmental Impact: Compared to conventional power generating techniques, a battery-based wind-based standalone AC micro grid has a lower environmental impact and emits no greenhouse gases.

Overall, a standalone AC micro grid powered by wind and batteries is a dependable and sustainable way to supply electricity to a company or local community. The micro grid can lessen its reliance on fossil fuels and contribute to a cleaner, more sustainable energy future by using renewable energy sources like wind turbines and batteries.

The energy storage device and DC-DC converter are shown which explains how the energy is kept in the battery and transferred to the inverter with the aid of a boost converter. A boost converter creates a DC output voltage that is larger than the DC input voltage It is obvious from the name alone that this is a boost converter used for DC voltage step-up. The inverter's AC output was sent to the load.

**III. CONTROL SCHEME:**

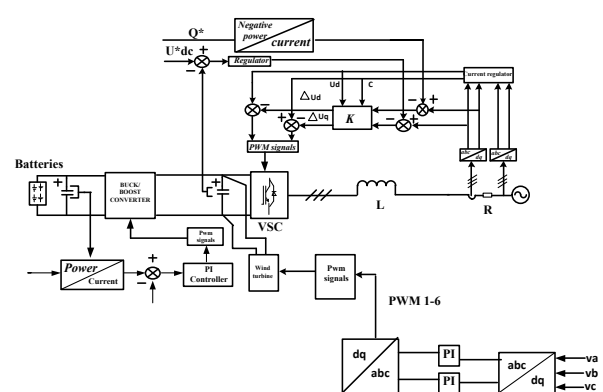


Figure2: control scheme



The primary objective of the control system is to manage and maintain the power flow between the various renewable energy sources. (Wind turbine), the battery, and the loads in the micro grid, to maintain a stable and reliable supply of AC power. Here is a step-by-step breakdown of the control scheme:

1. Measurement of system variables: The first step in the control scheme is to measure key system parameters such as wind speed, battery voltage and current, and load demand.
2. Power generation control: Based on the measured variables, the control system calculates the amount of power generated by renewable energy sources.
3. The power output can be adjusted by controlling the blade pitch angle of the wind turbine. The power output is then sent to the battery and the load
4. To regulate the charging and discharging of the battery, a PI controller is employed for control purposes. The PI controller compares the desired battery voltage with the actual battery voltage and adjusts the battery charging and discharging currents accordingly. The PI controller uses the proportional and integral terms to adjust the battery current in response to changes in the error between the desired and actual battery voltage.
5. Load control: The PI controller is also used to regulate the power flow to the load. The PI controller compares the desired AC voltage with the actual AC voltage and adjusts the power output of the renewable energy sources accordingly. The proportional and integral terms are used to adjust the power output of the

renewable energy sources in response to changes in the error between the desired and actual AC voltage.

6. System stability control: For maintaining a stable voltage and frequency in the micro grid, the PI controller is utilized for system stability control. It regulates the power output of renewable energy sources and the charging/discharging currents of the battery.

In general, the PI controller is a commonly used option for governing power flow in a battery-wind standalone AC micro grid due to its ability to regulate battery charging and discharging currents and control the renewable energy sources' power output straightforwardly and efficiently. Nonetheless, it's essential to acknowledge that the optimal control scheme selection will depend on the micro grid's design and the desired level of control precision.

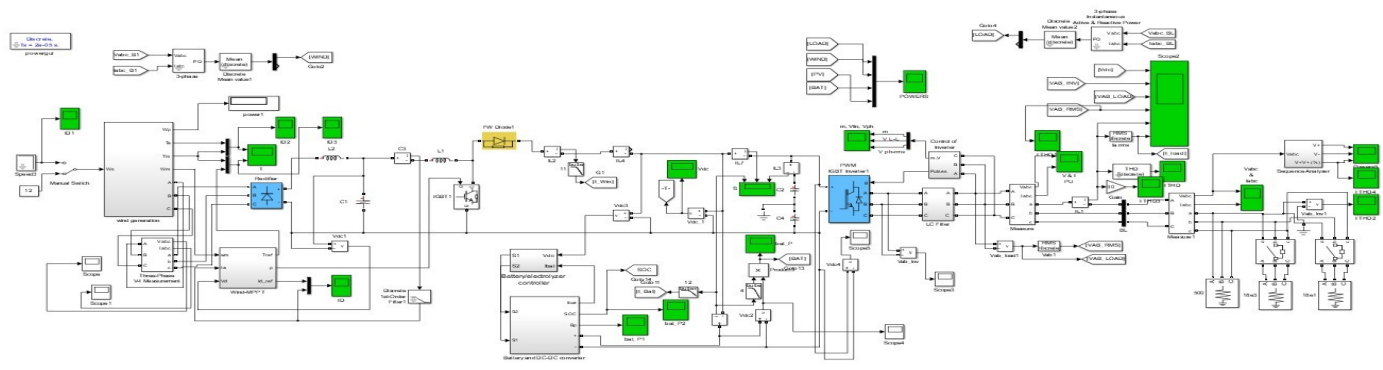


FIGURE 3: SIMULINK MODEL

#### IV.SIMULATION RESULTS

Once the MATLAB/simulation diagram was designed, the current and voltage waveforms for the wind model, battery, inverter, and load side input and output were extracted using MATLAB/Simulink. The figure shows the MATLAB/simulation diagram that was designed.

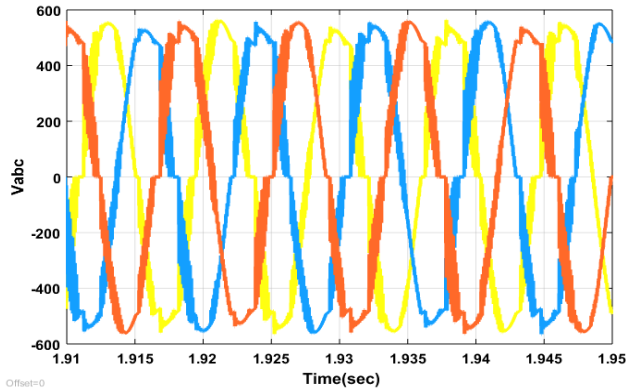


Figure 4: wind output voltage

From the above waveform, we can observe the output voltage of a wind turbine which is a three-phase ac waveform, consisting of R Y Bphases. The determination of the three phases involves the utilization of distinct colors, namely red, yellow, and blue... The waveform is distorted because of the inconsistency in power generation. As the wind is not constant, the power generation using wind energy will be inconsistent.

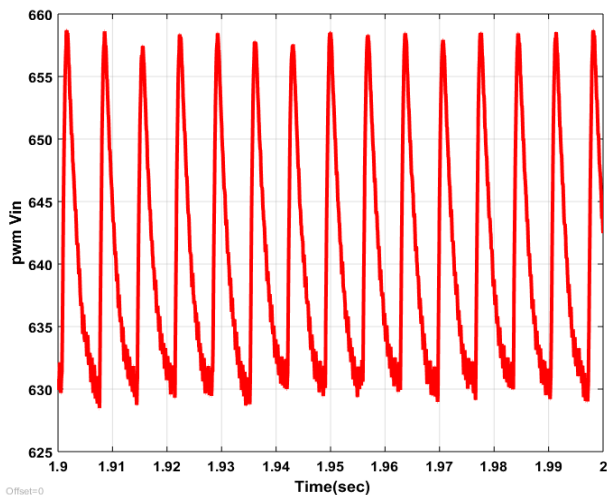


Figure 5:P-W-M Input Voltage Waveform

The above visual shows the pulse width modulation wave. That PWM is the minimum requirement wave for the operating condition. The x-axis shows the PWM voltage and the y-axis shows the time in a sec that the wave contributed to the operating conditions. Because of the PWM wave, only

requirement quantity is used hence the whole operation becomes optimal and efficient.

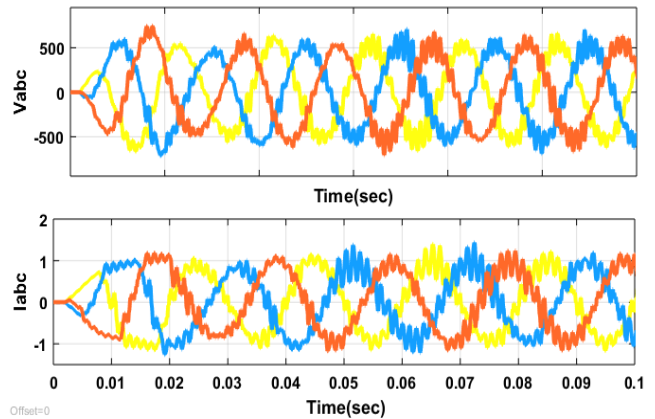


Figure 6: Vabc and Iabc load voltage and load current

The above waveform shows the output load for the voltage and current. The output voltage and current of an AC load powered by a wind generator are influenced by various factors, whereas the determination of the three phases is accomplished through the use of distinct colors, namely blue, orange, and blue. Firstly, wind speed is a significant factor as it affects the rotational speed of the turbine's blades and, in turn, the output voltage and current. Secondly, the size and design of the wind turbine can also influence the output voltage and current.

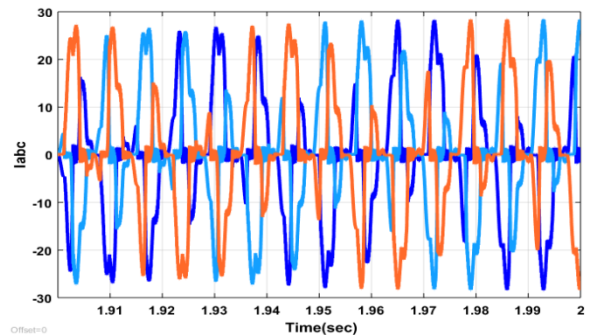


Figure 7 : waveform of the wind turbine's output current.

By analyzing the waveform depicted above, we can deduce that the wind turbine's output current takes the form of a three-phase AC waveform, characterized by three distinct phases represented by three different colors. The magnitude of the current waveform oscillates between -30 and 30.

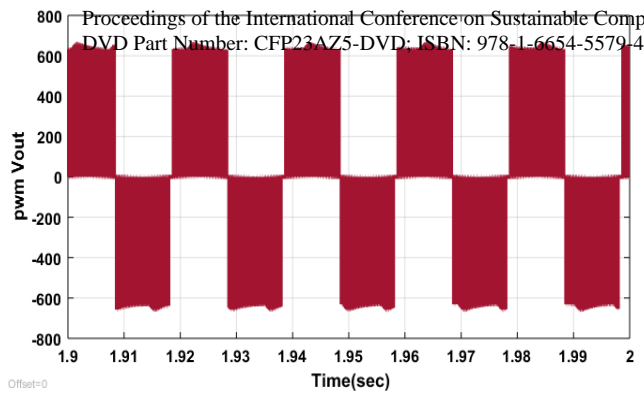


Figure8: PWM voltage output waveform

The above waveform represents the pulse width modulation waveform for output voltage. By altering the width of signal pulses, the voltage can be adjusted. The horizontal axis of the graph shows the output voltage, while the vertical axis represents time measured in seconds.

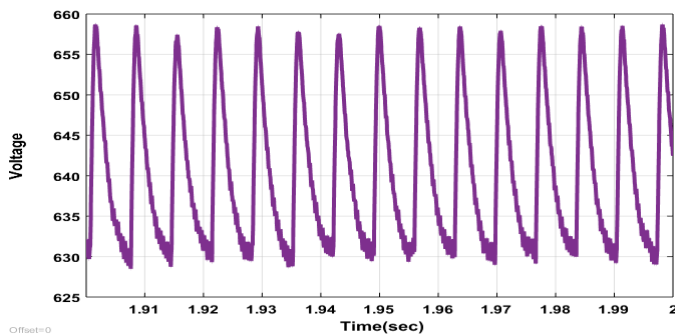


Figure9: battery output voltage

The above visual shows the output voltage waveform of the battery output. the voltage that comes out from the battery is alternating voltage Consumers make efficient and effective use of the voltage produced by the battery.

## VII.CONCLUSION

Due to their capacity to deliver dependable and sustainable power, standalone AC micro grid applications for wind-battery-based energy systems are growing in popularity. The management of electricity generation under varying conditions, however, continues to be difficult. The control methods proposed in this study tackle this issue and optimize the utilization of the generated power for standalone AC micro grid applications. These methods can help wind-battery-based energy systems become more effective and dependable, increasing their suitability for fulfilling remote places' power needs and lowering reliance on fossil fuels. For standalone micro grid applications, further study and improvement of these techniques may result in more effective and environmentally friendly energy solutions.

## REFERENCES

- [1] N. Miller and G. Strbac. "Cost-effective battery storage for standalone windpower plants." *Energy*, vol. 129, pp. 42-51, 2017.
- [2] Y. Dong, et al. "Optimal design and operation of a wind-battery-based standalone AC microgrid for remote communities in Canada." *Renewable Energy*, vol. 105, pp. 347-357, 2017.
- [3] A. J. Kim, et al. "Wind-battery standalone microgrids for mitigating climate change in developing countries." *Nature Climate Change*, vol. 7, no. 9, pp. 704-710, 2017.
- [4] A. Kumar, et al. "Design and control of a standalone hybrid wind-battery system for remote area power generation: A case study of the western Himalayas, India." *Journal of Renewable and Sustainable Energy*, vol. 12, no. 6, 063902, 2020.
- [5] R. Bhattarai, et al. "Design and techno-economic analysis of a wind-battery hybrid system for remote communities in Nepal." *Journal of Energy Storage*, vol. 40, 101562, 2021.
- [6] Chauhan, Priyesh J., et al. "Battery energy storage for seamless transitions of a wind generator in a standalone microgrid." *IEEE Transactions on Industry Applications* 55.1 (2018): 69-77.
- [7] Kücüker, Ahmet, et al. "Design and control of photovoltaic/wind/battery based microgrid system." *2017 International Conference on Electrical Engineering (ICEE)*. IEEE, 2017.
- [8] Chishti, Farheen, Shadab Murshid, and Bhim Singh. "Natural genetics adapted control for an autonomous wind-battery based microgrid." *IEEE Transactions on Industry Applications* 56.6 (2020): 7156-7165.
- [9] Parida, Adikanda, and Debashis Chatterjee. "Stand- alone AC- DC microgrid- based wind- solar hybrid generation scheme with autonomous energy exchange topologies suitable for remote rural area power supply." *International Transactions on Electrical Energy Systems* 28.4 (2018): e2520.
- [10] V. Kumar, K. Chenchireddy, M. R. Reddy, B. Prasad, B. Preethi and D. S. Raj, "Power Quality Enhancement In 3-Phase 4-Wire Distribution System Using Custom Power Devices," 2022 8th International Conference on Advanced Computing and Communication Systems (ICACCS), Coimbatore, India, 2022, pp. 1225-1228, doi: 10.1109/ICACCS54159.2022.9785339.
- [11] Kalla, Ujjwal Kumar, et al. "Adaptive sliding mode control of standalone single-phase microgrid using hydro, wind, and solar PV array-based generation." *IEEE Transactions on Smart Grid* 9.6 (2017): 6806-6814.
- [12] Rezkallah, Miloud, et al. "Comprehensive controller implementation for wind-PV-diesel based standalone microgrid." *IEEE transactions on industry applications* 55.5 (2019): 5416-5428.
- [13] K. Chenchireddy, V. Kumar, K. R. Sreejyothi and P. Tejaswi, "A Review on D-STATCOM Control Techniques for Power Quality Improvement in Distribution," 2021 5th International Conference on Electronics, Communication and Aerospace Technology (ICECA), Coimbatore, India, 2021, pp. 201-208, doi: 10.1109/ICECA52323.2021.9676019.
- [14] K. Santhosh, K. Chenchireddy, P. Vaishnavi, A. Greeshmanth, V. M. Kumar and P. N. Reddy, "Time-Domain Control Algorithms of DSTATCOM in a 3-Phase, 3-Wire Distribution System," 2023 International Conference on Intelligent Data Communication Technologies and Internet of Things (IDCIoT), Bengaluru, India, 2023, pp. 781-785, doi: 10.1109/IDCIoT56793.2023.10053535.
- [15] Chenchireddy, K., & Jegathesan, V. (2021). A Review Paper on the Elimination of Low-Order Harmonics in Multilevel Inverters Using Different Modulation Techniques. *Inventive Communication and Computational Technologies: Proceedings of ICICCT 2020*, 961-971.



# PERFORMANCE IMPROVEMENT OF GRID INTERFACED HYBRID SYSTEM USING DISTRIBUTED POWER FLOW CONTROLLER WITH MODEL PREDICTIVE CONTROL

<sup>1</sup>S Lavanya,<sup>2</sup>E Krishna, <sup>3</sup>B Sai Vandana, <sup>4</sup>L Akshay Kumar, <sup>5</sup>K Vijay

<sup>1</sup>Assistant Professor,<sup>2</sup>UG Student,<sup>3</sup>UG Student,<sup>4</sup>UG Student,<sup>5</sup>UG Student

<sup>1</sup>Department of Electrical and Electronics Engineering

<sup>1</sup>Teegala Krishna Reddy Engineering College, Hyderabad, India.

**Abstract :** This paper's essential objective is to introduce a structure for the plan and demonstrating of a PV-wind half and half framework and its control methods. Since the conveyance of energy today assumes a huge part in saving power steadfastness in dispersion frameworks, these control procedures plan to direct continuous changes in the working requirements of the crossover framework. In this exploration, a half and half PV and wind energy framework was added to the proposed cross breed framework. To capitalize on the predefined framework, approaches for most extreme power-point tracking (MPPT) have been introduced. This examination additionally focused on improving the half breed framework's solidness. We give another control technique called the dispersed power-stream regulator (DPFC) execution with an advanced controller called model predictive control (MPC) to upgrade the power quality and transient solidness of the proposed framework. The utilization of a DPFC regulator in a network associated framework prompted the underlying improvement of this MPC control approach. Signals from the framework's voltage and current attributes were utilized to fabricate the control approach. This work utilized fluffy rationale and MPC to tweak these boundaries. The proposed regulator prepared framework was assessed in MATLAB/Simulink, and the results were differentiated.

**IndexTerms :** DPFC, fuzzy logic controller, model predictive controller (MPC), wind energy system. grid interconnected ,PV system.

## I.INTRODUCTION:

The requirement for electrical energy has risen rapidly in the flow circumstance. Contamination and nursery impacts are welcomed on by the use of power creation strategies, like gas, coal, and thermal energy stations [1]. The flow energy producing frameworks intensely depend on non-traditional sources to address these natural issues and satisfy electrical interest [2]. These sustainable power sources' essential advantages are insignificant support costs, little contamination, and moderateness. In spite of the fact that there are more sustainable power frameworks available, wind and sun oriented energy frameworks are as yet significant due to their basic plan, openness to ecological assets, and elevated degrees of proficiency [3]. In crossover frameworks, PV and wind energy frameworks are significant essential energy sources [4]. When contrasted with other environmentally friendly power sources, PV frameworks are one of the most viable [5]. Nearby planet groups are very costly to assemble, and photovoltaic frameworks are not innately dependable concerning time, spot, season, or climate. The nearby planet group's result is affected by changes in the climate [6]. Thusly, MPPT strategies were utilized to expand yield and further develop sunlight based charger proficiency [7]. Wind energy frameworks are likewise a huge sustainable hotspot for PV frameworks, contingent upon the accessible regular conditions. How much electrical energy delivered relies heavily on how much wind there is in

the climate [8]. The results delivered by the breeze frameworks are affected by changes in the climate[9]. Thusly, MPPT techniques are utilized to expand creation and work on the adequacy of the breeze framework. The control outline in inverter was made utilizing an essential PWM approach, and the reference signals were chosen from the lattice boundaries [10]. Electric power networks these days are enormous and convoluted. In an interconnected power framework, regional repeat and tie-line power trade change when a power trouble demand fluctuates haphazardly. Age and load may be in struggle in the event that they are not taken care of [11]. Likewise, a control structure is fundamental to lessen the impacts of sporadic burden varieties, keep repeat at the standard worth, and have demonstrated the center idea of a rebuilt power framework [12].

**FIGURE 1. Structure of general microgrid system.**

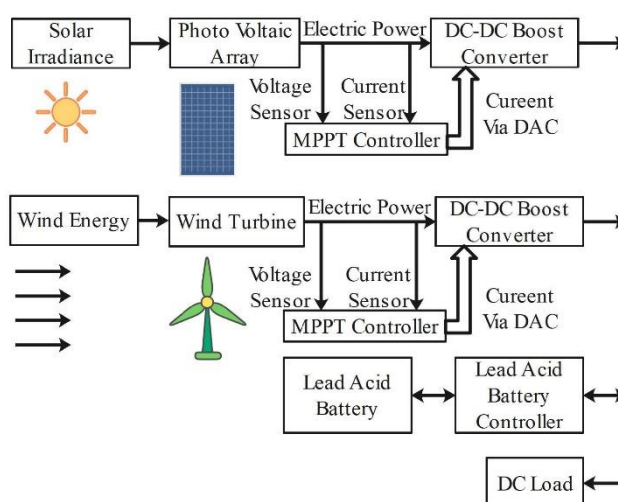


**TABLE 1. DC-DC boost converter specifications.**

Parameter Variable	Ratings
Input Voltage Range DC (Min)	150V
O/P voltage range DC (Max)	350V
Switching Frequency up to	100KHz
Inductor ( $L$ )	5mH
Capacitors ( $C$ )	1500 $\mu$ F
IGBT	1200V/100A

## II. Related Work

### Solar Power System

As a result of its accessibility in nature, steadfastness, and reasonableness, the sun based energy framework has had a critical impact throughout the entire existence of environmentally friendly power contrasted with other upset energy sources. Electric flow first moves from sun based cells & is a short time later changed into PV voltage with the guide of an identical electric circuit [14]. The resultant DC voltage shifts concurring on temperature and sun irradiance. A MPPT-based DC support converter is recommended to accomplish a reliable DC voltage from the planetary group, as found in Fig. 2. The's MPPT will probably screen sun oriented energy's pinnacle yield [15]. To accomplish the important voltage and current evaluations, these cells were set up in series and equal. The lift converter's details are displayed in Table 1. A PV framework's momentary power is followed by MPPT. Utilizing the PV-voltage & current, the PV not set in stone. A P&O MPPT is recommended for this framework [16] a standard PWM regulator delivers the obligation cycle fundamental for the DC converter.

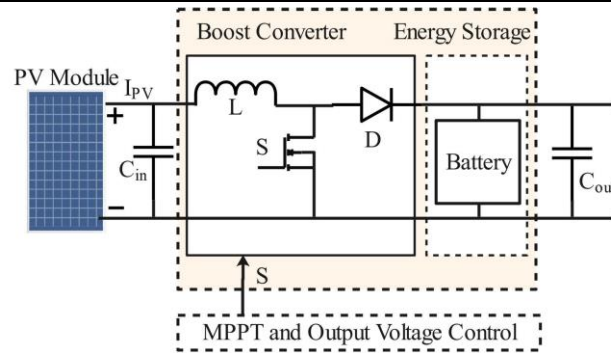


FIGURE 2. PV system with power converter.

### III. PROPOSED WORK

#### System For Wind Energy

One more significant calculate this uneven energy framework is wind turbines. To exploit the breeze's accessibility, energy transformation happens two times: first, turbine sharp edges convert wind speed to mechanical energy, and afterward, utilizing an electrical generator, they change it into electrical energy [18]. The wind turbine likewise incorporates a gearbox instrument that changes into a fast shaft alongside [19]. To increment reliability, a pitch point regulator was utilized to turn the breeze edges as per the course of the breeze [20]. A breeze vane was utilized to measure the breeze's speed as it moved toward the breeze turbine. Fig. 3 portrays the commonplace design of a breeze turbine framework utilizing a customary generator. The power delivered by the breeze turbine framework, as depicted in (1), is the manner by which the numerical displaying of the breeze energy framework is communicated.

$$P_{mech} = \frac{1}{2} C_p (\lambda, \beta) m A \rho v^3$$

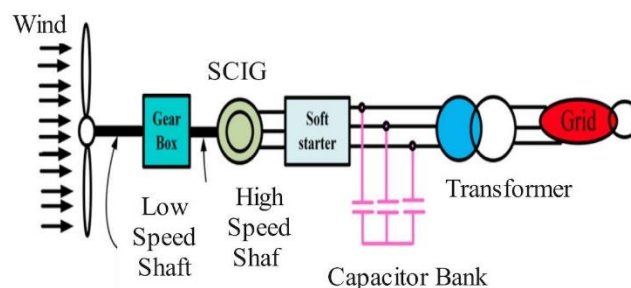


FIGURE 3. Basic diagram of SCIG wind turbine

An enlistment generator and a simultaneous generator are the two sorts of generators that are promptly open available [21].

#### Initiate And Screen The Mppt Calculation

Various exploration and innovation areas experience streamlining issues consistently. Because of the genuine and commonsense nature of the objective capability or model limitations, such issues may now and again be incredibly troublesome [23]. A goal capability exposed to convoluted, nonlinear highlights with huge uniformity or potentially equity limitations is limited or expanded in a normal enhancement issue. In the annoy and notice procedure, the framework screens changes in the cluster voltage prior to deciding how the result power has changed [24]. Fig. 4 portrays the P&O MPPT calculation's flowchart. This flowchart estimates the PV board's voltage and current and processes the PV power [25]. Prompt PV power was utilized to measure the gained PV power. The essential current sign is estimated as an outcome of these discoveries ceaselessly rehashed. This P&O procedure's essential downside is that it can't be utilized to represent progressing changes in natural variables like irradiance and daylight. To deliver an improved outcome, the ongoing result is persistently contrasted with the earlier output. This intricacy makes the regulator plan a decent contender for arrangement by utilization of enhancement techniques [26]. An ideal answer for high-intricacy plans is not too far off because of a deeply grounded part of study called electronic plan utilizing

enhancement calculations. The MPPT calculation (irritate and notice) in this paper shows how the sunlight powered chargers screen their greatest result.

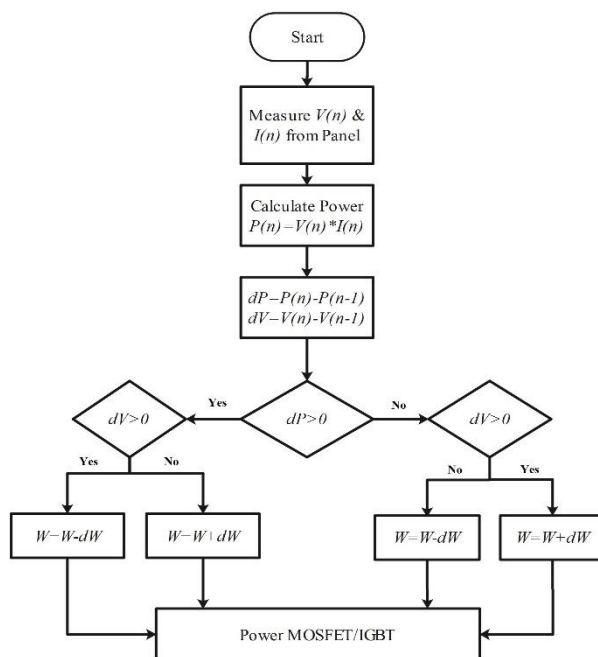


FIGURE 4. Flowchart representation of P&O technique.

**Diagram For Inverter Control**

As indicated by Fig. 5, this inverter control chart made utilizing a twofold circle of current regulators. In this occasion, the inward circle effectively expands the transient steadiness of the framework, while the external circle—otherwise called corresponding resounding regulators—assists with dealing with the consistent state blunder of the current comparator [28]. Fig. 6 shows the converter control schematic. The load, framework voltage, and current in this regulator were totally estimated. Utilizing Park's technique [29], these heap flows were changed into a d-q change. The heap, misfortune, and half and half framework influence are utilized to make the network dynamic influence. (2) was utilized to decide the framework power.

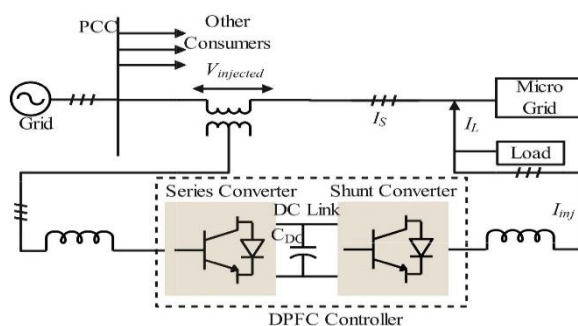
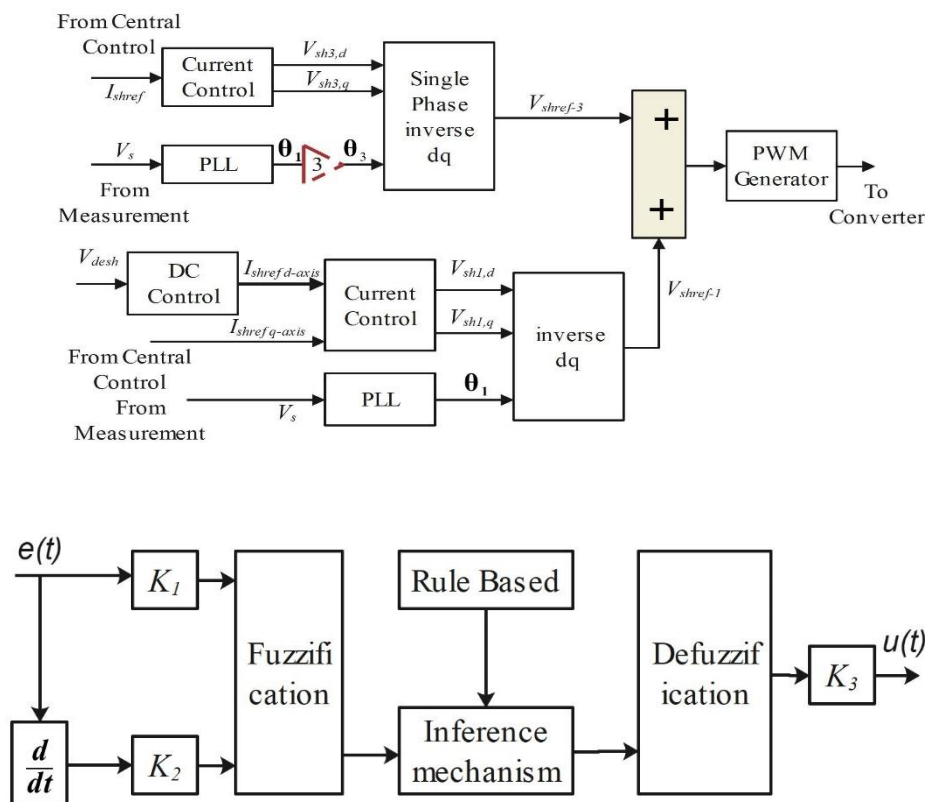


FIGURE 5. Proposed DPFC controller block diagram.



**FIGURE 6. Fuzzy Logic based DPFC block diagram**

### Controller of Fuzzy Logic

A mathematical system based only on digital logic is known as a fuzzy control system. Fuzzification, participation capabilities, rule-based, & defuzzification are the four steps of the controlling process in fuzzy logic [30]. Fuzzification is the method involved with changing over simple contribution to fluffy sets, which are then represented graphically under the membership function. In this instance, an if-then statement is used to define the rules, as shown in Fig. 7. The amount of enrollments in the fluffy rationale's bits of feedbacks, which are associated with the advanced administrators, decides the number of decides that are made.

### Controller of Model Predictive

The concept of MPC refers to a controller that explicitly uses the model of the system to select an optimal control action. The basic implementing structure for MPC is shown in Fig.7. A model of the system is used to predict the future behaviour of outputs based on the past and present values of both input and outputs. Based on the predicted outputs and corresponding reference trajectory, the future errors are obtained and will be given to the optimizer. Depending on the constraints and objectives given to the optimizer, future inputs for the system will be selected. In general, the input is referred as a control signal and output is considered as a control parameter in MPC techniques. The concept of MPC was introduced as an optimal control theory in the 1960s and by the end of 1970s, it was successfully implemented in industrial processes [26]. The slow dynamics and large sampling periods of the chemical process allow enough time for online optimization [25]. The first attempt to use the predictive control in power electronics was made in the early 1980 [28], [29]. This method was not popular at that time due to its high amount of calculations required in each sampling period. In the recent past, the inception of modern digital control platforms with high computational capabilities enabled the implementation of complex control techniques like MPC with more precision and ease.



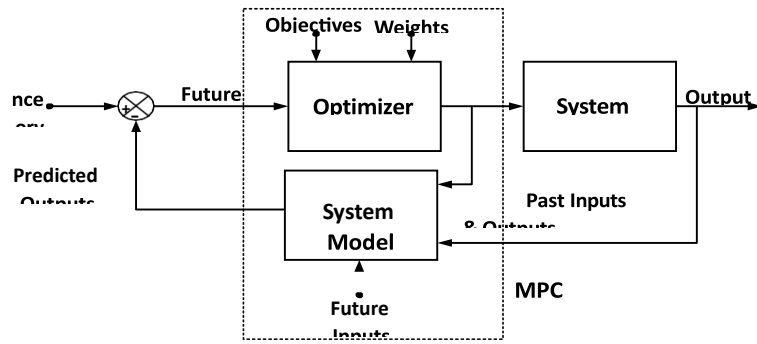


FIGURE 7: Structure for implementing model predictive control

IV. Simulation results and discussion:

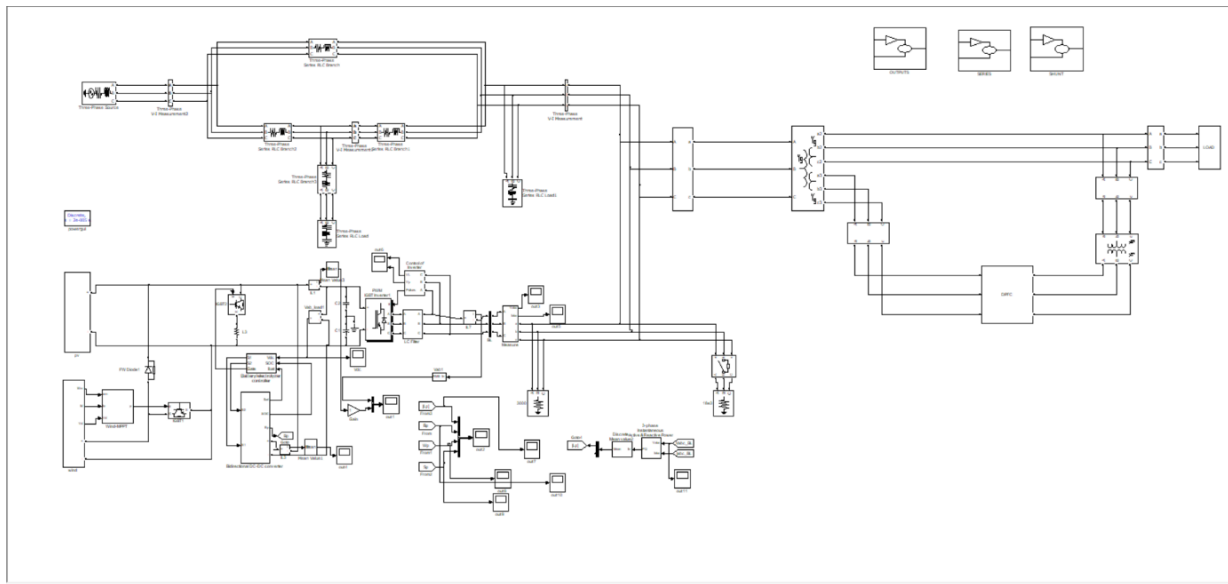


FIGURE 8: Simulation diagram

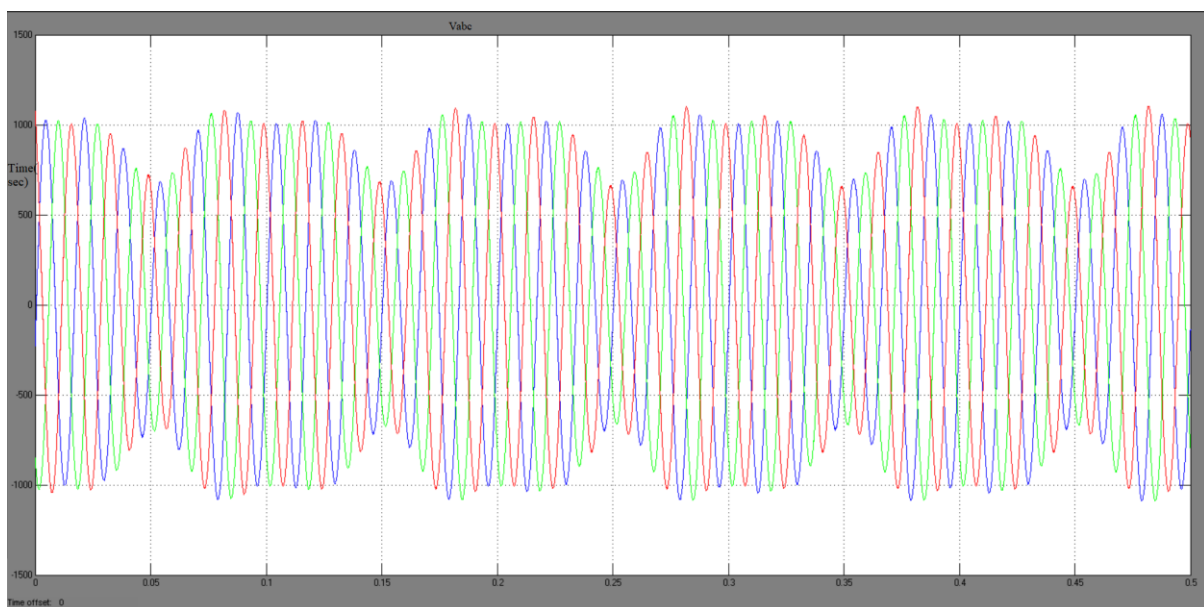


FIGURE 9. Output waveform for distorted micro grid voltage.

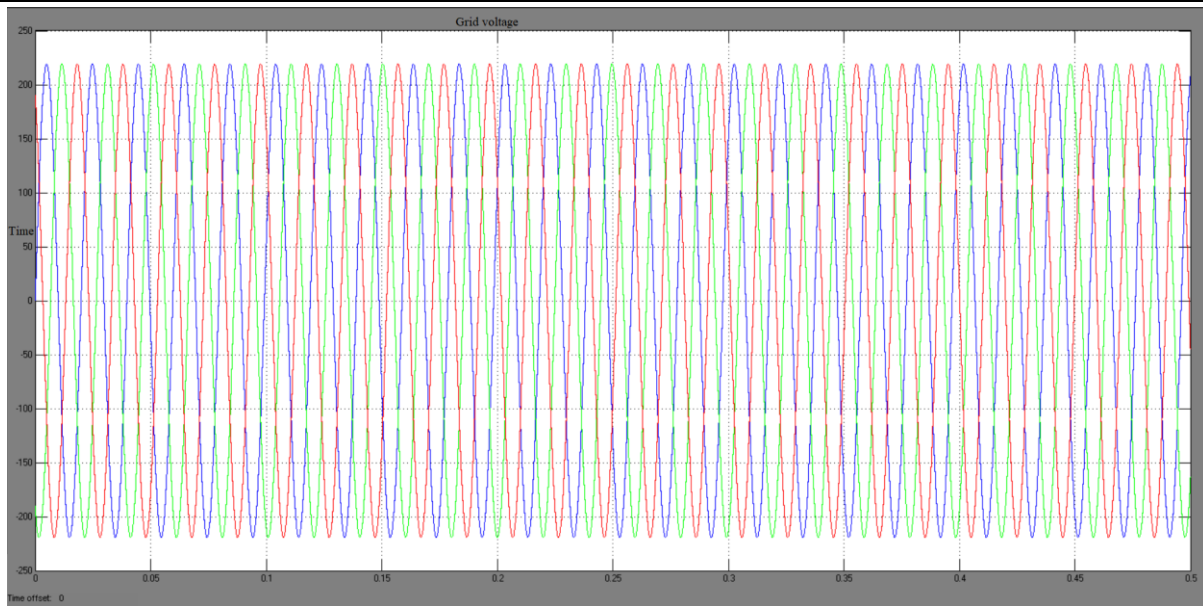


FIGURE 10. Output waveforms for grid voltage.

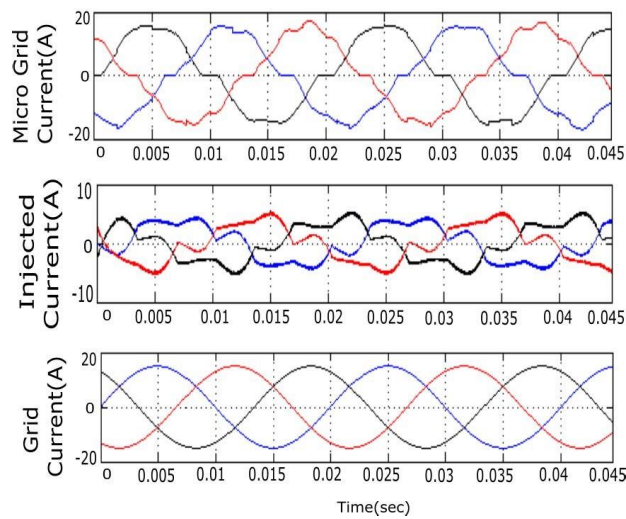


FIGURE 11. Output waveforms for uncompensated micro grid current, injected current, and compensated grid current

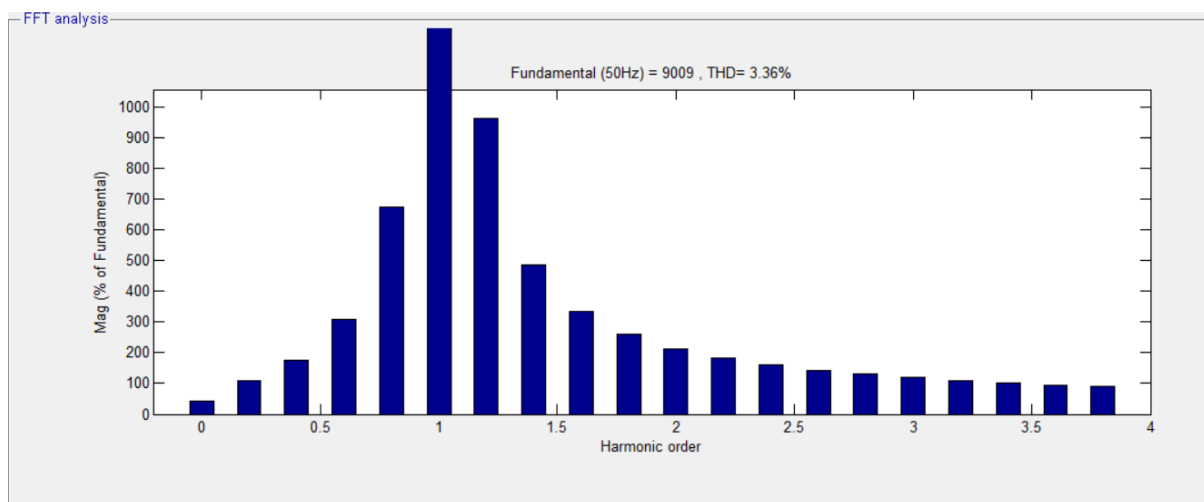


FIGURE 12. Total harmonics distortion for grid current using fuzzy based DPFC.

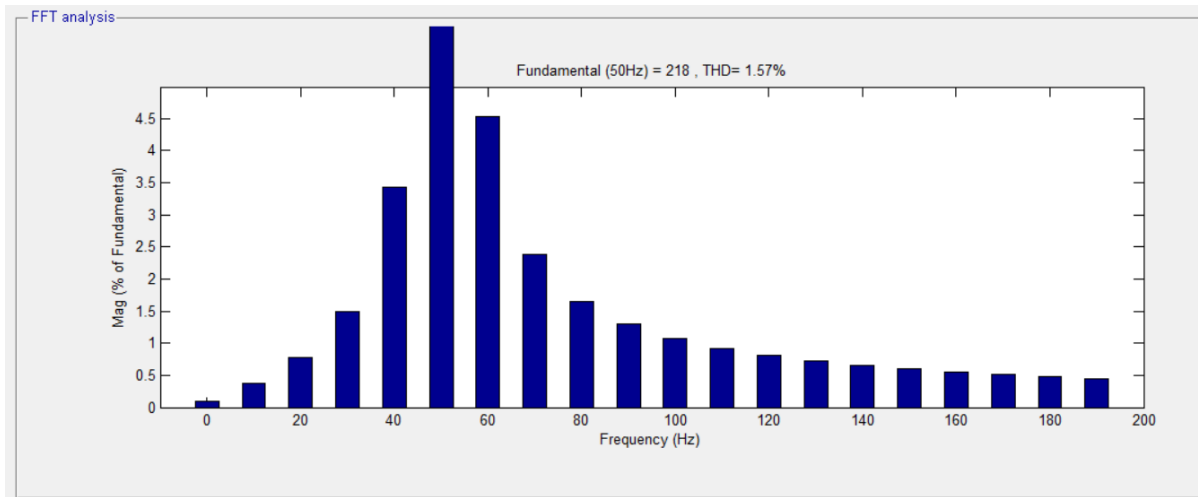


FIGURE 13. Total harmonics distortion for grid current using MPC based DPFC.

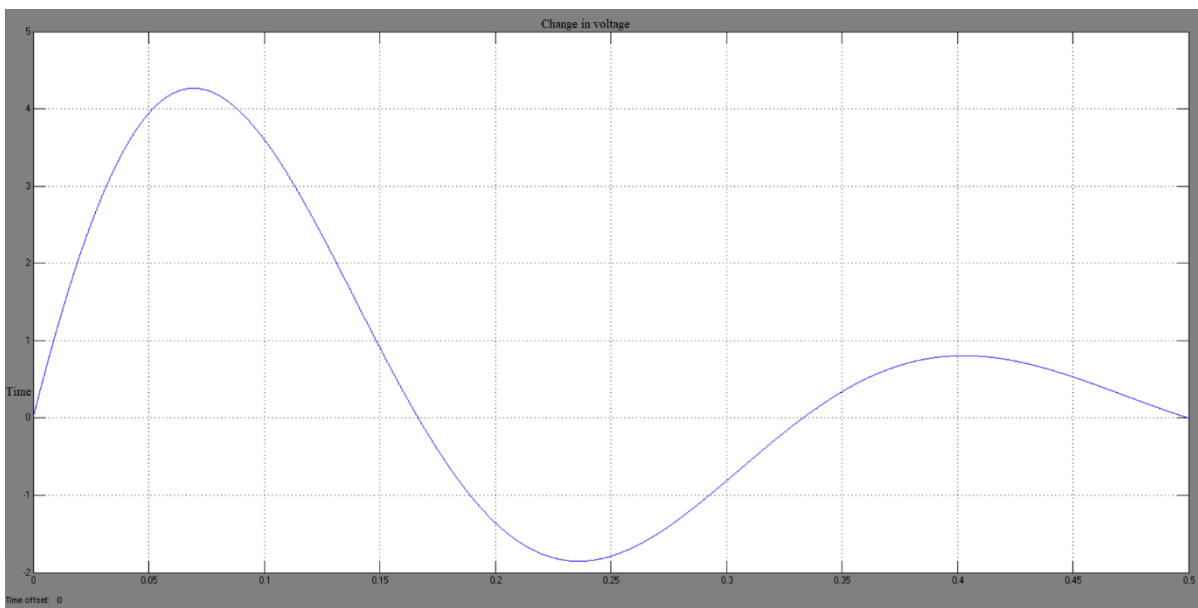


FIGURE 14. Simulation result for change in voltage under Fuzzy DPFC.

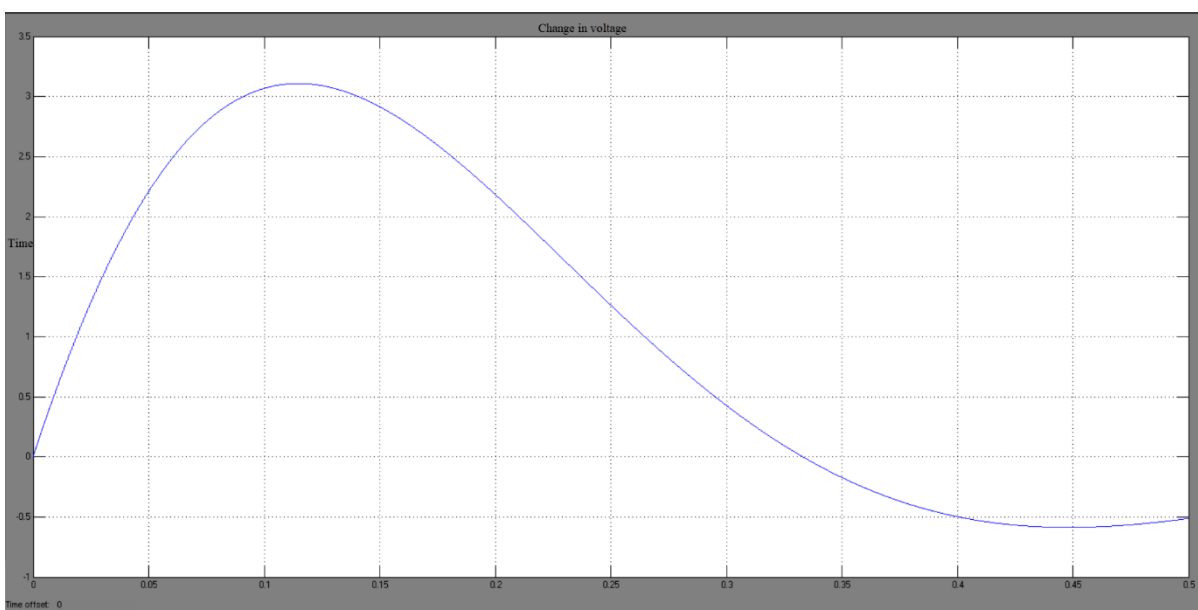


FIGURE 15. Simulation result for change in voltage under MPC DPFC.

Controller	Optimization Technique	%THD
DPFC	Fuzzy logic	3.36
DPFC	Model predictive	1.57

**TABLE 2. Comparative analysis for THD under different controllers**

**IMPROVEMENT OF POWER QUALITY IN A HYBRID SYSTEM USING FUZZY AND MPC-BASED DPFC CONTROLLERS:** In this case, the proposed system is tested with a DPFC fuzzy controller, and the experimental results are shown in the Fig. 10. The simulation result for non-linear grid voltage affected by DG system conditions, and the injected voltage of DPFC is shown in Fig.10. The simulation result for compensated output voltage of grid is shown in Fig.10. In this case, the proposed grid-connected system is affected by voltage distortions, which helps mitigate the distortions caused, and the compensated voltage is measured at the grid side. The unbalanced current affected by the unbalanced load is shown in Fig.11, and the injected current from the DPFC shunt converter under fundamental and 3rd order frequencies is shown in Fig.11. The compensated current in the grid system is shown in Fig.11. The proposed system is connected to different load conditions, that is, linear and unbalanced loads. Owing to the utilization of nonlinear loads, the microgrid current is affected by unbalanced conditions, the shunt converter of the DPFC helps to mitigate the unbalanced conditions, and the compensated current is measured at the grid side. The harmonic distortion of the grid current affected by the nonlinear and unbalanced loads was compensated using a DPFC controller. The THD for the grid current with the fuzzy-based DPFC controller was 3.36%, while that with the MPC-based DPFC controller was 1.57%, as shown in Fig.12 and 13, and the comparison of THD shown in Table 2.

## V. CONCLUSION

This study proposes an optimization-based control strategy for a distributed power flow controller to improve the reliability, power quality, and transient stability of a hybrid system. In addition, an MPPT controller was implemented for both the PV and wind energy systems to improve the performance of the hybrid system. In the literature, different control techniques have been applied to tune the parameters of DPFC series and shunt controllers. However, this study proposes a novel optimization technique for tuning the parameters of the DPFC. The series and shunt controls of the DPFC were tuned using fuzzy logic control and a model predictive controller to improve the power quality problems and the transient stability of the voltage, reactive power, rotor speed, and angle. These cases were successfully tested and verified in the MATLAB/Simulink environment. Based on these results, improvements in stability and power quality were achieved with the MPC-based controller as compared to the conventional fuzzy controller.

## VI. REFERENCES

- [1] K. Padmanathan, U. Govindarajan, V. K. Ramachandaramurthy, A. Rajagopalan, N. Pachaivannan, U. Sowmmiya, S. Padmanaban, J. B. Holm-Nielsen, S. Xavier, and S. K. Periasamy, "A sociocultural study on solar photovoltaic energy system in India: Stratification and policy implication," *J. Cleaner Prod.*, vol. 216, pp. 461-481, Apr. 2019.
- [2] R. M. Elavarasan, G. Shafiullah, S. Padmanaban, N. M. Kumar, A. Annam, A. M. Vetrichelvan, L. Mihet-Popa, and J. R. Holm-Nielsen, "A comprehensive review on renewable energy development, challenges, and policies of leading Indian states with an international perspective," *IEEE Access*, vol. 8, pp. 74432-74457, 2020.
- [3] S. Kumar, R. K. Saket, D. K. Dheer, J. B. Holm-Nielsen, and P. Sanjeevikumar, "Reliability enhancement of electrical power system including impacts of renewable energy sources: A comprehensive review," *IET Gener., Transmiss. Distrib.*, vol. 14, no. 10, pp. 1799-1815, May 2020.
- [4] L. Masenge and F. Mwasilu, "Hybrid solar PV-wind generation system coordination control and optimization of battery energy storage system for rural electrification," in *Proc. IEEE PES/IAS PowerAfrica*, Aug. 2020, pp. 1-5.
- [5] N. Priyadarshi, S. Padmanaban, M. S. Bhaskar, F. Blaabjerg, and J. B. Holm-Nielsen, "An improved hybrid PV-wind power system with MPPT for water pumping applications," *Int. Trans. Electr. Energy Syst.*, vol. 30, no. 2, p. el 2210, Feb. 2020.

- [6] S. Padmanaban, K. Nithiyananthan, S. P. Karthikeyan, and J. B. Holm-Nielsen, *Microgrids*. Boca Raton, FL, USA: CRC Press, 2020.
- [7] A. Suman, "Role of renewable energy technologies in climate change adaptation and mitigation: A brief review from Nepal," *Renew. Sustain. Energy Rev.*, vol. 151, Nov. 2021, Art. no. 111524. [Online]. Available: <https://www.sciencedirect.com/science/article/pii/S1364032121008029>
- [8] L. Varshney, A. S. S. Vardhan, S. Kumar, R. Saket, and P. Sanjeevikumar, "Performance characteristics and reliability assessment of self-excited induction generator for wind power generation," *IET, Renew. Power Gener.*, vol. 15, pp. 1927-1942, 2021.
- [9] M. Seapan, Y. Hishikawa, M. Yoshita, and K. Okajima, "Temperature and irradiance dependences of the current and voltage at maximum power of crystalline silicon PV devices," *Sol. Energy*, vol. 204, pp. 459-465, Jul. 2020. [Online]. Available: <https://www.sciencedirect.com/science/article/pii/S0038092X20305089>
- [10] F. Mebrahtu, B. Khan, P. Sanjeevikumar, P. K. Maroti, Z. Leonowicz, O. P. Mahela, and H. H. Alhelou, "Harmonics mitigation in industrial sector by using space vector PWM and shunt active power filter," in *Proc. IEEE Int. Conf. Environ. Electr. Eng., IEEE Ind. Commercial Power Syst. Eur. (EEEIC/I&CPS Europe)*, Jun. 2020, pp. 1-6.
- [11] S. Vadi, S. Padmanaban, R. Bayindir, F. Blaabjerg, and L. MihetPopa, "A review on optimization and control methods used to provide transient stability in microgrids," *Energies*, vol. 12, no. 18, p. 3582, Sep. 2019.
- [12] N. Priyadarshi, S. Padmanaban, R. K. Ghadai, A. R. Panda, and R. Patel, "Advances in power systems and energy management select proceedings of ETAEERE 2020," in *Power System and Energy*. Springer, 2020, p. 4.
- [13] E. Sundaram and M. Venugopal, "On design and implementation of three phase three level shunt active power filter for harmonic reduction using synchronous reference frame theory," *Int. J. Electr. Power Energy Syst.*, vol. 81, pp. 40-47, Oct. 2016.
- [14] A. Raj, S. R. Arya, and J. Gupta, "Solar PV array-based DC-DC converter with MPPT for low power applications," *Renew. Energy Focus*, vol. 34, pp. 109-119, Sep. 2020. [Online]. Available: <https://www.sciencedirect.com/science/article/pii/S1755008420300193>
- [15] C. H. Basha and C. Rani, "Different conventional and soft computing MPPT techniques for solar PV systems with high step-up boost converters: A comprehensive analysis," *Energies*, vol. 13, no. 2, p. 371, Jan. 2020.
- [16] J. D. Kumar, K. Mantosh, M. S. Bhaskar, P. Sanjeevikumar, J. B. H. Nielsen, and Z. Leonowicz, "Investigation studies of DC-DC boost converter with proportional-integral-derivative controller using optimization techniques," in *Proc. IEEE Int. Conf. Environ. Electr. Eng., IEEE Ind. Commercial Power Syst. Eur. (EEEIC/I&CPS Europe)*, Jun. 2020, pp. 1-5.
- [17] N. Hawkins, B. Bhagwat, and M. L. McIntyre, "Nonlinear currentmode control of SCIG wind turbines," *Energies*, vol. 14, no. 1, p. 55, Dec. 2020.
- [18] A. M. M. dos Santos, L. T. P. Medeiros, L. P. S. Silva, I. D. S. Junior, V. S. de C. Teixeira, and A. B. Moreira, "Wind power system connected to the grid from squirrel cage induction generator (SCIG)," in *Proc. IEEE 15th Brazilian Power Electron. Conf., 5th IEEE Southern Power Electron. Conf. (COBEP/SPEC)*, Dec. 2019, pp. 1-6.
- [19] A. K. S. Tomar, K. K. Gautam, and A. Lodhi, "Integration of SCIG wind energy conversion systems to the grid," *Int. J. Eng. Sci. Invention*, vol. 9, no. 6, pp. 28-36, 2020.
- [20] B. B. Adetokun, C. M. Muriithi, and J. O. Ojo, "Voltage stability analysis and improvement of power system with increased SCIG-based wind system integration," in *Proc. IEEE PES/IAS PowerAfrica*, Aug. 2020, pp. 1-5.
- [21] M. Xu, L. Wu, H. Liu, and X. Wang, "Multi-objective optimal scheduling strategy for wind power, PV and pumped storage plant in VSC-HVDC grid," *J. Eng.*, vol. 2019, no. 16, pp. 3017-3021, Mar. 2019.
- [22] P. Manoharan, U. Subramaniam, T. S. Babu, S. Padmanaban, J. B. Holm-Nielsen, M. Mitolo, and S. Ravichandran, "Improved perturb and observation maximum power point tracking technique for solar photovoltaic power generation systems," *IEEE Syst. J.*, vol. 15, no. 2, pp. 3024-3035, Jun. 2021.
- [23] M. H. Reza and M. A. Shobug, "Efficiency evaluation of P&O MPPT technique used for maximum power extraction from solar photovoltaic system," in *Proc. IEEE Region Symp. (TENSYP)*, Jun. 2020, pp. 1808-1811.
- [24] A. Ali, K. Almutairi, S. Padmanaban, V. Tirth, and S. Algami, "Investigation of MPPT techniques under uniform and non-uniform solar irradiation condition-A retrospection," *IEEE Access*, vol. 8, pp. 127368-127392, 2020.

- [26] G. S. Chawda, A. G. Shaik, O. P. Mahela, S. Padmanaban, and J. B. Holm-Nielsen, "Comprehensive review of distributed facts control algorithms for power quality enhancement in utility grid with renewable energy penetration," *IEEE Access*, vol. 8, pp. 107614-107634, 2020.
- [27] A. Sen, A. Banerjee, and H. Nannam, "A comparative analysis between two DPFC models in a grid connected hybrid solar-wind generation system," in *Proc. IEEE Int. Conf. Power Electron., Smart Grid Renew. Energy (PESGRE)*, Jan. 2020, pp. 1-6.
- [28] X. Zhai, A. Tang, X. Zou, X. Zheng, and Q. Xu, "Research on DPFC capacity and parameter design method," in *Proc. IEEE Int. Conf. Inf. Technol., Big Data Artif. Intell. (ICIBA)*, vol. 1, Nov. 2020, pp. 978-982.
- [29] J. H. Woo, L. Wu, S. M. Lee, J.-B. Park, and J. H. Roh, "D-STATCOM d-q axis current reference control applying DDPG algorithm in the distribution system," *IEEE Access*, vol. 9, pp. 145840-145851, 2021.
- [30] G. Balasubramani, V. Thangavelu, M. Chinnusamy, U. Subramaniam, S. Padmanaban, and L. Mihet-Popa, "Infrared thermography based defects testing of solar photovoltaic panel with fuzzy rule- based evaluation," *Energies*, vol. 13, no. 6, p. 1343, Mar. 2020.
- [31] S. V. K. Arun, U. Subramaniam, S. Padmanaban, M. S. Bhaskar, and D. Almakhlles, "Investigation for performances comparison PI, adaptive PI, fuzzy speed control induction motor for centrifugal pumping application," in *Proc. IEEE 13th Int. Conf. Compat., Power Electron. Power Eng. (CPE- POWERENG)*, Apr. 2019, pp. 1-6.
- [32] B. Alshammari, R. B. Salah, O. Kahouli, and L. Kolsi, "Design of fuzzy TS-PDC controller for electrical power system via rules reduction approach," *Symmetry*, vol. 12, no. 12, p. 2068, Dec. 2020.
- [33] D. Sharma and N. K. Yadav, "Lion algorithm with Levy update: Load frequency controlling scheme for two-area interconnected multi-source power system," *Trans. Inst. Meas. Control*, vol. 41, no. 14, pp. 4084-4099, Oct. 2019, doi: 10.1177/0142331219848033.
- [34] M. Yazdani and F. Jolai, "Lion optimization algorithm (LOA): A natureinspired metaheuristic algorithm," *J. Comput. Des. Eng.*, vol. 3, no. 1, pp. 24-36, 2016. [Online]. Available: <https://www.sciencedirect.com/science/article/pii/S2288430015000524>
- [35] R. Shankar, "Lion algorithm based load frequency control for interconnected power system incoordination with UPFC and electric vehicle," in *Proc. Int. Conf. Recent Innov. Electr., Electron. Commun. Eng. (ICRIEECE)*, Jul. 2018, pp. 575-580.



# Performance Improvement of Photo Voltaic fed Series Active Power Filters for Distributed Generation

**B Aravind Nayak<sup>1</sup>, CH Sai Deepak<sup>2</sup>, A Ajay Kumar<sup>3</sup>, M Rasagna<sup>4</sup>, N Naresh<sup>5</sup>**

Assistant Professor, Department of Electrical and Electronics Engineering, Teegala Krishna Reddy Engineering College, Hyderabad.

UG Students, Department of Electrical & Electronics Engineering, Teegala Krishna Reddy Engineering College, Hyderabad.

## ABSTRACT

This study examines the effectiveness of Series Active-Power Filters (SAPF) for enhancing power-quality using dispersed generating. The distribution system's voltage-related issues may be reduced by the SAPF. The PV system (Distributed Generation) provides the genuine power supply in order to offset voltage-related issues. The Synchronous Reference Frame (SRF) Theory is used to implement the control method for generating the reference in (V)voltage, which is then compared to constant in voltage for pulse-generation utilising hysteresis-band PWM. When it comes to resolving issues with voltage on the distribution side, the SAPF performs better. MATLAB and SIMULINK are used to model and simulate SAPF's performance.

**INDEX TERMS:** SAPP, PV-Photo-Voltaic, VSC-Voltage Source Converter, SRF-Synchronous Reference Frame-Distributed Generation.

## I.INTRODUCTION:

One of a utility system's primary duties is to provide consumers with electric-power in form of sinewave currents with the proper magnitudes & frequencies at the PCC Despite the virtually sinusoidal produced V of coeval machines in power-plants, certain undesirable circumstances, voltage & current disruptions. For instance, PEC produce contemporary harmonics & twine voltage waveforms, electric arc furnaces induce voltage variations, and short circuit defects cause voltage sags and swells [1-4]. On the other hand, the majority of consumer loads, including computers, microcontrollers, and medical equipment. are vulnerable to power quality disturbances and are not shielded from them, and the effectiveness of the voltage that is given to them determines how well they function. Only by guaranteeing a constant supply of electricity at the right voltage and frequency levels is this achievable. A strategy known as "custom power" is created largely to satisfy the needs of industrial & commercial customers. Power dispersal systems must provide unbroken stream of energy to its consumers at a smooth sinewave voltage at the agreed-upon[8-10]. Power-systems(PS) have a large number of nonlinear loads, which negatively impact power supply [11].[12].Voltage stability, supply reliability, and voltage are the three subcategories that make up power quality, a thorough analysis of compensatory type custom power devices, power quality concerns [13-16-21], a study of power-quality difficulties, standards and indices put out by various authorities, and various methods used to sometimes enhance power quality.

The SERIES ACTIVE POWER FILTER SAPF [17-18] corrects the voltage sags and swells on the load side by injecting a voltage component that is coupled in series with the supply voltage. A safe voltage supply is ensured under transient situations by the control-response, which is the decree of 3msec. Protecting network is the primary purpose of a SAPF. Based on sensitive loads, the SAPF is situated. DVR interlards series-voltage and adjusts load-voltage to value if a fault occurs on other lines. The three injected phase voltages momentary amplitudes are managed such that there are no negative impacts from a bus malfunction on the load voltage.

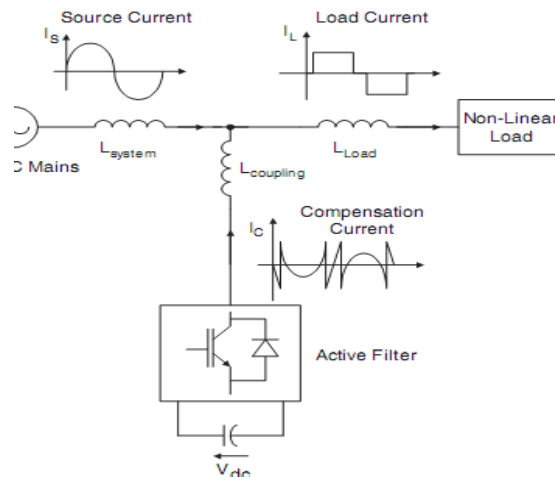
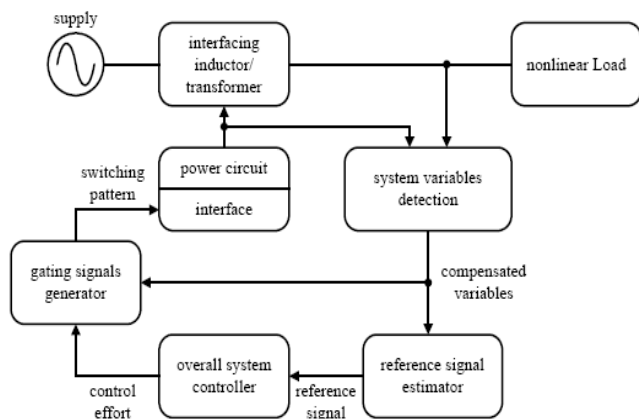


FIGURE 1. Generalized block diagram for APF

FIGURE 2. Configuration of a VSI based series APF

### ILPV Fed Series Active Power Filter, Basic Principles of Compensation

The ultimate replacement for passive filters is active filters. When the harmonic orders vary in terms of magnitudes and phase angles, the active filters are utilized. In these circumstances, it is possible to offer dynamic compensation by using active components rather than passive ones. In nonlinear load situations where the harmonics vary on time, active filters are utilised. Active filters may be linked in series or parallel depending on the types of sources that cause harmonics in the power system, much as passive filters. By employing active power conditions to provide equal amplitudes of opposite phase, the active filters eliminate the harmonics that are created in the nonlinear components and substitute the current wave from the load, minimizing the effects of harmonic current [7].

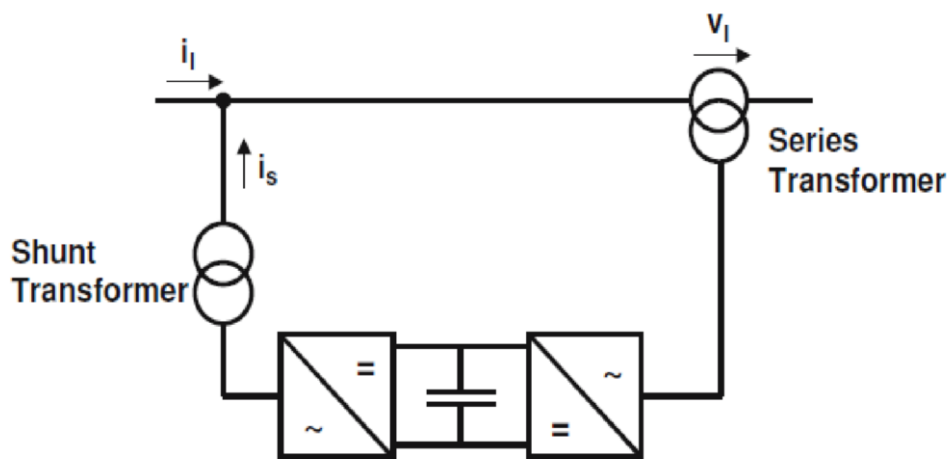


FIGURE 3. Principle configuration of an UPFC



III. PROPOSED WORK

III.I SRF, Synchronous Reference Frame

$$\begin{bmatrix} V_{s0} \\ V_{sd} \\ V_{sq} \end{bmatrix} = T \begin{bmatrix} V_{sa} \\ V_{sb} \\ V_{sc} \end{bmatrix} \tag{1}$$

$$T = \sqrt{\frac{2}{3}} \begin{bmatrix} \frac{1}{\sqrt{2}} & \frac{1}{\sqrt{2}} & \frac{1}{\sqrt{2}} \\ \sin(\omega t) & \sin(\omega t - 2\pi/3) & \sin(\omega t + 2\pi/3) \\ \cos(\omega t) & \cos(\omega t - 2\pi/3) & \cos(\omega t + 2\pi/3) \end{bmatrix} \tag{2}$$

$$T^{-1} = \sqrt{\frac{2}{3}} \begin{bmatrix} \frac{1}{\sqrt{2}} & \sin(\omega t) & \cos(\omega t) \\ \frac{1}{\sqrt{2}} & \sin(\omega t - 2\pi/3) & \cos(\omega t - 2\pi/3) \\ \frac{1}{\sqrt{2}} & \sin(\omega t + 2\pi/3) & \cos(\omega t + 2\pi/3) \end{bmatrix} \tag{3}$$

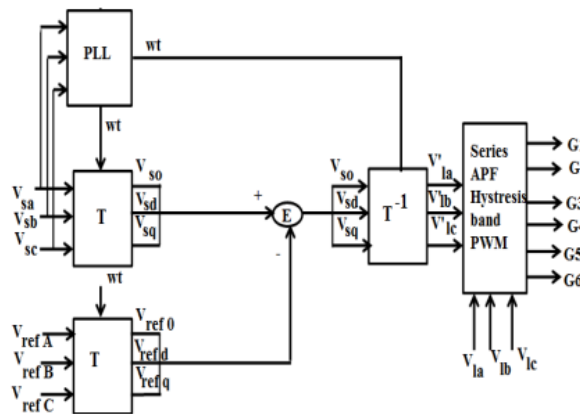


FIGURE 4. Series Active Power Filter (SAPF) configuration

III.II Sequential Control

The series converter has the ability to correct voltage issues like voltage sag. The PLL in the series controllers provides the sine and cosine values for the transformations from abc to dq0 and from dq0 to abc. In series continuation, abc to dq0 and dq0 to abc are used to produce the control signal. Using the hysteresis band, the reference signal produced is compared to the PCC point voltage. Pulse signals are produced; the converter receives the produced signals as the gate pulse. Figure 3 depicts the simulation diagram for a series controller. The system's control approach is to regulate the rectifier for the injection of -ve harmonics necessary for system restoration. The gate pulse sent to the IGBTs controls the converter output. The SRF Theory makes this possible. The direct & quadrature axis signals in dq0 are translated from the three-phase system abc. For the series APF, it is taken into account while calculating the reference signal and creating the pulse. The current for the three phases is represented by equations (3), (4), and (5), which are translated to dq0 for the balanced state.

$$i_a = I_m \sin \omega_s t \tag{3}$$

$$i_b = I_m \sin \left( \omega_s t - \frac{2\pi}{3} \right) \tag{4}$$

$$i_c = I_m \sin \left( \omega_s t + \frac{2\pi}{3} \right) \tag{5}$$

The transformation matrix for the  $i_a, i_b, i_c$  is given by equation (6),

$$\begin{bmatrix} i_a \\ i_b \\ i_c \end{bmatrix} = \begin{bmatrix} \cos \theta & -\sin \theta & 1 \\ \cos \left( \theta - \frac{2\pi}{3} \right) & -\sin \left( \theta - \frac{2\pi}{3} \right) & 1 \\ \cos \left( \theta + \frac{2\pi}{3} \right) & -\sin \left( \theta + \frac{2\pi}{3} \right) & 1 \end{bmatrix} \begin{bmatrix} i_d \\ i_q \\ i_0 \end{bmatrix} \tag{6}$$

To determine the transmutation of abc 2 dq0 & inverse transmute of dq0 2 abc are both carried out concurrently. Equations (7), (8), and (9) depict how dq0 changes in the balanced state. The quadrature, the direct, & zero-axis currents of system are denoted by the letters  $i_d$ ,  $i_q$ , and  $i_0$  and are produced by inverse transformation.

$$i_d = k_d \frac{3}{2} I_m \sin(\omega_s t - \theta) \tag{7}$$

$$i_q = -k_q \frac{3}{2} I_m \sin(\omega_s t - \theta) \tag{8}$$

$$i_0 = \frac{1}{3}(i_a + i_b + i_c) \tag{9}$$

The transformation matrix for the dq0 transform is given by (10)

$$\begin{bmatrix} i_d \\ i_q \\ i_0 \end{bmatrix} = \frac{2}{3} \begin{bmatrix} \cos\theta & \cos\left(\theta - \frac{2\pi}{3}\right) & \cos\left(\theta + \frac{2\pi}{3}\right) \\ -\sin\theta & -\sin\left(\theta - \frac{2\pi}{3}\right) & -\sin\left(\theta + \frac{2\pi}{3}\right) \\ \frac{1}{2} & \frac{1}{2} & \frac{1}{2} \end{bmatrix} \begin{bmatrix} i_a \\ i_b \\ i_c \end{bmatrix} \tag{10}$$

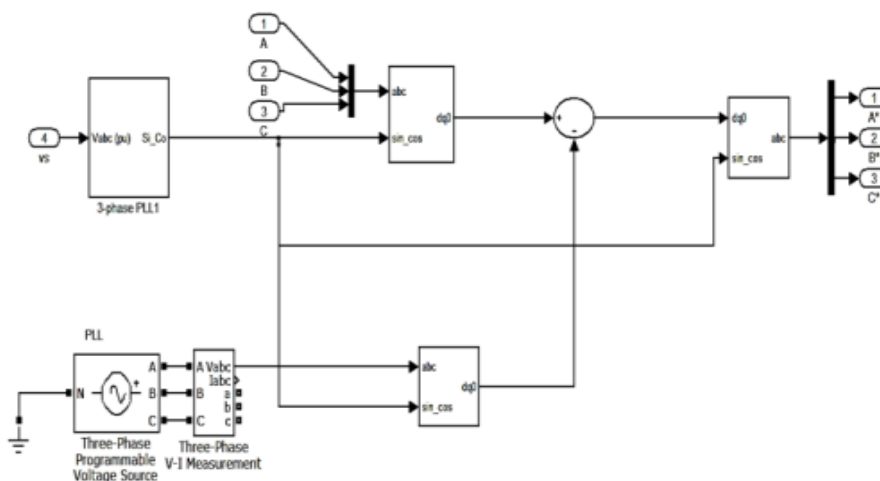


FIGURE 4. Simulation of Series Controller.

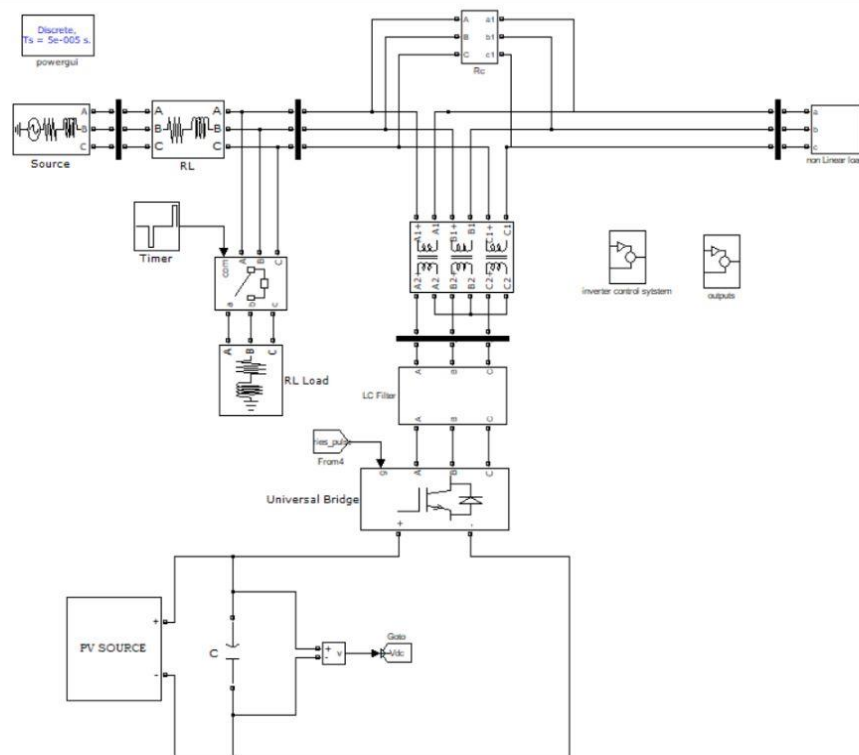


FIGURE 5 : Simulation diagram

### III.III SYSTEM CONFIGURATION

The grid is connected to nonlinear loads. The PV source is connected across the dc link. The PV fed filter can be utilized to compensate the voltage related problems and also it can help to maintain the supply across the load when there is no power supply. The specific model is designed to keep the voltage across the dc link capacitor constant for efficient operation of the filter. The filter can boost up and down the voltage as and when required and also provide the necessary voltage to the distribution line for forcing the load voltage to be balanced.

The control technique plays the vital role for proper operation of the filter. Various voltage related problems are required to be compensated to obtain balanced voltage across the load connected to the grid. Therefore, grid side voltage is sensed & provided to the controller for further processing to develop a signal which can be treated as the reference signal [6].

### III.IV CONTROL TECHNIQUES

In a PI controller, which is the existing model has no fuzzy FLC and the voltage calculations are being done automatically where in the FLC controller all the voltage issues are sorted out by means of a predefined rule set. The main role of the functionary is to set up decision-based rules by analyzing the system behavior and the linguistic input variables within the framework of the system. The inputs provided to the FLC have to process through three basic stages of fuzzification, decision-making stage, and defuzzification before generating the output [4]. In the fuzzification stage, the input variable is transformed into a linguistic variable with the help of predefined membership functions (MFs). The output of the fuzzification stage is then used to generate the fuzzified output according to the rules set defined.

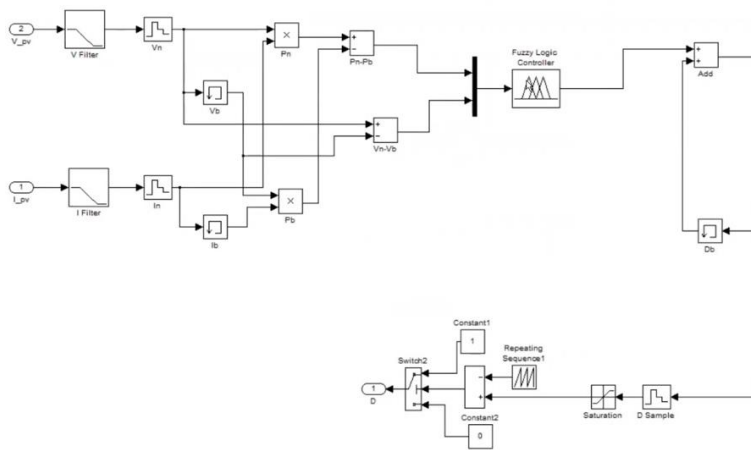


FIGURE 6. Proposed control technique (FLC) implementation in PV

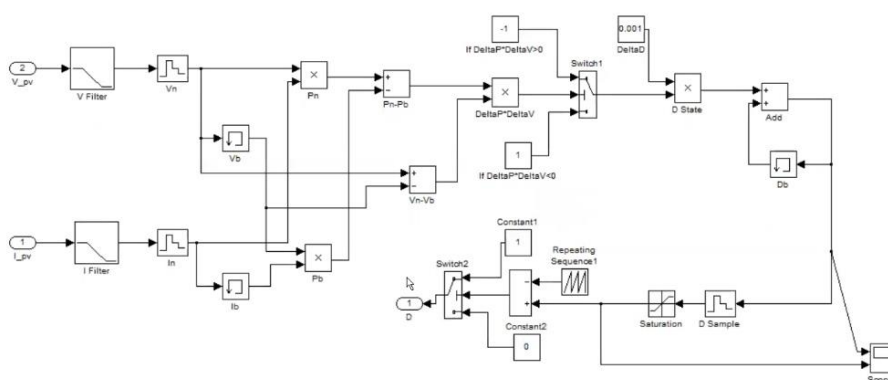


FIGURE 7. PV without FLC

IV.SIMULATION RESULTS AND ANALYSIS

To justify the superiority of this concept in static condition, at first the analysis is done by the series connected filter with unstabilized DC link voltage which indicates no PV associated with the filter. In second the verification is carried out with the same series connected filter with PV connected across the DC link and FLC controller in it which makes the voltage stabilized. And finally, a comparative analysis is carried out between the two models , In this paper only the voltage harmonics disturbances considered and the performance of the filter along with FLC and without FLC designed in PV

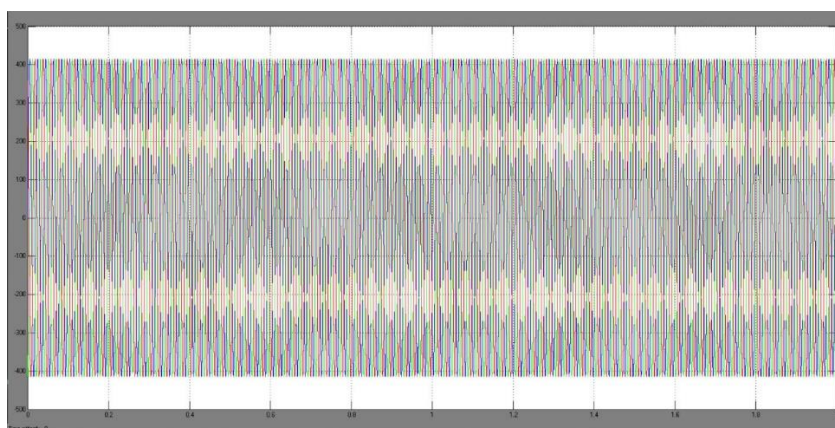
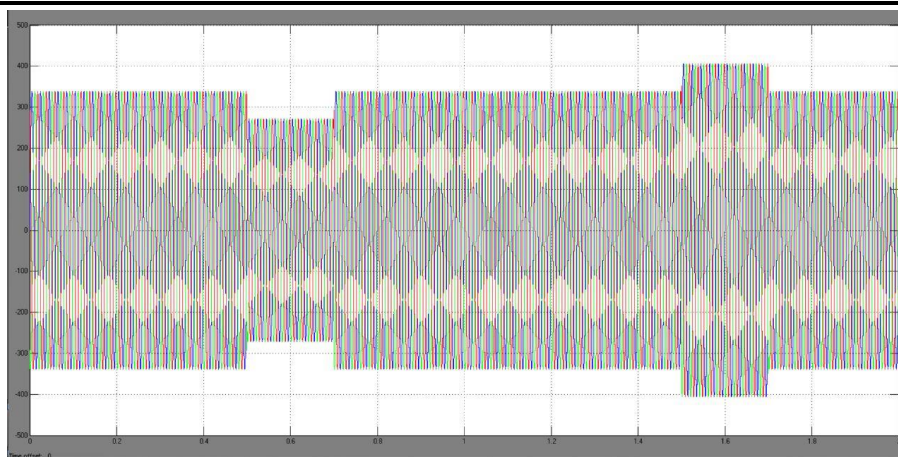


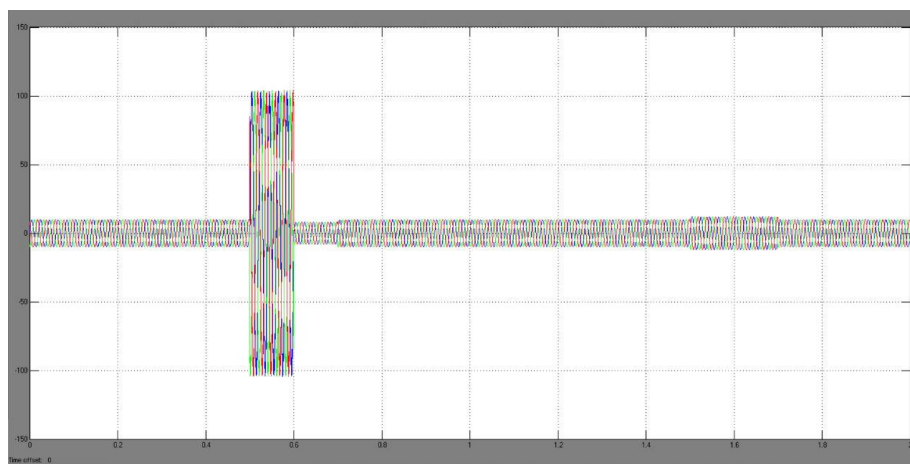
FIGURE 8. Load voltage waveforms

Figure 8. Shows the load voltage at static condition which is linear throughout where the waveform indicates load is safe, distortions generally occur when the fault hits the source



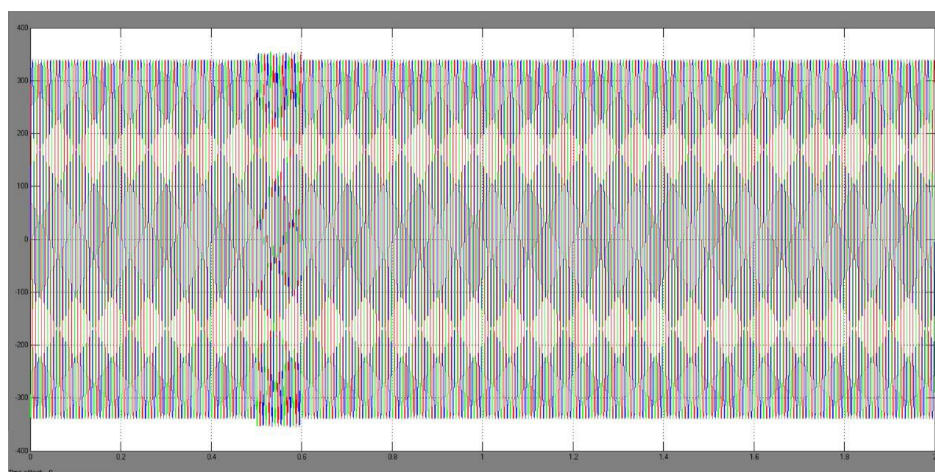
**FIGURE 9.** Voltage sag and swell from source

Figure 9. Shows Voltage sag, is a reduction in voltage for a short time. The voltage reduction magnitude is between 10% and 90% of the normal root mean square (RMS) voltage at 60 Hz. The duration of a voltage sag event, is less than 1 min and more than 8 msec, or a half cycle of 60-Hz electrical power. Voltage Swell is the increase in the RMS voltage level to 110% - 180% of nominal, at the power frequency for durations of  $\frac{1}{2}$  cycle to one (1) minute. It is classified as a short duration voltage variation phenomena, which is one of the general categories of power quality problems mentioned in the second post of the power quality basics series of this site. Voltage swell is basically the opposite of voltage sag or dip.



**FIGURE 10.** Injected voltage from filter to supply voltage

Figure 10. Shows the voltage to be injected and absorbed during sag and swell conditions respectively. If the voltage is reduced then with the help of PV as backup, voltage is injected to balance the system whereas it is absorbed if the voltage is increased.



**FIGURE 11.** Supply voltage after compensation

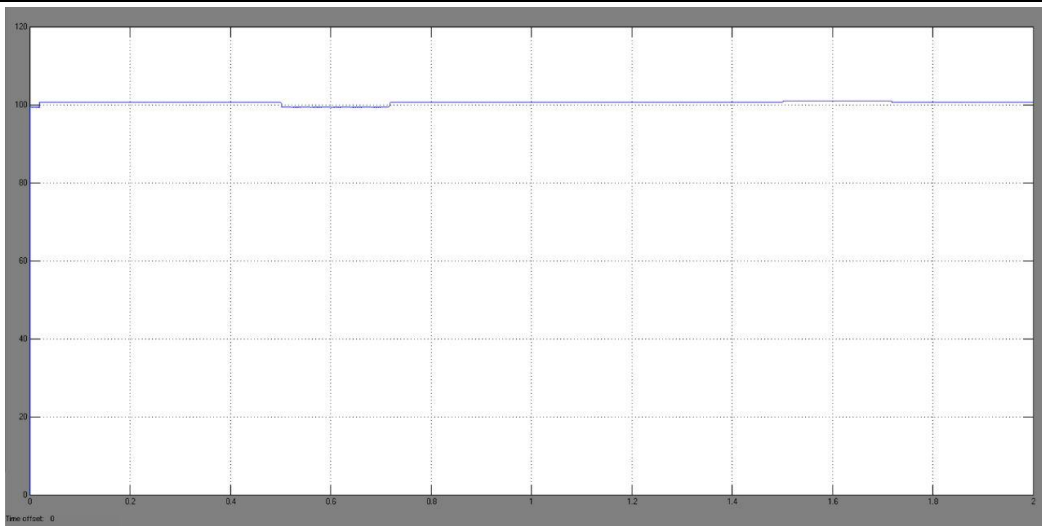


**FIGURE 12.** Voltage in DC link capacitor

Figure 12. The voltage of the DC link with PV Cell is shown in the fig.10 and it is constant in nature. This constant voltage across the DC link increases the overall performance of the series connected filter which leads to maintain the constant voltage across the load after compensation.

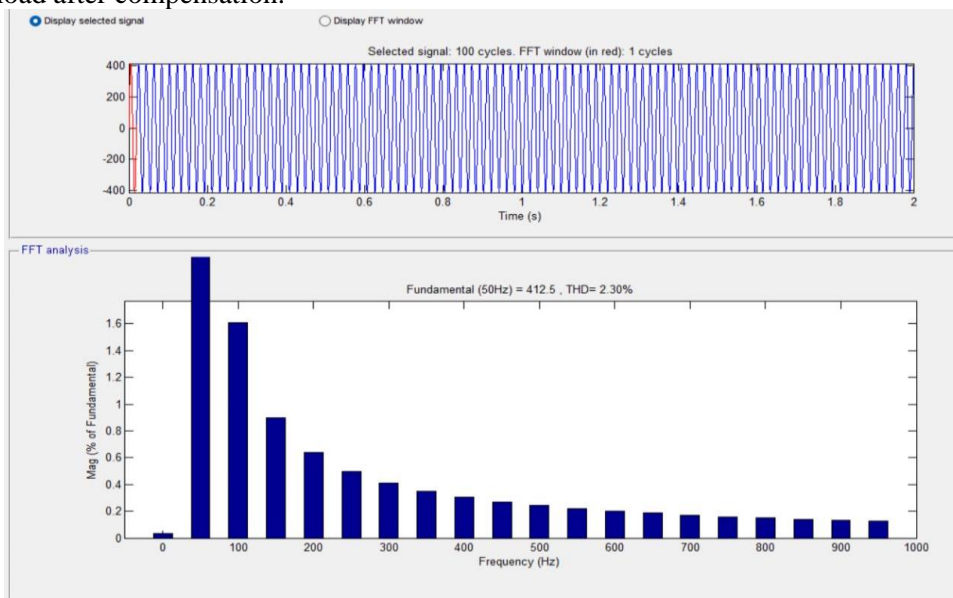


**FIGURE 13.** FFT analysis of PI based PV (THD)

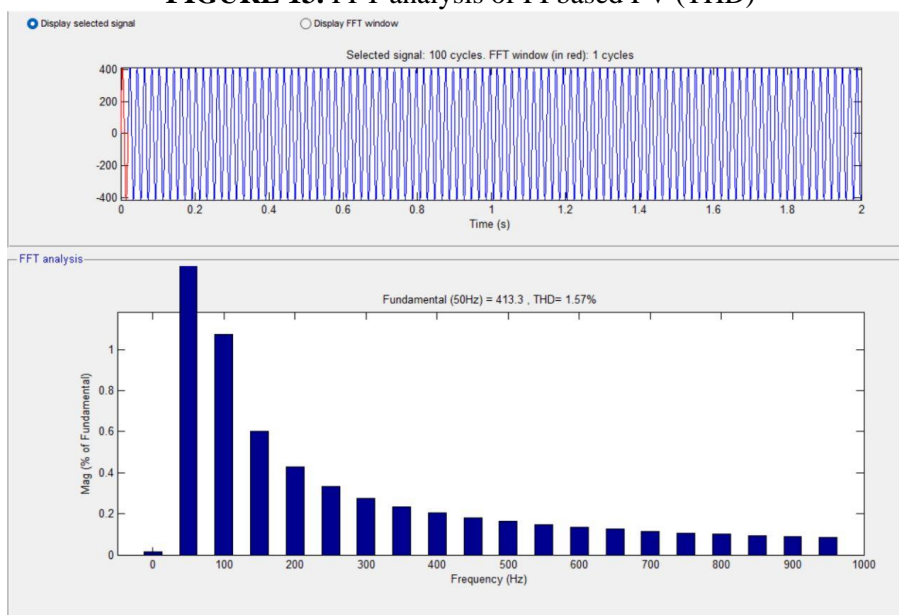


**FIGURE 14.** FFT analysis of FLC based PV (THD)

Model	Optimization Technique	% THD
PV fed series APF	PI	2.30
PV fed series APF	FLC	1.57

**TABLE 1.** Comparison of FFT analysis of THD under different controllers

The designed PV fed series connected filter verified under different voltage related problems for both PI and FLC controller condition of the system. It is concluded that PV fed series connected filters with FLC is able to compensate the voltage related problem satisfactorily and maintain the voltage across the load as pure as sinusoidal. In PI condition it is observed that the harmonics distortion level is 2.30 percentage of fundamental and same model with FLC the harmonics distortion level is 1.57 percentage. This encouraging results in each case proves the effectiveness of proposed series connected filter for power quality issues in power systems.

## V. CONCLUSION

In this paper, the Series Active Power Filter (SAPF) using Synchronous Reference Frame (SRF) Theory is implemented to control the SAPF for the sag and swell mitigation. The simulation results show that the device is capable of mitigating the sag, swell and the drop in voltage to maintain the voltage at 1 P.U. The Distributed Generation is used for the mitigation of power quality problems has the superior performance.

## VI. REFERENCES

- [1] Alexander Kusko, Sc.D. and Marc T.Thompson, "Power Quality in Electrical Systems", McGrawHill.2007.
- [2] ArindamGhosh and Amit Kumar Jindal, "A Unified Power Quality Conditioner for Voltage Regulation of Critical Load Bus", IEEE Conference on Power Delivery Transactions, Vol. 22, pp.364-372, 2007
- [3] ArindamGhosh and Gerard ledwhich, "Power Quality Enhancement Using Custom Power Devices", Kluwer Academic Publishers, 2002.
- [4] M.Basu, S.P. Das and G.K. Dubey, (2002), "Performance study of UPQC-Q for load compensation and voltage sag mitigation", Conference of the Industrial Electronics Society.Vol.1, pp.698–703.
- [5] T.Devaraju, V.C.Veera Reddy and M. Vijay Kumar(2012), "Modeling and Simulation of Custom Power Devices to Mitigate Power Quality Problems" International Journal of Engineering Science and Technology, Vol.26, pp.1880-1885.
- [6] GuJianjun, XuDianguo, Liu Hankui and Gong Maozhong, "Unified Power Quality Conditioner (UPQC): the Principle, Control and Application",Conference on Power Conversion, pp.80-85, 20002.
- [7] Hideaki Fujita and Hirofumi Akagi, "The unified power quality conditioner: the integration of seriesand shunt- active filters," IEEE Transactions on power electronics, pp.315-322, 1998.
- [8] H.Hingorani,"Introducing Custom Power" IEEE Spectrum, Vol.32,(6) pp. 41-48, 1995.
- [9] JiangyuanLe ,YunxiangXie , Zhang Zhi and Cheng Lin,"A Nonlinear control strategy for (UPQC)" International Conference on Electrical Machines pp.2067- 2070, 2008.
- [10] Juan W. Dixon, Gustavo Venegas and Luis A. Mor'an, "A Series Active Power Filter Based on a Sinusoidal Current-Controlled Voltage-Source Inverter" IEEE Transactions on Industrial Electronics, Vol. 44(5),pp.612-620, 1997.
- [11] MetinKesler and EnginOzdemir, "A Novel Control Method for Unified Power Quality Conditioner (UPQC) Under Non-Ideal Mains Voltage and Unbalanced Load Conditions", 25th Annual IEEE Applied Power Electronics Conference and Exposition (APEC), pp.374-379, 2010.
- [12] Olimpo Anaya - Lara and E. Acha, "Modeling and Analysis of Custom Power Systems by PSCAD/EMTDC", IEEE Transactions on Power Delivery, Vol.17, pp.266–272, 2002.
- [13] K.R.Padiyar, "Facts Controllers in Power Transmission and Distribution", New Age International Publishers, 2007.
- [14] Roger C. Dugan, Mark F. McGranaghan, Surya Santoso, and H.WayneBeaty, "Electrical Power Systems Quality", the McGraw-Hill, Second Edition, 2004.
- [15] RVD Rama Rao, Subhransu and Sekhar.Dash, "Power Quality Enhancement by Unified Power Quality Conditioner Using ANN with Hysteresis Control" International Journal of Computer Applications Vol.6, pp.9-15, 2010.
- [16] Rajasekaran Dharmalingam, Subhransu Sekhar Dash, Karthikrajan Senthilnathan, Arun Bhaskar Mayilvaganan, and Subramani Chinnamuthu, "Power Quality Improvement by Unified Power Quality Conditioner Based on CSC Topology Using Synchronous Reference Frame Theory," The Scientific World Journal, vol. 2014, pp.1-7, 2014.
- [17] C.Sankaran, "Power Quality", CRC Press LLC, 2002.
- [18] S Ravi, Vitaliy Mezhuhev, K Iyswarya Annapoorani, P Sukumar, "Design and implementation of a microcontroller

based buck boost converter as a smooth starter for permanent magnet motor” Indonesian Journal of Electrical Engineering and Computer Science.,vol. 1(3), pp. 566-574, Mar.2016.

[19] Karthikrajan Senthilnathan Iyswarya Annapoorani, “Implementation of unified power quality conditioner (UPQC) based on current source converters for distribution grid and performance monitoring through LabVIEW Simulation Interface Toolkit server: a cyber-physical model,” IET Generation, Transmission & Distribution, vol. 10(11), pp.2622–2630, 2016.

[20] Karthikrajan Senthilnathan, Iyswarya, A. K.. “Artificial Neural Network Control Strategy for Multi-converter Unified Power Quality Conditioner for Power Quality Improvements in 3-Feeder System,” Advances in Intelligent Systems and Computing, vol. 394, pp. 1105–1111, 2016.

[21] Senthilnathan, K., Annapoorani, K. I., “A Review on Back-to-Back Converters in Permanent Magnet Synchronous Generator based Wind Energy Conversion System”. Indonesian Journal of Electrical Engineering and Computer Science, vol. 2(3), pp. 583–591, June.2016.



## High voltage DC-DC converter with standalone application

Thiruveedula Madhu Babu, Kalagotla Chenchireddy, Jakkani Rohini, Mesaragandla Sai Suhas,  
Dara Ajitesh, Kanaparathi Rahul

Department of Electrical and Electronics Engineering, Teegala Krishna Reddy Engineering College, Hyderabad, India

### Article Info

#### Article history:

Received Mar 31, 2023

Revised May 20, 2023

Accepted May 25, 2023

#### Keywords:

High voltage step-up converter

High voltage transfer gain

MOSFET

PI controller

Ultra-lift Luo converter

### ABSTRACT

Designing DC-DC converters involves many voltage lift techniques. These techniques have been encouraged for their credible advantages. Most voltage lifting methods are applied in many areas of automotive, motor drives, telecom and electronic welfare in military applications. Voltage lifting techniques are known for their high voltage transfer gain and high efficiency. Ultra-lift converter yields very high output transfer gain with geometric progression compared to other voltage lift techniques such as super lift converters and classical boost converters. It also offers reduced size and improved efficiency when compared. In this proposed method ultra-lift converter operation is analyzed with continuous conduction mode.

This is an open access article under the [CC BY-SA](https://creativecommons.org/licenses/by-sa/4.0/) license.



### Corresponding Author:

Kalagotla Chenchireddy

Department of Electrical and Electronics Engineering, Teegala Krishna Reddy Engineering College

Hyderabad, Telangana 500097, India

Email: chenchireddy.kalagotla@gmail.com

## 1. INTRODUCTION

The DC-to-DC converters are applied for stand-alone applications. The input of the converter is applied from a PV panel with the output connected to a battery source and a DC load. The capacity of the PV array is 50 W. The simulation and experimental results are verified by comparing different converters [1]. A reduced switch count-based ultra step-up DC to DC converter is presented and the implemented converter has less number of components such as diodes inductors capacitors when compared to conventional converters. This type of converter gives high efficiency with high transfer gain. The simulation results with different pulse widths are taken and verified for better output [2].

An improved voltage lift technique is proposed for high voltage DC to DC converter this paper focused on the mathematical analysis of the converter operation in the continuous conduction and the simulation results along with the hardware results are implemented. The results obtained do have not much difference in the output waveforms when done with simulation and hardware [3]–[5]. In this paper, the converter yields a voltage gain of 3 when the duty cycle is 50%, which when compared with the boost converter is 2 times greater. The converter implemented in this system has a voltage transfer gain that is equal to the boost converter with a 50% duty cycle [6]–[8]. The dynamic analysis of the converter has a major role in this converter, as voltage obtained by the converter alone consists of a high value of ripple factor, there increased necessity of a control technique to overcome the effects of the ripples produced. There are many control techniques implemented to the voltage lift converters with a closed loop system in which we used the proportional integral (PI) control technique along with the ultra-lift converter, by which the voltage yielded is improved along with the efficiency [9]–[12].

In this voltage lift technique, the voltage transfer gain is obtained step by step as symmetric progress. Which is several times greater than other converters such as boost and super lift converters [13]–[15]. The converter topology implemented in this paper gives negative voltage as output. as it supplies the requirements of many applications. It is more advantageous of using a PI controller which supplies the gate pulses to the converter and gives a good response for linear systems, by which we can get an accurate dynamic response for the system [16]–[18]. The proportional constants of the controller deal with the current rate of error and the integral constants deal with the previous rate of error. The modes of operation of the converter are also explained in this methodology [19].

The negative output superlift Luo converter (NOSLC) uses the VL approach to produce a large negative voltage. The closed loop block gives the required control output and the output of this system is generated as an error this error value is given as the input to the converter system by comparing the reference voltage to that of the error signal. The controller produces the duty ratio as a result. The switch that creates the necessary pulse for the system's operation is assigned this duty ratio as a result the required output is obtained with reduced ripple values [9]. The following assumptions are made: the MOSFETs, the diodes D1 and D2 are considered to be the three switches in the basic circuit. Theoretically, 2' distinct switch states will be created by n switches. Assuming a low value of ripple the steady state value is DC and the small value of AC ripples [20].

**2. ULTRA-LIFT LUO CONVERTER**

DC-DC converters play a role in modern energy [21]–[25]. There are many applications for DC-DC converters DC motors, solar power plants, and DC drives. This paper mainly focuses on the ultra-lift converter, the ultra-lift converter 4 to 5 times increase input voltage. Compared to the boost converter, the proposed converter has high efficiency. Figure 1 shows the circuit diagram of the ultra-lift Luo converter. The input applied is Vs and the output is V0. Ultra-lift converter works in two modes based on the switch position. The converter operated in 2 modes here we discuss one of them.

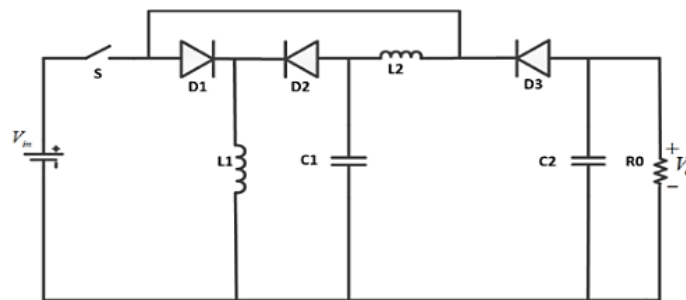


Figure 1. Ultra-lift converter

**2.1. Mode 1**

Figure 2 depicts the ultra-lift converter in mode 1 of operation. In this mode, the switch S is kept in the ON position A supply voltage is provided across an inductor L1, a forward-biased diode D1, and a pair of reverse-biased diodes D2 and D3. The inductor and capacitor are energy storage devices, and the figure depicts the current flow. When the switch is on the inductor current  $i_{L1}$  rises with a slope  $+\frac{V_1}{L_1}$ . The voltage across the inductor L1 is:

$$V_1 = L_1 \frac{di_{L1}}{dt} \tag{1}$$

applying the node analysis:

$$0 = L_1 \frac{di_{L1}}{dt} - L_2 \frac{di_{L2}}{dt} + V_3 \tag{2}$$

from (1) and (2):

$$\left(\frac{V_1+V_3}{L_2}\right) - \frac{di_{L2}}{dt} = 0 \tag{3}$$

$$\left(\frac{V_1-V_3}{L_2}\right) T_{ON} = \frac{di_{L2}}{dt} \tag{4}$$

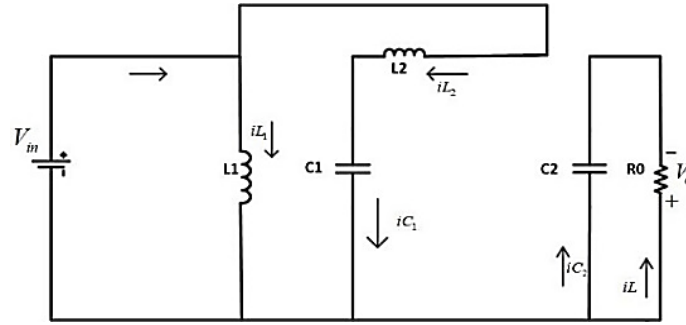


Figure 2. Mode 1: Switch is ON

**2.2. Mode 2**

Figure 3 depicts how the ultra-lift converter functions in mode 2. The switch S is in the off position in this mode. The inductor L2 discharges and the diodes D2, and D3 are forward-biased. When the inductor L2 transfers the stored energy in C2 through the diode, the current through the inductor  $i_{L2}$  diminishes and the inductor  $i_{L1}$  transfers stored energy in C2.

$$V_3 + V_{C2} - V_{C1} = 0 \tag{5}$$

Substituting  $V_{C2}$  as  $V_2$  we get:

$$V_3 + V_2 + V_{C1} = 0 \tag{6}$$

$$-L_2 \frac{di_{L2}}{dt} + V_2 - V_3 = 0 \tag{7}$$

$$V_2 - V_3 = L_2 \frac{di_{L2}}{dt} \tag{8}$$

$$T_{OFF} \left( \frac{V_2 - V_3}{L_2} \right) = \frac{di_{L2}}{dt} = i_{L2} \tag{9}$$

from (6) and (9):

$$KT \frac{V_1 + V_3}{L_2} = (1 - k)T \left( \frac{V_2 - V_3}{L_2} \right) \tag{10}$$

where  $KT$  = switch ON time and  $(1 - k) T$  = switch OFF time. Evaluating (10):

$$KT \frac{V_1 + V_3}{L_2} = \left( \frac{V_2 - V_3}{L_2} \right) T - KT \left( \frac{V_2 - V_3}{L_2} \right) \tag{11}$$

$$KT(V_1 + V_2) = (V_2 - V_3)T \tag{12}$$

$$K = \left( \frac{V_2 - V_3}{V_1 + V_3} \right) \tag{13}$$

$$\left( \frac{V_1 + V_3}{V_2 - V_3} \right) = \left( \frac{1 - K}{K} \right) \tag{14}$$

$$\frac{(V_1 + V_3)K}{(1 - K)} = \frac{V_2 - V_3}{1} \tag{15}$$

$$\frac{(V_1 + V_3)K}{(1 - K)} + V_3 = V_2 \tag{16}$$

$$V_3 = V_1 \left( \frac{K}{1 - K} \right) \tag{17}$$

$$V_2 = V_1 \left( \frac{K}{1 - K} \right) + \left[ \frac{\left\{ V_1 + V_1 \left( \frac{K}{1 - K} \right) \right\} K}{1 - K} \right] \tag{18}$$

$$G = \frac{V_2}{V_1} = \frac{K(2-K)}{(1-K)^2} \tag{19}$$

the (19) depicts the ultra-lift converter's voltage transfer gain, which, when compared to conventional voltage lift converters, is larger.

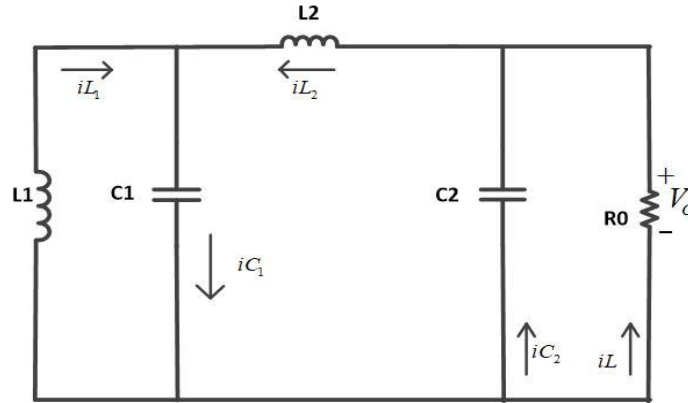


Figure 3. Mode 2: switch is OFF

### 3. PI CONTROLLER

Figure 4 shows the PI controller in this system. The proportional plus integral controller is another name for the proportional-integral controller. It's the result of combining proportional and integral control operations. As a result, it is known as a PI controller. The controller becomes more efficient when two separate converters are combined, eliminating the disadvantages of each controller. The suggested DC-DC converter can accomplish a high voltage transfer ratio, and low current ripple, according to the results. These data indicate that this converter is appropriate for use in a domestic FC system. Similarly, this Luo system can be employed in solar-powered Luo converters and electric vehicle (EV) chargers. Table 1 shows the pulse width modulation (PWM) and output voltage values.

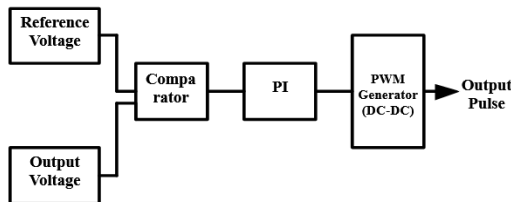


Figure 4. PI controller block

Table 1. Output values

S.L.	Pulse width (%)	Output voltage (V)
1	20	-11.7
2	40	-35.47
3	50	-59.69
4	60	-105.69
5	80	-404.5
6	90	-555.5
7	95	-209.9

### 4. SIMULATION RESULTS

Figure 5 shows the high voltage ultra-lift Luo converter is depicted in Figure 5. The circuit consists of a single MOSFET switch, a single load resistance, a single voltage source, two capacitors, two inductors, three diodes, and a pulse generator. Figure 6 shows that the ultra-lift converter output waveforms when the pulse width (PW) of the pulse generator is 50%. Vs is the input voltage of magnitude of 20 V. The capacitors C1 and C2 have voltages of magnitudes -20 V, -59 V. The output voltage magnitude across the load resistor is -59 V. Figure 7 shows that the ultra-lift converter output waveforms when the PW of the pulse generator is 60%. Vs is the input voltage of magnitude of 20 V. The capacitors C1 and C2 have voltages of magnitudes -30 V, -105 V. The output voltage magnitude across the load resistor is -105 V. Figure 8 shows that the ultra-lift converter output waveforms when the PW of the pulse generator is 80%. Vs is the input voltage of magnitude of 20 V. The capacitors C1 and C2 have voltages of magnitudes -70 V, -404 V. The output voltage magnitude across the load resistor is -404 V. Figure 9 shows that the ultra-lift converter output waveforms when the PW of the pulse generator is 90%. Vs is the input voltage of magnitude of 20 V. The capacitors C1 and C2 have voltages of magnitudes -50 V, -555 V. The output voltage magnitude across the load resistor is -555 V.

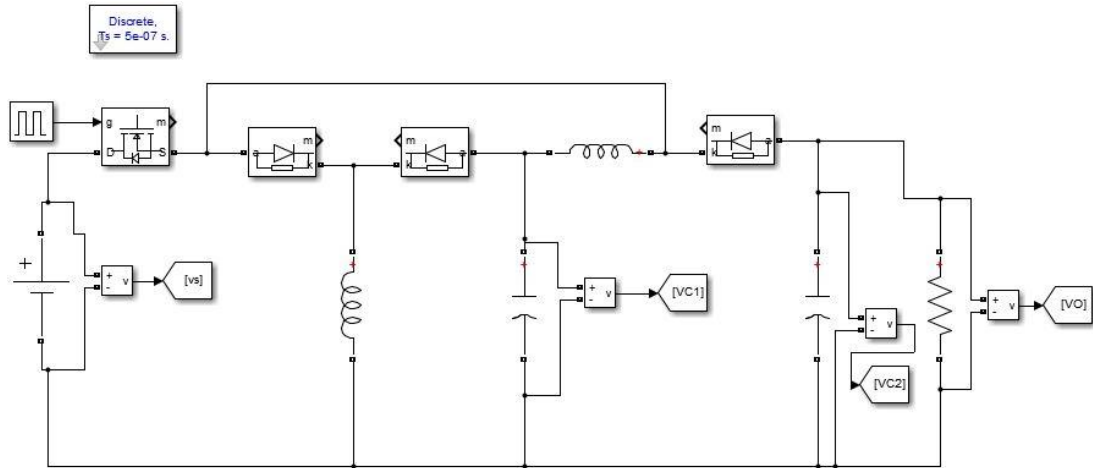


Figure 5. Ultra-lift Luo DC-DC converter

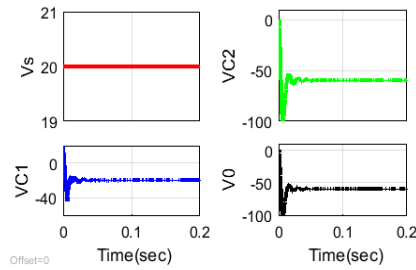


Figure 6. DC-DC converter with a PWM of 50%

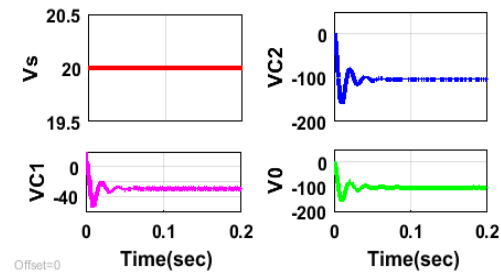


Figure 7. DC-DC converter with a PWM of 60%

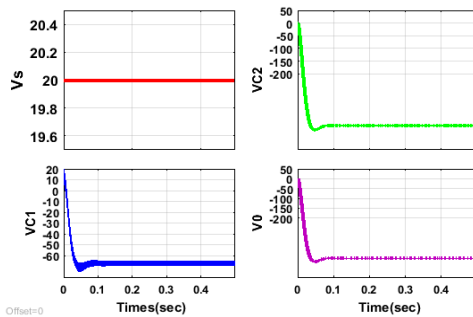


Figure 8. DC-DC converter with a PWM of 80%

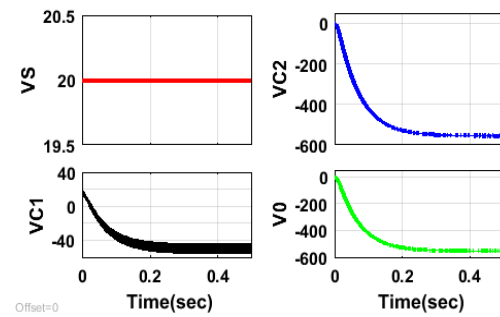


Figure 9. DC-DC converter with PWM of 90%

### 5. CONCLUSION

The ultra-lift converter operation is analyzed, and mathematical calculations and simulation results are verified. This converter produces a very high voltage transfer gain which is verified with different values of duty ratio. Good dynamic performance in the presence of input voltage variations and variant dynamic performance in the presence of varying operating conditions.




### REFERENCES

- [1] A. Kavitha and G. Uma, "Experimental Verification of Hopf Bifurcation in DC-DC Luo Converter," *IEEE Transactions on Power Electronics*, vol. 23, no. 6, pp. 2878–2883, Nov. 2008, doi: 10.1109/TPEL.2008.2004703.
- [2] K. R. Sreejyothi, Balakrishnakothapalli, K. Chenchireddy, S. A. Sydu, V. Kumar, and W. Sultana, "Bidirectional Battery Charger Circuit using Buck/Boost Converter," in *2022 6th International Conference on Electronics, Communication and Aerospace Technology*, Dec. 2022, pp. 63–68, doi: 10.1109/ICECA55336.2022.10009062.
- [3] J. Gupta and B. Singh, "Bridgeless Isolated Positive Output Luo Converter Based High Power Factor Single Stage Charging Solution for Light Electric Vehicles," *IEEE Transactions on Industry Applications*, vol. 58, no. 1, pp. 732–741, Jan. 2022, doi: 10.1109/TIA.2021.3131647.




- [4] R. Kushwaha and B. Singh, "Bridgeless Isolated Zeta–Luo Converter-Based EV Charger With PF Preregulation," *IEEE Transactions on Industry Applications*, vol. 57, no. 1, pp. 628–636, Jan. 2021, doi: 10.1109/TIA.2020.3036019.
- [5] F. L. Luo and H. Ye, "Positive Output Multiple-Lift Push–Pull Switched-Capacitor Luo–Converters," *IEEE Transactions on Industrial Electronics*, vol. 51, no. 3, pp. 594–602, Jun. 2004, doi: 10.1109/TIE.2004.825344.
- [6] B. Singh, V. Bist, A. Chandra, and K. Al-Haddad, "Power Factor Correction in Bridgeless-Luo Converter-Fed BLDC Motor Drive," *IEEE Transactions on Industry Applications*, vol. 51, no. 2, pp. 1179–1188, Mar. 2015, doi: 10.1109/TIA.2014.2344502.
- [7] B. Singh and R. Kushwaha, "Power Factor Preregulation in Interleaved Luo Converter-Fed Electric Vehicle Battery Charger," *IEEE Transactions on Industry Applications*, vol. 57, no. 3, pp. 2870–2882, May 2021, doi: 10.1109/TIA.2021.3061964.
- [8] S. Mahdizadeh, H. Gholizadeh, and S. A. Gorji, "A Power Converter Based on the Combination of Cuk and Positive Output Super Lift Luo Converters: Circuit Analysis, Simulation and Experimental Validation," *IEEE Access*, vol. 10, pp. 52899–52911, 2022, doi: 10.1109/ACCESS.2022.3175892.
- [9] R. Kushwaha and B. Singh, "Design and Development of Modified BL Luo Converter for PQ Improvement in EV Charger," *IEEE Transactions on Industry Applications*, vol. 56, no. 4, pp. 3976–3984, 2020, doi: 10.1109/TIA.2020.2988197.
- [10] M. Mahdavi, M. Shahriari-kahkeshi, and N. R. Abjadi, "An Adaptive Estimator-Based Sliding Mode Control Scheme for Uncertain POESLL Converter," *IEEE Transactions on Aerospace and Electronic Systems*, vol. 55, no. 6, pp. 3551–3560, Dec. 2019, doi: 10.1109/TAES.2019.2908272.
- [11] R. Kushwaha and B. Singh, "A Modified Luo Converter-Based Electric Vehicle Battery Charger With Power Quality Improvement," *IEEE Transactions on Transportation Electrification*, vol. 5, no. 4, pp. 1087–1096, Dec. 2019, doi: 10.1109/TTE.2019.2952089.
- [12] B. Faridpak, M. Farrokhifar, M. Nasiri, A. Alahyari, and N. Sadoogi, "Developing a super-lift Luo-converter with integration of buck converters for electric vehicle applications," *CSEE Journal of Power and Energy Systems*, vol. 7, no. 4, pp. 811–820, 2020, doi: 10.17775/CSEEJPES.2020.01880.
- [13] Z. Amjadi and S. S. Williamson, "Modeling, simulation, and control of an advanced Luo converter for plug-in hybrid electric vehicle energy-storage system," *IEEE Transactions on Vehicular Technology*, vol. 60, no. 1, pp. 64–75, Jan. 2011, doi: 10.1109/TVT.2010.2088146.
- [14] P. Anbarasan, M. Venmathi, M. Vijayaragavan, and V. Krishnakumar, "Performance Enhancement of Grid Integrated Photovoltaic System Using Luo Converter," *IEEE Canadian Journal of Electrical and Computer Engineering*, vol. 45, no. 3, pp. 293–302, 2022, doi: 10.1109/icjece.2022.3178696.
- [15] S. Pal, B. Singh, and A. Shrivastava, "A universal input CrCM Luo converter with low-cost pilot-line dimming concept for general purpose LED lighting applications," *IEEE Transactions on Industrial Informatics*, vol. 14, no. 11, pp. 4895–4904, Nov. 2018, doi: 10.1109/TII.2018.2808277.
- [16] H. N. Jazi, A. Goudarzian, R. Pourbagher, and S. Y. Derakhshandeh, "PI and PWM Sliding Mode Control of POESLL Converter," *IEEE Transactions on Aerospace and Electronic Systems*, vol. 53, no. 5, pp. 2167–2177, Oct. 2017, doi: 10.1109/TAES.2017.2684998.
- [17] F. Ghasemi, M. R. Yazdani, and M. Delshad, "Step-Up DC-DC Switching Converter with Single Switch and Multi-Outputs Based on Luo Topology," *IEEE Access*, vol. 10, pp. 16871–16882, 2022, doi: 10.1109/ACCESS.2022.3150316.
- [18] F. L. Luo and H. Ye, "Positive output super-lift converters," *IEEE Transactions on Power Electronics*, vol. 18, no. 1, pp. 105–113, Jan. 2003, doi: 10.1109/TPEL.2002.807198.
- [19] F. L. Luo and H. Ye, "Negative output super-lift converters," *IEEE Transactions on Power Electronics*, vol. 18, no. 5, pp. 1113–1121, Sep. 2003, doi: 10.1109/TPEL.2003.816185.
- [20] F. L. Luo and H. Ye, "Small signal analysis of energy factor and mathematical modeling for power DC-DC converters," *IEEE Transactions on Power Electronics*, vol. 22, no. 1, pp. 69–79, Jan. 2007, doi: 10.1109/TPEL.2006.886652.
- [21] M. Zhu, F. L. Luo, and Y. He, "Remaining inductor current phenomena of complex DC-DC converters in discontinuous conduction mode: General concepts and case study," *IEEE Transactions on Power Electronics*, vol. 23, no. 2, pp. 1014–1019, Mar. 2008, doi: 10.1109/TPEL.2008.917956.
- [22] S. Ding and F. Wang, "A New Negative Output Buck-Boost Converter with Wide Conversion Ratio," *IEEE Transactions on Industrial Electronics*, vol. 64, no. 12, pp. 9322–9333, Dec. 2017, doi: 10.1109/TIE.2017.2711541.
- [23] B. W. Williams, "Generation and analysis of canonical switching cell DC-to-DC converters," *IEEE Transactions on Industrial Electronics*, vol. 61, no. 1, pp. 329–346, Jan. 2014, doi: 10.1109/TIE.2013.2240633.
- [24] K. Chenchireddy, B. S. Goud, C. M. Sudhan Mudhiraj, N. Rajitha, B. S. Kumar, and V. Jagan, "Performance Verification of Full-Bridge DC to DC Converter Used for Electric Vehicle Charging Stations," in *2022 8th International Conference on Advanced Computing and Communication Systems (ICACCS)*, Mar. 2022, pp. 434–439, doi: 10.1109/ICACCS54159.2022.9785288.
- [25] K. R. Sreejyothi, K. Chenchireddy, N. Lavanya, R. M. Reddy, K. Y. G. Prasad, and R. Revanth, "Level-Shifted PWM Techniques Applied to Flying Capacitor Multilevel Inverter," in *2022 International Conference on Electronics and Renewable Systems (ICEARS)*, Mar. 2022, pp. 41–46, doi: 10.1109/ICEARS53579.2022.9752074.

## BIOGRAPHIES OF AUTHORS






**Thiruveedula Madhu Babu**    is received a B.Tech. from JNTU Hyderabad, Hyderabad, India, in 2010 and M.Tech. from NIT Calicut 2012 respectively and pursuing Ph.D. in Annamalai University, India. He is working presently as Assistant Professor and HOD in Teegala Krishna Reddy Engineering College, Hyderabad, India. He has presented technical papers in various national and international journals and conferences. He can be contacted at email: madhumk448@gmail.com.






**Kalagotla Chenchireddy**    is received the B.Tech. and M.Tech. from JNTU Hyderabad, Hyderabad, India, in 2011 and 2013 respectively and pursuing Ph.D. in Karunya Institute of Technology and Sciences, Karunyanagar, Coimbatore, TN, India. He is working presently as Assistant Professor in Teegala Krishna Reddy Engineering College, Hyderabad, India. He has presented technical papers in various national and international journals and conferences. His area of interest includes power electronics, power quality, and multilevel inverters. He is a regular reviewer of ISA Transactions, Cybernetics and Systems SCIE journals, IJPEDS, and IJAPE. He can be contacted at email: [chenchireddy.kalagotla@gmail.com](mailto:chenchireddy.kalagotla@gmail.com).






**Jakkani Rohini**    is presently UG Student in Electrical and Electronics Engineering, at Teegala Krishna Reddy Engineering College, Hyderabad, India. She has presented technical papers at various national and international conferences. His area of interest includes power electronics, power quality, and multilevel inverters. She developed a single phase inverter in Teegala Krishna Reddy Engineering College, Hyderabad. She can be contacted at email: [jakkanirohini027@gmail.com](mailto:jakkanirohini027@gmail.com).






**Mesaragandla Sai Suhas**    is presently UG Student in Electrical and Electronics Engineering Department, Teegala Krishna Reddy Engineering College, Hyderabad, India. He has presented technical papers in various national and international journals and conferences. His area of interest includes power electronics, power quality, and multilevel inverters. He got first prize national level project expo 2023 in VJIT college Hyderabad. He can be contacted at email: [sai123mesaragandla@gmail.com](mailto:sai123mesaragandla@gmail.com).



**Dara Ajitesh**    is presently UG Student in Electrical and Electronics Engineering Department, Teegala Krishna Reddy Engineering College, Hyderabad, India. He has presented technical papers in various national and international journals and conferences. His area of interest includes power electronics, power quality, and multilevel inverters. He got first prize national level project expo 2022 in NNRG college Hyderabad. He can be contacted at email: [daraajitesh8@gmail.com](mailto:daraajitesh8@gmail.com).



**Kanaparthi Rahul**    is presently UG Student in Electrical and Electronics Engineering Department, Teegala Krishna Reddy Engineering College, Hyderabad, India. He has presented technical papers in various national and international journals and conferences. His area of interest includes power electronics, power quality, and multilevel inverters. He got first prize national level project expo 2023 in Gitanjali Engineering college Hyderabad. He can be contacted at email: [kanaparthirahul35@gmail.com](mailto:kanaparthirahul35@gmail.com).



# AUTOMATIC FIRE CONTROL SYSTEM IN RAILWAYS

<sup>1</sup>Dr. B.Vidya Sagar, <sup>2</sup>K.Sai Priya, <sup>3</sup>B. Kurmi Naidu, <sup>4</sup>S. Sai Sagar, <sup>5</sup>M. Shivakanth Reddy, <sup>6</sup>M. S. Sujatha

<sup>1,2,3,4,5</sup>Teegala Krishna Reddy Engineering College

Hyderabad, Telangana, India

Sree Vidyanikethan Engineering College (Formerly), Mohan Babu University, Tirupati, India

vidyasagar@tkrec.ac.in

**Abstract.** The Present project will automatically help the railways to safeguard from Fire Accidents in a step-by-step process. When a fire occurs, the sensor will detect and starts alerting the security people. We designed four stages for controlling and monitoring. The siren will be turned ON in the first stage, in the second stage Blinker, in the third stage water flushes, and in the fourth stage, the train stops automatically by using LM3914 with LM35 Heat sensors and RF Wireless technology with relay switching is interfaced for the circuit.

**Keywords:** RF Technology, LM3914 IC, LM35 Heat sensors

## 1 INTRODUCTION

Fire accidents in trains are one of the most dangerous disasters to human lives and loss of costly components in Railways. Fire in a moving train is threatening because it quickly spreads to other coaches due to the interaction with air present in the surroundings. Automatic fire control in railroads is the topic of this study [1]. As we can see, there are frequent train fire catastrophes that result in fatalities for passengers. To overcome this challenge, we designed an autonomous fire control system. This project makes use of sensing components to measure temperature and fire [2]. Additionally, Wireless RF technology is being used to continuously manage the fire and check the temperature inside the train compartment [3] [4]. The system will use the Temperature Sensor to determine the temperature, and it will use the Siren and Blinker to inform those inside the compartments [5]. Water Sprinklers are utilized to put out the fire. In the entire functioning stages, an LM35 Heat Sensor, relay switching is interfaced and operated [6] [7].

The automatic fire control system applies to theatres, museums, exhibitions, complexes, Historical and cultural artifacts, and huge regions where there are high-rack warehouses, workshops, underground parking lots, etc. We use several electrical components in this project i.e. Step-down transformer, LM3914 IC, LM35 Heat Sensor, Relays, Encoder, Decoder, RF Technology, and Optocouplers [8].

A T/F is an electric device that can change the voltage without changing the frequency. Without any electrical contact between them, the electrical energy is transmitted from one circuit to another [9]. This is designed to alter the Voltage output between the circuits while keeping the current's frequency constant. This technique is used to step up the voltage and afterward step down the current to lower it. This shows that the current flowing via the overhead wires is frequently little and has a wide dispersion across the country.

A step-down T/F is a static device that has low current (LC) and high voltage (HV) from the transformer's principal side to the secondary side's High current (CV) and low voltage (LV). For a step-down transformer, the voltage ratio is roughly inversely proportional to the transformer turns ratio(n):

$$n = N_p/N_s = N_p/N_s(1)$$

Where NPS stands for the number of turns on the primary (LV) and secondary (HV) sides, representatively, VPS stands for, whereas voltage energy flow from the HV side to the LV side because the main side (HV Side) of a step-down transformer has more turns than the secondary side (LV Side). Stepping down the primary voltage (input voltage) to the secondary voltage (output voltage). This equation can be changed to include the output voltage formula (i.e., Secondary voltage). It is possible to refer to the following formula as the step-down transformer formula:

$$N_s * V_p / V_s = V_s(2)$$



The transformer in an electronic device is referred to as the low-voltage application a low-voltage value is needed to supply the electrical circuits (for example, 5V or even low values).

The temperature sensor LM35 measures external heat and gives the outputs as a signal in an analog form that is proportional to the immediate temperature is simple to interpret the output voltage to obtain a temperature reading in Celsius. Several forms of There are heat sensors available. a few works with hot temperature measures and Certain sensors are inappropriate for this project. The LM35 element is rated to operate over a range of  $-55^{\circ}\text{C}$  to  $150^{\circ}\text{C}$  [10] [11].

The LM3914 is an integrated circuit (IC) that has outputs that can power up fluorescent displays, LCDs, or LEDs. The device can be used, for instance, as a voltmeter thanks to the direct scaling of the output thresholds. The initial configuration offers a scale with ten steps that can be expanded to 100 pieces and ten vacuum floors with another LM3914 IC.

#### 4.1 DESCRIPTION: -

The LM3914 is an integrated circuit that senses analog voltage levels and drives 10 LEDs providing a linear analog display

## 5. RELAYS

A switch that is electrically actuated is called a switch. It consists of several input terminals, several functioning contact terminals, and one or more control signals. There could be any quantity of contacts on the switch relays used to open or close. There could be any number of contacts on the switch. Relays are used to open or close electrical circuits as well as protect electrical devices.

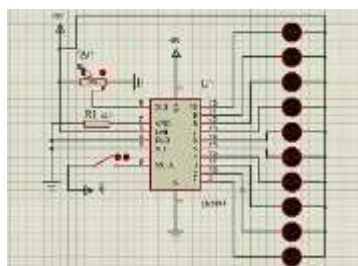


**FIG:6.IC PIN CONNECTIONS TO LEDS**

An electromagnet, armature, spring movable contact, and stationary contact make up an electromagnetic relay. The high power required to directly control a load may be handled by a relay, but the difference is in the voltage.

#### 1. Encoders

The encoder is a piece of technology that is used to encode the signals with the help of signals send by the transmitter.

#### 2. Decoders

The decoder is an electronic device that is used to decode the signals which are sent by the receiver.

An RF module is also called a radio frequency module. It's a tiny electronic gadget that's utilized to transmit and receive signals with the help of a transmitter and receiver between two devices.

Another name for an optocoupler is a photocoupler or an optoisolator. It is an electronic component that uses light to transmit electrical impulses between two shielded circuits. High voltages cannot damage the system entering the signal thanks to opt-isolators. optoisolators that are rapidly available in the marketplace can tolerate input-to-output voltages of up to 10kv and voltage transients of up to 25kv/s. To provide insulation between low and high-voltage circuits, optocouplers can either be employed alone as a switching device or in conjunction with other electrical biases. These gadgets are often used to switch the DC and AC power input and output of microprocessors. In this system, there are two components: an automatic control unit and a monitoring section

### 9. Automatic control unit

The step-down transformer, a sensor system, an LM3914 integrated circuit, a transmitter section, and a relay's sequential switching system are the automatic control unit's main systems.

In this system, the needed power is supplied by stepping down the system voltage using a step-down transformer. An LM3914 integrated circuit temperature level in the compartment is shown by the LED and a heat sensor in the sensing system detects an increase in temperature in the compartments when fire accidents occur. To notify the passengers, a siren is activated. Fire sensors also detect a fire within the compartment, and this information is conveyed through an RF module. The transmitter and receiver sections of an RF module. The transmitter section collects data from heat sensors and transmits it to the receiver section, which is in the monitoring section and locomotive, so that the monitoring section and locomotive may take appropriate action to protect the passengers.

Sequential relay switching is utilized to turn on the water pump, blinkers, and train brakes all at once. The water pump will start to circulate water throughout the cabin as the relay-controlled automatic braking system stops the train.

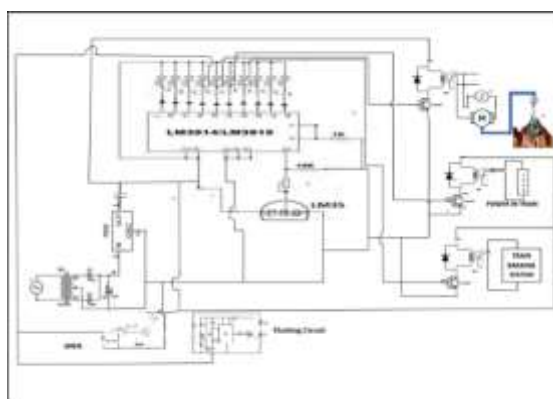


Fig:11Control unit Circuit diagram

### 10. Monitoring section

The receiver section is another name for the monitoring section. Data from the RF transmission module is received by it via an RF reception module. It informs the railroad safety measures to control fire accidents and save the lives of passengers by displaying the serial number of the bogie in which the fire accidents occur.

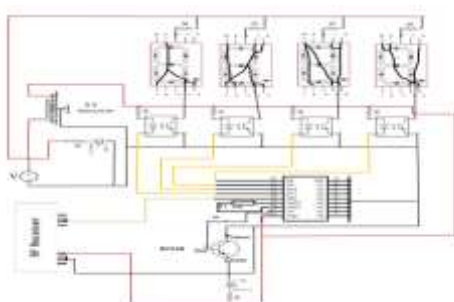


Fig:12.Schematic diagram



Fig:13. Monitoring circuit board

### 11. Block Diagram



Fig:14.Block diagram

### 12. SYSTEM OVERVIEW

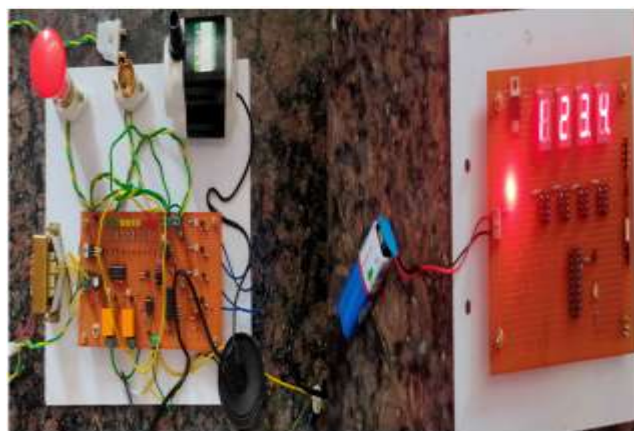


Fig.15.Automatic fire control unit and monitoring section.



Fig.16.Installation of circuits in a train compartment

### 13.Circuit diagrams

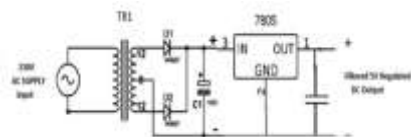


Fig.17.5v regulated supply circuit

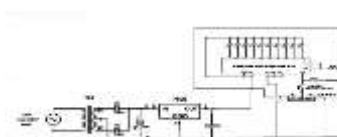


Fig.18.Temperature indicator circuit

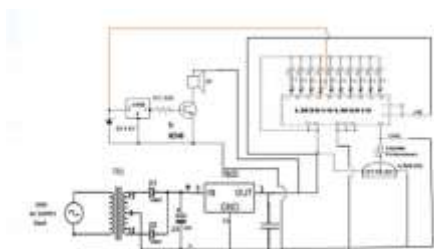


Fig.19.Siren circuit

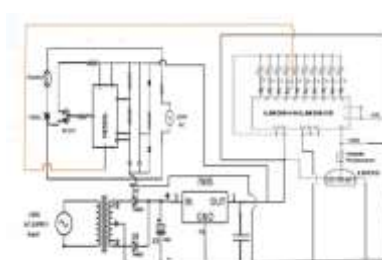


Fig.20.Flasher and Relay circuit

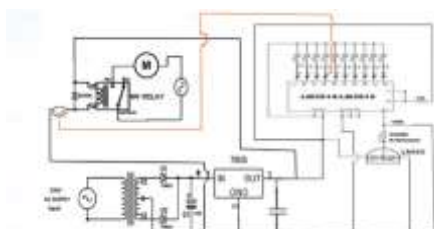


Fig.21.Water sprinkler circuit

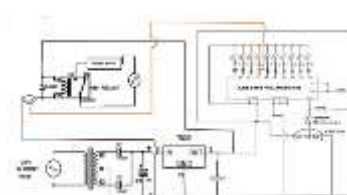


Fig.22.Train Breaking circuit

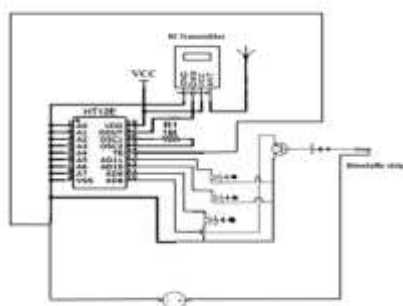


Fig.23.RF Transmitter circuit

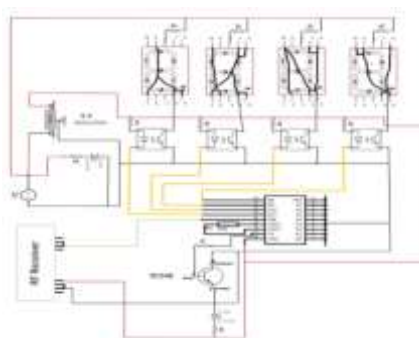


Fig.24.RF Receiver circuit

## 14.RESULT

As fire accidents occur the heat sensors sense the heat and the fire detector detects the fire and indicates the temperature, simultaneously siren and blinkers will be turned on to alert passengers, relays get operated and the water pump is turned on then the water sprinkling starts the same time train get stops by breakings. Hence, the fire in the train gets controlled and stops the spreading of the fire

## 15. CONCLUSION

This essay demonstrates the planning and execution of automatic fire control systems in railways at low-cost and trustworthiness. Using RF technology, which is completely wireless. this system is implemented mainly with electrical components, like heat sensors, fire detectors, relays, etc. heat sensors, fire detectors, and water storage is allotted at every compartment in railroads. so that whenever fire detects it is controlled. This is a more condensed version of the project and implemented and tested with success in this document.

## 16. REFERENCES

1. Devan, P. ArunMozhi, et al. "Fire Safety and Alerting System in Railways." *3rd IEEE International Conference on Recent Trends in Electronics, Information, and Communication Technology, 2018 (RTEICT). IEEE, 2018.*
2. Pandey, Sumit, et al. "Automatic fire-initiated braking and alert system for trains." *Second International Conference on Computer and Communication Engineering Advances 2015 IEEE, 2015.*
3. Peacock Richard W. Bukowski, VytenisBabrauskas, Paul A. Reneke, Walter W. Jones, and Richard D.. "Concepts for fire protection of passenger rail vehicles: past, present, and future *Inflammable Materials* 19, no. 2 (1995): 71-87.
4. Wang, W. Q., and Liu, X. L. (2013). An investigation of China's standardization of the use of fire detectors in rail vehicles. 240–244 in *Procedia Engineering*, 52.
5. Raman, R. R., Kumar, S. S., M. P., and Ramasamy, R. P. (2013). Using a Zigbee wireless sensor network, fire mishaps on moving trains can be prevented. 3(6), 583-592, *International Journal of Information and Computation Technology*.
6. Lee, T. S., Moon, Y. H., & Hong, H. S. (2004). A Study on the auto fire-extinguishing system in the subway train. Within the *KSR Conference Proceedings* (pp. 168-173). Railway Society of Korea.
7. Sathya, M. S., Khan, J. A. J., Velmurugan, M., &Kumar, M. A. A. (2020). FORESTALLING FIRE ACCIDENT IN TRAIN.
8. R. Mundra, A. Srinivasulu, C. Ravariu, A. Bhargav, M.Sarada, "Real Time Driver Alertness System Based on Eye Aspect Ratio and Head Pose Estimation", in *proc.of the International Conference on Smart Technologies in Urban Engineering*, 29 Nov. 2022, vol. 536, pp. 707-716. doi:10.1007/978-3-031-20141-7\_63
9. Liu, Y. Y. (2020, September). Analysis of Taihe East Station's drainage, fire suppression, and water supply system design aspects for the Shanghai Railway. *Earth and Environmental Science Conference Series, IOP Science* (Vol. 568, No. 1, p. 012022). IOP Publishing.
10. S .Sreelakshmi, M. S. Sujatha, Jammy Ramesh Rahul, " Improved Seven level Multilevel DC-Link Inverter with Novel Carrier PWM Technique", *Journal of Circuits Systems and Computers*, DOI.org/10.1142/S0218126623501086, 2023.
11. D.K.Gupta, A. Srinivasulu, et al., "Load Frequency Control Using Hybrid Intelligent Optimization technique for Multi-Source Power Systems", *Energies*, 2021, 14(6), 1581; doi:10.3390/en14061581.ISSN:1996-1073.
12. S .Sreelakshmi, M. S. Sujatha, Jammy Ramesh Rahul, " Multi-level inverter with novel carrier pulse width modulation technique for high voltage applications " ,  *Indonesian Journal of Electrical Engineering and Computer Science* Vol. 26, No. 2, May 2022, pp. 667~674.
13. D.K.Gupta, A. Srinivasulu, et al., "Hybrid Gravitational-Firefly Algorithm based Load Frequency Control for Hydrothermal Two-area System", *Mathematics*,2021, 9(7), 712; doi:10.3390/math9070712
14. Dr. M. S. Sujatha, B.Lakshmi, " Simulation and analysis of FLC & FOFLC based MPPT and charge controller for PV system, *International Journal of Condition Monitoring and Diagnostic Engineering Management*, Vol.24 no. 2, PP.29-34.



# Power Quality Improvement Using UPQC

Ankathi Manjula <sup>1</sup>, Kalagotla Chenchireddy <sup>2</sup>, Sankineni Vinay <sup>3</sup>, Nallabothu Swathi <sup>4</sup>, Ganduri Preamsagar <sup>5</sup> and Nayakallu Charan Raj <sup>6</sup>.

<sup>1</sup> Teegala Krishna Reddy Engineering College; [manju.ankathi708@gmail.com](mailto:manju.ankathi708@gmail.com)

<sup>2</sup> Teegala Krishna Reddy Engineering College; [chenchireddy.kalagotla@gmail.com](mailto:chenchireddy.kalagotla@gmail.com)

<sup>3</sup> Teegala Krishna Reddy Engineering College; [vinayrao012@gmail.com](mailto:vinayrao012@gmail.com)

<sup>4</sup> Teegala Krishna Reddy Engineering College; [swathinallabothu5@gmail.com](mailto:swathinallabothu5@gmail.com)

<sup>5</sup> Teegala Krishna Reddy Engineering College; [preamsagar6003@gmail.com](mailto:preamsagar6003@gmail.com)

<sup>6</sup> Teegala Krishna Reddy Engineering College; [ncharanraj99@gmail.com](mailto:ncharanraj99@gmail.com)

Correspondence: [vinayrao@gmail.com](mailto:vinayrao@gmail.com); Tel.: +91 9160767614

**Abstract:** This paper represents the improvement of power quality using Unified Power Quality Conditioner(UPQC). In modern days the use of power electronic converters has increased a lot which causes power quality issues and affects the equipment. Unified power quality conditioner is to mitigate the various concerns related to power quality such as harmonic current,voltage imbalance,sag and swell phenomena and reactive power compensation. The extensive simulation results are verified in matlab 2015a software. The simulation results are verified output voltage, output current and THD. By the results it is clear that using UPQC THD value reduced and achieved high capability of mitigating the harmonic current, voltage and current sag or swell and obtained improved power quality.

**Keywords:** Power Quality; UPQC(Unified Power Quality Conditioner); Voltage and Current Sag/Swell; Harmonics; THD(Total Harmonic Distortion).

## 1. Introduction

At the beginning, The main objective is to produce energy in the form of electrical and to supply this energy to the loads/devices at a felicitous voltage [1]. But the term power quality is much used and a very important aspect of power delivery mainly in the second half of the 1990s. Some examples for increasing interest in power quality in recent times are that loads/devices used becoming more sensitive to voltage disturbances, increase in use of electronic devices on a large scale, rapid growth of usage of electricity etc. Nonlinear loads and sensitive equipment are widely used in both the domestic sector and industrial sector. This power quality occurrence is a problem for users' equipment/loads[3]. The voltage quality and current quality combinedly known as power quality[2].

Voltage dip (or sag), extremely brief disturbances, extended disturbances, spikes in the voltage, swells in the voltage, fluctuations in the voltage, harmonic amplifications, voltage amplification and noise etc are the most frequent issues of quality of power [4]. Due to the above problems the sensitive equipment may damage or in the industrial sector they may get huge loss due to damages of high cost equipment or because of malfunctioning of equipment or stopping the devices due to power quality issues. So the interest in equipment for improving power quality is increasing i.e to mitigate the power quality issues[5].So as to continue proper power quality, it is required to include some kind of allowance of techniques[6]. Different ways have been proposed and developed to improve power quality and protect the sensitive loads against the disturbances[7]. There are many compensating type devices which are used for improvement of power factor, balancing load currents, filtering purpose, regulation of voltage. The compensating type devices are DVR (Dynamic Voltage Restorer), UPQC (Unified Power Quality Conditioner), DSTATCOM (Distribution static Compensator), Unified Power Quality Conditioner etc [8]. DVR, UPQC, and DSTATCOM solve the problems due to voltage and current on

power quality[11]. The DSTATCOM is a device which is shunt connected and it is mainly for power quality disturbances due to current[9]. The DVR is a series connected device, it is mainly for power quality disturbances due to voltage[10]. The UPQC includes both shunt converter and series converter[12]. The separate use of parallel, series converters may not be economical. Hence, the UPQC which includes both parallel, series converters is used to observe the power quality improvement [13]. UPQC is used for improving the quality of power because it has advantages over DVR and DSTATCOM. Many papers reported that UPQC is utilized to improve power quality at distribution level[14]. In this paper we see the comparison of power quality of a given network with using UPQC and without UPQC i.e voltage and current sag/swell and THD during nonlinear load.

## 2. Power Quality of Basic Given Electrical Network.

For any basic system or in ideal condition the power quality is constant. But in practical it is impossible due to loads connected to it. Loads are considered as two types, they are 1.Linear loads 2.Nonlinear loads. In general, most of the loads are integration of both loads which are linear and also nonlinear. Mainly the power quality issue occurs due to nonlinear loads only. Due to nonlinear loads the output waveforms are not in pure form or in pure sinusoidal form. Due to this power quality issues or working of the electrical loads without accurate power causes the electrical devices or loads to fail, break down, or not operate at all.

This paper reviews the power quality problem of basic electrical given network when connected to loads and how to overcome this issue. The below Fig 1 shows the Simulink model of the basic electrical network. This does not include any power quality improving techniques.

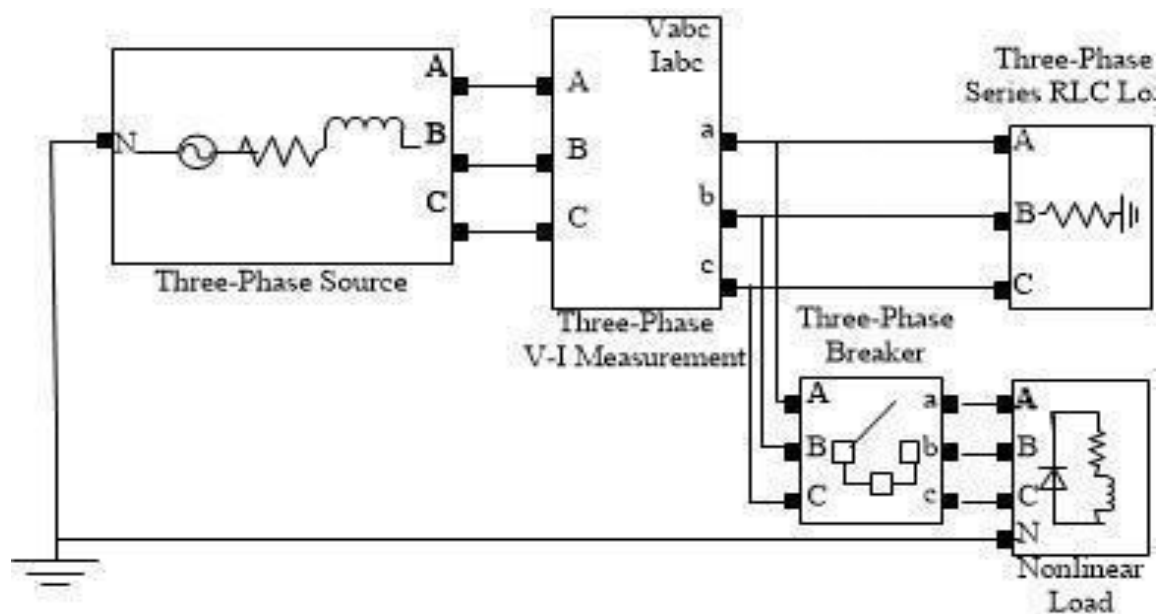


**Figure 1.** Simulink model of the basic electrical network

In this model supply source is three phase for a given network. V-I measurement is used to measure the magnitudes of the voltage and current. Linear load and Nonlinear loads are connected and nonlinear load is connected through circuit breaker as shown in Fig 1. Circuit breaker is used to connect the nonlinear load to the network for a specific duration.

The power quality error occurs when the circuit breaker is closed and nonlinear load connected to the network. This will cause the non-uniform waveform at the load side which may lead to the damage or malfunction of the electrical equipment or loads. This also induces the harmonics into the network which leads to increase the Total Harmonic Distortion (THD) value. To overcome the above power quality issues there are many power quality improvement techniques such as Active filter, Shunt filter, Static VAR Compensator (SVC), DSTATCOM, UPQC.

### 3. Proposed Topology

This topology proposes the UPQC (Unified Power Quality Conditioner) technique for boosting the quality of power in the given network. Below Fig 2 represents the Simulink model of the electrical network using UPQC.

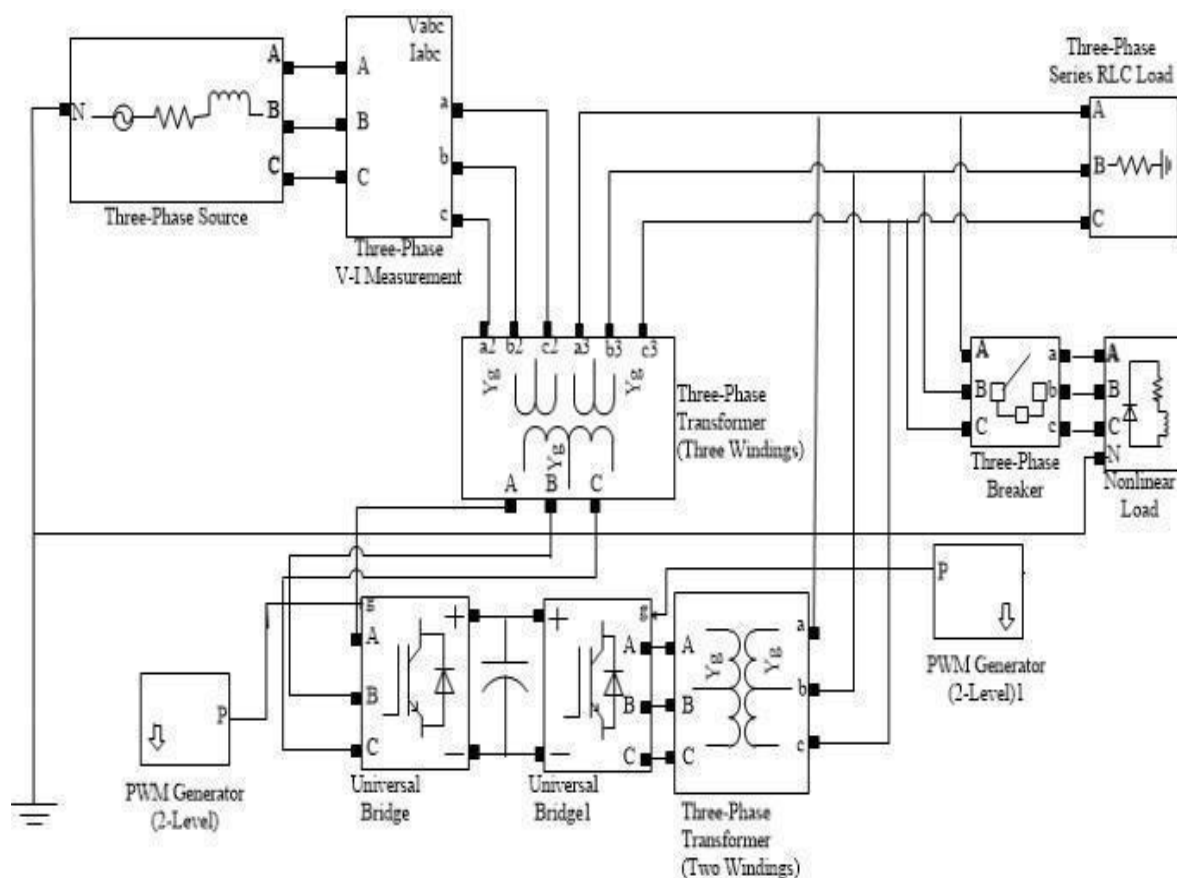


**Figure 2.** Simulink model of the basic electrical network with UPQC.

This Simulink model is similar to the basic electrical network Simulink model but it also includes Unified Power Quality Conditioner (UPQC) circuit as indicated in Fig. 2.

UPQC is an integration of active series and active parallel compensators. These compensators are Voltage Source Converters (VSCs). The UPQC's shunt device is also named as DSTATCOM or full form Distribution Static synchronous Compensator, mitigates the current based power quality problems. In addition to balancing of load, currents in the neutral, harmonic diminishing, and indemnity are offered by the DSTATCOM. DSTATCOM is normally operated in PWM (Pulse Width Modulation) suitable voltage current mode injection in parallel in the network/system. UPQC's series device is also denoted as



DVR indicates full form of Dynamic Voltage Restorer, mitigates the problems in the quality of power (voltage-based).

DVR keeps the load end voltage insensitive to the supply voltage quality problems such as sag/swell, surges, spikes, notches or unbalance etc. In order to inject the proper voltages in series with the ac mains, the DVR is often operated in pulse width modulation voltage control mode.

Using an injection transformer, the UPQC's ac sides are coupled in series (DVR) of ac lines with the series and parallel compensators on a shared dc bus. Shunt (DSTATCOM) normally attached through an isolation transformer for high ratings.

So, by using UPQC we can overcome the problems with voltage and current quality such as surge, unbalancing currents, harmonics can be eliminated and pure sinusoidal waveforms are obtained and can prevent the electrical equipment or loads from damages and malfunctioning etc.

#### 4. Results

Fig 3 depicts the output voltage waveform of the basic electrical network without UPQC Simulink model result. In the simulink model at initial the CB(Circuit Breaker) is at open position and only linear load acting on it. In order for the nonlinear load to be linked to the network at a certain time between 0.2 and 0.3 seconds, the CB must be in the closed position. At time 0.3 seconds, the CB must be opened to re-connect the load to the network. We can see that at linear load the waveform is in pure sinusoidal form but at the duration of nonlinear load connected to it the voltage sag is occurred, the voltage magnitude reduced to a very less value and the waveform also not in pure sinusoidal form.

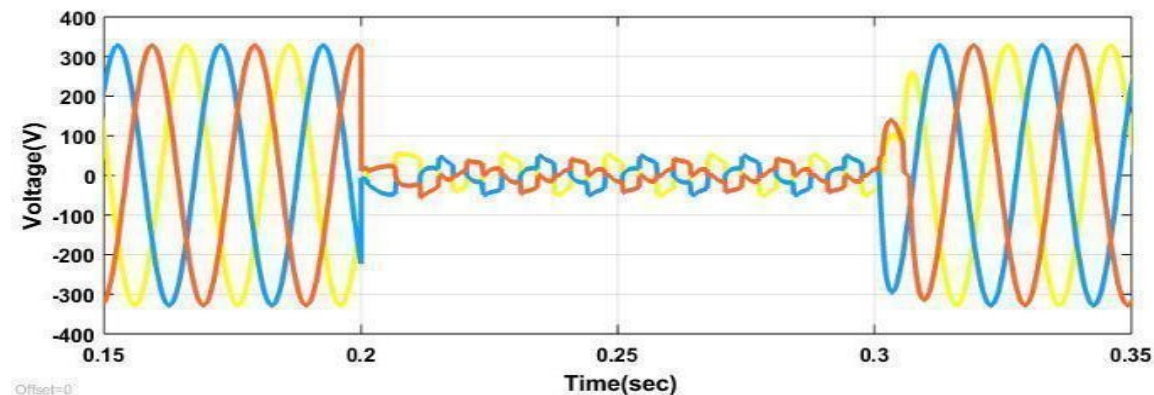


Figure 3. Output Voltage Waveform Without UPQC.

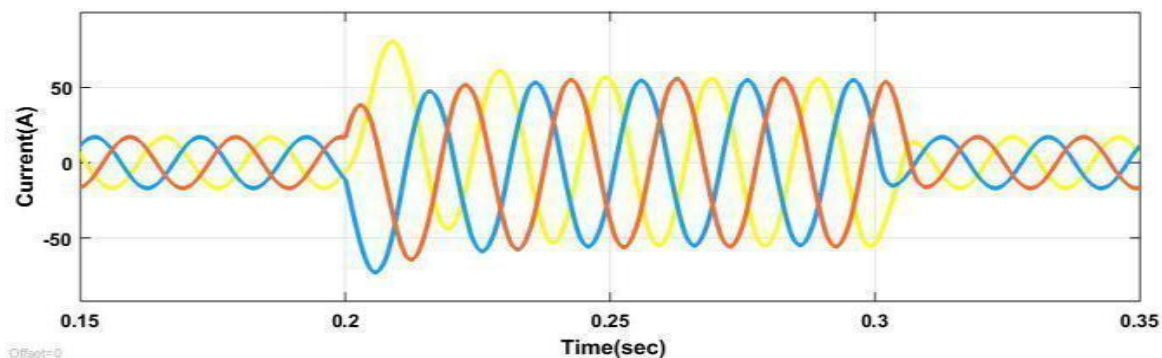


Figure 4. Output Current Waveform Without UPQC.

Fig 4 shows the output current waveform of the basic electrical network without UPQC Simulink model result. In this we can observe that current swell occurs during nonlinear load connected. The current magnitude becomes very high as we see in Fig 4.

Due to the above swelling and sagging of current and voltage respectively will cause the increase in THD (Total Harmonic Distortion) which results in power quality problems. Total Harmonic Distortion of a fundamental electrical network without the use of UPQC is displayed in Fig. 5 below, and we can see that it is quite high (43.47%), which is not permitted by IEEE regulations.

The following equation can be used to compute THD in current waveforms:

$$\text{THD} = \frac{\sqrt{\sum I_k^2}}{I_1}$$

Where  $I_1$  is the primary component of current and  $I_h$  is the harmonic current of the  $h^{\text{th}}$  order. In this case, MATLAB's FFT (Fast Fourier Transform) Analysis Toolbox is used to determine the THD.

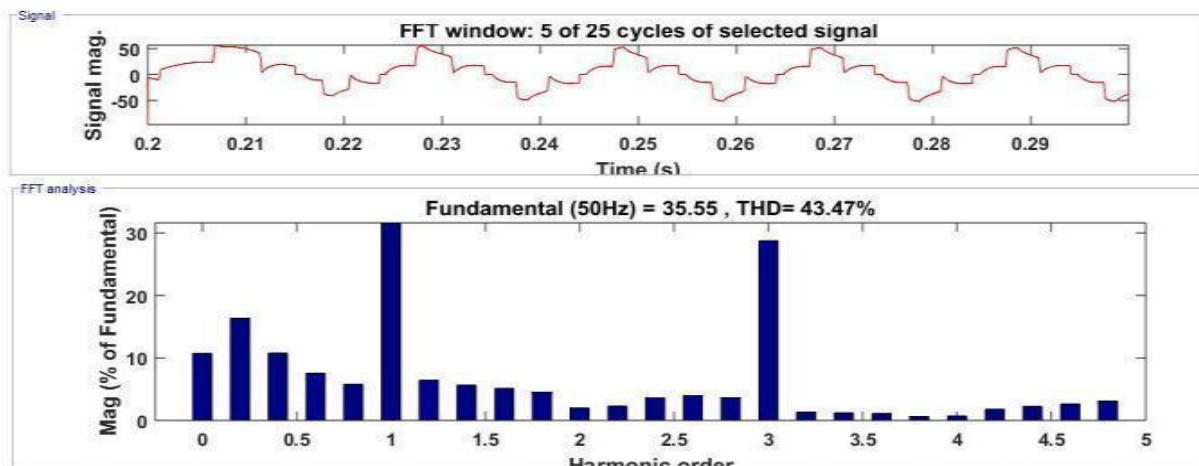


Figure 5. Without using UPQC THD of the electrical network.

Fig 6 depicts the electrical network's output voltage waveform and the UPQC Simulink model result. So, we can see that the output voltage waveform is in pure sinusoidal form even at nonlinear load connected duration. There is no voltage swell in the output voltage waveform. Thus by using UPQC the voltage waveform is in pure sinusoidal form and we avoided the disturbances at output waveform.

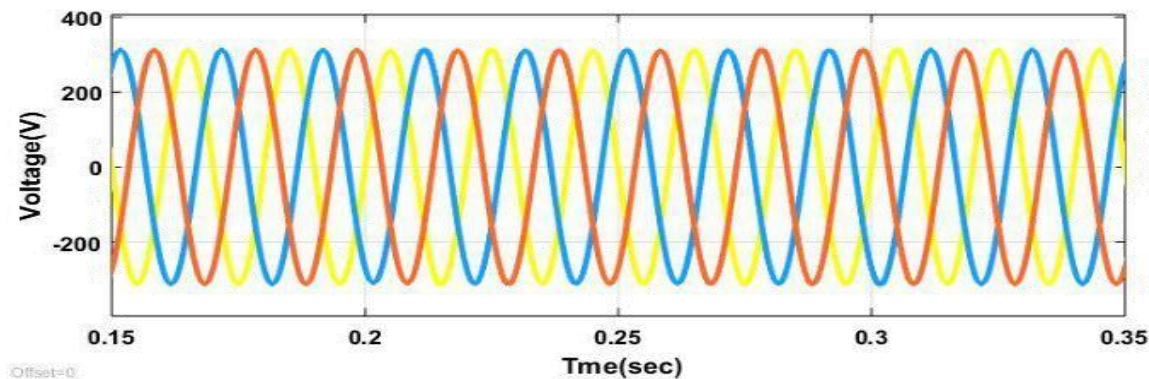


Figure 6. Output Voltage Waveform With UPQC.

Fig 7 shows the output current waveform of the electrical system with UPQC Simulink model result. We can see that the current waveform is in pure sinusoidal form and no current swells, rapid increase in magnitudes, and any disturbances in it.

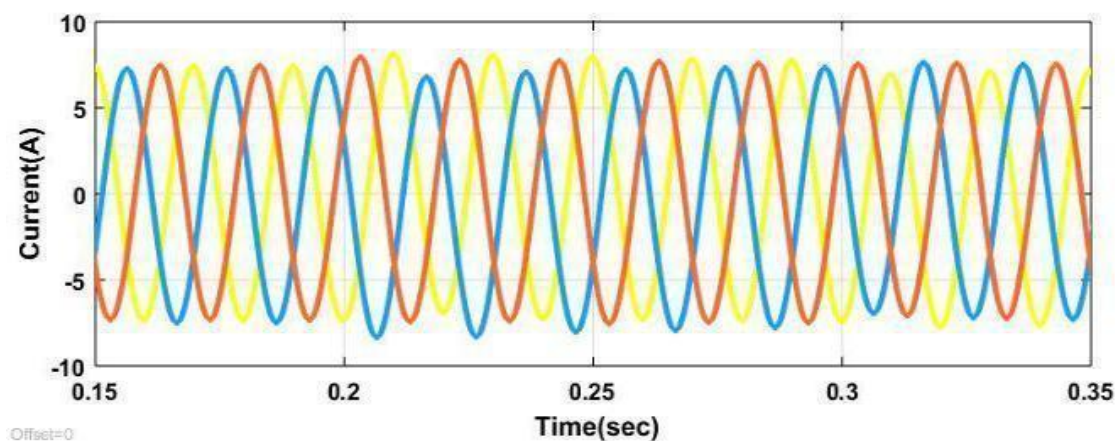


Figure 7. Output Current Waveform With UPQC.

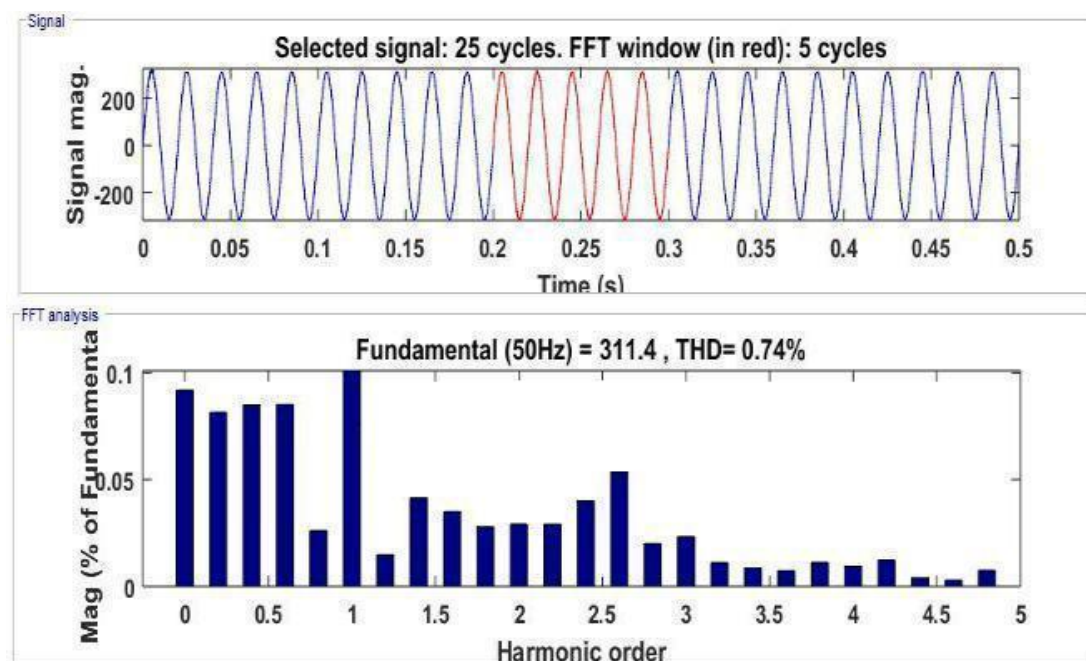


Figure 8. With using UPQC, THD of the electrical network.

Hence from above Fig 6 and Fig 7 we can say that power quality can be improved by using UPQC. Also, THD is decreased as depicted in Fig 8. Fig 8 shows the Total Harmonic Distortion of the electrical network using UPQC.

The THD is decreased to 0.74% by using UPQC, which is within IEEE requirements. By using UPQC we had achieved the power quality improvement as seen in the results waveforms such as output voltage and current waveforms and THD with using UPQC. The simulation results are verified output voltage, output current and THD i.e after successful running of the simulation model we had achieved it.

## 5. Conclusion

The goal of improving electricity quality has been achieved in this paper. The FFT analysis yields the THD using UPQC, which is displayed in Fig 8 It uses an electrical network simulation model with UPQC. The Total Harmonic Distortion (THD) in the data indicates that it is acceptable to fall below the 5% IEEE standard for THD. The output voltage waveforms and current waveforms are obtained and observed the results of waveforms without using UPQC and with using UPQC. We can see that the output voltage and current waveforms are in pure sinusoidal form by using UPQC.

## References

1. Bhosale, Swaroopa S., et al. "Power quality improvement using UPQC: A review." *2018 International conference on control, power, communication and computing technologies (ICCPCT)*. IEEE, 2018.
2. Bollen, Math HJ. "Understanding power quality problems." *Voltage sags & Interruptions*. Piscataway, NJ, USA: IEEE press, 2000.
3. Stones, John, and Alan Collinson. "Power quality." *power engineering journal* 15.2 (2001).
4. De Almeida, A., L. Moreira, and J. Delgado. "Power quality problems & new solutions." *International conference on renewable energies & power quality*. Vol. 3. 2003.
5. Goud, B. Srikanth, and B. Loveswara Rao. "Power quality enhancement in grid-connected PV or wind or battery using UPQC: atom search optimization." *Journal of Electrical Engineering & Technology* 16 (2021): 821-835.
6. Benachaiba, C., and B. Ferdi. "Power quality improvement using DVR." *American Journal of Applied Sciences* 6.3 (2009): 396.
7. a. "A review on power quality problems and its improvement techniques." *2017 Innovations in Power & Advanced Computing Technologies (i-PACT)* (2017): 1-7. Khan, Shazma, Balvinder Singh, and Prachi Makhij.
8. Chenchireddy, Kalagotla, et al. "A Review on D-STATCOM Control Techniques for Power Quality Improvement in Distribution." *2021 5th International Conference on Electronics, Communication & Aerospace Technology (ICECA)*. IEEE, 2021.
9. Khadem, Md Shafiuzzaman K., Malabika Basu, and Michael F. Conlon. "UPQC for power quality improvement in dg integrated smart grid network-a review." *International Journal of Emerging Electric Power Systems* 13.1 (2012).
10. Khadkikar, Vinod, and Amrisha Chandra. "A novel structure for three-phase four-wire distribution system utilizing unified power quality conditioner (UPQC)." *2006 International Conference on Power Electronic, Drives and Energy Systems*. IEEE, 2006.
11. Sydu, Shabbier Ahmed, Kalagotla Chenchireddy, and Khammampati R. Sreejyothi. "Novel pso-fuzzy logic based control method for unified power quality conditioner (upqc) for harmonic distribution." *Proceedings of the International Conference on Smart Data Intelligence (ICSMDI 2021)*. 2021.
12. Khadkikar, Vinod. "Enhancing electric power quality using UPQC: A comprehensive overview." *IEEE transactions on Power Electronics* 27.5 (2011): 2284-2297.
13. 14. Xu, Qianming, et al. "Analysis and control of M3C-based UPQC for power quality improvement in medium/high-voltage power grid." *IEEE Transactions on Power Electronics* 31.12 (2016): 8182-8194.
14. Han, B., et al. "New configuration of UPQC for medium-voltage application." *IEEE Transactions on Power Delivery* 21.3 (2006): 1438-1444.



# BI-DIRECTIONAL AC-DC CONVERTER FOR ELECTRIC VEHICLE CHARGING STATION

<sup>1</sup>B.Vignesh, <sup>2</sup>K.Santhosh, <sup>3</sup>K.Jahnavi, <sup>4</sup>J.Sai, <sup>5</sup>P.Sanjay

<sup>1</sup> Assistant Professor, <sup>2</sup>UG Student, <sup>3</sup> UG Student, <sup>4</sup>UG Student, <sup>5</sup> UG Student

<sup>1</sup> Department of Electrical and Electronics Engineering

<sup>1</sup> Teegala Krishna Reddy Engineering College, Hyderabad, India.

**Abstract :** This paper presents a bi-directional AC-DC converter for EV charging stations. The charging station is interconnection hybrid energy sources solar, Diesel generator, and grid. The proposed configuration has a bi-directional converter, which means AC-DC and DC-AC. The IGBT switches are used in this paper for high current and power ratings. The main objective of this paper is electrical vehicle charging. The operation of the converter in normal mode charges the battery (G2V), when the vehicle is in rest position it converts energy (V2G). The total operation was simulated by using MATLAB/simulation software. The battery current, state of charge (SOC) and voltage results were verified. The overall system operated well in steady state condition.

**IndexTerms – Electric Vehicle (EV), State of Charge (SOC), Vehicle to Grid (V2G)**

## I. INTRODUCTION

The presented paper says that In early 1918 they are there are rapidly grew in ev and at the end of 1930 they are decreased to zero, Now the world mainly focusing on two things i.e, energy conservation and environmental protection [1]. Electric vehicles (EVs) are now one of the most environmentally friendly forms of transportation because they are free from pollution and eco friendly, At the time of use, the EV produces no emissions. EVs are popular nowadays because they are eco-friendly, The development of new technology in electric motors, power electronics, and microelectronics brings change to the development of EVs so fast. Authors presented in reference [2] a cross 100 million vehicles by 2030. So there is a need to set charging stations for such large no of vehicles. Any end, fossil fuels going to deplete so we need not be depended upon a single source we need to grow through alternative sources along with renewable energy sources.

Urban areas are mainly focusing on environmental safety so they shifting conventional vehicles into hybrid vehicles, So they that can access to {minimize the pollution} reduce some amount of pollution [3]. In parallel-type hybrid electric vehicles the key point for efficient driving torque assisting and battery recharging control using the electric motor. The robust property of fuzzy logic enables the HEV to be operated with the improved battery charge balance, regardless of various disturbances. fuzzy logic is applied to the battery charge balance control of the parallel-type HEV. by using fuzzy logic control we can manage energy and optimize the torque between the distribution of energy between the ic engine and the electric motor [4]. The controller important part of HV which controls all performance of such as acceleration, and SOC of the battery engine speed [5]. The HEV synchronizes the electric power with the diesel engine has improved overall efficiency [6]. They used fuzzy logic control with trapezoidal membership and mamdani reference mechanism. 130 rules are used in the fuzzy-based torque distribution strategy and it is sorted into 4 rule bases. Simulation has also been compared with rule base strategy [7].

The proposed model is suitable for fast charging of EVs, The charging station consists of a single grid connected to the inverter with a dc bus where EVs are connected [8]. The charging station model also designs to support v2g and Reactive power compensation by this fast dc charging is possible [9]. Charging time is a key role in EV eco- friendly this model offer reduced time of 10 to 20n min [10]. EVs are attention much attention owing because of they are clean energy use and the huge development in batteries led to the development of EV also huge [11]-[12]. And implementation of new tech and altering clean energy sources to charge the EVs is a solar charging station. The charging station provides multi-port charging by providing a constant dc voltage bus [13]. This operated based on the concept of power balancing charging control and cc and cv charging 62.8 % of India depend on fossil fuels [14]. At low radiation, it is insufficient to meet the demand for EVs and BESS will meet the required demand if excess power generated stored energy [15]-[16]. In addition in rural areas accessibility to electric power is less so it is preferred to utilize renewable energy sources [17]. Storage in battery-depleted solar energy not suitable at the all-time charging station uses grid and diesel generator voltage synchronize at the PCC to achieve continuous charging [18]-[20]. Reduces emission and benefits the environment. The proposed charging station is primarily intended to charge electric vehicles using a solar PV array for voltage regulation Sepic converter is used to track MPPT to achieve max power tracking from the sun.

II. RELATED WORK

EV Charging Station

The structure of the charging station is shown in Fig. 2. It utilizes a two-leg VSC, which works as a rectifier, and as an inverter depending upon the working mode. The BDC is connected to the DC link of VSC to interface the storage battery. A solar PV array is also connected to the DC link of VSC without any DC-DC converter. A diode is connected in the solar PV array path to avoid the reverse power flow. A SEIG, the grid, two EVs and a nonlinear load, are connected at the point of common coupling (PCC) of charging station. An inductor is used to connect the grid, SEIG, EVs and the load to VSC. A ripple filter is also connected at PCC to eliminate switching harmonics from the grid and DG to make their currents sinusoidal. An excitation capacitor is connected across the auxiliary winding of SEIG. A small capacitor is also connected across the main winding of SEIG for filtering and voltage regulation across the main winding of SEIG for filtering and voltage regulation.

III. PROPOSED WORK

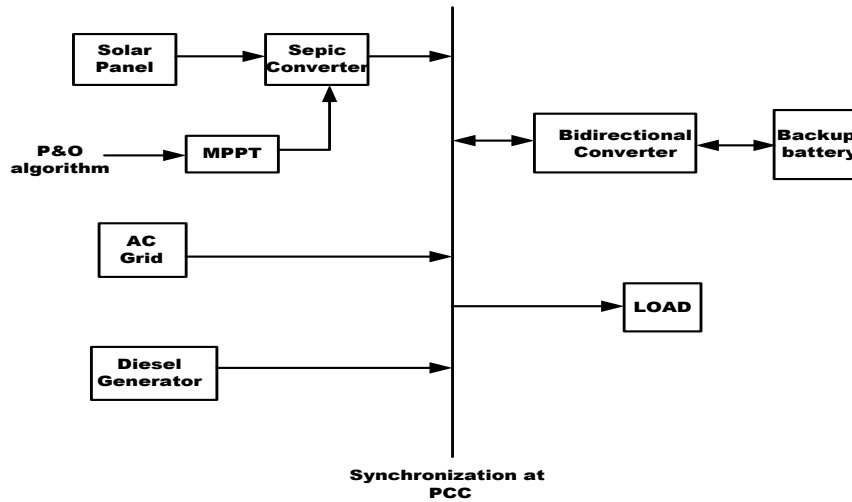


Fig.1 single line diagram EV charging station

The figure.1 represents the charging station of the Electrical vehicle. The three sources solar panel, AC grid, and Diesel generator are synchronized at the Point of common coupling (PCC). The Sepic converter is designed to permit a certain range of DC Voltage and also maintained constant output voltage. The Sepic converter is controlled by a Duty cycle to increase and decrease the input voltage. The synchronized sources will charge the Electrical vehicle with extreme value[21]-[23]. MPPT detects the solar panel voltage and also tracks the maximum voltage occurring point. The connected EVs are charged with a solar, AC grid if there is enough of it available to do so. If demand rises, power is drawn from the grid during base load hours and the The islanded control of the CS ensures the stable operation of the CS in absence of the grid, which means the AC as well as the DC charging of the EV remains intact along with the undisturbed solar power generation. The DC charging and the solar PV generation can be managed by the storage battery without much modification in the control. However, the AC charging needs a separate controller for VSC using which the local voltage reference is generated, because in absence of the grid no voltage reference is available. Therefore, the islanded controller generates the internal voltage reference of 230V and 50 Hz as per the logic presented in Fig. 2, which integrates the frequency and pass through the sin for generating the reference voltage. The generated reference is compared with the terminal voltage of the converter, which ultimately gives the reference converter current after minimisation of voltage error using proportional integral (FUZZY) controller

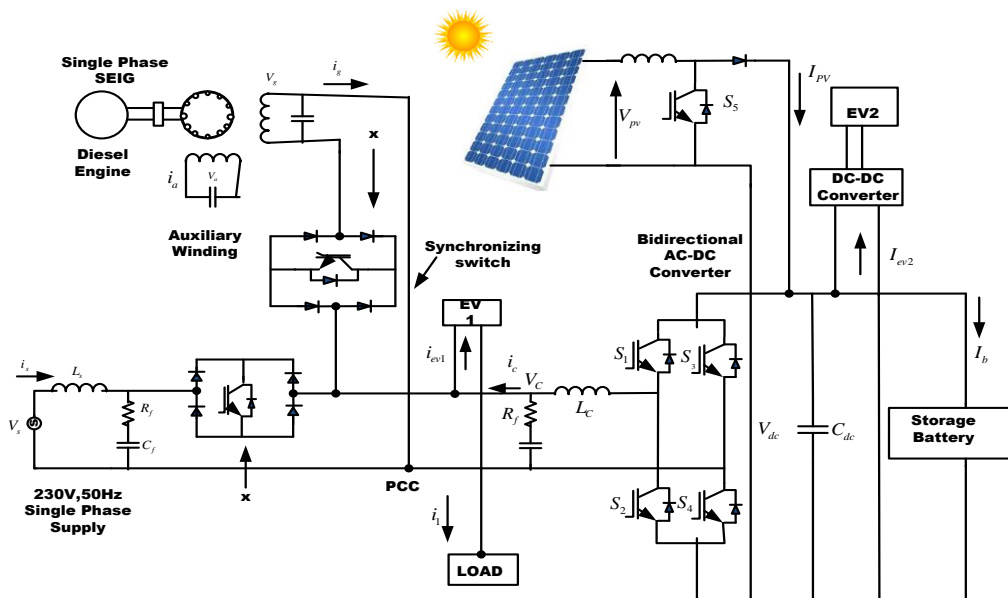


Fig.2 Topology of Charging Station



**Layer 4: Defuzzification layer**

$$\overline{Z}_{k1}f_{ki} = F_{kL3,i} = \frac{Z_{ki}}{Z_{k1} + Z_{k2}} (M_{k1}(E_k) + N_{k1}(CE_k) + C_{k1}) \quad i = 1, 2; \tag{4}$$

$$\overline{Z}_{k2}f_{kj} = F_{kL3,j} = \frac{Z_{kj}}{Z_{k1} + Z_{k2}} (M_2(E_k) + N_2(CE_k) + C_{k2}) \quad j = 1, 2;$$

**Layer5: Total output layer**

$$f_k = F_{kL5,i} = \sum \overline{Z}_{k1}f_i = \frac{\sum \overline{Z}_{k1}f_k}{\sum Z_{ki}} \tag{5}$$

**IV. RESULTS AND DISCUSSION**

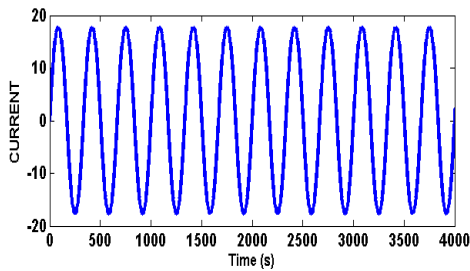


Fig 5 EV current

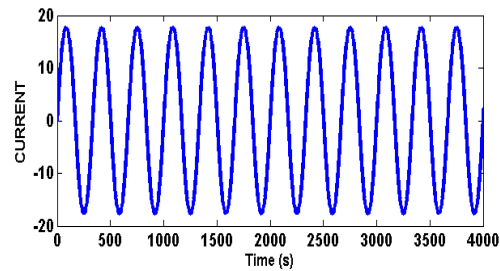


Fig 6 Load Current.

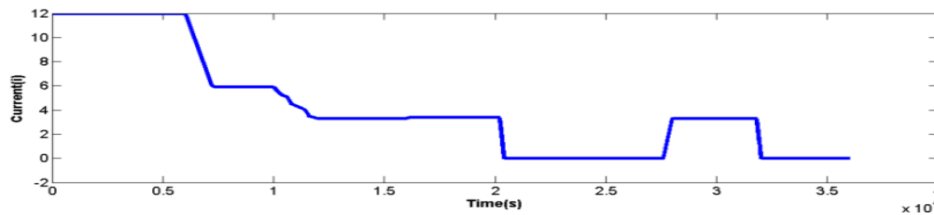


Fig 7 PV Generated Current

The fig 5 shows EV current at the port 1. On graph X-axis is time& Y-axis is current. The amplitude varies from -20 to20 .figure.6 shows the Load Current. On graph X-axis is time& Y-axis is current. The amplitude varies from -20 to20.The fig 7 represents PV Generated Current. On the graph X-axis is Time & Y-axis is Current And its range varies from -2 to 12.

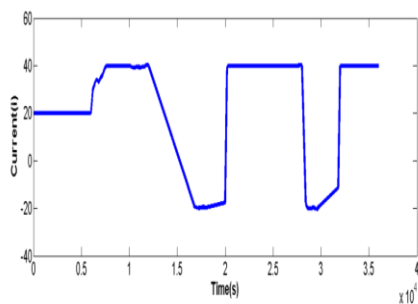


Fig 8 Battery Current

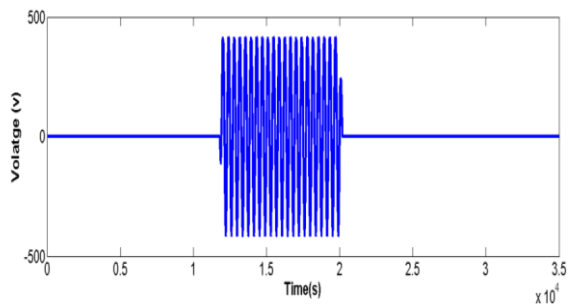


Fig 9 Grid Voltage



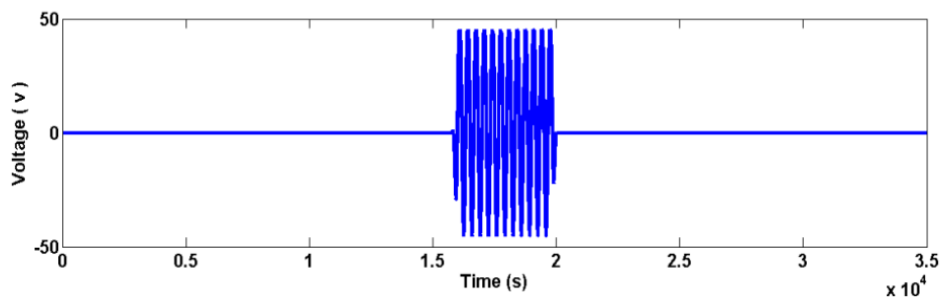


Fig 10 Grid Current.

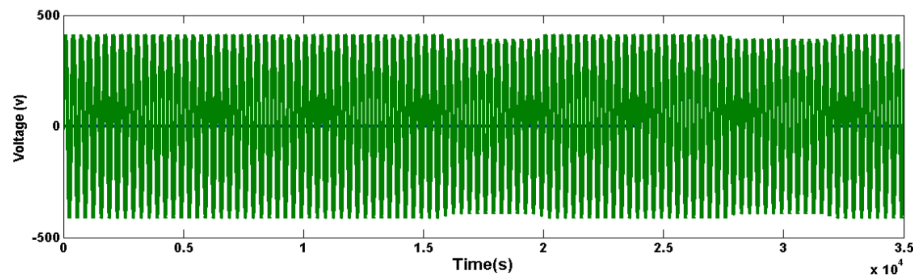


Fig 11 Diesel generated Voltage

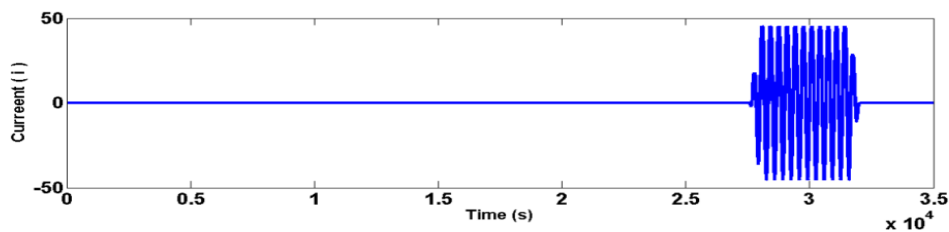


Fig 12 Current output from diesel generator

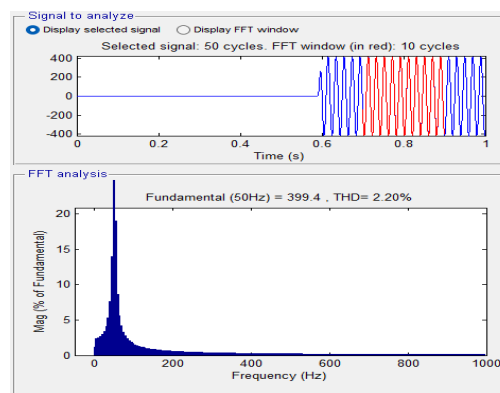


Fig 13 THD values

The Figure 8 shows the Battery Current .On the graph X-axis is Time & Y-axis is Current and its range varies from -30 to 50.The Figure 9 shows the Grid output Voltage. On the graph X-axis is Time & Y-axis Voltage. The voltage ranges varies from -500 to 500. The Figure 10 shows that Grid supplied Current. On the graph X-axis is Time & Y-axis is Current. The current range varies from the -50 to 50. The Figure 11 shows the voltage generated from diesel engine .On the graph x-axis is Time & Y-axis is Voltage. The voltage ranges varies from -500 to 500. The Figure 12 shows the diesel generated Current .On the graph x-axis is Time & Y-axis is Current. The Current ranges vary from -50 to 50. Figure 13 shows the THD values with the PI Controller and Fuzzy Controller has been showed and losses get minimized and response of the system is improved.

## V. CONCLUSION

This paper presents The Bi directional AC-DC converter converts for EV charging Station. The presented converter operated AC-DC and DC-AC. When the battery charging mode the converter it works as a rectifier and when the battery is discharging mode the converter working as an inverter. The EV charging station has many renewable energy sources solar, grid and diesel. The EV charging station results are verified in matlab/simulink software.

## REFERENCES

- [1] Hyeoun-Dong Lee and S. -K. Sul, "Fuzzy-logic-based torque control strategy for parallel-type hybrid electric vehicle," in *IEEE Transactions on Industrial Electronics*, vol. 45, no. 4, pp. 625-632, Aug. 1998, doi: 10.1109/41.704891.
- [2] A. Narula and V. Verma, "Bi – directional trans – Z source boost converter for G2V/V2G applications," 2017 IEEE Transportation Electrification Conference (ITEC-India), Pune, India, 2017, pp. 1-6, doi: 10.1109/ITEC-India.2017.8356947.
- [3] S. Nair, N. Rao, S. Mishra and A. Patil, "India's charging infrastructure — biggest single point impediment in EV adaptation in India," 2017 IEEE Transportation Electrification Conference (ITEC-India), Pune, India, 2017, pp. 1-6, doi: 10.1109/ITEC-India.2017.8333884.
- [4] Ustun, Taha Selim, Cagil Ozansoy, and Aladin Zayegh. "Recent developments in microgrids and example cases around the world—A review." *Renewable and Sustainable Energy Reviews* 15.8 (2011): 4030-4041. doi:10.1016/j.rser.2011.07.033
- [5] Mehrjerdi, Hasan, and Reza Hemmati. "Electric vehicle charging station with multilevel charging infrastructure and hybrid solar-battery-diesel generation incorporating comfort of drivers." *Journal of Energy Storage* 26 (2019): 100924.
- [6] M. C. Falvo, D. Sbordone, I. S. Bayram and M. Devetsikiotis, "EV charging stations and modes: International standards," 2014 International Symposium on Power Electronics, Electrical Drives, Automation and Motion, Ischia, Italy, 2014, pp. 1134-1139, doi: 10.1109/SPEEDAM.2014.6872107.
- [7] Hyeoun-Dong Lee and S. -K. Sul, "Fuzzy-logic-based torque control strategy for parallel-type hybrid electric vehicle," in *IEEE Transactions on Industrial Electronics*, vol. 45, no. 4, pp. 625-632, Aug. 1998, doi: 10.1109/41.704891.
- [8] Shen, Caiying, Peng Shan, and Tao Gao. "A comprehensive overview of hybrid electric vehicles." *International journal of vehicular technology* 2011 (2011). doi:10.1155/2011/571683
- [9] Hannan, Muhammad A., F. A. Azidin, and Azah Mohamed. "Hybrid electric vehicles and their challenges: A review." *Renewable and Sustainable Energy Reviews* 29 (2014): 135-150. Doi:10.1016/j.rser.2013.08.097
- [10] Narasipuram, Rajanand Patnaik, and Subbarao Mopidevi. "A technological overview & design considerations for developing electric vehicle charging stations." *Journal of Energy Storage* 43 (2021): 103225. Doi:10.1016/j.est.2021.103225
- [11] Hemavathi, S., and A. Shinisha. "A study on trends and developments in electric vehicle charging technologies." *Journal of Energy Storage* 52 (2022): 105013. Doi:10.1016/j.est.2022.105013
- [12] Hengsong Wang, Qi Huang, Changhua Zhang and Aihua Xia, "A novel approach for the layout of electric vehicle charging station," The 2010 International Conference on Apperceiving Computing and Intelligence Analysis Proceeding, Chengdu, China, 2010, pp. 64-70, doi: 10.1109/ICACIA.2010.5709852.
- [13] Mehrjerdi, Hasan, and Reza Hemmati. "Electric vehicle charging station with multilevel charging infrastructure and hybrid solar-battery-diesel generation incorporating comfort of drivers." *Journal of Energy Storage* 26 (2019): 100924. doi:10.1016/j.est.2019.100924
- [14] Kamali, A. R., and V. Prasanna Moorthy. "Design of Solar and Battery Hybrid Electric Vehicle Charging Station." *Journal of Trends in Computer Science and Smart Technology* 4.1 (2022): 30-37. doi:10.36548/jtcsst.2022.1.005
- [15] S. A. Parah and M. Jamil, "Techniques for optimal Placement of Electric Vehicle Charging Stations: A review," 2023 International Conference on Power, Instrumentation, Energy and Control (PIECON), Aligarh, India, 2023, pp. 1-5, doi: 10.1109/PIECON56912.2023.10085887.
- [16] D. A. Hussien, W. A. Omran and R. M. Sharkawy, "Smart Charging of Electric Vehicles in Charging Stations," 2023 5th International Youth Conference on Radio Electronics, Electrical and Power Engineering (REEPE), Moscow, Russian Federation, 2023, pp. 1-5, doi: 10.1109/REEPE57272.2023.10086885.
- [17] A. Gupta, S. Sarangi and A. K. Singh, "Wavelet Based Enhanced Fault Detection Scheme for A Distribution System Embedded with Electric Vehicle Charging Station," 2023 5th International Conference on Power, Control & Embedded Systems (ICPCES), Allahabad, India, 2023, pp. 1-6, doi: 10.1109/ICPCES57104.2023.10075986.
- [18] A. Bashaireh, D. Obeidat, A. A. Almezahia and L. Shalalfeh, "Optimal Placement of Electric Vehicle Charging Stations: A Case Study in Jordan," 2023 IEEE Texas Power and Energy Conference (TPEC), CollegeStation,TX,USA,2023,pp.10.1109/TPEC56611.2023.10078486.
- [19] R. Sushmitha, K. Asha, J. Tejaswini, V. Hemanthakumari, K. Harshitha and N. K. Suryanarayana, "Implementation of Electric Vehicles Charging Station and Battery Management System," 2023 2nd International Conference for Innovation in Technology (INOCON), Bangalore, India, 2023, pp. 1-5, doi: 10.1109/INOCON57975.2023.10101213.
- [20] K. V, M. K. R, N. V. K and H. S, "Design and Implementation of Common EV Charging Station," 2023 Third International Conference on Artificial Intelligence and Smart Energy (ICAIS), Coimbatore, India, 2023, pp. 1307-1313, doi: 10.1109/ICAIS56108.2023.10073755.
- [21] J. Xu, H. Wang, W. Zhang, T. Wang and C. Wu, "Prediction of Electric Vehicle Charging Demand in Rural Areas Based on Driving Track Data," 2023 IEEE 2nd International Conference on Electrical Engineering, Big Data and Algorithms (EEBDA), Changchun, China, 2023, pp. 292-296, doi: 10.1109/EEBDA56825.2023.10090607.
- [22] S. A. Nemmaniwar, K. D. Patil, S. P. Mali, A. S. Bhojugade, A. J. Patil and M. Dharme, "Renewable Energy Integration with Plug-In Electric Vehicles and Charging Stations," 2023 11th International Conference on Internet of Everything, Microwave Engineering, Communication and Networks (IEMECON), Jaipur, India, 2023, pp. 1-6, doi: 10.1109/IEMECON56962.2023.10092305.
- [23] R. Sriabisha and T. Yuvaraj, "Optimum placement of Electric Vehicle Charging Station using Particle Swarm Optimization Algorithm," 2023 9th International Conference on Electrical Energy Systems (ICEES), Chennai, India, 2023, pp. 283-288, doi: 10.1109/ICEES57979.2023.10110213.
- [24] N. Kaur and R. K. Bindal, "Modeling and Simulation Analysis of Solar Charging Station for Electric Vehicle," 2023 5th International Conference on Smart Systems and Inventive Technology (ICSSIT), Tirunelveli, India, 2023, pp. 344-349, doi: 10.1109/ICSSIT55814.2023.10061147.
- [25] G. Subramaniam, K. Hari Adithyan, S. Gogul, D. Heera Sree and E. Kumaresan, "Multi-Model Charger for Light Electric Vehicles," 2023 9th International Conference on Electrical Energy Systems (ICEES), Chennai, India, 2023, pp. 418-421, doi: 10.1109/ICEES57979.2023.10110215.



# Harmonic Reduction In VSG Using Fuzzy Logic Considering Nonlinear loads and Distorted Grid.

A Naga Sridhar <sup>1</sup>, G Raj Rohan Reddy <sup>2</sup>, P Alekhya<sup>3</sup>, N Pawan Kalyan <sup>4</sup>, S Madhusudhan<sup>5</sup> \*

Assistant Professor, Department of Electrical & Electronics Engineering, Teegala Krishna Reddy Engineering college, Hyderabad

UG Students, Department of Electrical & Electronics Engineering, Teegala Krishna Reddy Engineering College, Hyderabad

## ABSTRACT

Harmonics are always present in the electrical networks in both no-load and load conditions. Harmonics reduces the power quality of the VSG in the presence of nonlinear loads and distorted grid. Completely removing the Harmonics from the network is impossible but we need to reduce them to a minimum value so that the system efficiency improves. A hybrid harmonic suppression scheme is proposed to enable the further improvement of the adaptability of VSG, which mainly consists of a voltage harmonic control loop and a grid current-controlled loop. The voltage harmonic control loop aims to scale down the inverter output impedance via a negative feedback loop, while the grid current-controlled compensator is intended to counteract the adverse effects from a weak grid via an additional voltage, which leads to substantially lower total harmonic distortion for both the load voltage and the grid current at the same time. By using a proper controller we can reduce the THD value of the grid to the minimum.

Keywords: Distorted Grid, Active Power, Reactive Power, Inverter, THD, VSG.

## 1 INTRODUCTION

MPC uses a discrete-time model of the system to predict the optimal solution in the next instant according to the current system state acting as the initial value. The method proposed in belongs to a continuous control set model predictive control, with a fixed switching frequency. In this paper, an MPC method is proposed for grid connected DC/DC converters of a HESS with a double layer control strategy to realize the voltage regulation and power allocation between battery and UC [1]. In the recent years, there has been a considerable increment of diffused generators connected to distribution grids by means of power converters. These converters operate frequently below their rated power due to the fluctuation of the power generated by the renewable sources. In this scenario, power electronics interfaces could be also used as active harmonic compensators for other converters or distorting loads.[2] Typically, these converters do not have information on other loads or on the level of grid current distortion. For this reason, this paper presents a new control algorithm for the grid harmonics compensation that relies only on the measurement of the voltage at the point of connection of the power converter. The reference of the compensating current is calculated from the harmonic content of the voltage in a reference frame synchronous with the grid voltage. [3]. In this work, an adaptive observer supported fundamental extractor is developed to estimate the fundamental components of the load current for a three phase distribution static compensator (DSTATCOM) under nonlinear load. Main variations in the proposed work are the fundamental drawing out from the distorted load current and

estimation of PI controller gains. With this observer, salp swarm optimization algorithm (SSOA) is used for estimation of DC PI controller and AC PI controller gains. The estimated gains are used for DC bus voltage and AC terminal voltage error minimization respectively. This optimization algorithm commendably progresses the initial random solutions and converge to optimum. Pareto optimal solutions are approximated in SSOA with prodigious convergence and coverage. The SSOA can search unknown spaces and can deal with real world problems for solutions. This paper presents a method for improving the reliability of DC nanogrids by decreasing the input capacitance requirement.[4] The nanogrid DC bus capacitance requirement is reduced by utilizing the zero-sequence operation mode of the solid state converter (SSC). This SSC is often considered as the main DC nanogrid energy control unit that is linking the nanogrid with the main utility AC grid and managing the nanogrid elements. The proposed method injects a zero-sequence voltage in the SSC AC filter capacitors to compensate the low frequency power ripples that are imposed on the DC bus. The proposed method compensates power ripple due to non-linear loads, linear loads, distorted grids, and load variations. Moreover, the compensation method does not require additional components that are commonly used with the existing power ripple compensators. Furthermore, practical considerations of the proposed control are discussed in the paper regarding stabilization of the nanogrid in case of lack of critical damping[5]. In fuel-cell-connected utility networks, electrical loads attached to the power network often generate reactive power, which hinders the utility from normal functioning and reduces the system power factor. This condition results in wasted energy, increase demand for electricity, system overload, and higher utility costs for customers. Besides, a power system's poor power factor is often caused by a large distorted reactive power element because of the widespread use of non-linear loads. Moreover, power outages were brought on by voltage dips resulting from reactive power. In a fuel cell-based network, traditional utilities often use classical filters that are unable to remove harmonic properties, and incapable of compensating for the reactive power. Moreover, power outage compensation is overlooked in most fuel cell-based energy systems. To address this problem, the proposed article provides a novel unified linear self-regulating (LSR) active/reactive sustainable energy management system (SEM) that can adjust the power factor by compensating for power outages and reactive power, and precisely removing harmonics from the electricity network. As a result, the suggested mechanism may avoid power losses and allow users to save money on their power costs. Furthermore, notwithstanding grid availability, the critical loads receive an uninterrupted power supply due to the automatic transition circuit implemented in the SEM.[6]. DC-link voltage directly affects the compensation range and performance of shunt active power filters (SAPFs). DC-link voltage in SAPF is generally high, fixed, and dependent on rated power. DC-link voltage could become excessive in low-load conditions, which increases switching loss and switching noise. Optimized DC-link voltage was obtained in this study to enhance compensation adaptability for variable nonlinear loads and fluctuation in grid voltage. We proposed a novel adaptive DC-link voltage control for SAPFs, which reduced switching noise and switching loss during operation. The proposed DC-link voltage control method employed model predictive current control, proportional voltage control and calculation of optimal DC-link voltage. A real-time observer, which was insensitive to distorted grid condition, was used to capture peak grid voltage. [7]. The increasing use of power electronic devices can deteriorate the power quality by introducing voltage and current harmonics. In islanded microgrids, the presence of nonlinear loads can distort the point of common coupling (PCC) voltage, while the dead-time effect can also bring additional circulating current harmonics among parallel inverters. To simultaneously attenuate the PCC voltage harmonics and suppress the dead-time induced circulating current harmonics, this paper proposes a coordinated control strategy for harmonic mitigation of parallel inverters. The proposed control strategy allows inverter impedances to be properly reshaped at selective harmonic frequencies. As a consequence, the PCC voltage harmonics are filtered by the inverter operating in the harmonic compensation mode (HCM),[8] whereas the dead-time induced circulating current harmonics are suppressed by the inverter operating in the harmonic rejection mode (HRM).[9]. With the rapid development of industrialization, the proportion of electric arc furnaces (EAF) in distribution networks is getting higher and higher. Aiming at the problem that grid voltage is distorted by a large number of arc furnace nonlinear loads accessing to distribution networks, it is crucial to make dynamic analysis of distribution network voltage and adopt a control strategy of grid-connected converter based on the new phase-locked loop (PLL) technology. As a result, the harmonic distortion rate is reduced and the quality of grid-connected current and voltage is improved. In this paper, photovoltaic (PV) system model and the typical dynamic model of the EAF are established. By analyzing the influence of the EAF model on the PV grid-connected converter with the traditional phase-locked loop while connected to distribution network, a control

strategy of the PV grid-connected converter with the self-adjusting double SOGI (MAF-SASOGI) phase-locked loop with the ideal low-pass filter is proposed.[10]. an alternative control technique for producing reference current signal to manage operation of three-phase three-wire parallel-connected active power filter (PAPF) is presented. In the context of generating reference current, time-domain synchronous reference frame (SRF) technique has commonly been recognized to provide the benefit of control simplicity. However, its control structure is rather rigid which restricted its flexibility to be applied in different power system configurations. For instance,[11]SRF technique which is initially designated to work with three-phase system cannot be applied directly to single-phase network without intensive modification to its overall control structure. Hence, in this work, a control technique named as modular fundamental element detection (modular-FED) which exhibits modular structure is proposed, to manage mitigation of harmonic current under unbalanced and/or distorted grid. The design concept of the proposed technique was modeled using MATLAB-Simulink software. Two types of highly nonlinear loads are applied to assess the effectiveness of the proposed modular-FED technique under various unbalanced and/or distorted grids. In-depth comparative analysis with the standard SRF technique is performed to evaluate the benefits of using the proposed technique.[12]

## 2 PROPOSED TOPOLOGY

Harmonics are always present in the network even in ideal and non ideal conditions. We cannot remove harmonics totally from the network but we can reduce them to the minimum, so that the losses in the network will be reduced and electrical energy transmission will be done efficiently. Most common causes of harmonics in the circuit are from non-linear loads and distortions in the grid due to various reasons. In this simulation above hybrid harmonic sources are used to produce harmonics in the circuit. Our goal is to reduce these harmonics present in the circuit to a minimum value. Harmonics in the circuit are reduced by using a negative feedback loop consisting of PWM which injects Controlled outputs to the VSG. Control outputs are derived by comparing the derived quantities and desired quantities using fuzzy logic controller. The outputs from the fuzzy logic controller is given to the PWM .

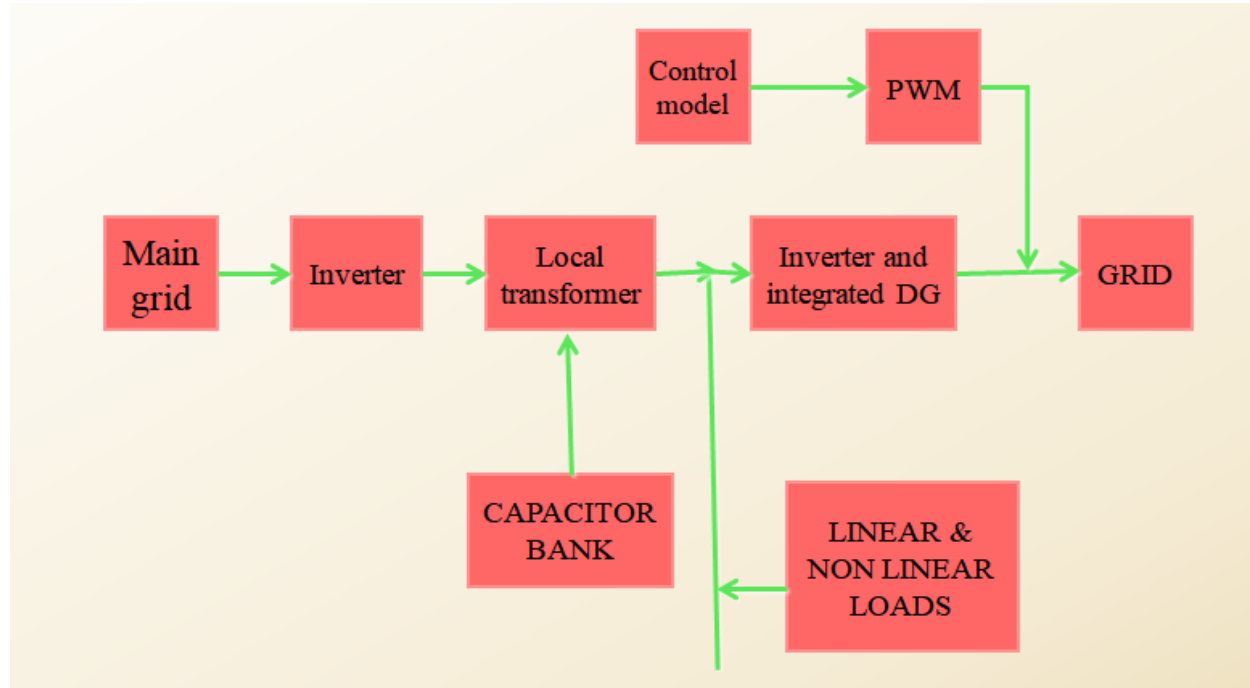


Fig 1. Block Diagram

## 3 CONTROL SCHEME

In order to control the bus voltage of the DC microgrid and the voltage of UC, the control structure includes two parts: the battery provides the UC with energy and the UC provides the DC bus with energy. Each part includes two layers of control: outer voltage control and inner current control. The purpose of outer voltage control is to calculate the predictive value of the inductor current needed to stabilize the voltage. The function of the inner current control is to make the actual current follow the predictive value calculated from the outer control, so as to realize the function of the outer layer steady-state predictive value calculation and

inner layer dynamic rolling optimization.

The battery provides the UC with energy to regulate UC voltage and UC regulates the bus voltage by the three-level DC/DC converter. There are two types of input voltage values on the bus side, i.e., the full bus voltage  $V_{dc}$  or half of the bus voltage  $V_{dc}/2$ . The input voltage can be selected according to the actual situation. This topology can effectively reduce the inductor current ripples and the voltage stress of each switch, thereby suppressing the DC bus power fluctuations of the higher voltage levels.

Changing the parameter  $\delta_i$  only affects the change rate of the current in the transition process, and has no effect on the steady-state value. By changing the value of parameter  $\delta_i$ , the charging/discharging rate of the battery can be controlled, and then the power fluctuations under different frequency ranges can be allocated between the battery and UC. The rated reference bus voltage is  $V_{dcref}$ , and the actual voltage  $V_{dc}$  is regulated by the UC charging/discharging through the three-level DC/DC converter.  $d_{uc}$  is the duty cycle of the switches on the UC side. The UC terminal voltage  $V_{uc}$  may be larger or smaller than  $V_{dc}/2$  in the dynamic process of the system, which is according to the principle of NPV balance. The input voltage on the bus side may be  $V_{dc}$  or  $V_{dc}/2$ , which will be discussed in the following two cases.

In case 1, when  $V_{uc} > V_{dc}/2$ , the UC is charged or discharged. The input voltage on the bus side is  $V_{dc}$ , and the equivalent capacitance  $C$  is the series value of  $C_1$  and  $C_2$ .

In case 2, when  $V_{uc} < V_{dc}/2$ , the UC is charged or discharged. Due to the NPV balance control strategy,  $V_{c1}$  almost equals  $V_{c2}$ . The input voltage on the bus side can be considered as  $V_{dc}/2$ , and the equivalent capacitance is  $C_1 = C_2 = 440 \mu\text{F}$ .

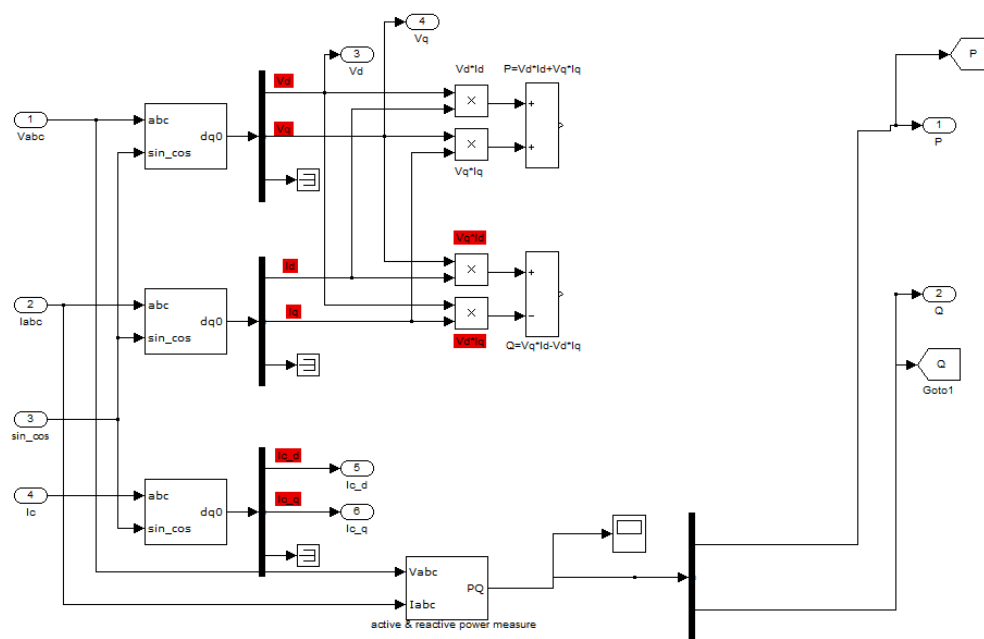


**Fig 2: Active and Reactive power measurements**

Above figure shows the simulation diagram for calculating active and reactive power. Load voltages and currents are given as input to this circuit. From these current and voltage values both active power and reactive power values are calculated using instantaneous active and reactive power measure tool.  $V_d$  and  $V_q$  values are also calculated in this circuit, which are used to compare with desired values. For finding  $V_d$  and  $V_q$  values load voltage and current values are converted into DQ quantities.

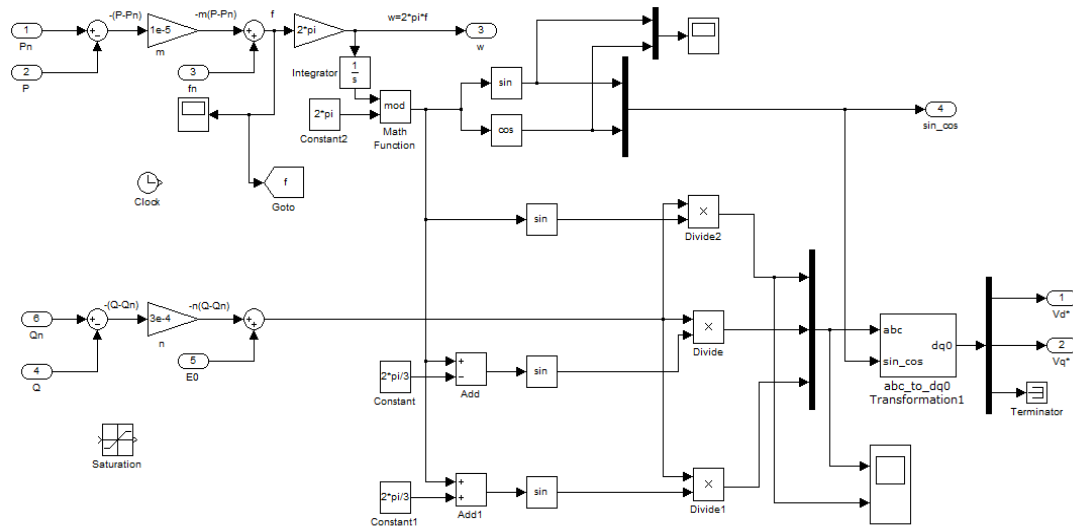


**Fig 3: Power loop controller**

In power loop controller  $V_d$  and  $V_q$  values are derived from the active and reactive power values. Reference active and reactive power, voltage, frequency values are given as inputs for this circuit based on the requirement.  $V_d$  and  $V_q$  and  $W$  values are calculated in this circuit using reference values. These values are used to compare with the values from active and reactive power measurement circuit.

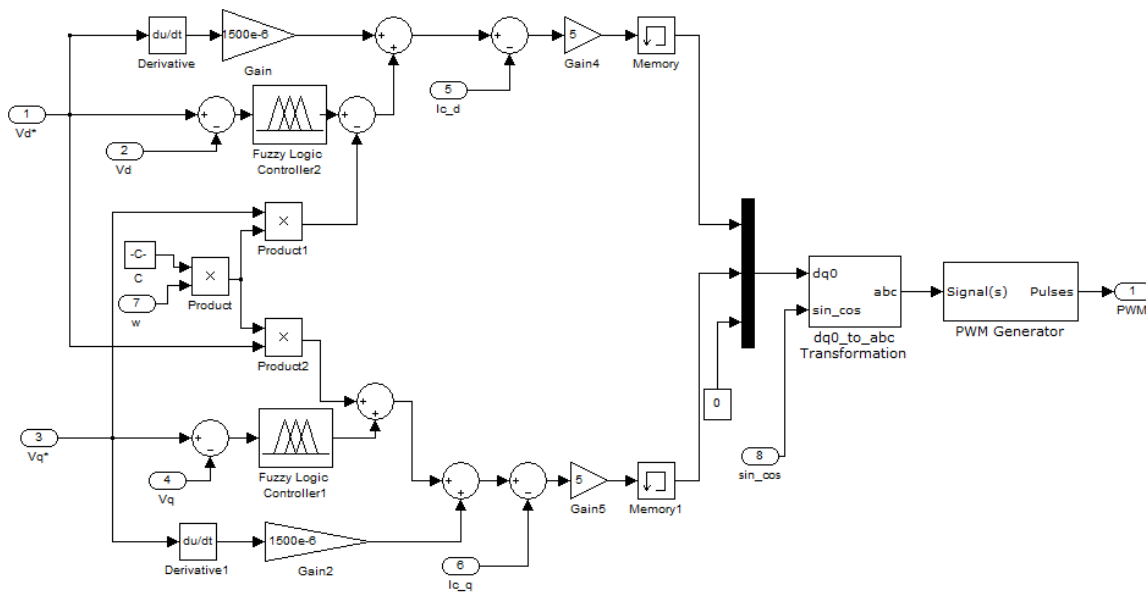


**Fig 4: UI control diagram :**

Above control loop only controls the values of PWM in the main simulation diagram. In this UI control loop inputs are derived and desired conditions of the transmission line. Fuzzy logic performs the control function in this loop. Inputs of this loop are derived active power and reactive power from active and reactive power measurement. Desired conditions are obtained from the power loop controller. Fuzzy logic compares these values and give output to the PWM accordingly.

4. SIMULATION RESULTS

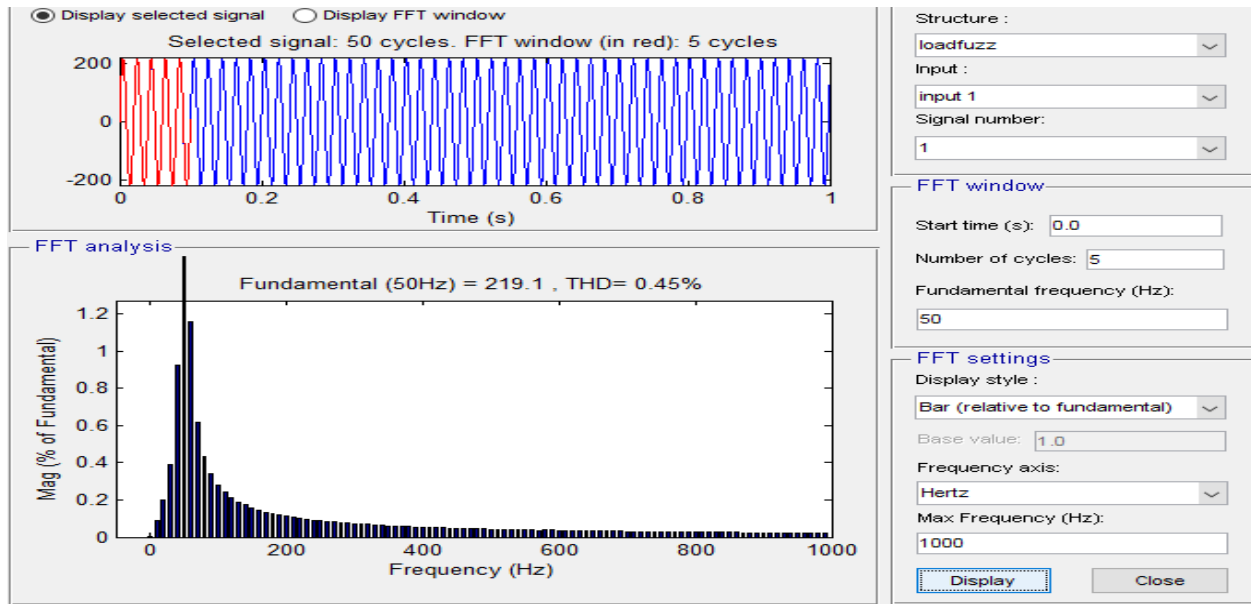


Fig 5. Total harmonic distortion value

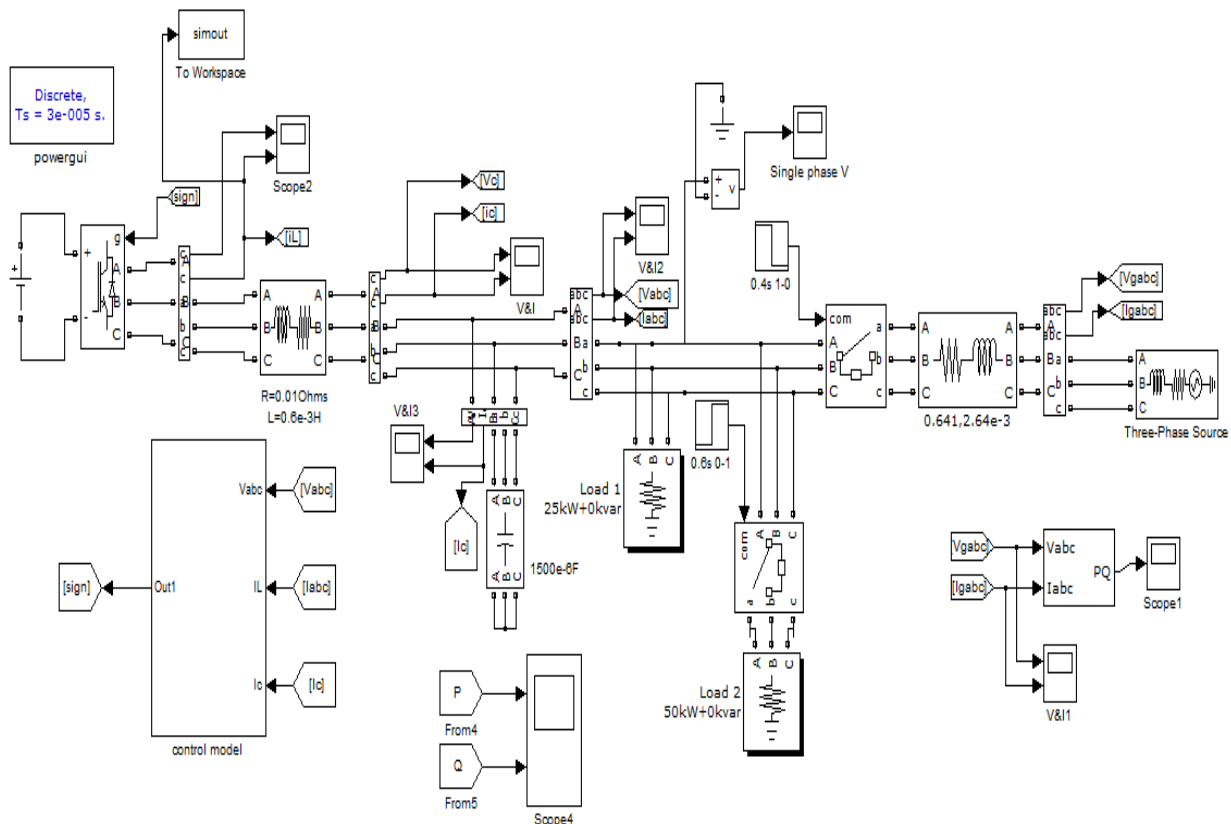


Fig 6 :Simulation diagram

There are two loops. First loop is DG (distributed energy generator) is connected to the inverter. The loops are connected across the inverter and the inverter is connected to the grid. We take the voltage feedback value and current loop, powerloop through that values harmonics eliminates from the loop. The output of the voltage, current and power values we take as the reference value and the reference value is given input to the pwm modulator. The pwm modulator is connected to the inverter and the DG is suppress the values and this value is connected to the grid. The DG is connected to the inverter. For the inverter we assign some pulses and the local transmission line we connected to the



inverter. In local transmission line we use capacitor and linear and non linear loads arranged to the transmission line. The capacitor is used to reduce the power factor correction and the linear and non linear loads are arranged to the transmission. In control loop we take the input values of the active and reactive power values, the output values of active and reactive values taking as reference values and these reference values given input to the power loop and the output of the power loop is connected to the the UI control loop. Using the reference values are given to the converter and using these values reduces the harmonics.



Fig 7. Supply Voltage and Current

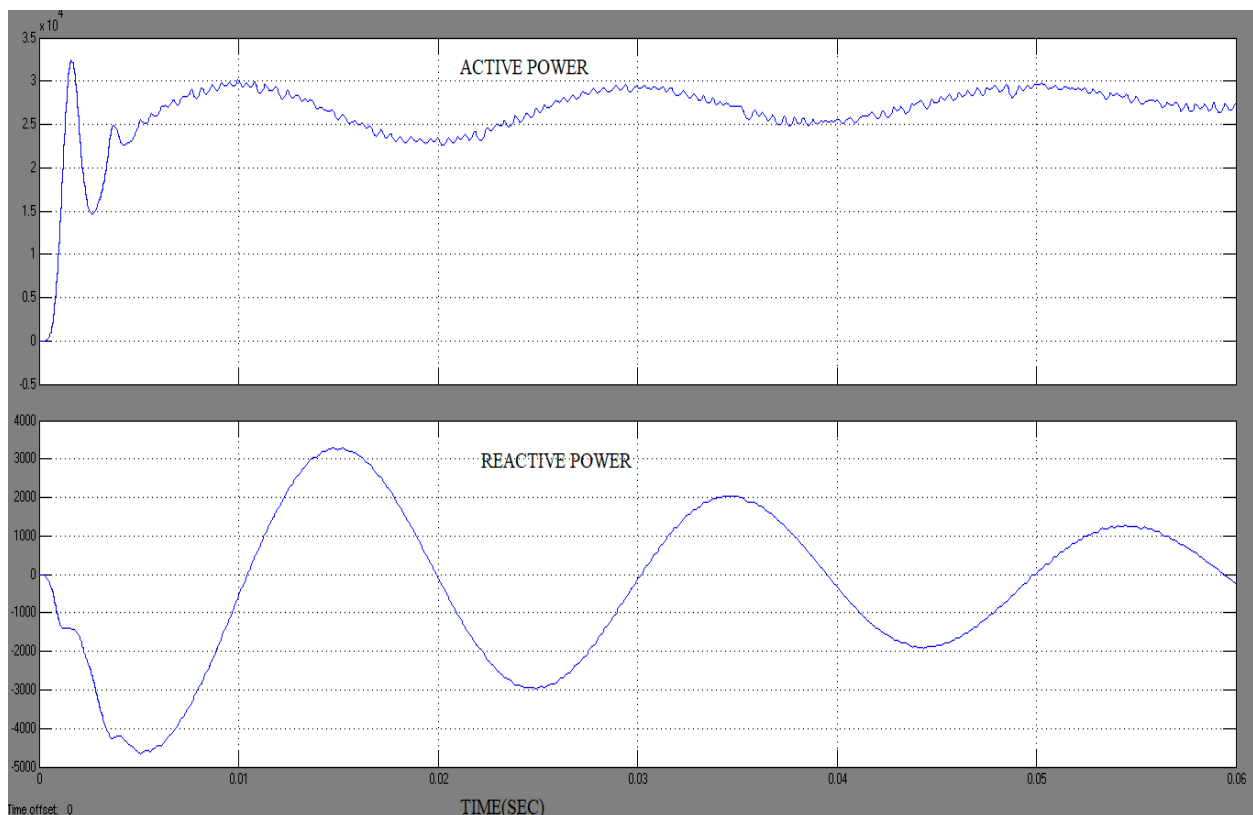
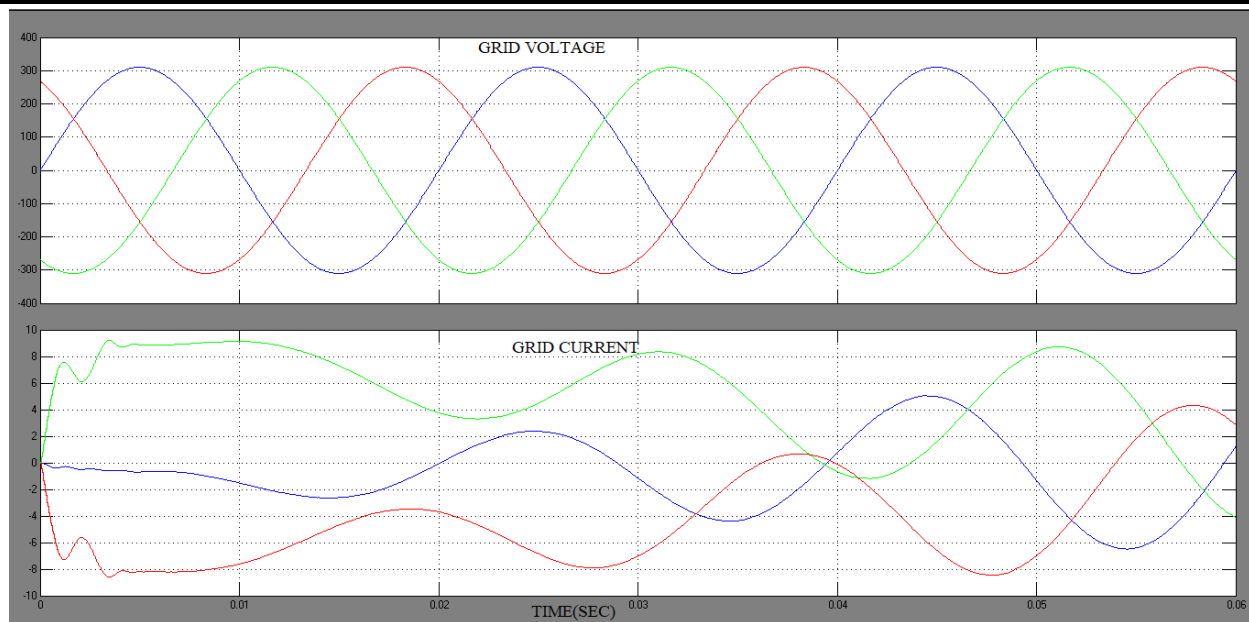


Fig 8. Active power and Reactive power



**Fig 9. Grid Voltage and Grid Current**

## 5. CONCLUSION

In this paper, the advantages of a three-level bidirectional DC/DC converter for battery/UC HESS and the effectiveness of the proposed MPC method are discussed. At the same grid voltage level, the battery can suppress higher voltage level fluctuations after a two-stage boosting structure. Compared with the fuzzy logic controller, the MPC controller doesn't need a tedious step of adjusting parameters and various state variables are considered in each sampling instant. Moreover, the MPC algorithm based on the constant switching frequency achieves fast and accurate regulation of voltage and current with diminished ripples. Finally, the system does not need filters to allocate power fluctuations, and the control structure is optimized while the battery life is prolonged.

## 6. References

1. Chen, Siyuan, et al. "A model predictive control method for hybrid energy storage systems." *CSEE Journal of Power and Energy Systems* 7.2 (2020): 329-338.
2. S. D'Arco, L. Piegari and P. Tricoli, "Harmonic compensation with active front-end converters based only on grid voltage measurements," 3rd Renewable Power Generation Conference (RPG 2014), Naples, 2014, pp. 1-6, doi: 10.1049/cp.2014.0935.
3. J. Srikakolapu, S. R. Arya and R. Maurya, "Distribution static compensator using an adaptive observer based control algorithm with salp swarm optimization algorithm," in *CPSS Transactions on Power Electronics and Applications*, vol. 6, no. 1, pp. 52-62, March 2021, doi: 10.24295/CPSSTPEA.2021.00005.
4. A. Khan, M. B. Shadmand, S. Bayhan and H. Abu-Rub, "A Power Ripple Compensator for DC Nanogrids via a Solid-State Converter," in *IEEE Open Journal of the Industrial Electronics Society*, vol. 1, pp. 311-325, 2020, doi: 10.1109/OJIES.2020.3035073.
5. K. Hasan, M. M. Othman, S. T. Meraj, M. Ahmadipour, M. S. H. Lipu and M. Gitizadeh, "A Unified Linear Self-Regulating Method for Active/Reactive Sustainable Energy Management System in Fuel-Cell Connected Utility Network," in *IEEE Access*, vol. 11, pp. 21612-21630, 2023, doi: 10.1109/ACCESS.2023.3249483.
6. J. Zhou, Y. Yuan and H. Dong, "Adaptive DC-Link Voltage Control for Shunt Active Power Filters Based on Model Predictive Control," in *IEEE Access*, vol. 8, pp. 208348-208357, 2020, doi: 10.1109/ACCESS.2020.3038459.
7. Y. Qi, J. Fang, J. Liu and Y. Tang, "Coordinated control for harmonic mitigation of parallel voltage-source inverters," in *CES Transactions on Electrical Machines and Systems*, vol. 2, no. 3, pp. 276-283, September 2018, doi: 10.30941/CESTEMS.2018.00034.
8. L. Kong, Z. Shi, G. Cai, C. Liu and C. Xiong, "Phase-Locked Strategy of Photovoltaic Connected to Distribution Network With High Proportion Electric Arc Furnace," in *IEEE Access*, vol. 8, pp. 86012-86023, 2020, doi: 10.1109/ACCESS.2020.2989896.

9. H. K. M. Paredes, D. T. Rodrigues, J. C. Cebrian and J. P. Bonaldo, "CPT-Based Multi-Objective Strategy for Power Quality Enhancement in Three-Phase Three-Wire Systems Under Distorted and Unbalanced Voltage Conditions," in IEEE Access, vol. 9, pp. 53078-53095, 2021, doi: 10.1109/ACCESS.2021.3069832.
10. Q. -N. Trinh and H. -H. Lee, "Improvement of grid current performance for grid-connected DG under distorted grid voltage and nonlinear local loads," 2014 IEEE 23rd International Symposium on Industrial Electronics (ISIE), Istanbul, Turkey, 2014, pp. 2607-2612, doi: 10.1109/ISIE.2014.6865031.
11. G. Lou, Q. Yang, W. Gu, X. Quan, J. M. Guerrero and S. Li, "Analysis and Design of Hybrid Harmonic Suppression Scheme for VSG Considering Nonlinear Loads and Distorted Grid," in IEEE Transactions on Energy Conversion, vol. 36, no. 4, pp. 3096-3107, Dec. 2021, doi: 10.1109/TEC.2021.3063607.
12. H. Ahmed, S. Biricik and M. Benbouzid, "Extended Self-Tuning Filter-Based Synchronization Technique for Unbalanced and Distorted Grid," 2020 2nd International Conference on Smart Power & Internet Energy Systems (SPIES), Bangkok, Thailand, 2020, pp. 350-355, doi: 10.1109/SPIES48661.2020.9242953.



# MODELLING AND SIMULATION OF GRID INTERCONNECTION OF VARIABLE SPEED WIND TURBINE ENERGY SYSTEM

B Ramesh<sup>1</sup>, G Madhu<sup>2</sup>, T Aravind<sup>3</sup>, E Bhanu Kovindh<sup>4</sup>, B Srikanth<sup>5</sup>

<sup>1</sup>Assistant Professor, <sup>2</sup>UG Student, <sup>3</sup>UG Student, <sup>4</sup>UG Student, <sup>5</sup>UG Student

<sup>1</sup>Department of Electrical and Electronics Engineering

<sup>1</sup>Teegala Krishna Reddy Engineering College, Hyderabad, India.

**ABSTRACT:** Renewable energy from wind is the safest form of energy. Wind turbine based energy generators have the potential to generate high amount of electric power if there is a proper wind velocity and control mechanisms. This can certainly reduce the dependency on solar photovoltaic based energy systems, which needs huge space to install the solar photovoltaic panels. However, the output power of wind turbine is affected by the uncertain wind velocity. The output mechanical power has to be properly controlled. Hence, the wind energy system efficacy depends on how well this uncertainty is addressed. The major challenge is to design and control the wind turbine systems that has a suitable mediator between the power generator and the load, which counters the damage to the load due to variable voltages produced by the varying wind velocity. Keeping this in view, this paper implements all-important converter design methods for wind energy application and recommends the most suitable method for its controller design. The overall analysis is presented via detailed quantitative results that are evaluated with the help of time-domain performance index parameters.

**Index terms** - Wind power, renewable energy, turbine model, pitch angle, battery, dc to dc converter, pi controller

## I. INTRODUCTION:

In the world energy point of view, there are two types of energy sources i.e., nonconventional (renewable) energy sources and conventional energy sources. Renewable energy sources are the type of resources which are derived from earth or its ecology, and are plenty in quantity. There are different types of renewable resources in general such as, wind energy, hydro-energy, solar energy, biomass, geothermal energy, etc., which are inexhaustible in nature. Apart from the abundancy, these resources are pollution free in usage when compared to the conventional fossil fuel-based energy systems. So, presentday energy sector is depending more and more usage of renewables rather than fast depleting conventional fossil fuels. Many researches has been done on the generation of the electricity from these renewable energy resources [1]. Among all these renewable resources, wind energy generation is cleanest and more efficient source of energy. The main advantage of this is, it doesn't pollute the air, water, or soil in any form and other major advantage is it doesn't contribute to global warming. However, the major challenge in the wind turbine-based energy system is to design and control the wind turbine systems such that there should be a suitable interface between the power generator and the load such that no (or minimum) damage to the load due to variable voltage produced by the variable wind speed. Normally wind turbines operates in two different ways one with variable speed and other with fixed speed. Wind speed is uncontrollable and changes within a very short period of time, which makes the wind power control operations very complex. If the wind power generated cannot be controlled, it damages the load. This can be solved by controlling the speed of wind turbine generator which can be used to control the power generated over a wide variety of speeds. So, to resist the damage to the load, proper design of controller unit is required to control the wind turbine's speed against all the uncertain wind velocities. Many researches are on-going in this area to regulate the wind turbine speed, such as, speed control for direct drive permanent magnet wind turbine [2], non-variable speed control of wind turbine [3], sensor less control scheme for wind turbine in 1.5 MW doubly-fed induction generator

(DFIG) application with maximum power point tracking (MPPT) facility [4], full range speed control mechanism given for an electromagnetic doubly-salient wind turbine plant [5], disturbance observer based speed control mechanism for fixed-pitch angle based wind turbine [6], and modern or intelligent speed control novel methods, such as wind velocity forecasting concept based predictive control method for wind turbines [7], adaptive MPPT based rotor speed control of DFIG wind turbine [8], intelligent speed control integrated with MPPT facility for medium power wind energy systems [9], protection and control mechanism for full wind speed range of a wind turbine power system [10], imperialist competitive algorithm based induction motor's speed control provision that was supplied by wind turbine [11], and model predictive control approach for speed control of a wind turbine energy system [12]. However, all these controllers that are implemented in literature are normally based on PID (proportional cum integral cum derivative) controllers [13]. The fundamental issue with the PID controller is, this can suitably work well for linear error variations, however, for nonlinear deviations of the system response may not be settled with a PID controller. Variable-Speed and Constant-Speed Wind Turbines.

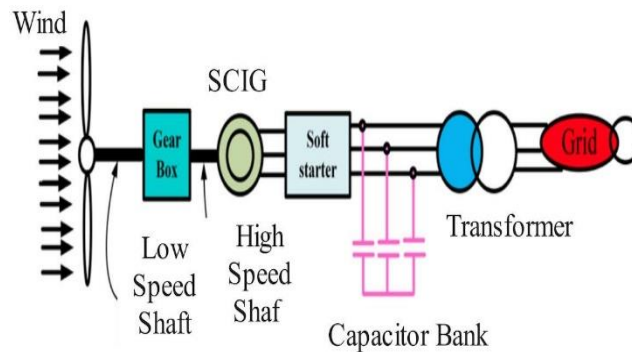


**FIGURE 1. Basic diagram of SCIG wind turbine**

A major distinction in the wind turbines includes variable and constant speed wind turbines i.e. the rotor is allowed to run at variable speed or constrained to operate at constant speed. The constant speed wind turbines allow the use of simple generators whose speed is fixed by the frequency of the electrical system. Although the power electronics needed for variable speed wind turbines are more expensive, this type of turbines can spend more time operating at maximum aerodynamic efficiency than constant speed turbines. This can be seen clearly if the performance coefficient,  $C_p$  of a wind turbine is plotted against the tip speed ratio,  $\lambda$ . The tip speed ratio,  $\lambda$ , is defined as the ratio between the speed of the tips of the blades of the wind turbine and the speed of the wind.

$$\lambda = \frac{v_{tip}}{v_{wind}} = \frac{\omega R}{v} \quad (1)$$

The coefficient of performance,  $C_p$ , is defined as the fraction of energy extracted by the wind turbine of the total energy that would have flowed through the area swept by the rotor if the turbine had not been there.

$$C_p = \frac{P_{extracted}}{P_{wind}} \quad (2)$$

The coefficient of performance  $C_p$  has a theoretical optimum of 0.59. Only a portion of the power in the wind can be converted to useful energy by wind turbine. The power available for a wind turbine is equal to the change in kinetic energy of the air as it passes through the rotor. This maximum theoretical  $C_p$  was formulated in 1919 by Betz and applies to all types of wind turbines. A typical  $C_p$  vs  $\lambda$  characteristics is depicted in the figure.1. The figure.1 represents the characteristics of coefficient of performance,  $C_p$  versus tip speed ratio,  $\lambda$

.From figure.1 we infer that maximum value of  $C_p$  i.e. 0.5 is achieved for a tip speed ratio of 10 and pitch angle of 0. For a fixed-speed wind turbine, where  $\omega$  is constant, this corresponds to a particular wind speed. For all other wind speeds the efficiency of the turbine is reduced. The aim of variable-speed wind turbines is to always run at optimal efficiency, keeping constant the particular  $\lambda$  that corresponds to the maximum  $C_p$ , by adapting the blades velocity to the wind speed changes. Hence, variable speed wind turbines are designed to operate at optimum energy efficiency, regardless of the wind speed. On the other hand, due to the fixed-speed operation for constant speed turbines, all

fluctuations in the wind speed are transmitted as fluctuations in the mechanical torque and then as fluctuations in the electrical power grid. This together with the increased energy capture obtained by using a variable-speed wind turbine provides enough benefit to make the power electronics cost effective. Therefore, the wind industry trend is to design and construct variable-speed wind turbines.

## II. EXISTING SYSTEM

An analysis of the available storage technologies for wind power application. The advantage of battery energy storage for an isolated WECS is discussed. With battery energy storage it is possible to capture maximum power from the available wind. A comparison of several maximum power point tracking (MPPT) algorithms for small wind turbine (WT) is carried out. In order to extract maximum power from WECS the turbine needs to be operated at optimal angular speed. However, do not take into account the limit on maximum allowable battery charging current nor do they protect against battery overcharging. With battery energy storage it is possible to capture maximum power from the available wind. A comparison of several maximum power point tracking (MPPT) algorithms for small wind turbine (WT) is carried and. In order to extract maximum power from WECS the turbine needs to be operated at optimal angular speed. However do not take into account the limit on maximum allowable battery charging current nor do they protect against battery overcharging. In order to observe the charging limitation of a battery a charge controller is required

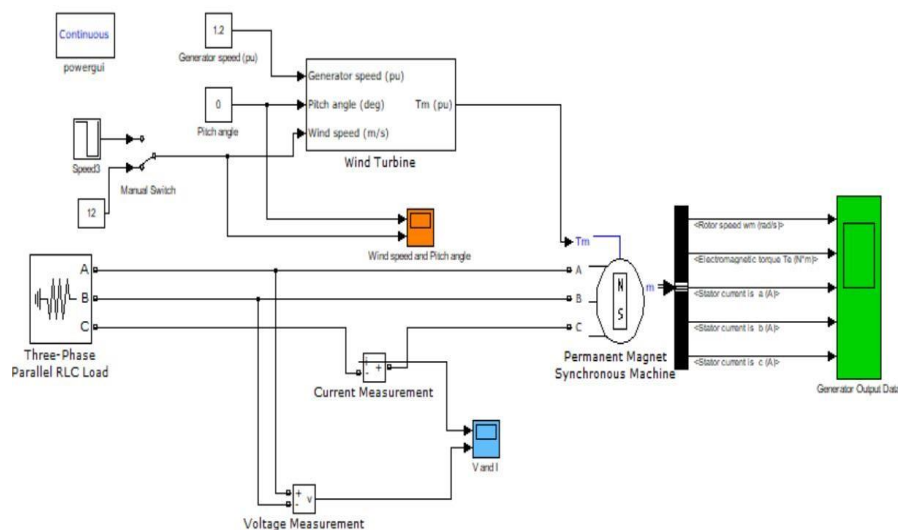


FIGURE 2. Existing circuit configuration

## III. PROPOSED SYSTEM

A hybrid wind-battery system is considered to meet the load demand of a stand-alone base telecom station (BTS). The BTS load requirement is modeled as a dc load which requires a nominal regulated voltage of 50 V. The WECS is interfaced with the stand-alone dc load by means of ac-dc-dc power converter to regulate the load voltage at the desired level.

that MPPT schemes with and without battery charging mode control and pitch control technique have been implemented independently for stand-alone wind energy applications.

The proposed control scheme utilizes the turbine maximum power tracking technique with the battery SoC limit logic to charge the battery in a controlled manner. Unlike, the MPPT logic used here actually forces the turbine to operate at optimum TSR and hence is parameter independent. The battery charging current is always continuous with very low ripple thus avoiding harmonic heating. The changeover between the modes for battery charging is affected based on the actual value of the SoC. Further it also provides protection against turbine over speed, over loading, and over voltage at the rectifier output by using pitch control.



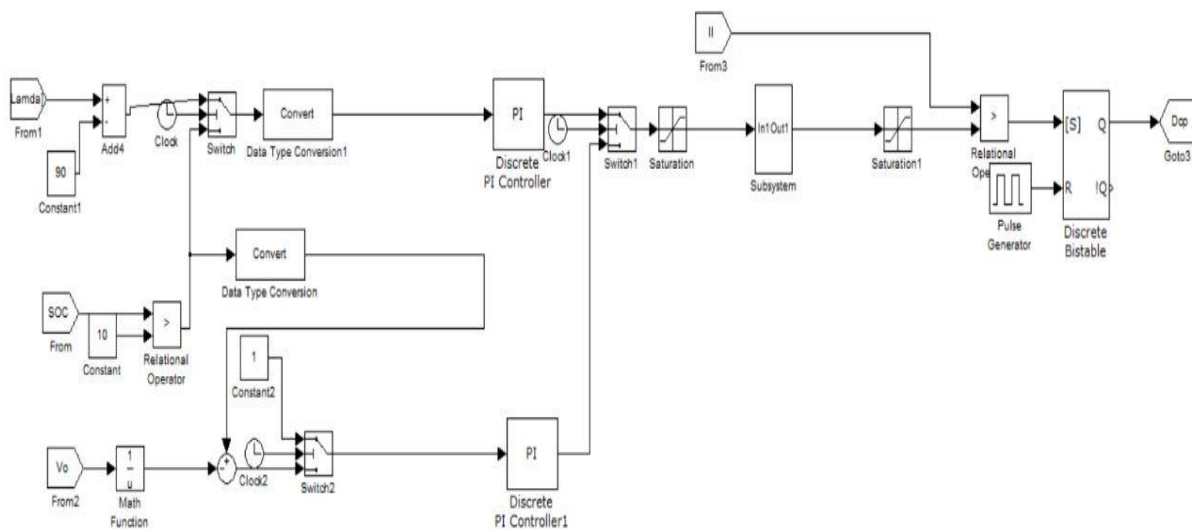
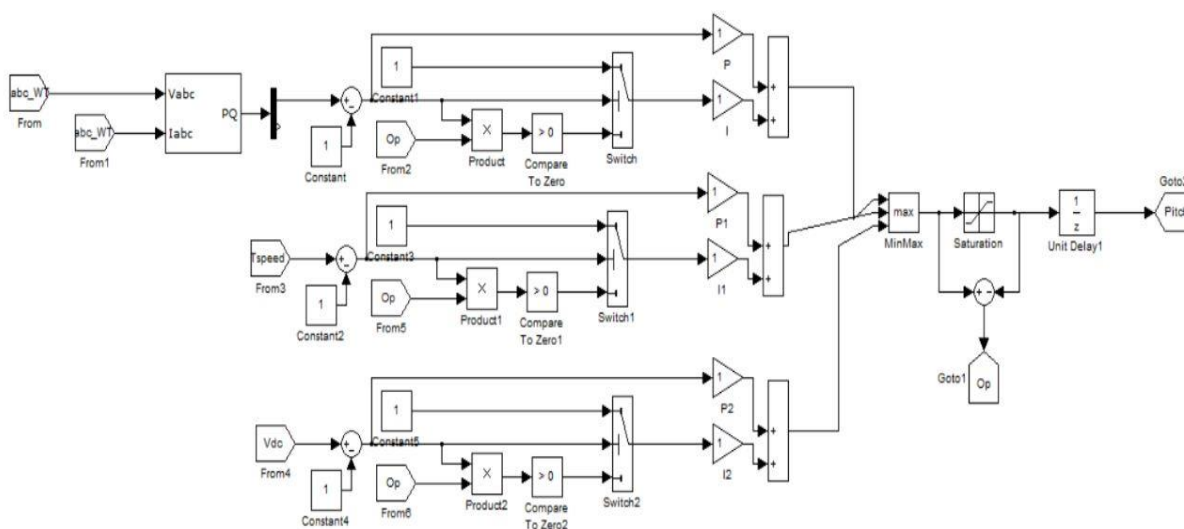


FIGURE 5.DC-DC Converter

### III.III PITCH ANGLE CONTROL

Pitch angle control has the same idea as active stall control except that the blades' movement is not into the wind as in active stall control but out of the wind. It can be accomplished by decreasing angle  $\beta$ . It can be explained as follows: When the wind speed is higher than the rated value, the angle  $\beta$  will be decreased to decrease the pressure on the lower surface of the blade and hence decrease the torque force. The decrease in torque force will decrease the rotor speed and hence output power so that it will be kept at its rated value. The opposite procedure will happen when wind speed is lower than its rated value where angle  $\beta$  will be increased to increase the output power and keep it at its rated value. Figure shows the difference between impact on the blade position due to pitch angle control and active stall control. From it can be observed that in active stall control angle  $\beta$  is increased with the increase of wind speed but in pitch angle control angle  $\beta$  is decreased with the increase of wind speed. This is the main difference between the principle operations of active stall control and pitch angle control angle.

FIGURE 6. Pitch angle control



### IV. SIMULATION RESULTS AND ANALYSIS

As mentioned in the above-section, all the important tuning methods have been implemented and the corresponding results are deposited through Fig.7 to Fig.9. MATLAB/SIMULINK is a graphical software package for modelling, simulating and analysing dynamic systems. It supports linear and nonlinear systems both in continuous time and sample time. There are various researches presented the PMSG based on WECS in MATLAB/SIMULINK [8-9]. In order to understand the principle of producing electricity from wind with WECS and analyze before it will be implemented in practical case. Thus, it is needed to further study and investigate the PMSG based on WECS.



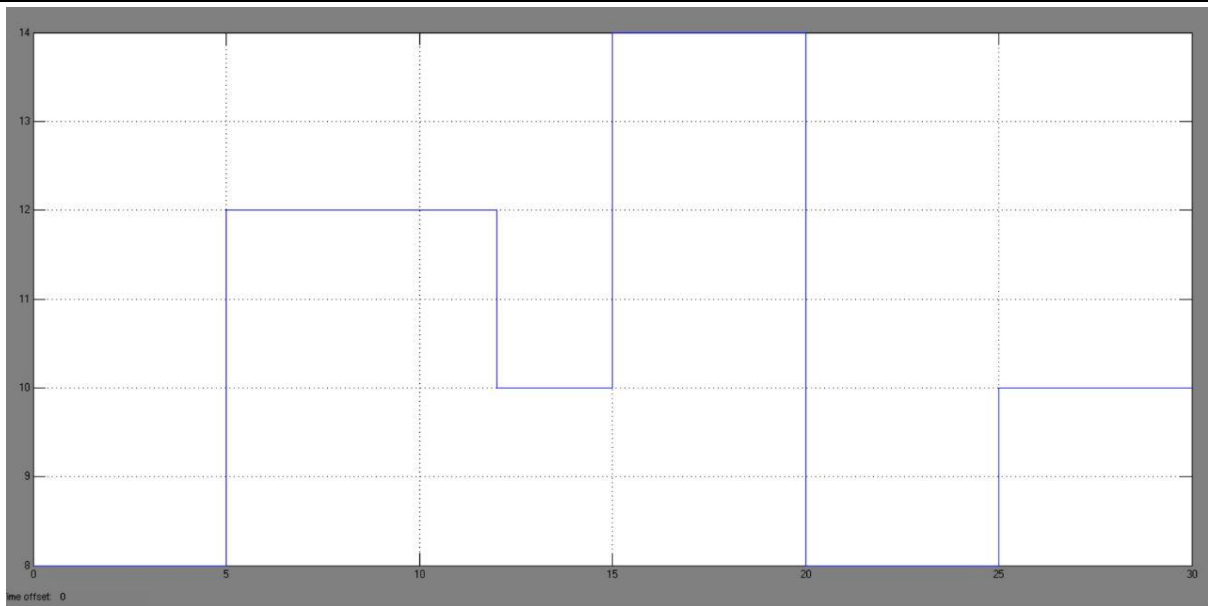


**FIGURE 7. Input Wind speed characteristics**

In order to evaluate the efficacy of these methods, various time domain specifications of the wind turbine system response are computed. The parameters of interest are delay time ( $T_d$ ), peak time ( $T_p$ ), rise time ( $T_r$ ), settling time ( $T_s$ ), peak overshoot ( $M_p$  in %), and steady state error (eSS).

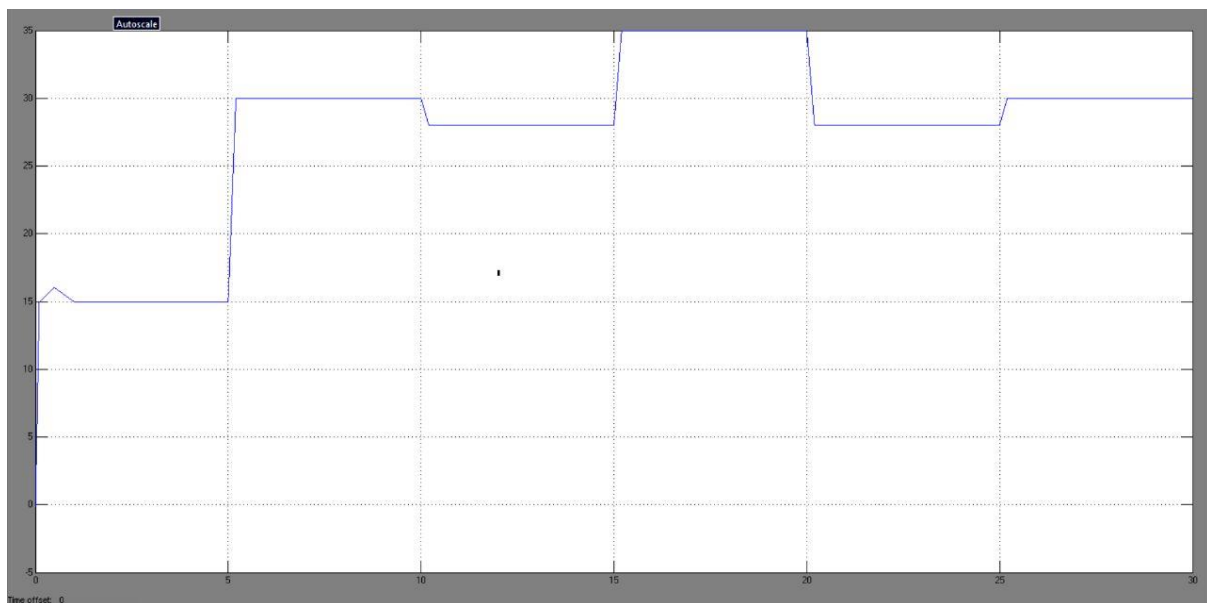


**FIGURE 8. Torque characteristics**

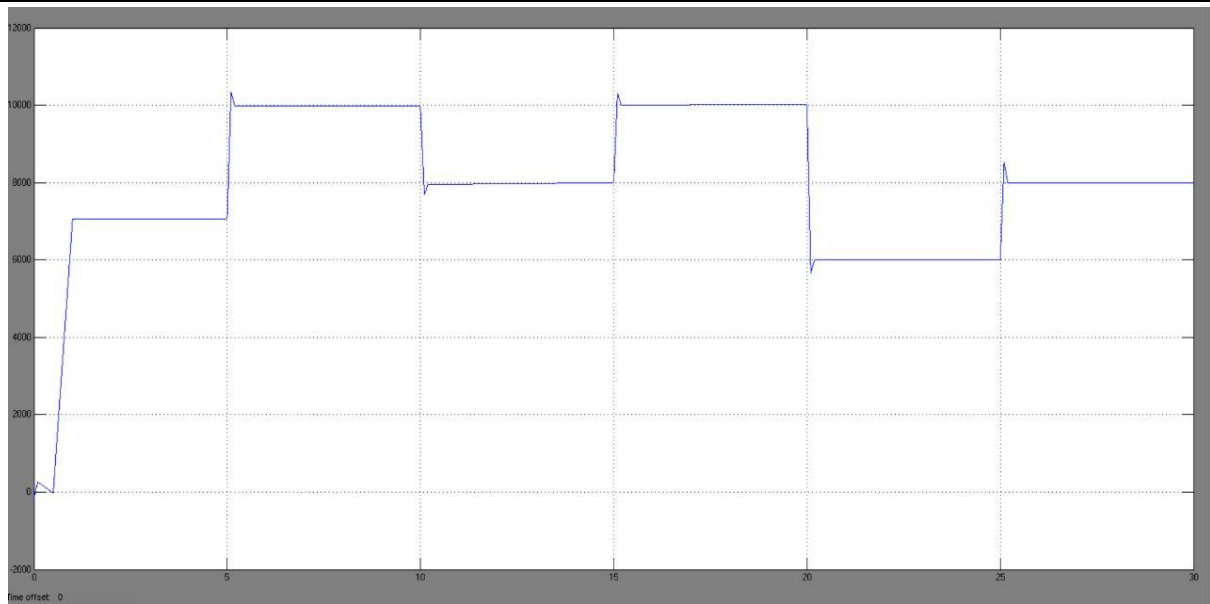


**FIGURE 9. Active and Reactive power**

The best response, i.e., the best design method is decided such way that the method which produces lower values for all the abovementioned time domain performance specifications. From the computed values shown , it is clearly observed that, Ziegler – Nichols 1 (ZN-1) method is leading to produce superior time domain performance indices in terms of delay time ( $T_d$ ), peak overshoot ( $M_p$  in %), and settling time ( $T_s$ ) when compared with the other methods. Hence, this method is a suitable choice to design the controller for the considered wind turbine energy system.

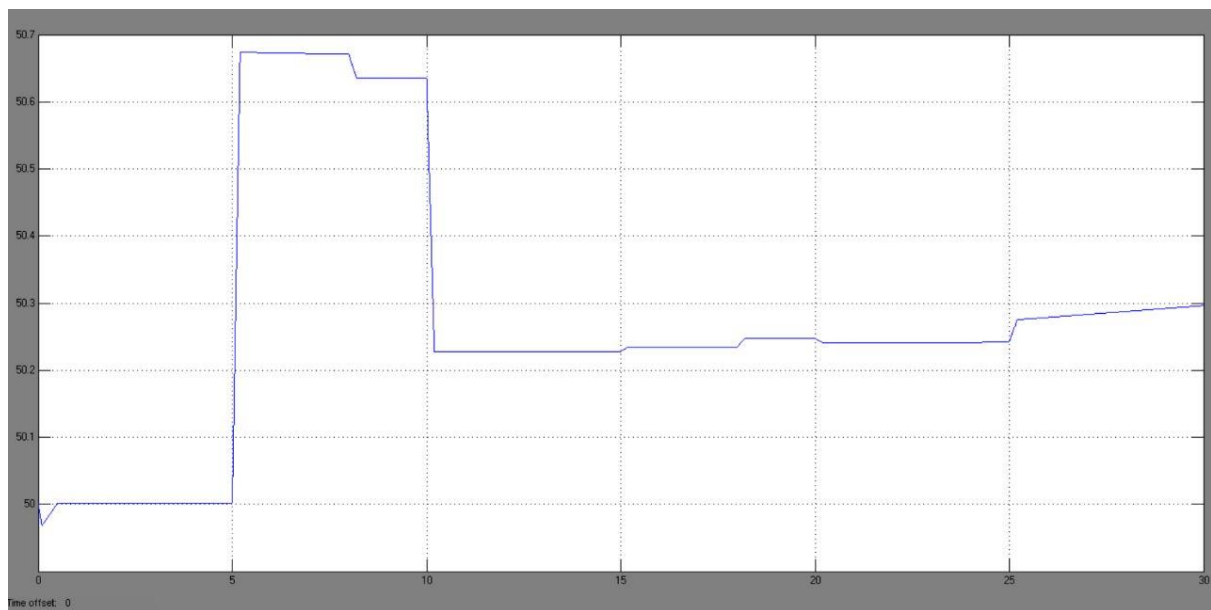


**FIGURE 10. Battery voltage**

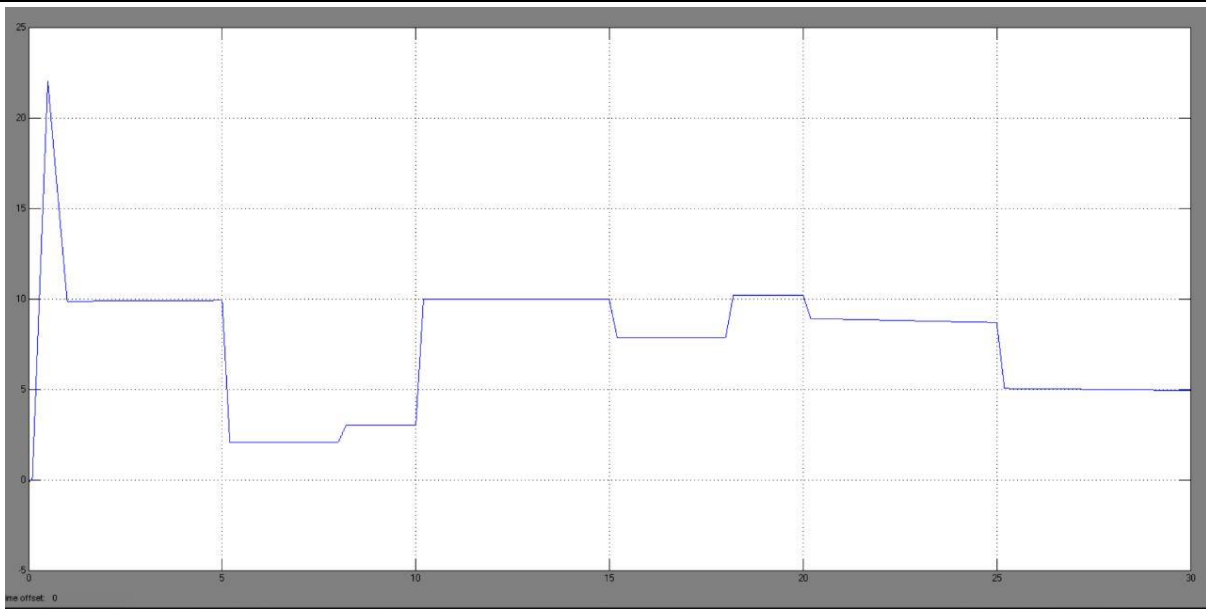


**FIGURE 11. Battery current**

## V.CONCLUSION

WECSs are widely employed nowadays in stand-alone systems for providing power to isolated loads, as well as in distributed generation systems, microgrids, and smartgrids. In all of these applications, appropriate energy management processes must be performed in order to maximize the energy production of the wind turbines and transfer the wind-generated energy to the consumer with high efficiency and adequate power quality. This paper presented the modelling of PMSG based on WECS. It consists of wind turbine, drive train, PMSG, pitch angle control and ac/dc converter model. PMSG and converter are established in proposed model. A great number of workable technology choices prevail in wind turbine designs. Certain manufacturers champion gearless or direct drive wind turbines. These direct drive turbines have no gearbox, which lessens the number of moving parts and teeth issues as well as the oil cooling system resulting in fire hazard and environmental spillage issues. Feasible knowledge depicts that the gearless wind turbine technology works and is very efficient. A complete valid simulation model of a gearless variable speed wind turbine scheme with permanent magnet synchronous generator have been confirmed in MATLAB/Simulink software environment, the suggested wind turbine system allows the independent control of active and reactive power according to the applied reference values at variable wind speeds. Thus, the suggested gearless wind turbine scheme is practical and permits the generation of power at variable speeds achieving stability throughout the course or duration of various wind speed operational values investigated.

## VI.REFERENCES

- [1] Y. V. Pavan Kumar, Ravikumar Bhimasingu, "Renewable energy based microgrid system sizing and energy management for green buildings," Springer Journal of Modern Power Systems and Clean Energy, Vol. 3, No. 1, pp. 1-13, 2015.
- [2] Moein Lak, V. K. Ramachandaramurthy. "Speed control for direct drive permanent magnet wind turbine," in Proc. 2014 International Conference on Renewable Energy Research and Application (ICRERA), Milwaukee, WI, USA, pp. 317-321, 2014.
- [3] Y. D. Song, B. Dhinakaran, "Nonlinear variable speed control of wind turbines," in Proc. 1999 IEEE International Conference on Control Applications (Cat. No. 99CH36328), vol. 1, pp. 814-819, 1999.
- [4] Essam H. Abdou, Abdel-Raheem Youssef, Salah Kamel, Mohamed M. Aly, "Sensorless Wind Speed Control of 1.5 MW DFIG wind turbines for MPPT," in Proc. 2018 Twentieth International Middle East Power Systems Conference (MEPCON), pp. 700-704, 2018.

- [5] Ying Liu, Guofen Tang, Haidong Liu, Bo Zhou, Honghao Guo, Guangjie Zuo. "Speed control method of double salient electro-magnetic wind power generator in full range of wind speed," in Proc. 2010 World Non-Grid-Connected Wind Power and Energy Conference, Nanjing China, pp. 1-5, 2010.
- [6] Zurong Hu, Junqi Wang, Yundong Ma, Xing Yan "Research on speed control system for fixed-pitch wind turbine based on disturbance observer," in Proc. 2009 World Non-Grid-Connected Wind Power and Energy Conference, Nanjing, China, pp. 1-5, 2009.
- [7] Mahinsasa Narayana, Ghanim Putrus, Milutin Jovanovic, Pak Sing Leung, "Predictive control of wind turbines by considering wind speed forecasting techniques," in Proc. 2009 44th International Universities Power Engineering Conference (UPEC), Glasgow, UK, pp. 1-4, 2009
- [8] Dinh-Chung Phan, Shigeru Yamamoto, "Rotor speed control of doubly fed induction generator wind turbines using adaptive maximum power point tracking." Elsevier Energy Journal, Vol. 111, pp. 377-388, Sep. 2016.
- [9] Vlaho Petrovic, Carlo L. Bottasso, "Wind turbine envelope protection control over the full wind speed range," Elsevier Renewable Energy Journal, Vol. 111, pp.836-848, Oct. 2017.
- [10] Ehab S. Ali, "Speed control of induction motor supplied by wind turbine via imperialist competitive algorithm," Elsevier Energy Journal, Vol. 89, pp. 593-600, Sep. 2015.
- [11] Andrea Tilli, Christian Conficoni, "Speed control for medium power wind turbines: an integrated approach oriented to mppt," IFAC Proceedings Volumes, Vol. 44, No. 1, pp. 544-550, Jan 2011.
- [12] Christian Leisten, Uwe Jassmann, Johannes Balshusemann, Dirk Abel, "Model predictive speed control of a wind turbine system test bench," IFAC-PapersOnLine, Vol. 51, No. 32, pp.349-354, 2018.
- [13] Zhenyu Zhang, Yongduan Song, Peng Li, WenLiang Wang, Ming Qin, "Adaptive and robust variable-speed control of wind turbine based on virtual parameter approach," in Proc. 324 Chinese Control Conference, pp. 8886-8890, 2013.
- [14] A. J. Mahdi, W. H. Tang, Q. H. Wu, "Derivation of a complete transfer function for a wind turbine generator system by experiments," in Proc. 2011 IEEE Power Engineering and Automation Conference, Vol. 1, pp. 35-38, 2011.
- [15] Y. Jaganmohan Reddy, Y. V. Pavan Kumar, K. Padma Raju, Anilkumar Ramsesh, "Retrofitted hybrid power system design with renewable energy sources for buildings," IEEE Trans. Smart Grid, Vol. 3, No. 4, pp. 2174-2187, Dec. 2012.
- [16] B. Vasu Murthy, Y. V. Pavan Kumar, U. V. Ratna Kumari, "Application of neural networks in process control: Automatic/online tuning of PID . controller gains for  $\pm 10\%$  disturbance rejection," in Proc. 2012 IEEE International Conference on Advanced Communication Control and Computing Technologies (ICACCCT), 2012.
- [17] B. V. Murthy, Y. V. P. Kumar, U. V. R. Kumari, "Fuzzy logic intelligent controlling concepts in industrial furnace temperature process control," in Proc. 2012 IEEE International Conference on Advanced Communication Control and Computing Technologies, 2012.

See discussions, stats, and author profiles for this publication at: <https://www.researchgate.net/publication/368018991>

# 3-Phase 7-Level Diode Clamped Inverter for Standalone Application

Conference Paper · February 2023

---

CITATIONS

0

READS

42

1 author:



[Kalagotla Chenchireddy](#)  
Karunya University

53 PUBLICATIONS 160 CITATIONS

SEE PROFILE

# 3-Phase 7-Level Diode Clamped Inverter for Standalone Application

Kalagotla Chenchireddy  
Assistant Professor  
Department of EEE  
Teegala Krishna Reddy Engineering  
College  
chenchireddy.kalagotla@gmail.com

V Kumar  
Assistant Professor  
Department of EEE  
Teegala Krishna Reddy Engineering  
College  
kumarpoma@gmail.com

N Shiva Shankar  
UG Student  
Department of EEE,  
Teegala Krishna Reddy Engineering  
College  
Shankarnani640@gmail.com

P Vamshi  
UG student  
Department of EEE,  
Teegala Krishna Reddy Engineering  
College  
vamshi16233@gmail.com

S.Tulasi  
UG student  
Department of EEE,  
Teegala Krishna Reddy Engineering  
College  
tulasi2502@gmail.com

K. Radhika  
Assistant Professor  
Department of EEE,  
Megha Institute of engineering and  
technology for women  
kanchariradhika11@gmail.com

**Abstract:** *This article presents a three-phase, seven-level diode clamped multilevel inverter method. This circuit can be used for applications requiring medium to low industrial power. The three operational modes for this three-phase, seven-level, diode-clamped MLI structure are presented in this study. It consists of three phases each phase consists of the upper and lower leg each leg consists of 12 switches. This circuit operation is presented and simulated with PWM control techniques and output waveforms are obtained. By using this circuit design the THD is better.*

**Keywords:** *Inverter, MLI, DC MLI, PWM technique, THD*

## I. INTRODUCTION

Multi-level inverters are now increasingly in demand for high-power applications. In the past ten years, multi-level inverters have caught the interest of both the industry and the academic community. The optimal topologies for this multilevel inverter are the diode-clamped inverter and capacitor clamping. explains the various diode-clamped inverters and MLIs [1]. According to the literature on the principles of diode clamped inverters, their functioning, and clamping issues [2]. The best SVPWM method for diode-clamped multilevel inverters for industrial induction motors is evaluated, along with the method's explanation [3]. The statcom/BESS applications for diode-clamped multilevel inverters are reviewed[4]. The comparative analysis of two, three, and five-level inverters based on THD was evaluated by this author [5]. presented the harmonic distortion removal in diode-clamped MLIs using an evolutionary method [6]. The optimal control strategies for THD and RMS voltage as

well as a variety of PWM strategies for three-phased diode multilevel inverters are presented [7]. The SPWM approaches use different modulation indices to observe the presented fluctuations of total THD [8]. A three-level diode clamped multilevel inverter's simple neutral point voltage regulator was designed, analysed, and implemented [9]. MLIs with diode clamps were modulated at a fundamental frequency. This article examines the design of a three-phase standalone solar system with a six-level inverter [10]. The outflow current and dv/dt switch damage are reduced using multilevel inverters. The methods for lowering and removing the common mode voltage (CMV) utilising a five-level diode-clamped multilevel inverter are discussed in this study [11]-[12]. Chopper circuits with a new topology are used in diode clamped multilevel inverters to balance the voltage across DC capacitors. The suggested structure is very reliable and modular [13]-[15]. Reduced switching components, high level voltage, and low THD are just a few benefits of MLIs. Electric and hybrid automobiles, microgrids, and transmission systems are among the MLI's applications. The drawbacks include a high switching loss.

## II DIODE CLAMPED MLI

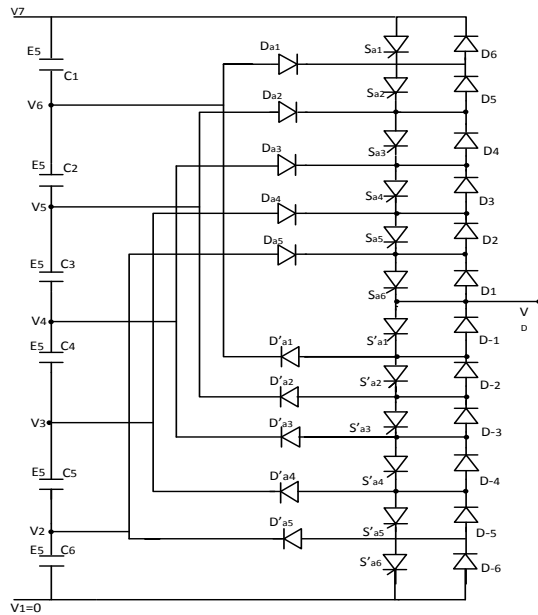


Fig.1 Seven-Level Diode Clamped Inverter

Fig.1 shows the 7-stage diode clamped inverter consisting of three legs. One leg per each phase each leg consists of 12 switches. Which are divided into two parts upper leg and lower leg each has 6 switches. The inverter consists of a total of 36 switches. The implemented inverter has six DC-Link capacitors, 10 auxiliary diodes, and 12 switches connected. The implemented circuit has for standalone application. The load is resistance.

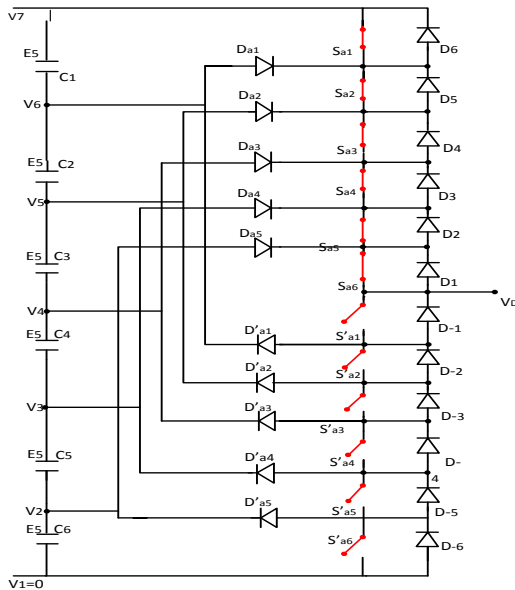


Fig.2 Mode-I operation

**Mode I:** Fig. 2 shows the first mode of operation of the multi-level inverter leg a .consists of 12 switches total. Upper leg switches are the first six, lower leg switches are the last six.

The output voltage in mode 1 is  $E/2$  because the upper switches (sa1, sa2, sa3, sa4, sa5, sa6) are in the ON position while the bottom switches (sa1', sa2', sa3', sa4', sa5', sa6') are in the OFF position.

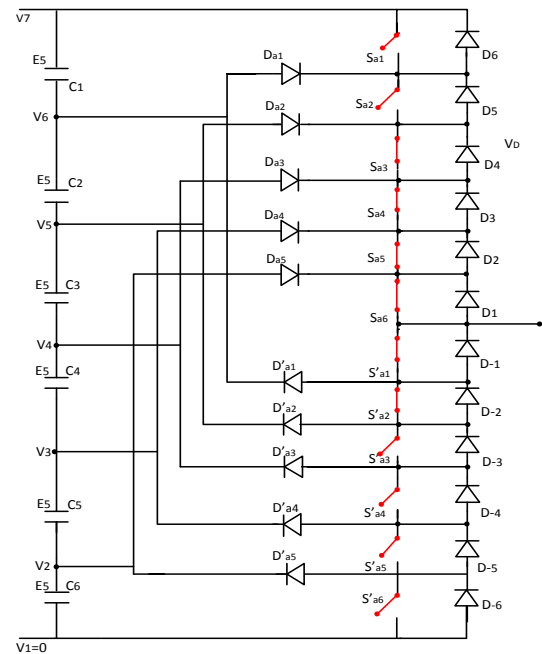


Fig.3 Mode-II operation

**Mode II:** Fig.3 shows mode 2 of operation of the multi-level inverter .in this mode the switches sa1 of the upper leg are in off condition and the remaining switches sa2,sa3,sa4,sa5, and sa6 are in on condition and the switches sa1' of the lower leg is in on condition and remaining switches sa2',sa3',s4',sa5',sa6' is in off condition and gives output voltage E

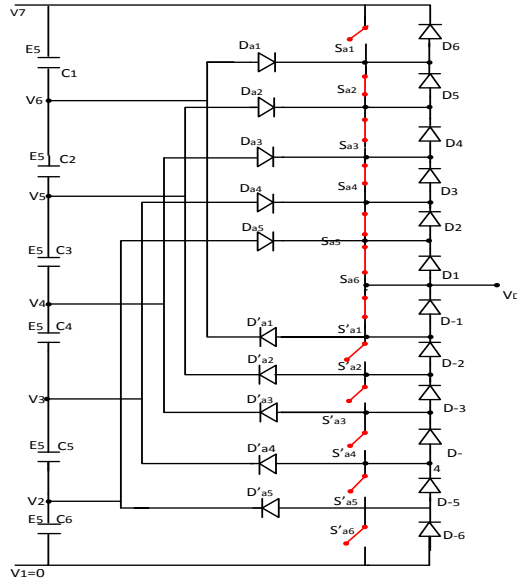


Fig.4 Mode-III operation

**Mode III:** Fig 1.4 shows mode 3 of operation of multilevel inverter. In this mode of operation, switches  $sa_1$  and  $sa_2$  of the upper leg are in off condition, and the remaining switches  $sa_3, sa_4, sa_5$ , and  $sa_6$  are in on condition, and the switches  $sa_1', sa_2'$  of the lower leg are in on condition, and the remaining switches  $sa_3', sa_4', sa_5', sa_6'$  are in off condition, and gives output VOLTAGE  $E/6$

Table: 1 switching sequence

VOLTAGE $V_{a0}$	SWITCH STATE											
	A1	A2	A3	A4	A5	A6	A1,	A2,	A3,	A4,	A5,	A6,
V7	+	+	+	+	+	+	-	-	-	-	-	-
V6	-	+	+	+	+	+	+	-	-	-	-	-
V5	-	-	+	+	+	+	+	+	-	-	-	-
V4	-	-	-	+	+	+	+	+	+	-	-	-
V3	-	-	-	-	+	+	+	+	+	+	-	-
V2	-	-	-	-	-	+	+	+	+	+	+	-
V1	-	-	-	-	-	-	+	+	+	+	+	+

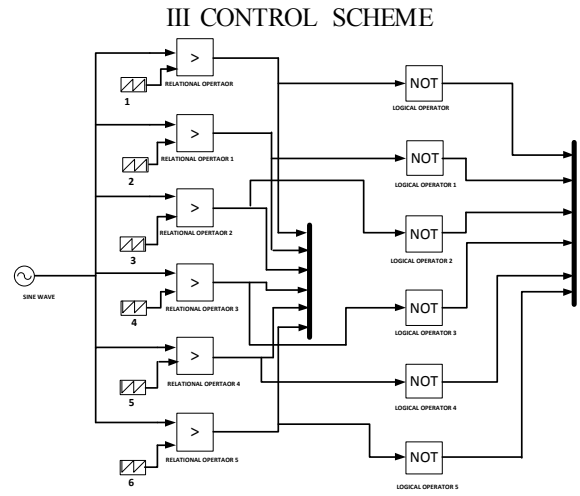


Fig.5 switching pulse generation circuit

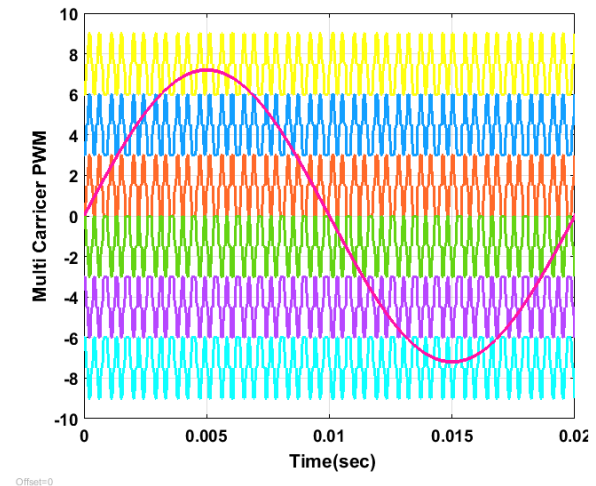


Fig.6 phase disposition control technique

Fig.5 shows the PWM generating circuit for MLI. They are a neutral extension of sine PWM the modulation scheme, used for two-level inverters. In two-level inverters, we have different modulation schemes are there: SPWM (sine PWM), SHE (Selective Harmonic Elimination), and also SVM technique. In the case of multilevel modulation, we simply extend this technique to a higher level. All these accent techniques are divided into two levels (a) SV Based Algorithm (all the 3-phase are controlled together) (b) Voltage Level Based Algorithm (each phase is separately controlled) have based on the resultant vector we are in 3-switching stages. In SVBA, again we have two different techniques (a) space vector modulation (b) Space Vector Control. In VLBA, the first thing is the multicarrier PWM is the extension of a higher level in this again there are two methods (a) Phase Shifting PWM (b) Level Shifting PWM. In the level-shifting PWM, there are three possible ways to arrive at the carrier: (a) POD (b) APOD (c) PD



Hybrid modulation is used for asymmetrical cascade inverter H hybrid

Selective harmonic elimination is the extension of multilevel inverters these can be used for any multilevel inverter topologies. Sometimes known as a trapezoidal modulate scheme.

Nearest Level Control, especially used in a higher number of levels this method is preferred. Ex: HVDC (200 no. of level)

(b) Level-Shifted Multicarrier Module

Fig.6 shows the level shift PWM. These waveforms are six triangular waveforms and one sine wave. The first triangular wave output values it varies from [6 9 6], the second triangular wave varies from [3 6 9] and the third one varies from [0 3 0]. All three carrier waves are controlling upper switches. The remaining all the three carrier waves are varied from [0 -3 0], [-3 -6 -3] and [-6 -3 -6].

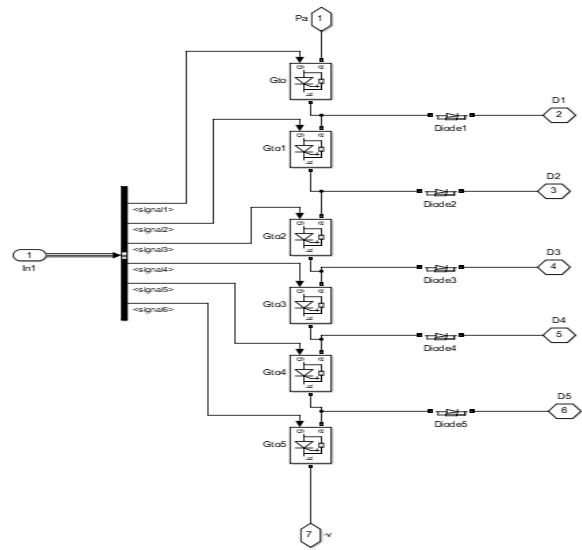


Fig.8 Diode-Clamped Multilevel Inverter Leg-A lower switches

Fig. 7 shows the R-Phase inverter leg-A. These inverters have six switches and six diodes are connected with anti-parallel. The implemented topology have simulated in MATLAB/simulink software. The GTO based MLI is presented this paper. The total 12 GTO switches and 10 Diodes used this paper. The GTO main advantages are operated at high voltage MV, current rating KA and power rating is MW. Fig.8 shows the lower switches' R-phase inverter. The inverter has six switches and six diodes like an upper leg.

#### IV SIMULATION RESULTS

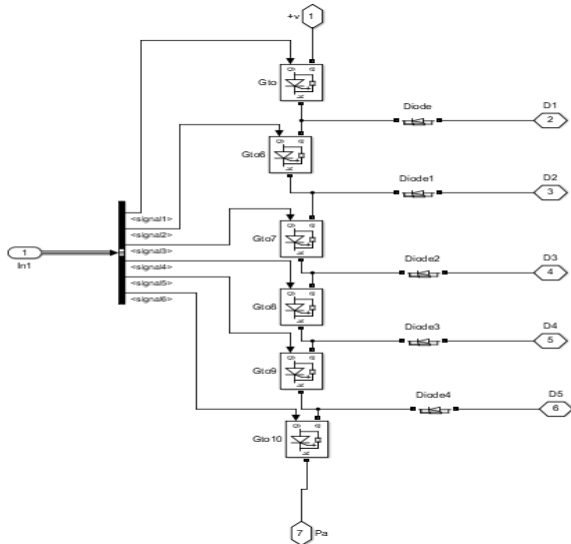


Fig.7 Diode-Clamped Multilevel Inverter Leg-A Upper switches

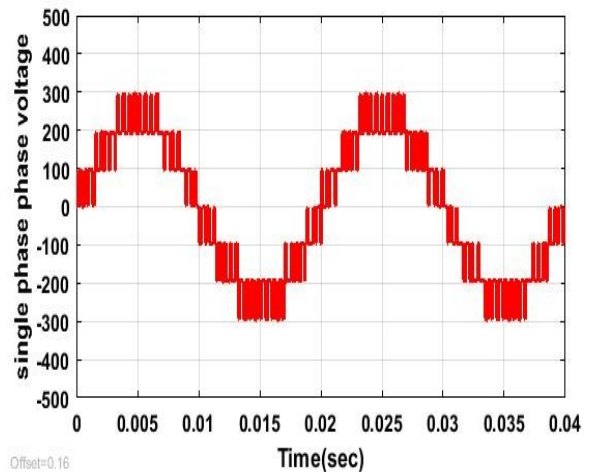


Fig.9 Single-leg Inverter output phase voltage

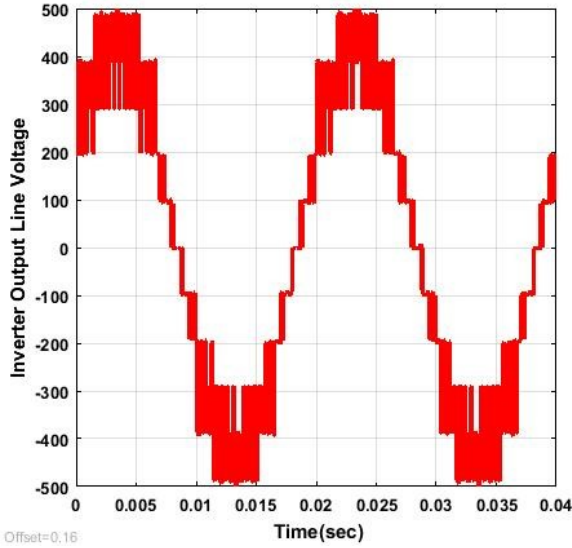


Fig. 10 Single-leg inverter output Line Voltage

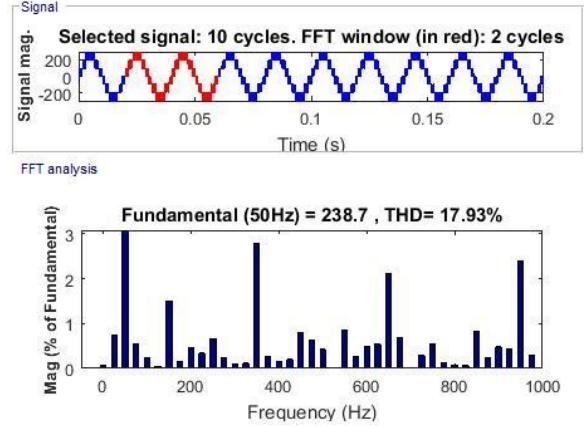


Fig.13 the THD value of the inverter output voltage

Fig.9 shows the single-phase inverter phase voltage Fig.10 shows the 11-level inverter output voltage.

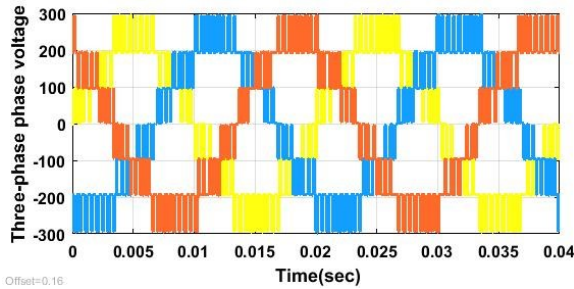


Fig.11 Three-phase inverter phase voltage

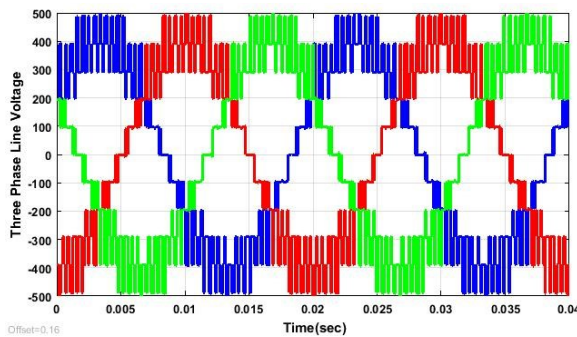


Fig.12 Three-phase inverter Line Voltage

The inverter's output phase-to-phase voltage is shown in Fig. 11. The inverter output line-to-line voltage is depicted in Fig. 12. There is no doubt about the phase or line voltages. GTO switches created the inverter that was put into use. The inverter output voltage THD waveform is shown in Fig. 13.

## V CONCLUSION

A 7-level diode-clamped MLI with fewer switches is shown in this study. For both three-phase inverter phase voltage and line voltage as well as single-leg phase voltage and line voltage, the Multi-carrier approaches are examined. The MLIs' benefits include producing output waves that are close to sine waves. The output voltage that was obtained had a staircase pattern. The inverter's THD value is lower than average at 17.93%.

## REFERENCES

- [1]. S. Pal, K. Gopakumar, U. Loganathan, H. Abu-Rub and D. Zielinski, "A Hybrid Seven-Level Dual-Inverter Scheme With Reduced Switch Count and Increased Linear Modulation Range," in IEEE Transactions on Power Electronics, vol. 38, no. 2, pp. 2013-2021, Feb. 2023,
- [2]. D. Niu and F. Gao, "Flexible Third Harmonic Voltage Modulation of Boost Seven-Level Active Neutral-Point-Clamped Inverter With Reduced Voltage Ripple," in IEEE Transactions on Industrial Electronics, vol. 70, no. 2, pp. 1150-1160, Feb. 2023
- [3]. N. V. Kurdkandi et al., "A New Seven-Level Transformer-Less Grid-Tied Inverter With Leakage Current Limitation and Voltage Boosting Feature," in IEEE Journal of Emerging and Selected Topics in Industrial Electronics, vol. 4, no. 1, pp. 228-241, Jan. 2023
- [4]. Chenchireddy, K., Jegathesan, V., & Ashok Kumar, L. (2020). Different topologies of inverter: a literature survey. Innovations in Electrical and Electronics Engineering, 35-43.
- [5]. Kumar, T. A., Kaliamoorthy, M., & Rai, I. (2023). Genetic Algorithm Based 7-Level Step-Up Inverter with Reduced Harmonics and Switching Devices. Intelligent Automation & Soft Computing, 35(3).
- [6]. Al-Atbee, O. Y. K., & Abdulhassan, K. M. (2023). A cascade multi-level inverter topology with reduced switches and higher efficiency. Bulletin of Electrical Engineering and Informatics, 12(2), 668-676.

- [7]. Sreejothi, K. R., Chenchireddy, K., Lavanva, N., Reddy, R. M., Prasad, K. G., & Revanth, R. (2022, March). Level-Shifted PWM Techniques Applied to Flying Capacitor Multilevel Inverter. In 2022 International Conference on Electronics and Renewable Systems (ICEARS) (pp. 41-46). IEEE.
- [8]. Parimalasundar, E., Kumar, R. S., Chandrika, V. S., & Suresh, K. (2023). Fault diagnosis in a five-level multilevel inverter using an artificial neural network approach. *Electrical Engineering & Electromechanics*, (1), 31-39.
- [9]. Ramu, V., Satish Kumar, P., & Srinivas, G. N. (2023). Comparative Analysis of Multi-level Inverters with Various PWM Techniques. In *Information and Communication Technology for Competitive Strategies (ICTCS 2021)* (pp. 325-351). Springer, Singapore.
- [10]. Ayub, M. A., Aziz, S., Liu, Y., Peng, J., & Yin, J. (2023). Design and Control of Novel Single-Phase Multilevel Voltage Inverter Using MPC Controller. *Sustainability*, 15(1), 860.
- [11]. Sakasegawa, E., Chishiki, R., Sedutsu, R., Soeda, T., Haga, H., & Kennel, R. M. (2023). Comparison of Interleaved Boost Converter and Two-Phase Boost Converter Characteristics for Three-Level Inverters. *World Electric Vehicle Journal*, 14(1), 7.
- [12]. Parimala, P. V. S. S. A., & Mathew, R. (2023). Maximum Boost Control of Quasi-Z-Source Inverter with DST AT COM for a Wind Energy System. In *Proceedings of the International Conference on Cognitive and Intelligent Computing* (pp. 205-214). Springer, Singapore.
- [13]. Bhatt, K., & Chakravorty, S. (2023). Optimum regulation of THD profile in multilevel inverter using parameter-less AI technique for electrical vehicle application. *International Journal of Power Electronics*, 17(1), 78-96.
- [14]. Revathi, M., & Rama Sudha, K. (2023). A New Cascaded H-bridge Multilevel Inverter Using Sinusoidal Pulse Width Modulation. In *International Conference on Innovative Computing and Communications* (pp. 261-268). Springer, Singapore.
- [15]. Chenchireddy, K., & Jegathesan, V. (2022, March). Multi-Carrier PWM Techniques Applied to Cascaded H-Bridge Inverter. In 2022 International Conference on Electronics and Renewable Systems (ICEARS) (pp. 244-249). IEEE.

See discussions, stats, and author profiles for this publication at: <https://www.researchgate.net/publication/369816525>

# Reduction of THD and Power Quality Improvement by using 48-pulse GTO-based UPFC in the Transmission Systems

Conference Paper · February 2023

DOI: 10.1109/ICCMCS56507.2023.10083821

CITATIONS

0

READS

22

6 authors, including:



**Khammampati R Sreejyothi**  
Karunya University

20 PUBLICATIONS 78 CITATIONS

[SEE PROFILE](#)



**Kalagotla Chenchireddy**  
Karunya University

53 PUBLICATIONS 160 CITATIONS

[SEE PROFILE](#)

# Reduction of THD and Power Quality Improvement by using 48-pulse GTO-based UPFC in the Transmission Systems

Khammampati R Sreejyothi  
*Electrical and Electronics Engineering  
Teegala Krishna Reddy Engineering  
College*  
Hyderabad, India.  
krs.jyothi@gmail.com

Sandarikari Umesh  
*Electrical and Electronics Engineering  
Teegala Krishna Reddy Engineering  
College*  
Hyderabad, India.  
umesh.sandarikari1234@gmail.com

Valluri Ranjith Kumar  
*Electrical and Electronics Engineering  
Teegala Krishna Reddy Engineering  
College*  
Hyderabad, India.  
vallriranjith2662662@gmail.com

Kalagotla Chenchireddy  
*Electrical and Electronics Engineering  
Teegala Krishna Reddy Engineering  
College*  
Hyderabad, India.  
chenchireddy.kalagotla@gmail.com

Yerroju Abhinay Sai  
*Electrical and Electronics Engineering  
Teegala Krishna Reddy Engineering  
College*  
Hyderabad, India.  
Yerrojuabhinayabhi1333@gmail.com

Bontha Nagarjun  
*Electrical and Electronics Engineering  
Teegala Krishna Reddy Engineering  
College*  
Hyderabad, India.  
Bonthanagarjun2526@gmail.com

**Abstract:** This paper presents a 48 Pulse GTO-based Unified Power Flow Controller (UPFC) for power quality development in the Transmission system. It consists of a shunt converter which is operating as a Static Synchronous Compensator (STATCOM) to control the voltage at the source side and a Series converter which is operating as a Static Synchronous Series Capacitor (SSSC) to control the injected voltage and reactive power at the load side. This paper proposed Synchronous Reference Theory (SRF) based Phase locked loop for controlling the voltage at the source site. The Total Harmonic Distortion (THD) with UPFC resulted inside 43.93% and without UPFC resulted in 1.81% as per IEEE 519 standards. The results were simulated in MATLAB/SIMULINK.

**Keywords:** UPFC, STATCOM, SSSC, SRF theory, PI controller

## I INTRODUCTION

This paper [1] proposed a 48-pulse GTO-based Center node (C-Node) UPFC. The main implementation of the C-Node compensates for the unbalanced line current and it will control the dc bus voltage in the transmission line. The 48-pulse multilevel inverter has fast control and the best-performed d-q-based algorithm. Different types of FACTS controllers are proposed for improving the power quality in transmission lines. The main use of FACTS devices is can control the output voltage without harmonics and also it will regulate the voltage in

transmission lines [2]. In this paper [3] UPFC under control and grid protection can be done with a coordination strategy for improving fault ride-through capability. The strategy is verified by a 220kv power grid and a closed loop test is also performed in Simulink results. In this article, a novel IPFC and UPFC-based voltage control strategy were proposed [4]. This paper's in-depth analysis focuses on the coordination of actual and reactive powers using IPFC and UPFC. This paper [5] implemented a new control technique of PV-UPFC to establish the stability of the power grid. A single inverter is used to perform the DC-AC as well as AC-DC Conversion. The maloperation function is implemented by using a fault detection module. This paper [6] discussed FACTS devices used in the Transmission system. Compared to all, UPFC improves the system performance and reduces power oscillations. The other advantage of UPFC controls the line parameters, phase angle, and output power. This research [7] implements and analyses a UPFC to control the power flow in the system. The proposed control parameters are voltage and reactive power. This paper [8] discussed the performance of UPFC under fault conditions such as LG fault and LLL-G fault. To perform these two faults, considered a two-machine-double line system in four different modules. This paper [9]-[10] performed UPFC on distance protection in transmission lines. The line impedance

values are investigated under underperformed standards. This paper [11]-[13] implemented a Neuro-Fuzzy UPFC controller for reducing the low-frequency oscillations in power systems. The controller was designed for an infinite bus system to control the adaptive changes in neural networks.

## II. TOPOLOGY

UPFC is a grouping of SSSC and STATCOM. SSSC consists of one voltage source converter and a DC link through a series transformer. SSSC performs the functions, You can exchange both active and reactive power.

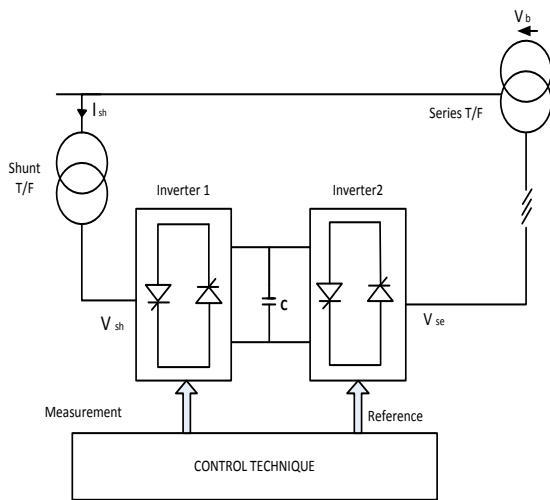


Fig. 1 Basic Diagram of UPFC

UPFC can regulate both the real and reactive in the timeline if the initial voltage and the current-voltage are in phase. Normally UPFC consists of two converters, namely converter 1 Which is called a shunt converter, and converter 2 called As series converter. These two converters are connected by a DC storage capacitor to a common link that powers them. Real power can easily flow between the two converters in any way, but the reactive powers independently are generated and observed by its output terminal.

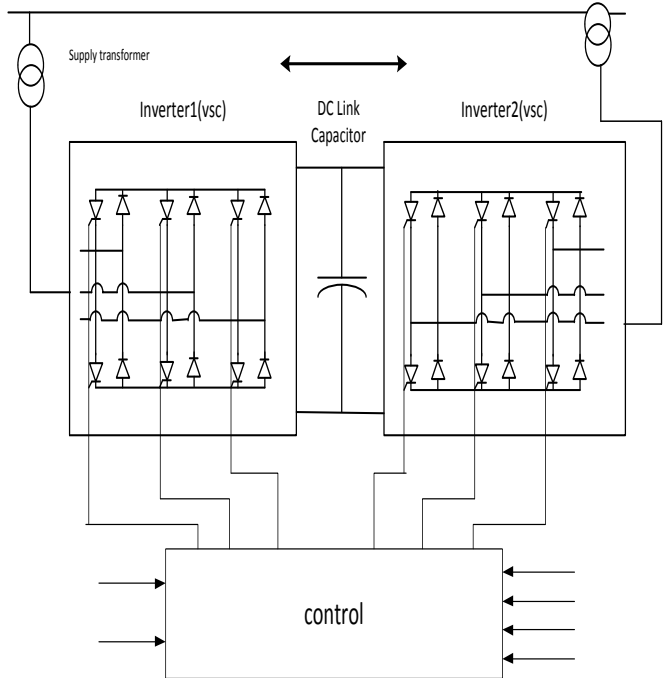


Fig.2 Switching Diagram of UPFC

The voltage  $v_{pq}$  with magnitude and phase angle is introduced by the series converter into the transformer line.

$$P - jQ_r = V_r \left( \frac{V_s + V_{pq} - V_r}{jX} \right)^* \quad (1)$$

Where () denotes the injected compensatory voltage and (\*) the complex value's conjugate value.

$$P - jQ_r = V_r \left[ \frac{V_s - V_r}{jX} \right]^* + \frac{V_r V_{pq}^*}{jX} \quad (2)$$

$V_s, V_r$  and  $V_{pq}$  can be calculated as below :

$$V_s = V e^{j\frac{\delta}{2}} = V \left[ \cos \frac{\delta}{2} + j \sin \frac{\delta}{2} \right] \quad (3)$$

$$V_r = V e^{-j\frac{\delta}{2}} = V \left[ \cos \frac{\delta}{2} - j \sin \frac{\delta}{2} \right] \quad (4)$$

$$V_{pq} = V_{pq} e^{j\left(\frac{\delta}{2} + \rho\right)} = V_{pq} \left[ \cos \left( \frac{\delta}{2} + \rho \right) + j \sin \left( \frac{\delta}{2} + \rho \right) \right] \quad (5)$$

By changing (2) to read as (3), (4), (5), the answer to and can be found as follows.

$$P(\delta, \rho) = P_0(\delta) + P_{pq}(\rho) = \frac{V^2}{X} \sin \delta - \frac{VV_{pq}}{X} \cos\left(\frac{\delta}{2} + \rho\right)$$

(6)

$$Q_r(\delta, \rho) = Q_{or}(\delta) + Q_{pq}(\rho) = \frac{V^2}{X} (1 - \cos \delta) - \frac{VV_{pq}}{X} \sin\left(\frac{\delta}{2} + \rho\right)$$

### III CONTROL TECHNIQUE

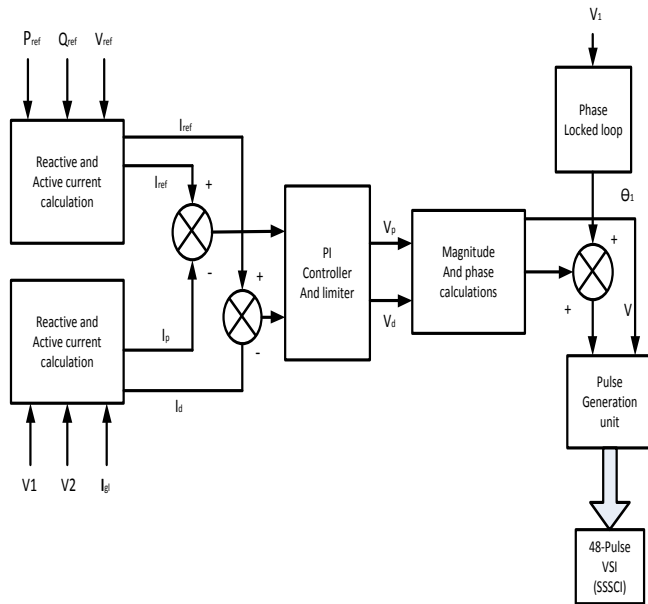


fig.3 shows the UPFC control scheme

The control scheme is three reference one is active power (Pref), second is Reactive power (Qref) and Reference Voltage (Vref). These three-phase references are generated by Idref values. The DC reference currents are Id and Iq, these currents are generated by V1, V2, and Id. This control scheme has a summation block it compares the Idref and Id values. The PI controller control and converter input currents to output DC voltages. The magnitude and phase angle block generates magnitude and phase angle. The PLL block locks the voltage in the transmission. The pulse generator block generates 48 pulses for UPFC.

### IV SIMULATION RESULTS

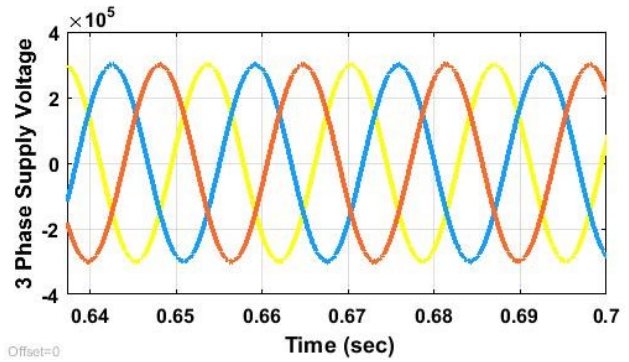


Fig.4 Three Phase supply voltage

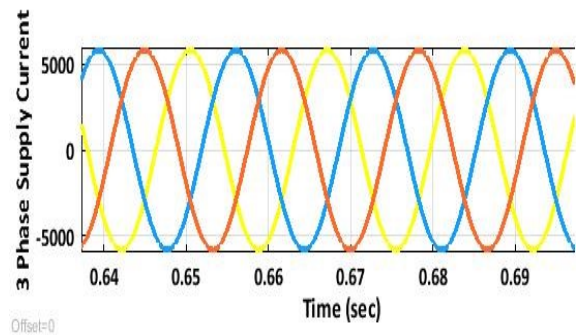


Fig.5 Three-phase Supply Current

A three-phase supply voltage is shown in Fig. 4 at the grid side; the average voltage is 300 kV. The voltage rating is very high; transmission cables for HVAC use this voltage. The three-phase supply current is depicted in Fig. 5. The current is extremely high at 5000A in magnitude. R, Y, and B phases make up these three phase currents.

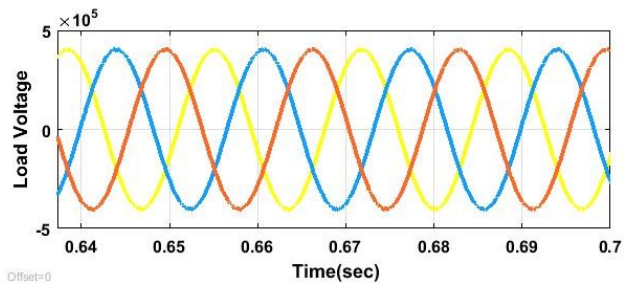


Fig.6 Three-Phase Load Voltage

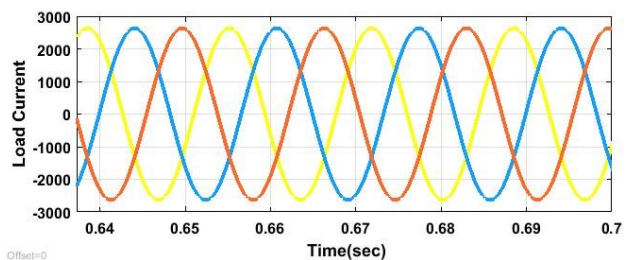


Fig.7 Three-Phase Load current

The three-phase load side voltage waveform is depicted in Fig. 6; the loading waveforms are 300 KV, and the x-

axis ranges from 0.64 to 0.7 sec. These three-phase waveforms have 1200 phase shifts between one another and are used in industrial loads. The three-phase load currents, which are rated at 2500A, are shown in Fig. 7. The current magnitudes do not change during the total during the 0.64 to 0.7 sec X-axis period.

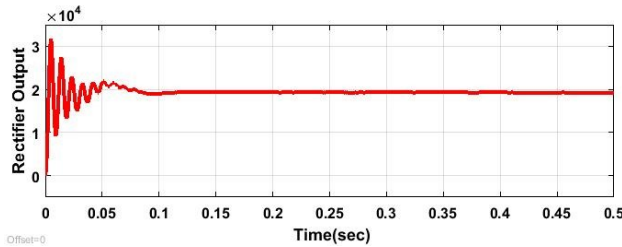


Fig.8 Rectifier Output

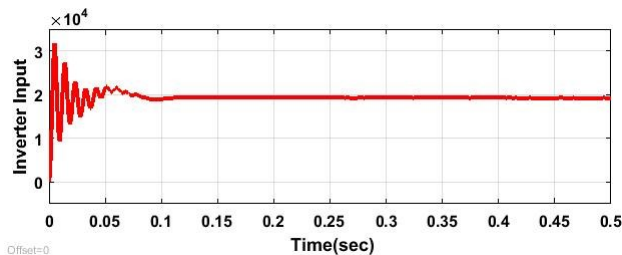


Fig.9 Inverter input

Fig.8 shows the rectifier output voltage, the magnitude of the DC output voltage is 20KV; the voltage is 0 to 0.05 have high distortions; it took time for 0.05sec for the transient state to steady state. The magnitude is 0.1 sec to 0.5 it is maintained constant. Fig.9 shows the inverter input voltage, this voltage same as the rectifier output voltage.

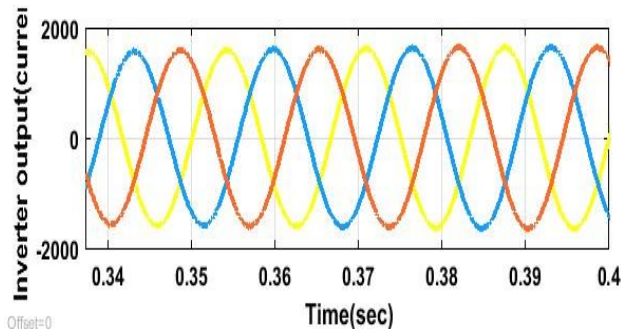


Fig.10 Inverter Output (Current)

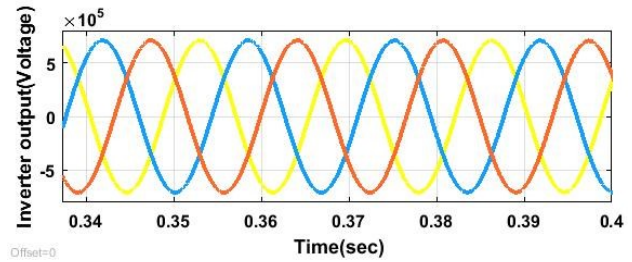


Fig.11 Inverter Output (Voltage)

The three-phase inverter output current waveform is depicted in Fig. 10, and it has a 1500A current magnitude. The 550KV output voltage waveform of the inverter is shown in Fig. 11.

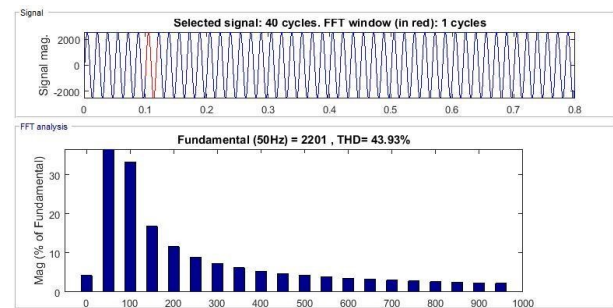


Fig.12 THD without UPFC

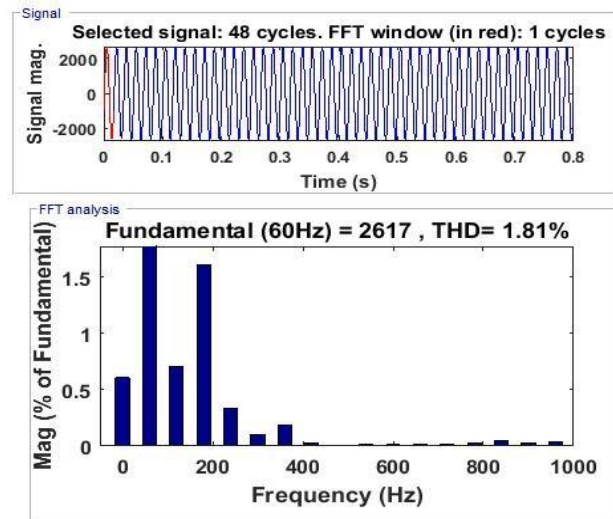


Fig.13 THD with UPFC

Without UPFC, as shown in Fig.12, the supply current has a THD value of 43.13%. The THD value of the Supply current using the UPFC controller is 1.81%, as shown in Fig. 13. In this circuit, the current harmonics are corrected for using the UPFC controller.



## V CONCLUSION

This paper implemented 48 Pulse GTO-based Unified power flow controllers (UPFC). This UPFC controller is improved power quality in the Transmission system. It consists of a series converter that functions as a static synchronous series capacitor (SSSC) to control the injected voltage and reactive power at the load side and a shunt converter that operates as a static synchronous compensator (STATCOM) to regulate the voltage at the source site. SRF-based PLL is controlled at source side voltage in this paper. In Matlab/Simulink, many simulation results are validated. These outcomes include the average AC voltage input, load voltage, inverter output voltage, and rectifier output voltage. This study explains the steady-state and dynamic outcomes. The Total harmonic distortion (THD) with UPFC resulted in 43.93% and without UPFC resulted in 1.81% as per IEEE 519 standards. The results are simulated in MATLAB/SIMULINK.

## REFERENCES

- [1] Aali, Seyedreza, and Daryoush Nazarpour. "48-Pulse GTO center node unified power flow controller." *European Journal of Scientific Research* 42.1 (2010): 106-113.
- [2] Kadandani, Nasiru B., and Yusuf A. Maiwada. "An overview of facts controllers for power quality improvement." *The International Journal Of Engineering: And Science (IJES)* 4.9 (2015): 9-17.
- [3] Lin, Jinjiao, et al. "Coordination strategy and its realization of UPFC control protection system and power grid protection for improving fault ride-through capability." 2017 China International Electrical and Energy Conference (CIEEC). IEEE, 2017.
- [4] Murugan, A., and S. Thamizmani. "A new approach for voltage control of IPFC and UPFC for power flow management." 2013 International Conference on Energy Efficient Technologies for Sustainability. IEEE, 2013.
- [5] Ramya, L., and J. Pratheebha. "A novel control technique of solar farm inverter as PV-UPFC for the enhancement of transient stability in the power grid." 2016 International Conference on Emerging Trends in Engineering, Technology and Science (ICETETS). IEEE, 2016.
- [6] K. R. Sreejyothi, P. V. Kumar and J. Jayakumar, "SRF Theory-Based PI Controller Applied to Micro Grid Interfaced with hybrid sources for Power Quality Improvement," 2022 8th International Conference on Advanced Computing and Communication Systems (ICACCS), 2022, pp. 01-06, doi: 10.1109/ICACCS54159.2022.9785173.
- [7] Choudante, Smitkumar D., and A. A. Bhole. "A review: Voltage stability and power flow improvement by using UPFC controller." 2018 International conference on the computation of power, energy, information and communication (ICCPEIC). IEEE, 2018.
- [8] Shahgholian, G., et al. "Analysis and simulation of UPFC in electrical power system for power flow control." 2017 14th

- International Conference on Electrical Engineering/Electronics, Computer, Telecommunications and Information Technology (ECTI-CON). IEEE, 2017.
- [9] Deepak, Kumara, et al. "Performance of UPFC on system behavior under fault conditions." 2005 Annual IEEE India Conference-Indicon. IEEE, 2005.
- [10] K. R. Sreejyothi, K. Chenchireddy, N. Lavanya, R. M. Reddy, K. Y. G. Prasad and R. Revanth, "Level-Shifted PWM Techniques Applied to Flying Capacitor Multilevel Inverter," 2022 International Conference on Electronics and Renewable Systems (ICEARS), 2022, pp. 41-46, doi: 10.1109/ICEARS53579.2022.9752074.
- [11] Deshmukh, Nisha, Amandeep S. Bedi, and N. R. Patne. "Analysis of distance protection performance for line employing UPFC." 2016 IEEE 1st International Conference on Power Electronics, Intelligent Control and Energy Systems (ICPEICES). IEEE, 2016.
- [12] Talebi, Nasser, and Ali Akbarzadeh. "Damping of low frequency oscillations in power systems with neuro-fuzzy UPFC controller." 2011 10th International Conference on Environment and Electrical Engineering. IEEE, 2011.
- [13] K. Chenchireddy, V. Kumar, K. R. Sreejyothi and P. Tejaswi, "A Review on D-STATCOM Control Techniques for Power Quality Improvement in Distribution," 2021 5th International Conference on Electronics, Communication and Aerospace Technology (ICECA), 2021, pp. 201-208, doi: 10.1109/ICECA52323.2021.9676019.



# Power Optimization Scheme On Induction Motor Using Artificial Neural Network For Electrical Vehicle

CH Prasanna <sup>1</sup>, Punumalli Naga Ganesh <sup>2</sup>, N.Bharath Kumar <sup>3</sup>, Botte Sathish <sup>4</sup>, Vempalla Naveen <sup>5\*</sup>

Assistant Professor, Department of Electrical & Electronics Engineering, Teegala Krishna Reddy  
Engineering College, Hyderabad.

UG Students, Department of Electrical & Electronics Engineering, Teegala Krishna Reddy  
Engineering College, Hyderabad .

## ABSTRACT

In electric vehicles (EVs) and hybrid EVs, energy efficiency is essential where the energy storage is limited. Adding to its high stability and low cost, the induction motor efficiency improves with loss minimization. Also, it can consume more power than the actual need to perform its working when it is operating in less than full load condition. This study proposes a control strategy based on the Artificial Neural Network (ANN) for EV applications. ANN controller can improve the starting current amplitude and saves more power. Through the MATLAB/SIMULINK software package, the performance of this control was verified through simulation. As compared with the conventional proportional integral derivative controller, the simulation schemes show good, high-performance results in time-domain response and rapid rejection of system-affected disturbance. Therefore, the core losses of the induction motor are greatly reduced, and in this way improves the efficiency of the driving system. Finally, the suggested control system is validated by the experimental results obtained in the authors' laboratory, which are in good agreement with the simulation results.

**Keywords:** Induction motor, electric vehicle, Proportional–integral derivative controller, fuzzy logic, artificial neural networks.

## 1. Introduction

With increasing global awareness of air quality and reduce greenhouse gas emissions, electric vehicles (EVs) have increasingly attracted the attention of manufacturers, governments, international organizations, and consumers. According to the European Renewable Energy Council (EREC) [1], many governments promote EV as an important part of their proposals for technologies required to reduce greenhouse gas emissions in the long term and to improve energy efficiency in the transport sector. In addition to reducing pollution in the environment, the electric vehicle gives good performance in terms of efficiency and torque [2]. The only drawback of electric vehicles is their cost [3]. It is, therefore, necessary to choose the appropriate drive motor and its control technology. In the previous literature review, a DC motor is preferred used in EV applications due to the simplicity of the control unit design and its characteristics well matched with an electric vehicle motor. With the increasing research progress of control technology, induction motors are among the best candidates for driving electric

vehicles and are widely used in modern electric vehicles [4]. The structure of the induction motor is simple, it has strong durability, it is inexpensive, it is very reliable, and it requires no maintenance [5]. Although it has more advantages than DC motors, it has some disadvantages such as non-linear properties; as a result, analysis becomes very complex [6, 7] and flux in induction motor is not measurable [8]. To overcome these drawbacks, several modern control techniques have been invented to control the two main parameters, torque and flux of induction motor for electric vehicle applications.

There are various control technologies for induction motors in electric vehicle applications. They are: (1) proportional–integral (PI) controller, (2) PID controller, (3) sliding mode controller (SMC), (4) fuzzy logic controller (FLC), (5) neural network controller (NNC), (6) model predictive control (MPC), (7) hybrid controllers, and more. Few important algorithms are reviewed here. One can choose the best algorithm for controlling the IM drives. In [9], this paper presents a compound sliding mode control (CSMC) method for controlling the speed of surface-mounted permanent magnet synchronous motors (SPMSMs). The proposed CSMC consists of a new sliding mode controller (SMC) based on a new hybrid reaching law and an extended sliding mode disturbance observer (ESMDO), and due to the complexity of organization of the brain, are interconnected to form a network, this is called a neural network (NN). An artificial network composed of structural units of perceptron that mimic these neurons is called ANN. A single-layer perceptron is a linear classifier that divides an input vector into two classes. MLP is a multi-layered perceptron and learns by using a hidden layer addition and a back-propagation algorithm between the input layer and the output layer to enable nonlinear classification that the single-layer perceptron cannot solve [29]. [30] proposes an artificial neural network (ANN) controller to reduce both torque and flux ripples by considering appropriate input and feedback values through online mode. By using both simulation and process, it shows that the proposed controller is more efficient than the traditional controller. [31] Improves the transient analysis using the ANN controller but without changes in the torque and flux ripples.

Finally, all of these algorithms have their advantages and disadvantages. So the choice of these algorithms for induction motor depends on cost, accuracy, and application. A fuzzy logic controller is used where the system behavior is more complicated and semantic rules are necessary to explain the system. Compared to the artificial neural network, it is good for modeling in these conditions as ANN is more suitable for controlling nonlinear devices. As induction motor has a nonlinear model, ANN is highly suitable for controlling induction motor drive in electrical vehicles. In this paper, a neural network controller-based method using simulation in the MATLAB/Simulink Power system cluster environment is then linked to the prototype reflector through the use of a micro ds PACE laboratory box control panel. The proposed neural network control is then compared with conventional PID control based on its effect on IM performance.

The main problem is to reduce the life cycle cost of the drive, i.e., manufacturing, maintenance, and energy costs.

- Efficiency is an indicator of energy cost, particularly important at rated speeds and above.
- Also, the efficiency of the inverter is very important as it affects the overall driving efficiency.
- The power factor is an indicator of the apparent power that the inverter must deliver.
- The inverter kVA rating is determined by the peak current of the maximum torque at low speeds and the maximum output voltage at high speeds

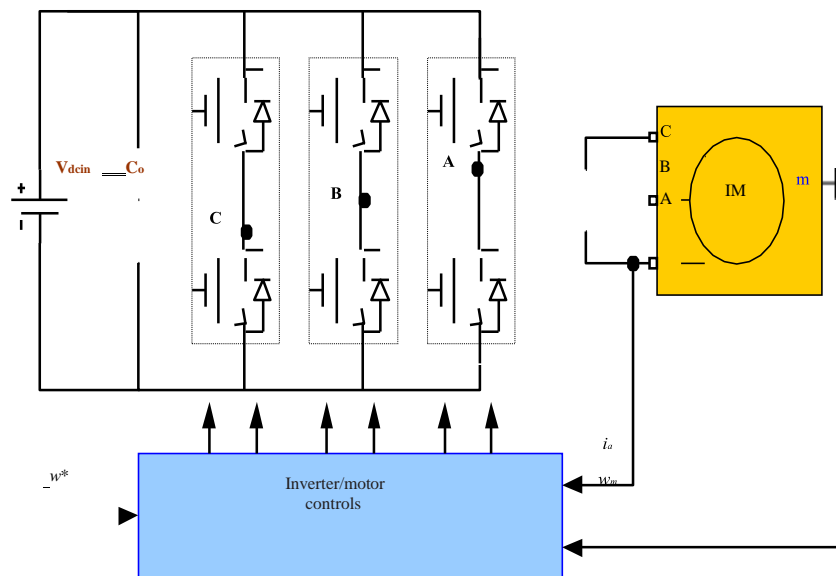


**Fig.1 Electrical vehicle drive with an induction motor**

This paper presents a comparative study between the PID controller and the ANN-based controller which is organized as follows: after introduction in the first section. In Sect. 2, the circuit description and control principle are given in Sect. 3. In Sect. 4, simulation results are provided. In Sect. 5, the experimental results are performed. In Sect. 6, conclusion is discussed, and future work is discussed in Sect. 7. is connected by the acceleration pedal and/or the brake pedal. In Fig. 1, the traction process is done by controlling the 3-phase induction motor. The right and left wheels are controlled separately by a differential system with a gear ratio to adapt to the high speed of the low-speed electric wheel shaft. The IM torque and speed are controlled by the DC/AC inverter which converts the DC voltage to the 3-phase AC voltage. To run the EV system efficiently, a robust controller is designed and implemented with adaptive capabilities in the process of network learning.

## 2. INDUCTION MOTOR DRIVE SYSTEM MODEL

Figure 1 shows the power circuit of the electric vehicle which consists of three main parts as follows: The first is the 3-phase induction motor. The second is a battery unit that is used as an energy storage element. The battery DC voltage is converted to 3-phase AC voltage by a DC/AC power converter. Third, the AC/DC controller controls the converter output voltage magnitude and frequency that is applied to the induction motor. The voltage magnitude is adjusted depending on the driver's current request, which is connected by the acceleration pedal and/or the brake pedal. In Fig. 1, the traction process is done by controlling the 3-phase induction motor. The right and left wheels are controlled separately by a differential system with a gear ratio to adapt to the high speed of the low-speed electric wheel shaft. The IM torque and speed are controlled by the DC/AC inverter which converts the DC voltage to the 3-phase AC voltage. To run the EV system efficiently, a robust controller is designed and implemented with adaptive capabilities in the process of network learning.



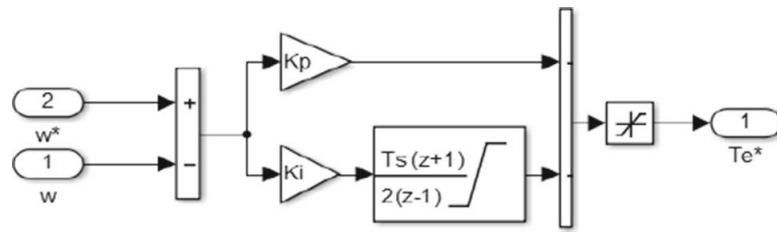


Fig 3. Block diagram of the conventional PID controller

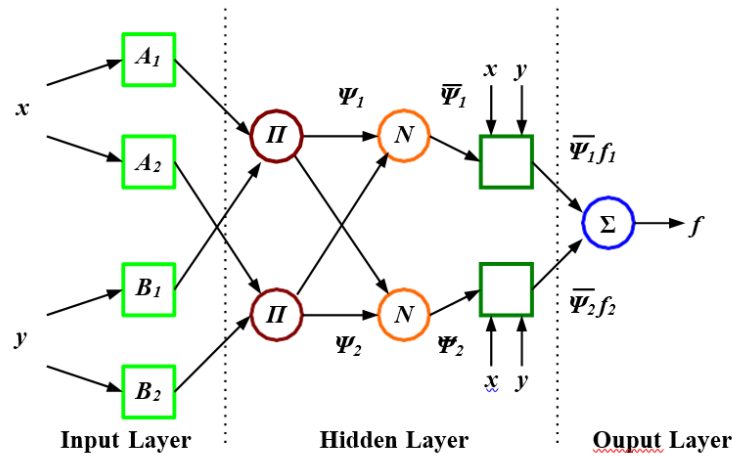


Fig 4. Neural Network Internal structure

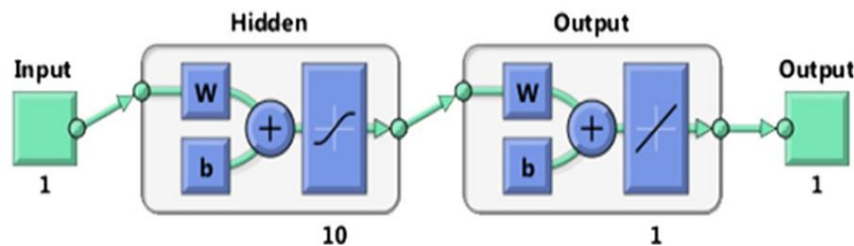


Fig 5. Training Network Model in Matlab

The operating ratios ( $d_d$  and  $d_q$ ) are obtained by normalizing by using the results ( $e_d$  and  $e_q$ ) by the disengagement condition which is normalized by the DC voltage as follows.

$$d_d = \frac{1}{V_{dc}} \begin{matrix} e_d + u_d + 3\omega L & X & i_q \\ e_q + u_q - 3\omega L & X & i_d \end{matrix}$$

Equation (4)

### 3.2 A proposed artificial neural network controller

ANN is an algorithm that models a human brain and processes various data like that of two brains. When neurons, the basic structural organization of the brain, are interconnected which imitates these neurons, is called an ANN, an artificial network composed of structural units. Single-Layer Perceptron (SLP) is a linear classifier that divides input vectors into two classes. MLP is a multilayer perceptron that learns by adding a hidden layer and back-propagation algorithm between the input layer and output layer so that nonlinear classification cannot be solved by a single-layer perceptron. It is possible to express all functions as a single hidden layer, but it is generally more accurate to use multiple hidden layers. Multilayer perceptron (MLP) and radial basisfunction (RBF) are two of the most widely used neural network architecture. In this study, a controller based on RBF for network adaptation is considered [XYZ1]. The common RBF is a Gauss function in the RBF neural network that can be expressed as [34]. which imitates these neurons, is called an ANN, an

artificial network composed of structural units. Single-Layer Perceptron (SLP) is a linear classifier that divides input vectors into two classes. MLP is a multilayer perceptron that learns by adding a hidden layer and back-propagation algorithm between the input layer and output layer so that nonlinear classification cannot be solved by a single-layer perceptron. It is possible to express all functions as a single hidden layer, but it is generally more accurate to use multiple hidden layers. Multilayer perceptron (MLP) and radial basis function (RBF) are two of the most widely used neural network architecture. In this study, a controller based on RBF for network adaptation is considered [XYZ1]. The common RBF is a Gauss function in the RBF neural network that can be expressed as [34].

$$R(X_p - C_i) = \exp - X_p - C_i / 2\sigma_i^2$$

**Equation (5)**

Where  $X_p$   $C_i$ .. the Euclidean norm;  $c$  the center deviation of the Gauss function  $\sigma$  the mean square deviation of the Gauss function. The output of the RBF is as follows [35].

$$y_j = \int_{i=1}^h \omega_{ij} \exp - X_p - C_i / 2\sigma_i^2 \quad j = 1, 2, 3, \dots, n$$

**Equation (6)**

Where  $x_p = (x_1^p, x_2^p, \dots, x_m^p)$  the  $p$ th input sample;  $p=1, 2, \dots, P$ , with  $P$  total number of samples;  $c_i$  the center of the celebration of the output layer;  $i= 1, 2, \dots, h$  the number of hidden layer points;  $y_j$  the true output form the output node  $j$ th corresponding to the input sample. The proposed ANN in this research consists of an input layer, output layer, and several hidden layers as shown in Fig. 4. The input layer depends on the control in the current, which is composed of two axes ( $d$ -axis and  $q$ - axis). The output layer is represented by the control signal axis.

Neurons number in each layer and structure of multilayer feed-forward propagation NN are mostly variable and thus determined by experience and trial and error. So many of the trials are implemented until reaching the best design. And the final design consists of a hidden layer constructed of 10 neurons whose activation function is a tangent sigmoid and the output layer has 1 neuron in which activation function is a linear transfer function. The building of the ANN is illustrated in Fig 5. Figure 6 shows block diagram of ANN with two layers. We have used only ten neurons in the hidden layer because using more neurons may result in a relatively large error due to the overrun problem [36]. The results of the training are given in Fig . The correlation coefficient of 0.8 or higher shows good training of the ANN controller. The histogram is shown in Fig it shows an indicator of errors during the training process, where the blue bars represent training data, the green bars represent the verification data, and the red bars represent the test data [38–40].

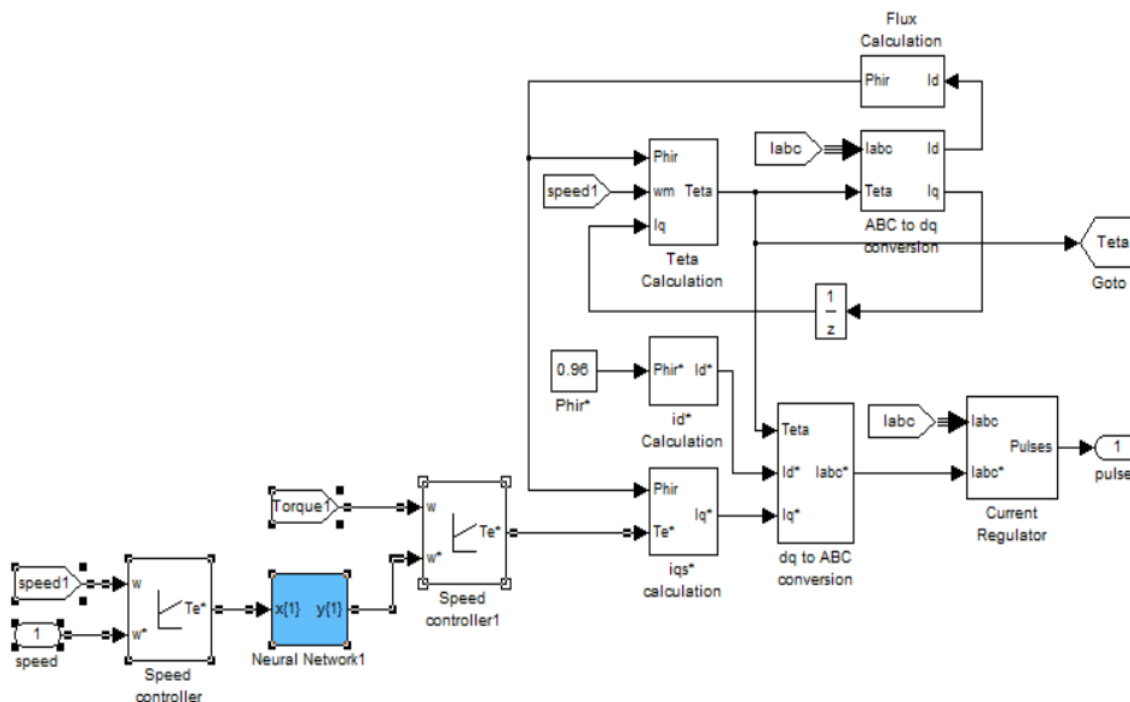


**Fig 6. Block diagram of three phase IM drive and speed control using ANN.**

#### 4. Simulation results and discussion

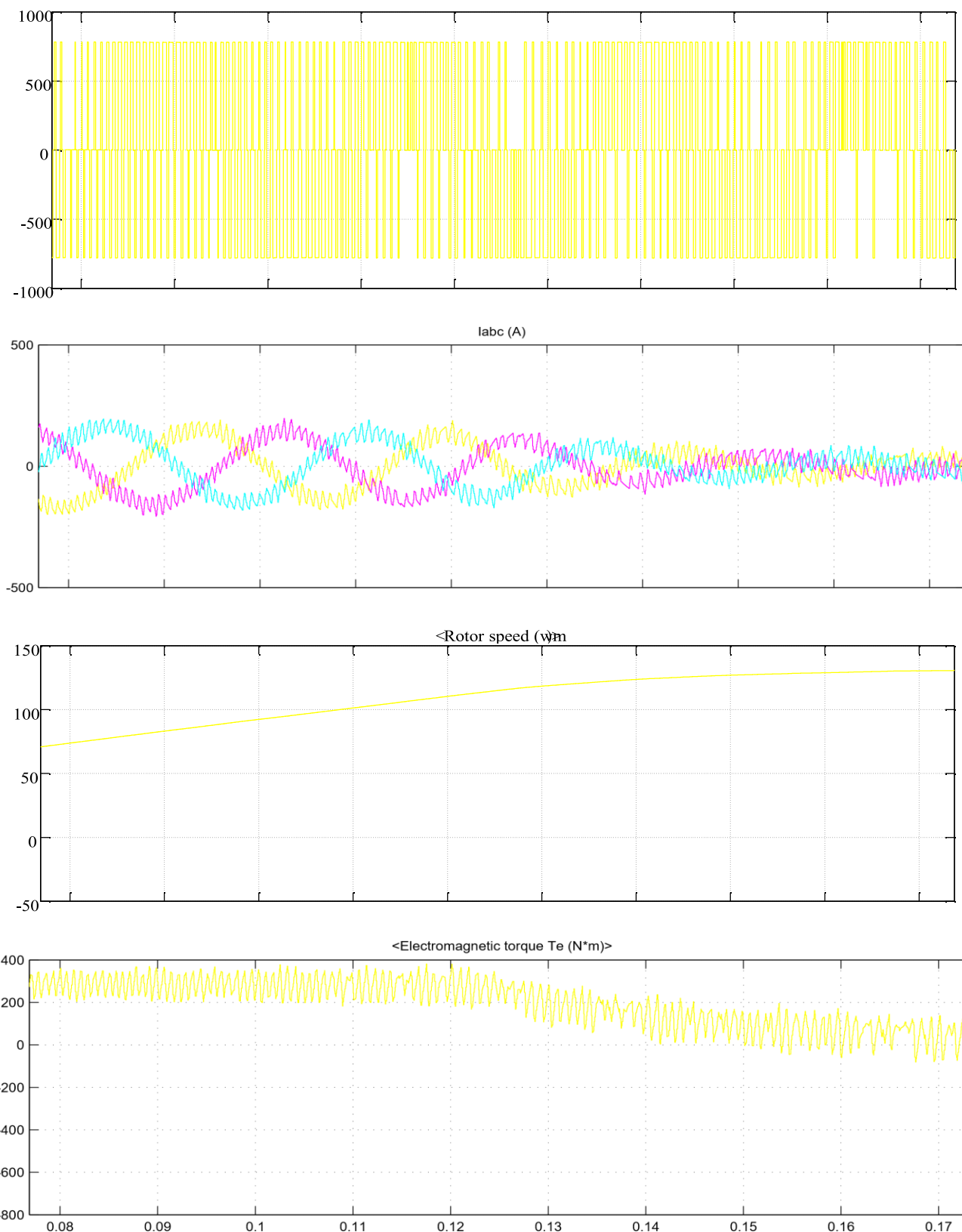
In this paper, two cases were studied. In both, MAT-LAB/Simulink toolboxes are used as shown in Fig. 9. In the first case study, a 50 hp IM is run and controlled by a PID controller. The 3-phase voltages and currents are measured and planned in the first 5 s of operation. Also, the acceleration curve and output torque are checked. In the second case, the engine itself is operated and controlled by the ANN controller. The PID controller response is compared with the ANN controller response, and the simulation results are presented in Fig. 10 through Fig. 13. As shown in Figs. 10 and 11, the outputs were improved concerning the size of the starting currents as well as the acceleration time response in the proposed ANN method. The phase current using the proposed ANN method has lower loss components or lower capacity in the same arrangement components.

From Figs. 12 and 13, from interval 0.7 s to 2 s, it is seen that for the desired speed there are spikes in the torque wave-form due to the conventional torque controller that draws more power and these ripples are suppressed using an ANN torque controller. For the actual torque in the steady state, the average loss capacity in the proposed ANN is reduced compared to the PID controller. This shows that the system generates actual torque smoother and reduces speed fluctuation.

The fluctuation in the mechanical speed  $\omega_m$  and load torque  $T_L$  is reduced with the ANN method. Furthermore, the ANN method shows a faster response in speed tracking. The ANN control achieves better robustness and less over-shoot than PID control by the same velocity reference. By equal initial conditions, the ANN control achieves a shorter duration of the transients. Another advantage of the ANN control is less deviation from the reference signal as shown in Fig. 13. As the figures showed, the proposed ANN method presents better dynamic performance than the PID scheme. Figures illustrate the harmonic velocity wave-form of PID and ANN, respectively. The simulation results show a net superiority of the proposed control as compared to the conventional PID. It can be observed from the simulation results that the torque and flux ripples have substantially reduced. Consequently, the stator current becomes

$$V_{ab} \text{ (V)}$$





Time offset: 0 **Fig14. Electromagnetic torque response of PID and ANN simulation results)**

more smoother and its harmonic contents become smaller as shown in Fig. 11. The THD is reduced by 49.57% compared to conventional PID. Figure shows the efficiency of the IM drive vs. percent load. From the figure, the energy efficiency increases when the IM runs at optimal performance. By comparison between the results obtained by the controller tuned using some known tuning rules and the results obtained by the suggested rules in a worthwhile performance is achieved by the proposed controller. A comparison between PID and ANN control of this system is presented. Fine-tuning of the PID controller for the actual parameters of the model could lead to better results, but it could hardly outperform the ANN-based control. Furthermore, the PID controller is sensitive to changes in the system model (i.e., simulations of a vehicle with different mass or aerodynamics) and requires repetitive fine-tuning of the controller. Therefore, another advantage of ANN control is that training and tuning are performed automatically. ANN showed a faster response in both the settling time and the overshoot compared

to the PID response for multi-step speed input. As a result, ANN showed better performance compared to the PID controller. ANN has also demonstrated the ability to control the speed of the 3-ph. IM and provide an accurate and fast response with no relatively large overshoot and stable state error. This shows the dynamic response for a 20-s simulation result. At time  $t = 0$ , the vehicle is completely stopped and the accelerator is suddenly pushed to 70%. The car starts in electrical mode until the power required by the vehicle reaches 10 kW (at  $t = 0.8$  s). At the time  $t = 12$  s, the brakes are pushed to 70%. This turns on the electric motor to transfer the brake energy to the battery and charge it for 4s. At the time  $t = 16$  s, the accelerator is suddenly pushed to 70% again [41, 42].

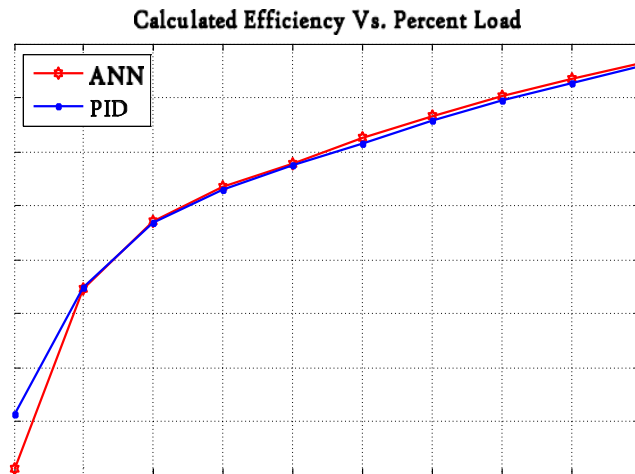


Fig Efficiency of the IM drive using PID vs. ANN

## 5. Experimental results

Some experimental results are presented for the 1.5 kW induction motor employing the indirect rotor field-oriented control system as shown in Fig. In this case, a multilayer feedforward ANN is used to estimate the rotor speed. The developed circuit controller is designed and implemented using the ds PACE Micro Lab Box controller. Fig shows the experimental setup circuit that consists of IM, 3-ph. inverter, Lithium-ion batteries, and voltage and current sensors. The experimental results of the proposed control system show good stability and better performance of the suggested ANN on the traditional PID controller in full harmonic distortion. The experimental results were in good agreement with the simulated results. Figure shows the experimental waveforms of the gate control signal ( $Q_1, Q_2, Q_3$ ). Figure shows currents through switches  $i_{ds1}$  &  $i_{ds2}$  &  $i_{ds3}$ . Figure shows stator current of the PID model. Figure shows an experimental validation of the stator current of the ANN model. Figure shows harmonic speed waveform of the PID model. Figure shows harmonic speed waveform of the ANN model. As shown in Figs. and, the experimental results reveal that ANN yields a 30% increase in core output with improved quality (i.e., less THD compared to PID). The experimental results exhibit the minimum ripples as previously obtained from the simulation results. The proposed control offers significantly torque and flux ripples reduction than the conventional PID and keeps the current harmonics content at low levels. Experimental results show that when IM operates at optimal flux, energy efficiency increases. These experimental results are more close to those obtained by simulation results. As the figures show, there is the superiority of the proposed controller in reducing the losses during drive cycles in an electric vehicle.

## 6. Conclusions

In this paper, a simulation study was conducted on an electric motor driven by 50 horsepower; the results showed that the phase current contains fewer loss components or less capacity in the same arrangement components. For the actual torque in the steady state, the amplitude of the loss is reduced on average. This shows that the system generates the actual torque more smoothly and reduces the speed fluctuation of the higher system performance and satisfactory system response is obtained. Various performance indicators were

measured such as override peak or lower condition, steady-state error, climb time, stability time, etc. The results of the proposed control scheme simulation show very good stability. The simulation results showed better performance of the ANN proposed on the conventional PID controller in ascension time, time stability, and peak step, and the experimental results were in good agreement with the simulation results obtained using the micro ds PACE laboratory box controller. The main contributions resulting from this work can be summarized as follows:

- ANN is more suitable for controlling nonlinear devices. Since the induction motor has a nonlinear model, the ANN is very suitable for the control of the induction motor in electric vehicles.
- Using the ANN controller, you can control the startup capacity as well as save more power during this time.
- Also, the cost and complexity of the console are reduced when designed by the ANN method, because it does not need data about the system used in detail.
- These controllers are capable of handling nonlinear signals with high efficiency, handling digital and analog data, and are powerful controllers.
- The proposed controller can produce smooth torque and improve system performance.

## 7. References

1. Lin F-J et al (2012) Digital signal processor-based probabilistic fuzzy neural network control of in-wheel motor drive for light electric vehicle. *IET Electr Power Appl* 6(2):47–61
2. Aktas M, Awaili K, Ehsani M, Arisoy A (2020) Direct torque control versus indirect field-oriented control of induction motors for electric vehicle applications. *Int J Eng Sci Technol* 23:1134–1143
3. Chau KT (2015) *Electric vehicle machines and drives: design, analysis and application*. Wiley, Hoboken
4. Tabbache B, Kheloui A, Benbouzid MEH (2010) Design and control of the induction motor propulsion of an electric vehicle. In: *IEEE vehicle power and propulsion conference*, pp 1–6. IEEE
5. Butler KL, Ehsani M, Kamath P (1999) A Matlab-based modeling and simulation package for electric and hybrid electric vehicle design. *IEEE Trans Veh Technol* 48(6):1770–1778
6. Karagiannis D, Astolfi A, Ortega R, Hilairet M (2009) A nonlinear tracking controller for voltage-fed induction motors with uncertain load torque. *IEEE Trans Control Syst Technol* 17(3):608–619
7. Sen PC (1990) Electric motor drives and control past, present, and future. *IEEE Trans Industr Electron* 37(6):562–575
8. Trabelsi R, Khedher A, Mimouni MF, M'sahli F (2012) Back-stepping control for an induction motor using an adaptive sliding rotor-flux observer. *Electric Power Syst Res* 93:1–15
9. Sun X, Cao J, Lei G, Guo Y, Zhu J (2021) A composite sliding mode control for SPMSM drives based on a new hybrid reaching law with disturbance compensation. *IEEE Trans Transp Electrif* 7(3):1427–1436. <https://doi.org/10.1109/tte.2021.3052986>
10. Abdelfatah N, Abdeldjebar H, Bousserhane IK, Hadjeri S, Sicard P (2008) Two-wheel speed robust sliding mode control for electric vehicle drive. *Serbian J Electr Eng* 5(2):199–216
11. Alagna S, Cipriani G, Corpora M, Di Dio V, Miceli R (2016) Sliding mode torque control of an induction motor for automotive application with sliding model flux observer. In: *IEEE international conference on renewable energy research and applications (ICR-ERA)*, pp 1207–1212. IEEE
12. Ltifi A, Ghariani M, Neji R (2014) Performance comparison of PI, SMC and PI-sliding mode controller for EV. In: *2014 15th international conference on sciences and techniques of automatic control and computer engineering (STA)*, pp 291–297. IEEE
13. Nasri A, Gasbaoui B, Fayssal BM (2016) Sliding mode control for four wheels electric vehicle drive. *Procedia Technol* 22:518–526
14. Boumediène A, Abdellah L (2012) A novel sliding mode fuzzy control based on SVM for electric vehicles propulsion system. *ECTITrans Electr Eng Electron Commun* 10(2):153–163
15. Nasri A, Hazzab A, Bousserhane IK, Hadjeri S, Sicard P (2009) Fuzzy-sliding mode speed control for two wheels electric vehicle drive. *J Electr Eng Technol* 4(4):499–509
16. Viswanathan P, Thathan M (2016) Minimization of torque ripple in direct torque controlled switched reluctance drive using neural network. *Asian J Res Soc Sci Humanit* 6(8):65–80
17. Kousalya V, Rai R, Singh B (2020) Predictive torque control of induction motor for electric vehicles. In: *IEEE transportation electrification conference & Expo (ITEC)*, pp 890–895. IEEE

17. Pushparajesh V, Balamurugan M, Ramaiah NS (2019) Artificial neural network based direct torque control of four-phase switched reluctance motor. Available at SSRN 3371369
18. Singh B, Jain P, Mittal AP, Gupta JRP (2006) Direct torque control: a practical approach to electric vehicle. In: IEEE power India conference, pp 4-pp. IEEE
19. Haddoun A et al (2008) Modeling, analysis, and neural network control of an EV electrical differential. IEEE Trans Industr Electron 55(6):2286–2294
20. Das S, Pal A, Manohar M (2017) Adaptive quadratic interpolation for loss minimization of direct torque controlled induction motor driven electric vehicle. In: 2017 IEEE 15th international conference on industrial informatics (INDIN). IEEE
21. Morsalin S, Mahmud K, Town G (2016) Electric vehicle charge scheduling using an artificial neural network. In: IEEE innovative smart grid technologies-Asia (ISGT-Asia). IEEE
22. Saleeb H, Sayed K, Kassem A et al (2019) Control and analysis of bidirectional interleaved hybrid converter with coupled inductors for electric vehicle applications. Electr Eng 102(1):195–222
23. Sayed K, El-Zohri E, Mahfouz H (2017) Analysis and design for interleaved ZCS buck DC-DC converter with low switching losses. Int J Power Electron 8(3):210–231
24. Singh B et al (2006) Neural network based DTC IM drive for electric vehicle propulsion system. In: IEEE conference on electric and hybrid vehicles. IEEE
25. Chan C (1993) An overview of electric vehicle technology. Proc IEEE 81(9):1202–1213
26. Asaii B, Gosden D, Sathiakumar S (1996) A new technique for highly efficient sensor-less control of electric vehicles by using neural networks. In: Power electronics in transportation. IEEE
27. Kalogirou SA (2003) Artificial intelligence for the modeling and control of combustion processes: a review. Prog Energy Combust Sci 29(6):515–566
28. Mediouni H et al (2017) Artificial neural networks applied on double squirrel cage induction motor for an electric vehicle motorization. In: International conference on electrical and information technologies (ICEIT). IEEE
29. Bouhoune K, Yazid K, Boucherit MS, Nahid-Mobarakeh B (2018) Simple and efficient direct torque control of induction motor based on artificial neural networks. In: IEEE international conference on electrical systems for aircraft, railway, ship propulsion and road vehicles & international transportation electrification conference (ESARS-ITEC), pp 1–7
30. Zegai ML, Bendjebbar M, Belhadri K, Doumbia ML, Hamane B, Koumba PM (2015) Direct torque control of Induction Motor based on artificial neural networks speed control using MRAS and neural PID controller. In: IEEE electrical power and energy conference (EPEC), pp 320–325
31. Kassem R, Sayed K, Kassem A et al (2020) Power optimization scheme of induction motor using FLC for electric vehicle. IET Electr Syst Transp 10(3):301–309
32. Sayed K, Kassem A, Saleeb H, Alghamdi AS, Abo-Khalil AG (2020) Energy-saving of battery electric vehicle powertrain and efficiency improvement during different standard driving cycles. Sustainability 12(24):10466. <https://doi.org/10.3390/su122410466>
33. Shi Y, Lorenz RD (2017) Induction machine design for dynamic loss minimization along driving cycles for traction applications. In: IEEE energy conversion congress and exposition (ECCE)
34. Ericsson E (2001) Independent driving pattern factors and their influence on fuel-use and exhaust emission factors. Transp Res Part D: Transp Environ 6(5):325–345
35. Lee J-S et al (2000) A neural network model of electric differential system for electric vehicle. In: IEEE international conference on industrial electronics, control and instrumentation. 21st century technologies. IEEE
36. Topic J, Skugor B, Deur J (2019) Neural network-based modeling of electric vehicle energy demand and all electric range. Energies 12(7):1396
37. Ericsson E (2000) Driving pattern in urban areas: descriptive analysis and initial prediction model. Univ
38. Zhao J et al (2019) Optimization and matching for range-extenders of electric vehicles with artificial neural network and genetic algorithm. Energy Convers Manage 184:709–725
39. Demuth H, Beale M, Hagan M (1992) Neural network toolbox. For use with MATLAB. The MathWorks Inc, Natick
40. Saleeb H, Sayed K, Kassem A et al (2019) Power management strategy for battery electric vehicles. IET Electr Syst Transp 9(2):65–74
41. Almutairi A, Sayed K, Albagami N, Abo-Khalil AG, Saleeb H (2021) Multi-port PWM DC–DC power converter for renewable energy applications. Energies 14:3490. <https://doi.org/10.3390/en14123490>